NCO-sP(EO-*stat*-PO) as functional additive for biomaterials' development

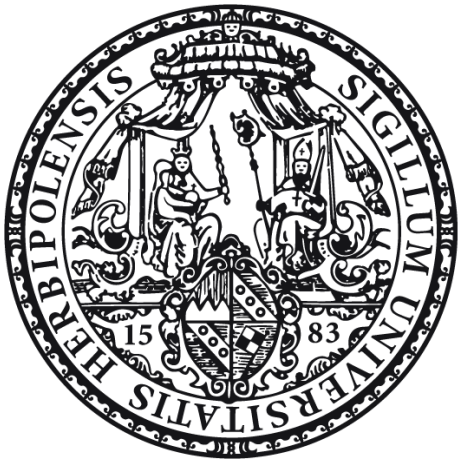

Dissertation zur Erlangung des naturwissenschaftlichen Doktorgrades
der Julius-Maximilians-Universität Würzburg

vorgelegt von

Apothekerin

Laura Wistlich

aus Kreuzwertheim

Würzburg 2018

Eingereicht bei der Fakultät für Chemie und Pharmazie am

_____

Gutachter der schriftlichen Arbeit

1. Gutachter: _____
2. Gutachter: _____

Prüfer des öffentlichen Promotionskolloquiums

1. Prüfer: _____
2. Prüfer: _____
3. Prüfer: _____

Datum des öffentlichen Promotionskolloquiums

_____

Doktorurkunde ausgehändigt am

_____

This thesis was performed from April 2013 until August 2017 at the Department for Functional Materials in Medicine and Dentistry (FMZ) of the University Hospital of Würzburg under the supervision of Prof. Dr. Jürgen Groll.

„Ich bin immer noch verwirrt, aber auf einem höheren Niveau.“

Enrico Fermi, 1901-1954

Table of contents

Abbreviations and symbols

%	percent
°C	degree Celsius
µg	microgram
µl	microliter
µm	micrometer
^{125}I	iodine-125, radioisotope
1D	one-dimensional
2D	two-dimensional
3D	three-dimensional
4-META	4-methacryloyloxyethyl trimellitate anhydride
^{68}Ge	germanium-68, radioisotope
AFM	atomic force microscopy
ANOVA	analysis of variance
APS	ammonium persulfate
ATR-FTIR	Fourier transform infrared spectroscopy with attenuated total reflection
BCA	bicinchoninic acid
Bcl2	B-cell lymphoma 2
BS	bending strength
BSA	bovine serum albumin
BSE	backscattered electrons
CD20	cluster of differentiation 20
CE	cellulose ether
CGEFYFDLRLKGDK	cysteine-glycine-glutamic acid-phenylalanine-tyrosine-phenylalanine-aspartic acid-leucine-arginine-leucine-lysine-glycine-aspartic acid-lysine
CGIKVAV	cysteine-glycine-isoleucine-lysine-valine-alanine-valine
CGRGDS	cysteine-glycine-arginine-glycine-aspartic acid-serine
CGYIGSR	cysteine-glycine-tyrosine-isoleucine-glycine-serine-arginine
cm	centimeter
CO_2	carbon dioxide
CPC	calcium phosphate cement
CQ	camphorquinone
CsA	Cyclosporin A
d	days
Da	Dalton
Dex-MA	methacrylate modified dextran
DMEM	Dulbecco’s modified Eagle’s medium
DMSO	dimethyl sulfoxide
DOPA	3,4-dihydroxy-L-phenylalanine
DSC	differential scanning calorimetry
dSTORM	direct stochastic optical reconstruction microscopy

DTS	diametral tensile strength
e.g.	example given
ECM	extracellular matrix
ELISA	enzyme linked immunosorbent assay
etc.	et cetera
FCS	fetal calf serum
fitcBSA	fluorescein isothiocyanate-conjugated bovine serum albumin
fmol	femtomole
FN	fibronectin
Fn14	fibroblast growth-factor-inducible 14 molecule
FRP	fiber-reinforced polymers
FT-IR	Fourier transform infrared spectroscopy (here: abbreviated version of ATR-FTIR)
g	gram
GEFYFDLRLKGDK	glycine-glutamic acid-phenylalanine-tyrosine-phenylalanine-aspartic acid-leucine-arginine-leucine-lysine-glycine-aspartic acid-lysine
GLF	glycine-leucine-phenylalanine
GpL	*Gaussia princeps* luciferase
GpL-FLAG-TNC-TNF	*Gaussia princeps* luciferase coupled with octapeptide FLAG, tenascin C and tumor necrosis factor, substrate
GRGDS	glycine-arginine-glycine-aspartic acid-serine
GRGDY	glycine-arginine-glycine-aspartic acid-tyrosine
h	hour
HA	hydroxyapatite
HaCaT	human keratinocyte cell line
HEMA	2-hydroxyethylmethacrylate
HEPES	4-(2-hydroxyethyl)-1-piperazineethanesulfonic acid
hFOB	human fetal osteoblast cell line
(h)MSC	(human) mesenchymal stromal / stem cells
HRP	horse radish peroxidase
HT1080-Bcl2-TNFR2	fibrosarcoma cell line with overexpressed Bcl2 and TNFR2
HyA	hyaluronic acid
IDT	interdigitated transducer
Ig	immunoglobulin
IL	interleukin
IPDI	isophorone diisocyanate
IPN	interpenetrating network
IR	infrared (spectroscopy)
kDa	kilo Dalton
kN	kilo Newton
kP	kilo pascal
kV	kilovolt
L929	mouse fibroblasts
M	molar
MEA	β-mercaptoethylamine

mg	milligram
MHz	megahertz
min	minute
ml	milliliter
mm	millimeter
mm^2	square millimeter
mmol	millimole
mol	mole, amount of substance
MPa	mega pascal
MPC	magnesium phosphate cements
ms	milliseconds
MTS	3-(4,5-dimethylthiazol-2-yl)-5-(3-carboxymethoxyphenyl)-2-(4-sulfophenyl)-2H-tetrazolium
MTT	3-(4,5-dimethylthiazol-2-yl)-2,5-diphenyltetrazolium bromide
n	sample size
N	Newton
NCO	isocyanate
NCO-sP(EO-*ran*-PO)	star-shaped random copolymer with 80% ethylene oxide and 20% propylene oxide and isocyanate groups at the end of the polymer chains
NCO-sP(EO-*stat*-PO)	star-shaped statistical copolymer with 80% ethylene oxide and 20% propylene oxide and isocyanate groups at the end of the polymer chains
ng	nanogram
NHS	N-hydroxysuccinimide
nm	nanometer
P(LLA-CL)	poly(L-lactic acid)-*co*-poly(ε-caprolactone)
PAA	poly(acrylic acid)
PBS	phosphate buffered saline
PC	polymer concrete
PCC	polymer cement concrete
PCL	poly(ε-caprolactone)
PCLEEP	poly(ε-caprolactone-*co*-ethyl ethylene phosphate)
PCM	polymer cement mortar
PDF	powder diffraction file
PDO	polydioxanone
PE	polyethylene
PEG / PEO	poly(ethylene glycol) / polyethylene oxide
PEGDMA	polyethylene glycol dimethacrylate
PET	poly(ethylene terephthalate)
pg	picogram
PGA	poly(glycolic acid)
PIC	polymer-impregnated concrete
PIM	polymer-impregnated mortar
PLA	poly(lactic acid)
PLGA	poly(D,L-lactide-*co*-glycolide)

PLLA	poly(L-lactic acid)
PLR	powder-to-liquid ratio
PM	polymer mortar
PMC	polymer-modified concrete
PMM	polymer-modified mortar
PMMA	poly(methyl methacrylate)
PP	polypropylene
PS	poylstyrene
PU	polyurethane
PVA	polyvinyl alcohol
PVC	polyvinyl chloride
QCM	quartz crystal microbalance
®	registered (USA)
RGD	arginylglycylaspartic acid, short peptide sequence which can be found in matrix proteins, e.g. fibronectin
RLU	relative light units
rpm	rounds per minute
RPMI	Roswell Park Memorial Institute medium
s	second
SA	streptavidin
SAM	self-assembled monolayer
SaOS-2	Sarcoma osteogenic cell line derived from primary osteosarcoma with osteoblastic features
SAW	surface acoustic wave
SBF	simulated body fluid
SEM	scanning electron microscopy
SGEFYFDLRLKGDK-Cys(2-thiopyiridine)	serine-glycine-glutamic acid-phenylalanine-tyrosine-phenylalanine-aspartic acid-leucine-arginine-leucine-lysine-glycine-aspartic acid-lysine-cysteine-2-thiopyridine
SGRGDS	serine-glycine-arginine-glycine-aspartic acid-serine
SGRGDSC-thiopyridine	serine-glycine-arginine-glycine-aspartic acid-serine-cysteine-2-thiopyridine
SIM	structured illumination microscopy
SPR	surface plasmon resonance
TAN	tetra-hydroperfluorooctyl acrylate
TBO	Toluidine Blue O
TCEP	*tris*(2-carboxy-ethyl)phosphine
TCP	tricalcium phosphate
TE	tissue engineering
TEM	transmission electron microscopy
TEMED	N,N,N',N'-tetramethylethylenediamine
TFA	trifluoroacetic acid
THF	tetrahydrofuran
™	trademark
TNC-scTNF (143N/145R)	human trimeric fusion protein from tenascin C and single chain TNF with changed amino acids in position 143 and 145

TNC-scTNF(mu) (221N/223R)	murine trimeric fusion protein from tenascin C and single chain TNF with changed amino acids in position 221 and 223
TNF	tumor necrosis factor
TNFR	tumor necrosis factor receptor
ToF-SIMS	time-of-flight secondary ion mass spectrometry
vs.	versus, means: in comparison to
WST-1	water-soluble tetrazolium salt
wt%	weight percent
XPS	x-ray photoelectron spectroscopy
XRD	x-ray diffractometry
α-TCP	alpha tricalcium phosphate
β-TCP	beta tricalcium phosphate

1 Scope and structure of the thesis

Scope and structure of the thesis

In the last 3 decades, various definitions of the word “biomaterials” arose and were modified during these years.[1-2] In 2007, biomaterials were specified as “*any materials used to make devices to replace a part or a function of the body in a safe, reliable, economic, and physiologically acceptable manner*”.[3] Ten years ago, a redefinition was set by Williams: ‘‘*A biomaterial is a substance that has been engineered to take a form which, alone or as part of a complex system, is used to direct, by control of interactions with components of living systems, the course of any therapeutic or diagnostic procedure, in human or veterinary medicine*.’’[4]

These definitions are differently phrased, but all show the same background of considering this topic. In general, it is difficult to find a universal definition due to the variety of materials, applications and current state of research. To use a biomaterial successfully in the human body, three conditions have to be fulfilled according to Park and Lakes: biocompatibility, a defined state of health of the host organisms and an experienced surgeon for monitoring the process of implantation.[3] The use of the word “biocompatibility” demands from a biomaterial to be non-toxic or not to injure biological tissue and at the same time, an interaction between the host and the material itself is necessary. Therefore, biocompatibility was defined by Williams as “*the ability of a biomaterial to perform its desired function with respect to a medical therapy, without eliciting any undesirable local or systemic effects in the recipient or beneficiary of that therapy, but generating the most appropriate beneficial cellular or tissue response in that specific situation, and optimizing the clinically relevant performance of that therapy*.”[5] Here, it was described as characteristic of a whole system and not of the single material components.[6]

The use of biomaterials ranges from restorage to enhancement of damaged or ill tissues; biomaterials can serve as replacement or regeneration device.[7] Here, it is crucial to consider the initial immune response of the hosting body. After implantation of a biomaterial, a foreign body reaction may occur leading to a rejection of the implant or to a severe inflammation process due to the implanted biomaterial[8] as shown in **Figure 1**.

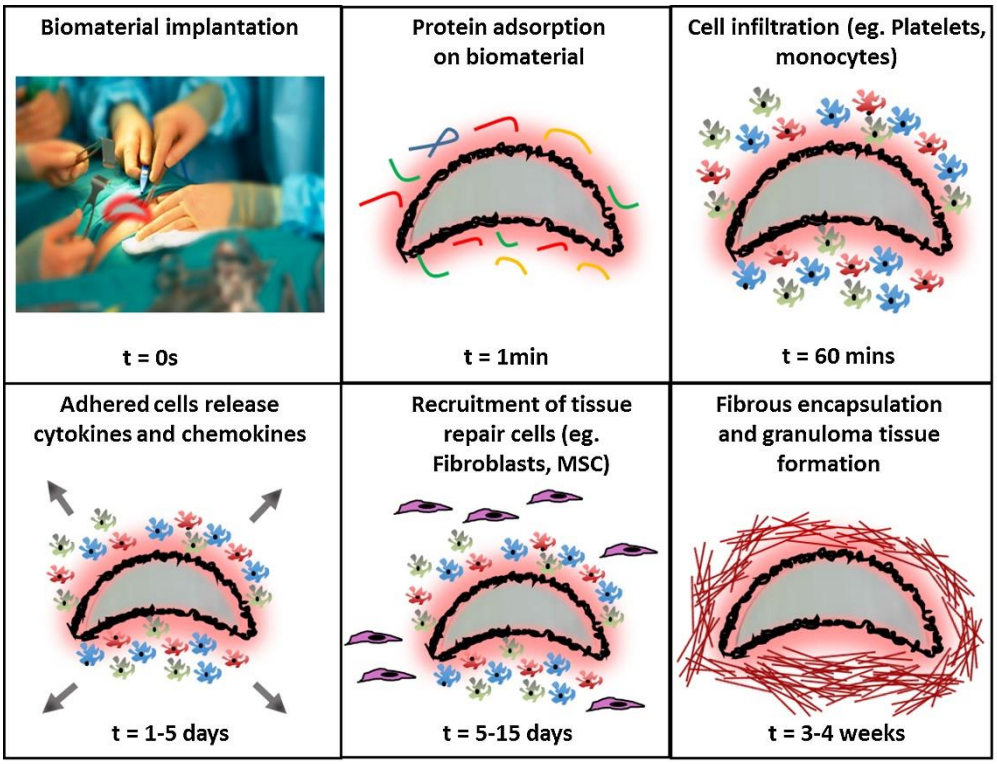

Figure 1: Innate immune response after biomaterial implantation. (Reprinted from [7]. Copyright (2015) with permission from Elsevier)

First, biomolecules such as proteins adsorb non-specifically on the surface of biomaterials within minutes recruiting cells which are able to bind via hydrophobic and electrostatic interactions. The release of cyto- and chemokines leads to further cell attraction of the innate immune system followed by collagen deposition and encapsulation after a timeframe of weeks.[9]

Focusing on the use of polymers as biomaterials, many types have been applied for medical applications and tissue engineering (TE) in literature until now.[10] Both natural and synthetic polymers were examined in detail.

For example, collagen as compound of the connective tissue was used for chondrocyte transplantation in terms of sponges[11] or hydrogels.[12] Chitosan was applied for wound healing or drug delivery,[13] whereas fibrin could serve as material for cartilage[14] or cardiac muscle regeneration.[15] Hyaluronan from hyaluronic acid (HyA) as non-sulfated glycosaminoglycan was found to be suitable for biomaterial applications as scaffold for skin and soft tissue replacement.[16] In general, these natural materials were mainly used because of their high biocompatibility and the absence of the above mentioned severe inflammation reactions.

Regarding synthetic polymers, polyethylene (PE), e.g. as hip implant,[17] poly(methyl methacrylate) (PMMA) for producing intraocular lenses,[18] contact lenses,[19] or bone cements,[20] poly(ε-caprolactone) (PCL) for example for chondrocyte cultivation,[21] polyurethane (PU) as porous structure for soft tissue,[22] and poly(lactic acid) (PLA) as surgical implant material and for drug delivery[23] are the most examined in literature. An advantage of synthetic polymers like PLA, PCL and PU is the degradability with controlled degradation rates.

Bioceramics based on calcium phosphate chemistry are suitable biomaterials for the application as bone replacement materials. Although they show brittle properties with high compressive strength, they could support new bone formation because of their chemical similarity to the inorganic component of bone tissue.[24] Here, hydroxyapatite (HA) and tricalcium phosphate (TCP) are the most prominent examples whereas HA shows a lower resorbability compared to TCP which is completely transformed into bone tissue after 3-9 months.[25-26] Both materials were shown to be osteoconductive[27] and augment each other regarding their advantageous properties by using biphasic calcium phosphate ceramics. By tuning the ratio of the components, materials were enhanced regarding their mechanical properties (higher HA content) or better degradability and ion release (more TCP).[28-29]

For the development of novel biomaterials, calcium and magnesium phosphate cements (CPCs, MPCs) play a significant role. For example, CPCs were used for orthopedic applications,[30-31] and for substitution of bone.[32-34] Furthermore, they were introduced as scaffold for drug delivery[35-36] or for replacement of complex bone defects[37-38] fabricated via the method of three-dimensional (3D) printing.[39] MPCs were developed to achieve an alternative to CPCs which show higher dissolution rates and faster bone remodeling.[40] Therefore, MPCs were also used mainly for hard tissue engineering, e.g. bone regeneration[41-42], and for dental treatments[43-44] showing antimicrobial properties.

Nowadays, the development of biomaterials is mainly focused on using composites rather than monolithic material approaches to adjust both mechanical and biological material properties to the respective application site. This applies for both the modification of the material surface to alter the biological response as well as the bulk for adaption of the mechanical performance. Such modifications often require the use of functional molecules, which are able to bind to the material and in addition offer

further reaction sites. A prominent example of such a molecule is the star-shaped prepolymer NCO-sP(EO-*stat*-PO), which was initially used as coating material as alternative to linear polymer chains to achieve surfaces repelling protein adsorption.[45] Previously, NCO-sP(EO-*stat*-PO) was applied to modify the surface of electrospun poly(D,L-lactide-*co*-glycolide) (PLGA) fibers[46] and was also introduced as a hydrogel phase in self-setting cement formulations.[47]

The **aim of this thesis** was to exploit and broaden the use of NCO-sP(EO-*stat*-PO) as reactive additive in various applications such as electrospun meshes and bone adhesive modification and to investigate these functionalizations in detail. These studies may contribute to the further development of innovative biomaterials.

Chapter 2 is dedicated to an overview of the state of the art and is divided into three parts reflecting the separation of three topics of this thesis described in the chapters 3-6. The first section focuses on the most relevant material approaches using NCO-sP(EO-*stat*-PO) for inorganic issues, additionally bone adhesives were described including their clinical requirements. In the second section, a summary of the literature background of the previous use of NCO-sP(EO-*stat*-PO) as coating material and electrospinning additive is given. Furthermore, the multimodal functionalization possibilities of NCO-sP(EO-*stat*-PO) modified electrospun fibers are described. In the last part, a literature review about quantification of molecules present on electrospun scaffolds is provided.

In **Chapter 3,** a reactive ceramic system is introduced consisting of tricalcium phosphate and star-shaped molecules with three polymer arms bearing isocyanates at the end of the polymeric chains. This system was examined in detail regarding the mechanical properties, composition and morphology.

Chapter 4 describes the development of a bone adhesive by using a common UV-curing system known from dental applications and the modification with six-armed NCO-sP(EO-*stat*-PO) to enhance the bonding strength on bovine bone. Here, especially the cytocompatibility and influence of the components on the mechanical properties were examined.

Chapter 5 addresses the fabrication of electrospun fibers and their application for fluorescent labeling and as immobilization tool for proteins and antibodies exploiting the NCO-sP(EO-*stat*-PO) macromers present on the surface of freshly electrospun

fibers. Binding capacities of electrospun meshes and cellular responses on antibodies immobilized on RGD-modified meshes were investigated.

In **Chapter 6**, new quantification methods of biomolecules immobilized on electrospun fibers are introduced. Here, a microscopic analysis approach was tested for quantification and an established method of quantifying RGD molecules was applied to other scales and used for collagen sequences to prove the reliability and applicability of the method.

Chapter 7 gives a summary of this thesis and an outlook on future approaches.

2 Theoretical background

2.1 Enhancement of mineral biocements by polymers

Mineral cements for both civil engineering and biomedical applications are usually brittle materials due to their ceramic character. While the chemistry of technical cements is based on the setting of calcium silicate and calcium aluminate compounds,[48-50] mineral biocements are commonly composed of calcium[51-52] and magnesium phosphates.[53] The setting reaction of such cements occurs by a dissolution-reprecipitation reaction, in which the raw powders dissolve and a less soluble, often hydrated mineral phase is precipitated. In the limited volume of the cement paste, the precipitates form an entangled network which finally leads to a hardening of the paste. A reduction of cement brittleness can be achieved by either fiber reinforcement strategies[54-56] or by creating cement-polymer composites.

A classification of the latter composites was already done in 1976 by Manson[57] for civil engineering cements and mentioned again by Ohama[58] determining the subsequent names:

- Polymer-modified (or cement) mortar (PMM or PCM) and concrete (PMC or PCC)
- Polymer mortar (PM) and concrete (PC)
- Polymer-impregnated mortar (PIM) and concrete (PIC)

The modification of mortar and concrete with polymers as cement hydrate binder and plasticizer is known since decades to improve several properties like fracture toughness, impermeability, durability, bonding strength,[59] water retention, and rheology,[60] since polymers are able to intercalate between cement particles which might lead to a more free flowing paste.[61] While non-modified cements and concretes exhibit several drawbacks such as low chemical resistance, marginal tensile strength and large drying shrinkage, these properties could be augmented by building of a polymer film or a redispersion during hardening.[62] Also microcracks could be bridged by forming polymer membranes.[63] These prerequisites qualify the material for application in building pavements and bridges, and as anticorrosive or decorative coatings.[64] In general, PMMs exceed the conventional mortars regarding their properties and therefore are used as render, masonry mortar or tile adhesive.[65]

Until now, various additives were used such as polymer latexes, redispersible polymer powders,[66] polymers with water-soluble properties (e.g., cellulose derivatives, polyvinyl alcohol), liquid resins or also *in situ* polymerizable monomers.[58] Additionally,

fiber-reinforced polymers (FRP) were applied for strengthening or rehabilitation of concrete structures.[67-69] For example, Nguyen et al. examined the addition of water-soluble polymers, in this case cellulose ether (CE). This led to delayed cement hydration and enhanced microstructural properties because of entrapped air causing an altered pore structure and a more homogeneous surface by migration of the polymer into the mortar. Mechanical and rheological properties were improved as well by building complex chemical interactions and by decrease of viscosity.[65] Another approach by Aggarwal et al. introduced epoxy-functionalized emulsions and compared them with acrylic modified mortar.[64] The authors found that the novel system showed better mechanical properties concerning flexural and compressive strength, and it could resist to water absorption and chloride ion penetration. A relatively new approach by Han et al[70] presented smart concretes as intelligent materials which could reply to an external stimulus such as mechanical stress or temperature changes additional to their self-healing character.

In contrast to civil engineering, the improvement of the mechanical properties of mineral biocements by polymer addition is much less explored. Approaches to reduce biocement brittleness include the incorporation of Ca^{2+} chelating reagents, e.g. polyacrylic acid,[71-72] gellan gum for calcium binding and hydrogel formation,[73] or swellable polymer additives which can be added as water-soluble monomers to the cement's liquid and then subsequently polymerized during cement setting.[74-75] The latter mechanism is usually termed as dual-setting cement, whereby the advantage compared to a direct addition of polymers lies in practically not altered rheological properties and a strong increase of the work of fracture after setting. As example for an organic polymer, Christel et al. used alpha tricalcium phosphate (α-TCP) together with 2-hydroxyethylmethacrylate (HEMA) as water soluble monomer, which was polymerized during setting by a system of N,N,N',N'-tetramethylethylenediamine (TEMED) and ammonium persulfate (APS).[76] By addition of various HEMA amounts, the setting time could be accelerated and a 4-point bending test revealed an increase of the bending strength from 9 to 14 MPa. Another approach was the application of ammonium acrylate for α-TCP cements to enhance their compressive and tensile strength. Here, an increase from 23 to 55 MPa and 12.5 to 21.2 MPa for tensile testing was demonstrated after storage in simulated body fluid (SBF) for 7 d.[77] Later, the diametral tensile strength was tested as well for different acrylates and N-vinyl-2-pyrrolidone to create a dual-setting cement.[78] A different chemical approach was

applied by Schamel et al.[47] who used NCO-sP(EO-*stat*-PO) in α-TCP cement for the fabrication of highly mineralized and mechanically strong hydrogels. NCO-sP(EO-*stat*-PO) forms a polyurethane matrix after partial hydrolysis of isocyanates, which afterwards is mineralized with nanosized hydroxyapatite crystals formed by α-TCP hydrolysis. Although the approach was successful, the large size of NCO-sP(EO-*stat*-PO) with only 2 % of isocyanate moieties is a limiting parameter for a further increase of the mechanical properties.

2.2 Material approaches for bone adhesives

While the previously mentioned mineral bone cements are used for filling larger sized bone defects, they have usually no adhesion to the bone matrix and hence, they are unsuitable to fix small bone fragments. Here, other sufficient surgical methods like nailing and plate osteosynthesis are needed for refixation.[79-80] However, the use of rigid plates on the one side and compression plates, which allow motion for bending, torsion and shear, on the other side might lead to problems such as restricting usual bone physiology or inadequate mechanical fixation.[81] Nevertheless, in literature, studies exist investigating the use of micro- or miniplates for osteosynthesis applications.[82-84] Furthermore, surgeons are able to decide between minimal invasive plate application and open reduction internal fixation.[85-86]

For the treatment of fractures in aesthetically challenging areas like the midface, which have a fragment size of about 1 cm, conventional metal plates, nails, pins and screws are available at present. However, by these general methods, it is difficult to fix smaller bone pieces, thus alternative fixation techniques are needed , e.g. *in situ* crosslinkable bone adhesives.[87-88] Such a bone glue would be advantageous for a consistent planar force distribution with an enhanced load transfer between the fracture surfaces.[89] A principle prerequisite for such adhesives from a clinical perspective (**Table 1**) is a sustained adhesion during the healing period while supporting bone tissue regeneration and a sufficient bonding to wet bone surfaces, because it is highly demanding to fix bone when the fracture surface is wet or even contaminated, e.g. by blood or fat. Existing systems in clinical use like BioGlue®, which contains glutaraldehyde,[90-91] show good adhesion properties but are cytotoxic,[92] and the adhesion decays rapidly in aqueous environment. Further demands are the cytocompatibility of both the adhesive and degradation products without any immune response applied to bone cells and an easy and suitable application regime for the surgeon.[87, 93] For a possible clinical application, only a short-time fixation of bone fragments is needed bearing moderate mechanical loads, since the adhered pieces will be further fixed to intact bone structures by plates and screws. Furthermore, the distortion of innate fracture healing should be avoided, thus an appropriate degradation time of several weeks to months is demanded for the adhesives without building a barrier for newly forming bone.[88, 94]

Table 1: Properties for a successful bone adhesive. (Reprinted from [87]. Copyright (2012) with permission from Elsevier)

Preferred properties
▪ high level of adhesion to bone, often in presence of contaminants such as fats, proteins, etc.
▪ bonds to wet surfaces / bond strength stable in wet environment
▪ mechanical stability under tension, compression, shear
▪ easy and quick to prepare and apply in operating room conditions
▪ adequate working time for the surgeon to apply and form bond
▪ rapid setting time (typically 1-10 min)
▪ low exotherm on setting → no thermal necrosis
▪ non-toxic and biocompatible including leachables, degradation products, etc.
▪ allows healing of the fracture
▪ sterilizable
▪ adequate shelf-life
▪ cost effective to use
▪ commercially viable to manufacture
Desirable properties
▪ adhesion to surgical alloys
▪ biodegradable in a controlled manner and timescale
▪ no special storage conditions and stable at room temperature
▪ ability to deliver drugs or bioactive agents, e.g. for stimulation of bone healing, prevention of infection, etc.

Material approaches for bone adhesives can be divided into biological / natural or synthetic inspired types. As described in literature, synthetic materials which for example are formed *in situ* by chemical crosslinking often show better bonding abilities in comparison to biological ones. Otherwise, natural components could lead to an improved biocompatibility and degradation.[87, 95]

2.2.1 Natural adhesives

Regarding biological derived glues, fibrin adhesives are the most extensively examined materials. A drawback of natural glues are their low mechanical properties and adhesion[93] and the fast degradation which might be too short for an application on bone.[88] Therefore, biological adhesives are mainly examined concerning the use for soft tissue adhesion and sealing.[87]

As example, Song et al. used a commercially available fibrin glue (Tisseel®) for a special fracture occurring in the anterior wall of the maxillary sinus after trauma like car accidents.[96] They achieved a grafting of bone fragments and could decrease shearing stress by adjacent tissue. Another application field of the fibrin glue is the fixation of an implant applied to the medial wall or orbital floor of the eye which areas are consisting of very thin bones.[97] Furthermore, a biomaterial called Greenplast composed of human fibrinogen and thrombin was investigated for comminuted nasal bone fractures by Jeong et al.[98] Earlier publications dealt with the use of fibrin adhesives on bovine femur[99] and porcine fibula,[100] but with very low adhesion strengths to bone and without proper storage. The benefit of fibrin glue is restricted to the use as operative sealant[101] or in non-load bearing areas.[102]

Other natural derived materials for adhesive applications are mussel proteins which are adhesive due to the presence of 3,4-dihydroxy-L-phenylalanine (DOPA). Ho and Ding reviewed about recent findings about this adhesive mussel-inspired polydopamine regarding the preparation and application.[103] This material was often used in literature as adhesive coating of biomaterials, for example by Madhurakkat Perikamana et al. for graded functionalization of different substrates and immobilization of biomolecules on the adhesive polydopamine layer.[104] The same group examined the coupling of DOPA to poly(ethylene glycol) (PEG) in hydrogels which led to a minimal inflammatory response. However, it was shown that these hydrogels only could be exploited as soft tissue adhesive.[105] Similar to this adhesive is “sandcastle glue” adapted from a marine worm, which was tested as glue material on wet bovine femur bone applied for 24 h by Shao et al.[106] and in a rat model by Winslow et al.[107]

Another approach is the use of biocompatible and degradable polysaccharides like chitosan and dextran.[108] Again, as additive, DOPA was conjugated to the biopolymer. This system revealed a higher adhesive strength than fibrin glue tested by tear-off measurements on bovine bone in wet environment, but with a limited storage time of only 3 h, and showed a good biocompatibility in cell tests with MC3T3 mouse fibroblasts. Newest findings compared DOPA together with styrene in a biomimetic co-polymer. By lap shear bonding tests, this group could achieve adhesion strengths, which were similar to a commercially available ethyl cyanoacrylate.[109]

However, natural materials often show disadvantages because of possible immunogenic reactions and high costs for extracting proteins from their host organisms.[104, 110]

2.2.2 Synthetic adhesives

A first example for synthetic-derived bone adhesives are cyanoacrylates, which provide high adhesion strengths and fast hardening, but are at the same time known to be toxic for cells and tissue.[111-113] Ethyl, iso- and n-butyl cyanoacrylates were examined in different tests on bovine or porcine bone with an achieved adhesive strength ranging from 0.5 to 12 MPa without and with storage in water at 37°C.[99, 114] Commonly, cyanoacrylates with shorter alkyl chains showed a significantly higher bonding strength;[115] however, compounds with butyl or octyl chains seemed to have a decreased adhesive toxicity.[116-117] Nevertheless, cyanoacrylates are subject of current research because of the enormous adhesion strength to bone as shown by Sohn et al.[118] who compared commercially available short- and long-chain cyanoacrylates regarding their toxicity and effect on bone development. Hochuli-Vieira et al. studied fixation of bone grafts using commercially available *n*-butyl-cyanoacrylate (Histoacryl® and Tissuacryl®) in comparison to titanium screws and could reveal that in general, the adhesives are comparable to titanium screws regarding the examined inflammation processes in rabbits.[119]

Methacrylate monomers which polymerize to poly(methyl methacrylate) (PMMA) are often used for hip replacement or knee arthroplasty. As adhesive, PMMA seems to be inappropriate for bone adhesion at first sight because the material itself is not very adhesive and shows different wetting properties in comparison to the bone surface.[120] This is why an additional amphiphilic bonding agent is needed which could also increase the bonding strength to bone surfaces from 0.2 to 8 MPa as described by Smeets et al.[121-122]. Additionally, a pretreatment of the osseous surface with bonding material or etching using weak acids such as citric or phosphoric acid improves the adhesiveness of PMMA.[123] Another enhancement is the addition of 4-methacryloyloxyethyl trimellitate anhydride (4-META) proved by measuring of bone adhesion via a tensile test.[124] Nevertheless, PMMA needs supplemental agents as shown by Jiang et al., who used PMMA together with mineralized collagen. These

adhesives demonstrated defined compressive strengths and good cytocompatibility of pre-osteoblasts, whereas injectability and process time remained the same.[125]

For preparation of glass ionomer cements, a polymeric acid, for example poly(acrylic acid), is bound via ionic interaction to metal ions like zinc or aluminum ions present in bioactive glass.[87] Brauer et al. used these zinc containing glass ionomer cements and could determine a higher adhesion strength than evaluated for cements without zinc addition. However, the authors discovered an acute cytotoxicity *in vitro*.[126] Latest research dealt with injectable cements consisting of bioactive borate glass particles and a chitosan bonding solution. Here, an increased compressive strength and a proper bone formation in a rabbit model could be achieved.[127]

Due to their similarity to the composition of mineralized bone, magnesium and calcium phosphate cements are common materials for bone substitution materials. Several publications exist about CPCs dealing with their brittle behavior and possible enhancements to alter their properties for application as bone cements.[32, 55, 128-129] An improvement is depicted for example by polymer-modification with poly(propylene glycol-*co*-lactide) dimethacrylate as shown by Abou Neel et al.[130] Here, the flexural strength was measured revealing an alteration from brittle to flexible behavior of the modified CPC. Furthermore, they showed an immediate bone fixation being beneficial for an early support of bone fractures. Another approach for enhancement of adhesion ability of calcium phosphates was introduced by Grover et al. by incorporating pyrophosphoric acid into a brushite cement. The authors showed adhesive tensile strengths on different surfaces, e.g. on cortical ovine bone and could achieve a tensile adhesion up to 1.3 MPa.[131]

In comparison to CPC, magnesium phosphate cements reveal some advantages such as a more rapid setting time, enhanced mechanical properties and a good biocompatibility *in vitro* and degradability *in vivo*.[40, 132-133] MPCs were evaluated by Yu et al.[132] regarding their toxicology and biocompatibility which are prerequisites for their use as bone adhesives as mentioned above. Gulotta et al. tested the tendon-to-bone interaction *in vivo* using the commercially available magnesium phosphate Osteocrete® in a rabbit animal model and could find an improvement in healing after 6 weeks.[134] Although magnesium phosphate cements are thought to represent the better bone adhesives,[87] studies revealing an appropriate testing regime of bonding strength are still missing for MPCs.

In situ crosslinking polyurethanes are also promising materials for bone adhesives because of their ability to react with water, amines, and alcohols during the interaction.[135-136] For example, the FDA approved castor oil Kryptonite™, which consists of oil based polyols, reactive isocyanate groups and a calcium carbonate filler, was investigated by Fedak et al.[137-139] Here, the conventional method of wire closure in human patients was enhanced by the use of Kryptonite™. The support by the wire is needed for several hours until adhesion of the material with the bone which was analyzed by mechanical testing with various loads.[137] As revealed in current studies, highly porous polyurethane foams used together with polyols for crosslinking and hydroxyapatite (HA) crystals were investigated regarding their mechanical properties like shear, compressive and tensile strength. For example, Schreader et al. used PU reinforced with 1% HA and could reveal an enhanced adhesion on treated or untreated bone surfaces in comparison to a commercially available acrylic bone cement. The authors further demonstrated that these HA-modified polyurethane foams were biocompatible *in vitro* and *in vivo*.[140] Sahan et al. also used castor oil based polyurethanes together with beta tricalcium phosphate (β-TCP) filler showing a Young's modulus around 44 MPa, such that these materials were proposed for load-bearing defects.[141]

2.3 Advancement of organic biomaterials

During the last 50 years of biomaterials research, a huge variety of materials for biomedical applications were developed. These materials can be distinguished in three different generations: bioinert materials, which lead to no or only marginal tissue response (first generation); bioactive and biodegradable materials, which are able to interact with the biological environment (second generation); and materials which could lead to an interaction with the host and an enhanced formation of new tissue materials (third generation).[28, 30] In literature, various compounds were used until now: polymers which could be inert or resorbable, metals which are usually inert (except magnesium alloys),[142] and ceramics and composites which show inert, active or degradable properties.

Recently, a fourth generation of biomaterials has appeared: the so-called smart or biomimetic materials. The purpose was to create biomimetic constructs to imitate hierarchical structures, for example the extracellular matrix, achieving a certain degree of complexity. It is important to change from a static replacing implant to a bioactive material which interacts with the body with the purpose to build new tissue or to regenerate tissue functions.[143]

A possible approach to create such a biomimetic organic material is described in this section. As mentioned in **chapter 1**, among others, the development of biocompatible biomaterials challenges scientists to avoid the rejection of implants *in vivo*. For this purpose, the control of unspecific protein adsorption on the surfaces has a tremendous influence on the compatibility of biomaterials.[144] To create a new type of material, the surface could be functionalized to protect it from the reactions of the host, because the surface chemistry and microstructure both influence protein adsorption and therefore cell adherence.[8] This can be achieved by introducing hydrophilic groups on the materials surface, e.g. poly(ethylene glycol) as previously examined in detail.[145-149] Together with its hydrophilic character, PEG is biocompatible and withstands unspecific protein adsorption, resulting in non-fouling surfaces.[150] To achieve a higher density of functional groups on surfaces of biomaterials, alterations in the molecular architectures of the PEG molecules could enhance the properties of resisting protein immobilization which was shown by Gasteier et al. The authors used six-armed star-shaped PEG-based molecules for coating surfaces and observed an even better

reduction of protein adsorption on such modified surfaces compared to linear PEG molecules.[45]

On the other side, biomaterials transferred into the body should be able to interact with the surrounding cells allowing regeneration and formation of new tissue.[151] Therefore, a specific immobilization of bioactive molecules is necessary to induce desired biological processes by tuning the surface specifically for cell adhesion, as mentioned by Ratner and Bryant.[8] This was realized by incorporating or immobilizing of short peptide sequences or even whole proteins on biomaterials' surfaces.[152] The peptide sequence RGD is likely the most investigated biomolecule and can be found in matrix proteins such as fibrinogen, laminin and collagen.[153] In literature, this cell-mediating sequence was used in combination with non-fouling PEG as demonstrated by VandeVondele et al.[154] and also applied together with star-shaped PEG-based polymers as a subsequent biofunctionalization after the coating process. This method of creating an RGD-modified star PEG layer was demonstrated to be beneficial for several applications like the culture of mesenchymal progenitor cells[155] or HaCaT keratinocytes.[156] In addition, this peptide modification could be also used for advanced structures such as electrospun fibers.[157]

Aside from that, the microarchitecture of surfaces plays a significant role for protein and cell adhesion on surfaces. For example, a porous structure enables vascularization and supply with nutrients and oxygen which is useful for cell migration and ingrowth.[158] This could be realized by building 3D structures from synthetic materials and providing them with biological anchor points for specific cell adhesion.[159] *In vivo*, cells are usually surrounded by the extracellular matrix (ECM), a fibrillar structure composed of collagen and elastin, which contains different biomacromolecules such as proteoglycans and glycosaminoglycans. Furthermore, adhesion sites for interaction with cells can be found which results in various cell-ECM interactions.[160] Via mimicking these ECM structures by means of electrospun polymeric fibers with immobilized biological anchor points for cells, it is possible to create 3D structures which are found to be suitable for many applications in tissue engineering and regenerative medicine.[161]

Another important point is the immune response of the human body when biomaterials are implanted. Detrimental inflammations could occur which lead to fibrosis, encapsulation of the material and finally rejection or accelerated degradation.[162]

Therefore, it would be beneficial to develop materials which can act immunomodulating because of their non-fouling, ECM-mimicking and bioactive properties.[163] A solution might be for example the delivery of pharmacological anti-inflammatory molecules from materials such as hydrogels.[164]

The possible improvements mentioned above were addressed in the following chapters of these thesis. First, the method of solution electrospinning is described.

2.3.1 Solution electrospinning

Besides electrospraying, the method of electrospinning belongs to the electro-hydrodynamic fabrication methods, where the dynamics of electrically charged fluids are exploited.[165] The process of solution electrospinning achieved its patenting already in 1934 by Formhals,[166] but did not gain attention for biomedical applications until in the 1990s and early 2000s. Then, Reneker and co-workers examined electrospinning and its parameter in detail regarding influences on the process and various morphologies.[167-171]

Electrospinning is depicted as easy and versatile method to produce fiber meshes with diameters in the micro- to nanometer range. These fibers could be used for example as scaffolds for tissue engineering applications[172-173] including cartilage,[174] bone,[175-176] skin[177-178] and cardiovascular tissues.[179-180] or for textiles,[181-182] sensing[183-184] and filtration issues.[185-187] There are many advantages, which argue for using the method for development of biomaterials, such as high porosity, large surface to volume ratio, controllable mechanical properties and easy functionalization of electrospun meshes.[188-189] Furthermore, the fibrillar structure of scaffolds show similarity to ECM structures.[190-191]

For solution electrospinning, an electrical charge is used to draw very fine fibers from a polymer solution. If a sufficiently high voltage is applied, the body of the liquid becomes charged resulting in an electrostatic repulsion. When these electrical forces exceed the surface tension of the polymer solution, a droplet is stretched out of the syringe needle and the so-called Taylor cone is built forming a charged liquid jet. The building of this Taylor cone is demonstrated in **Figure 2**.

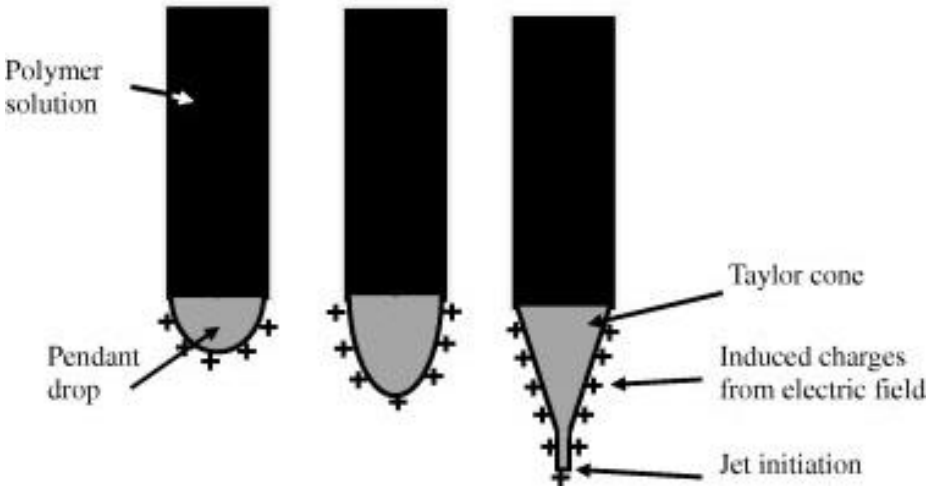

Figure 2: Schematic illustration of the Taylor cone formation from a pendent drop via elongation and deformation due to the charge-charge repulsion. (Reprinted from [192]. Copyright (2010) with permission from Elsevier)

Subsequently, the solvent evaporates, and the jet is elongated by a whipping process ("whipping instability") until it is finally deposited on a grounded collector forming an electrospun fiber mesh.[193-194] The complete process is shown in **Figure 3**.

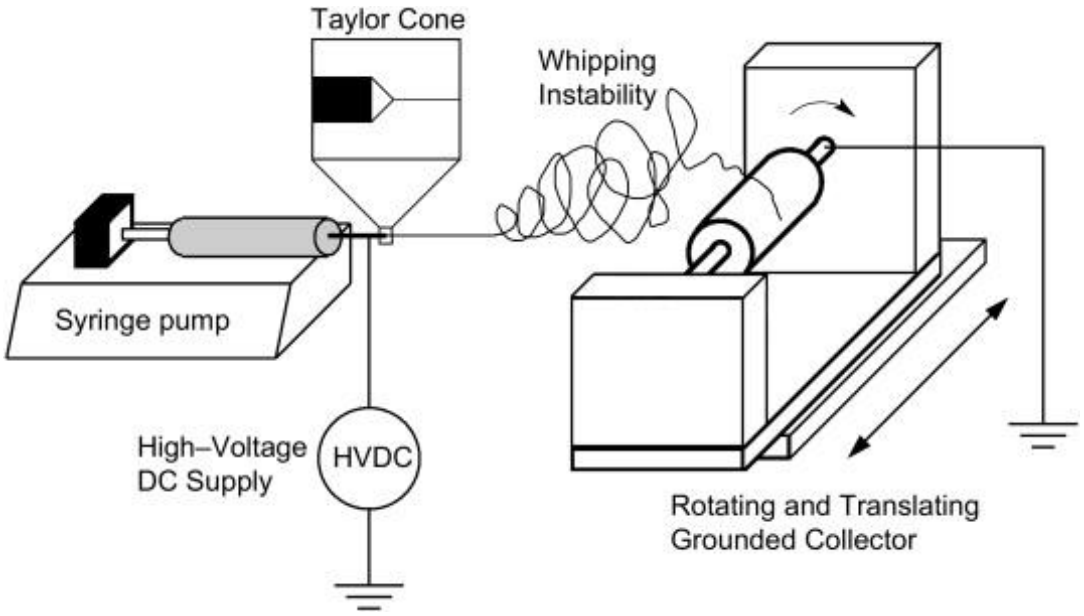

Figure 3: Typical electrospinning setup. The polymer solution is forced through a needle using a syringe pump. The high voltage injects charge of a certain polarity into the solution. If the electrostatic force created by the repulsion of similar charges is sufficient to overcome the surface tension the Taylor cone is formed, and a fiber jet is emitted. While the fiber jet is traveling toward the grounded collector it undergoes a chaotic whipping instability. The fiber jet is then deposited on the rotating collector. (Reprinted from [195]. Copyright (2008) with permission from Elsevier)

The structure of electrospun fibers is influenced both by the properties of the spinning solution (viscosity, surface tension, conductivity) but also by process parameters as applied voltage, spinneret to collector distance, flow rate as well as spinneret design and collector geometry.[195-196] Environmental influences such as air humidity, temperature and air velocity also affect electrospinning.[197-198]

2.3.1.1 Natural polymers

For fabrication of electrospun scaffolds, natural or synthetic derived polymers could be used. For spinning of natural polymers, their intrinsic biocompatibility and biofunctional motifs are both clear advantages in comparison to synthetic polymers.[199] In literature, an enormous number of studies dealt with natural polymers such as the proteins collagen[200-202] and silk fibroin[203-204] or polysaccharides like alginate,[205] hyaluronic acid[206-207] and chitosan.[208-209] Although natural polymers are appropriate for an electrospinning procedure revealing good biocompatibility, problems might occur by batch-to-batch variability and limited functionalization possibilities. Additionally, restrictions may result from the risk of immunogenicity and pathogen transfer.[178] Regarding industrial fiber production, a problem might also be the limited availability of natural materials.[210]

2.3.1.2 Synthetic polymers

In contrast, synthetic materials show a lower immunogenic risk and a better availability in huge amounts with reproducible material properties. Other advantages are the controllable structural and mechanical characteristics and the adaptable degradation properties.[178] Nevertheless, in comparison to natural polymers, the biocompatibility might be reduced because of possible residues of organic solvents or catalysts. Synthetic polymers like polyurethane (PU),[211-213] poly(ε-caprolactone) (PCL),[175, 214] polyethylene oxide (PEO),[215-216] poly(L-lactic acid) (PLLA),[217-218] poly(glycolic acid) (PGA),[219-220] and poly(D,L-lactide-*co*-glycolide) (PLGA)[221-222] are often examined for TE applications using scaffolds produced by electrospinning. Here, especially PLGA leads to fibers with proper biocompatibility and a tunable degradation rate[223] without toxicity of metabolites.[224]

Various modifications of electrospun fibers were performed, for example to incorporate drugs and other molecules. An overview is given in **Figure 4**. The first possibility is the addition of substances before the process; accordingly, bulk modification of polymers used for preparing the spinning solution is performed[225] or peptides are added directly into the electrospinning solution.[226] Another method is to functionalize the surface after the spinning procedure; this can be done by immersion of electrospun nonwovens in an aqueous solution which contains the desired molecule leading to coating of the fibers with the immobilizing agent.[46]

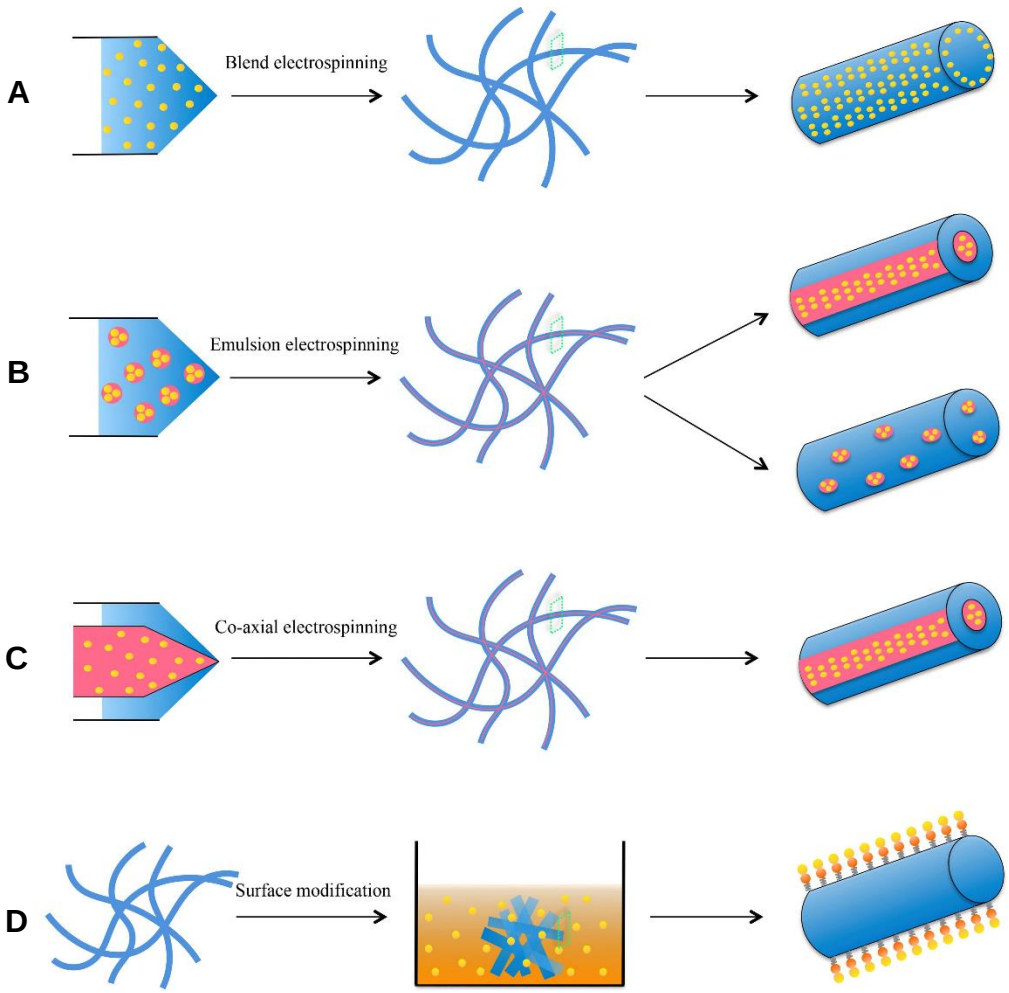

Figure 4: Schematic illustration of molecule incorporation strategies. **A**) Blend electrospinning: molecules and polymers are dissolved in solvents in order to be spun together; **B**) emulsion electrospinning: solutions are emulsified into immiscible polymer solutions, followed by spinning; **C**) co-axial electrospinning: molecule and polymer solutions are separately spun through two concentric nozzles; **D**) post-immobilization: substances are conjugated onto fabricated nanofiber matrices through physical or chemical interaction. (Reprinted from [178]. Copyright (2017) with permission from Elsevier)

2.3.2 NCO-sP(EO-*stat*-PO)

Recently, Ren et al. reviewed the use of star polymers which are composed of several linear polymer chains fixed at a core point while bearing a large number of functionalities.[227] The authors revealed several synthetic approaches and mentioned many possible applications in life sciences such as gene or drug delivery systems or for imaging issues. Star polymers can be formed as symmetric or asymmetric shapes carrying polymeric or peptide arms.[228] Beneficial in comparison to their linear analogs is the decreased arm entanglement in solution, which results in lower viscosities, and a quite low steric hindrance because of the length of the polymeric chains. Another advantage is the high reactivity due to several functional moieties.

Star polymers were previously used for surface passivation by building up thin layers[229] as shown by Groll and coworkers. Poly(ethylene glycol) is known to form a non-fouling surface where unspecific protein adsorption could be avoided. In comparison to linear PEG chains, star molecules bearing PEG groups are advantageous due to an increased amount of functional moieties per molecule.[230] Furthermore, they show a high coverage of surfaces, when prepared as a coating, and a proper localization of functional groups near the surface.[231] A prominent example is the NCO-sP(EO-*stat*-PO) prepolymer, which was used in the following chapters of this thesis (**Figure 5**).

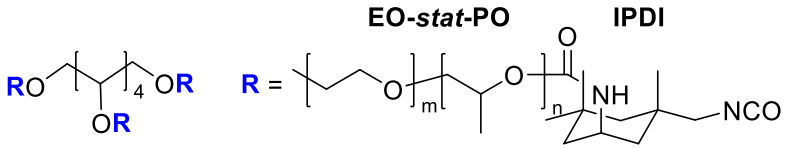

Figure 5: Chemical composition of NCO-sP(EO-*stat*-PO). The sorbitol core bears six arms with ethylene oxide and propylene oxide in a ratio of 4:1. The molecular weight of each arm is 2 kDa.

NCO-sP(EO-*stat*-PO) is a six-armed star-shaped molecule with reactive functional isocyanate groups at the end of the polymer chains. The backbone is built from a statistical copolymer of ethylene and propylene oxide in a ratio of 80% to 20%. Each arm with a molecular mass of 2 kDa is attached to a sorbitol core. As described by Götz et al.,[232] the high functionality of these prepolymers was introduced by endcapping of hydroxy functionalized poly(alkylene oxides) with isophorone

diisocyanate (IPDI) creating highly reactive polymers. These prepolymers are water-soluble and show an intermolecular crosslinking reaction in H_2O building a hydrogel (**Figure 6**).

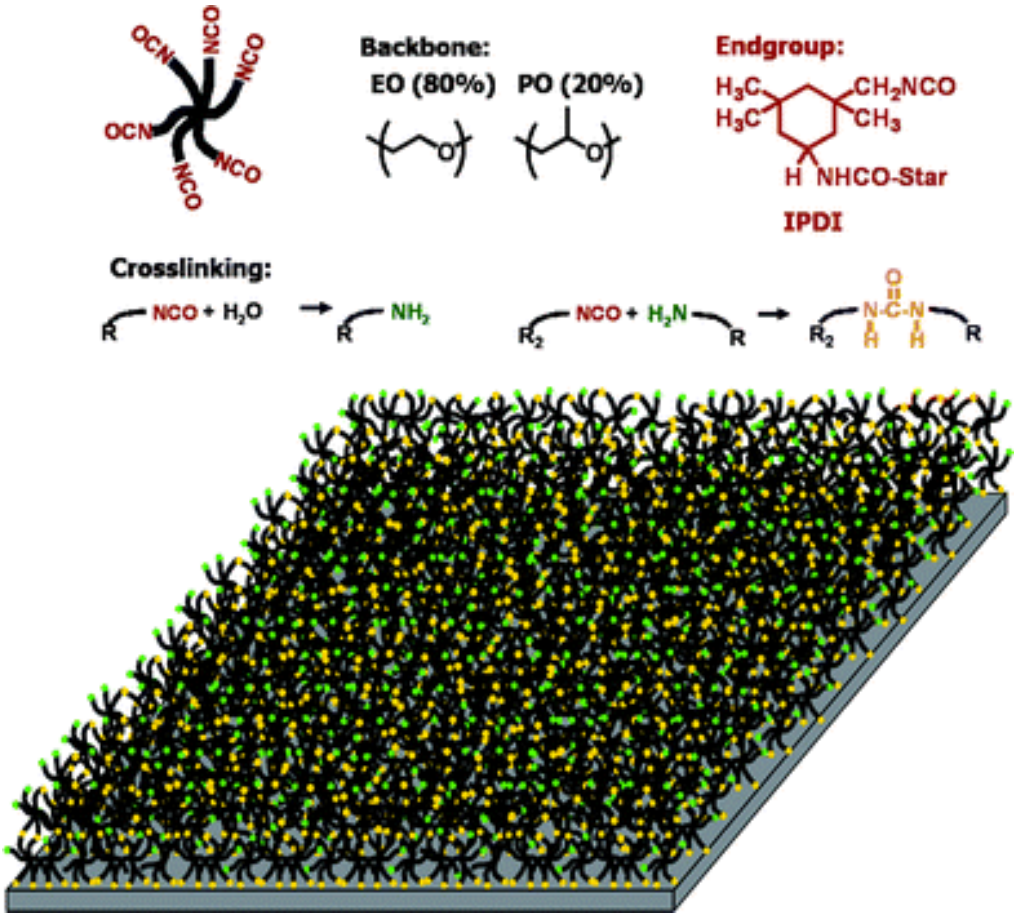

Figure 6: Scheme of chemical crosslinking of NCO-sP(EO-*stat*-PO) and surface coating with urea bridges shown in yellow and free amino groups shown in green. The crosslinked NCO-sP(EO-*stat*-PO) layer consists of a densely packed network. (Reprinted from [233] with permission of The Royal Society of Chemistry)

These resulting hydrogels were used in literature for example by Dhanasingh et al.[234] Here, a type of prepolymer with a molecular weight of 18 kDa was examined as crosslinker for hyaluronic acid hydrogels altering stability, degradability and porosity by interaction of hydroxyl groups of HyA with isocyanates of the six-armed star polymers. With this method, it was possible to create crosslinked and multi-layered hydrogels with drug releasing properties.[235] Pure hydrogels prepared from NCO-sP(EO-*ran*-PO) varying the molecular weight of macromers from 3 kDa to 18 kDa were investigated by differential scanning calorimetry (DSC) and rheological measurements by Dalton et

al.[236] Here, it was revealed that the solution ability and the quality of the formed hydrogels depended on the molecular weight of the macromers, and that by uniaxial freezing of gels, the formation of oriented pores could be achieved. This method of preparing hydrogels was applied later for a sustained drug release of the glucocorticoid dexamethasone in combination with silicone tubes for inner ear implants.[237]

2.3.2.1 Coating with NCO-sP(EO-*stat*-PO)

The crosslinking reaction according to **Figure 6** can be exploited for building up dense hydrogel layers as flat surfaces by means of the spin coating technique as demonstrated by Groll et al.[230, 238] The authors were able to show that these ultrathin coatings built by interaction between the isocyanate moieties via an urea bond were extremely resistant against unspecific protein adsorption in a biological environment and therefore, exhibited cell-repellent properties,[239] as also demonstrated extensively for linear PEG.

The preparation of thin coatings and the crosslinking reaction was visualized by Heyes et al. (**Figure 6**, lower image). By examination of several multi-arm star molecules, the researchers could reveal that NCO-sP(EO-*stat*-PO) with a molecular weight of 12 kDa led to the most resistant layers maintaining the non-fouling coating for more than 7 days at 37°C. Due to the reactivity of the isocyanate groups, it was demonstrated that several protein modifications could be performed on the surface of NCO-sP(EO-*stat*-PO) coatings such as using enzymes,[240] biotin-streptavidin,[238] or amino-reactive dyes.[241] Possible applications for these coatings were shown for antibacterial implant surfaces,[242] specific cell alignment,[243] or for quartz crystal microbalance (QCM) measurements.[244]

Another important functionalization of NCO-sP(EO-*stat*-PO) coatings is the immobilization of cell mediating peptide sequences such as RGD via exploiting the reactivity of NCO-sP(EO-*stat*-PO) towards nucleophilic groups like alcohols, amines and thiols.[245] By this modification, the properties of the surface were transformed from a cell-repellent to a specific cell-attaching character.[155] For immobilization, the desired amount of peptides was simply dissolved in the aqueous part of the spin coating solution. A terminal cysteine or lysine amino acid was found to be advantageous for a covalent binding of peptides. Furthermore, the interaction was proved by Salber et al. for several peptide sequences which appear in ECMs.[156] Cell culture of different cell

types like human fibroblasts, human mesenchymal stem cells and others was demonstrated to be successful. Fiedler et al. used coatings which were covalently functionalized with both linear and cyclic RGD to verify cell adhesion and proliferation of mesenchymal stromal cells (MSCs) and SaOS-2 cells.[246] Latest research dealt with polypropylene meshes which were functionalized with NCO-sP(EO-*stat*-PO) via plasma-introduced amino groups. After covering these meshes with additional electrospun fibers and modification with the matrix metalloproteinase inhibitor GM6001, it was found that these meshes used in a hernia model led to a partial compensation of inflammation responses in the bodies of rats.[247]

2.3.2.2 Electrospinning with NCO-sP(EO-*stat*-PO)

Besides the functionalization of flat surfaces with NCO-sP(EO-*stat*-PO), the macromers were also used as additives for solution electrospinning to create a very thin coating on the surface of electrospun fibers. This was demonstrated by Grafahrend et al.,[157] who used PLGA for solution electrospinning of thin fibers while adding NCO-sP(EO-*stat*-PO) as functional additive to the spinning solution. The additive was found to segregate to the surface during the electrospinning process being present over the entire surface area of the fibers. However, until now, it is not completely understood how the hydrophilic NCO-sP(EO-*stat*-PO) are able to accumulate at the surface of the fibers. Solvent evaporation might contribute to this phenomenon as well as electrostatic forces.[46] Electrospun fibers created with this method showed a minimized protein adsorption and cell-repellence, as demonstrated for flat surfaces. At the same time, via addition of cell-mediating peptide sequences such as RGD, a rapid and at the same time more specific biofunctionalization of the meshes was achieved by mixing these molecules into the spinning solution. A combined surface segregation of both NCO-sP(EO-*stat*-PO) and functional molecule occurred.[248]

The same effect could be demonstrated for electrospun fibers fabricated from PCL and functionalized with NCO-sP(EO-*stat*-PO) by mixing it into the spinning solution for examination of neural guidance.[249] Alternatively, it was demonstrated that coating of fibers with NCO-sP(EO-*stat*-PO) happened by incubation of electrospun fibers in an aqueous solution of the functional additive, as performed by Böhm et al..[250] They examined the behavior and biocompatibility of such meshes *in vivo.*

Table 2 gives an overview of the fabrication of electrospun fibers using NCO-sP(EO-*stat*-PO) as functional additive for immobilization with different peptide sequences and their cultivation with cells.

Table 2: Summary of literature dealing with NCO-sP(EO-*stat*-PO) as additive for solution electrospinning and corresponding biological modification.

Polymer	Peptide sequence	Functionalization	Cells	Ref.
PLGA	GRGDS, GEFYFDLRLKGDK, mixture	incubation in an aqueous peptide solution	keratinocytes	[157]
PCL	GRGDS	mixing of peptide into the spinning solution	Schwann cells	[249]
PLGA	/	incubation with an aqueous solution of NCO-sP(EO-*stat*-PO)	*in vivo* examination	[250]
PLGA	GRGDS	mixing peptide into the spinning solution	human dermal fibroblasts	[46]
PLGA	GRGDS, GLF	mixing of peptide into the spinning solution	primary human monocytes, macrophages	[251-252]
PLGA	growth factor Neuregulin-1	mixing protein into spinning solution	*in vivo* examination	[253]
PLGA	CGRGDS, CGYIGSR, CGIKVAV, CGEFYFDLRLKGDK	mixing protein into spinning solution	Co-culture of human dermal fibroblasts and HaCaT	[226]

2.3.2.3 Multimodal functionalization using NCO-sP(EO-*stat*-PO)

In 2007, Gasteier et al. reviewed the different functionalization steps which can be applied to NCO-sP(EO-*stat*-PO) layers.[45] (1) The functional prepolymers bear reactive isocyanate groups which may be modified in solution with reactive groups like thiols, amines and alcohols before the following process such as coating of flat surfaces or solution electrospinning together with a backbone polymer like PLGA. (2) After processing of NCO-sP(EO-*stat*-PO), isocyanates remain reactive on freshly prepared layers or freshly spun meshes for several minutes and can be used for an additional interaction with protic groups. (3) After the hydrolyzation of isocyanates to amines, these moieties are able to react with amino-reactive molecules. These three

functionalization steps were described in the above-mentioned literature but only in a combination of (1) and (2).

So far, previous publications dealt with methods of functionalizing electrospun fibers which took place in a multistep procedure after the processing.[254] If fibers were modified after the electrospinning process, this was done by plasma treatment,[255] surface graft polymerization,[256] aminolysis,[257] standard or enzymatic hydrolysis,[258-259] or via wet chemical reaction,[260] and required various altering steps.[261-264] For example, Viswanathan et al. applied diblock copolymers, which performed self-assembly on electrospun PLGA fibers, and they were able to alter the hydrophilicity.[265] Latest studies addressed PCL fibers in the micrometer range which were modified *in situ* by using a coagulation bath filled with polydopamine as collector for electrospinning.[266] Afterwards, differentiation studies of hMSCs were performed on these meshes. PCL nanofibers were treated with carboxyl or amine modified particles for RGD immobilization in another study.[267]

2.4 Quantification of biological active groups on electrospun fiber meshes

Parts of this chapter may be reworked for a publication reviewing literature about the quantification of ligands on electrospun fibers where L. Wistlich will hold first authorship. However, this manuscript is not submitted or published by the time of the submission of this thesis.

So far, many publications dealt with functionalization of electrospun surfaces by cell-mediating peptide sequences, but the quantification of peptides or other ligands was rarely examined in detail although ligand concentration plays a crucial role in the biomaterials' performance.[268-272] However, it is essential for a biomaterial regarding its function and application to examine the number of ligands which are immobilized and the stability of the interaction between material and active groups.[273-274] As addressed by Spatz and co-workers,[275-278] another important factor might be the distance between anchor points, for example RGD molecules, which were available for cells on the surface of biomaterials. For the function of the material, it is essential to answer the question of the presence of functional groups (qualitatively) and the amount of modified groups on the biomaterial surface (quantitatively).

The methods described in the following chapters are divided into characterization and quantification methods. In general, the amount of publications concerning analysis of flat surfaces exceeds the number of methods describing quantification on fibers by orders of magnitude.[279-281] Many materials are not adequately quantified for surface ligand density even it is decisive for the biomaterial's performance.

2.4.1 Characterization methods

The morphology of fibers is an important parameter affecting the activity of scaffolds *in vitro* and *in vivo*. In order to control the impact of all parameters relevant for the electrospinning process and influencing the morphology, it is pivotal to characterize electrospun fiber surfaces. A simple method to determine the hydrophilicity or hydrophobicity is the measurement of the contact angle. The extent of a water droplet spreading on the surface is a parameter for hydrophilicity of the surface. Many research groups use contact angle measurements to confirm successful grafting of fibers.[282-283] For example, Campos et al. applied the method to electrospun PLGA scaffolds to demonstrate a successful fibronectin (FN) coating for enhanced cell adhesion.[284]

Electron microscopy is a widely-used technique to characterize the structure of different sample surfaces. Scanning electron microscopy (SEM) and transmission electron microscopy (TEM) are applied to study the surface morphology and topography as well as cellular responses to biomaterials. Both techniques produce images of a sample by scanning it with a beam of electrons in a vacuum. These electrons interact with the sample resulting in an ejection of electrons and X-rays. Either the primary (BSE = backscattered electrons) or the secondary electrons are collected, and detectors convert them into a signal producing the final image which is close to 3D impression. SEM works with the principle of electron diffraction and scattering, TEM uses electrons which pass through the specimen and are collected below the sample. The magnification ranges from 20x to approximately 200 000x. SEM has a spatial resolution between 50 and 100 nm while TEM shows a much higher resolution and provides details about internal composition.

Therefore, TEM can show many characteristics of different samples, such as nanotubes,[285] hollow fibers,[286] nanocrystals,[287] and nanoparticles.[288] Non-conducting polymers must be sputter-coated prior to analysis. High vacuum is required, so obtained information might not be truly representative. Another drawback of the method could be the proper preparation of samples when Cryo-SEM is needed due to formation of ice crystals or overcritical drying of sensitive specimens such as proteins present on the samples which could destroy the surface.

SEM is used for the analysis of the topography of biomaterials[289-294] but also to investigate cell adhesion.[295-299] TEM examination is, for instance, applied to study fiber and nanotube morphology,[300-302] to explore microstructures,[303] and to characterize

nanoparticles.[304-305] The preparation of TEM samples involves fixation, embedding and sectioning to prepare very thin slices since electrons will not penetrate samples with more than 1 µm in thickness. These processes may alter the structure of the samples. With TEM, only small amounts of samples can be analyzed at a certain time whereas the acquisition of SEM micrographs are usually running quite quickly.

Another microscopic technique which gives information about the morphology and topography of samples is atomic force microscopy (AFM). Samples are measured by analyzing the bending of a cantilever as a response to external forces detected by a laser beam focusing on the back of the cantilever. A photodetector converts the laser beam into an electrical signal.[306] It is possible to use this method to determine the structure of fibers,[307] the fiber diameter,[308] the roughness of materials,[309-310] the cross sectional morphology of nanofibers,[311] liquid wetting,[312] but also the cell morphology.[313] In recent years, the application of AFM has been enlarged by using coated cantilever tips to enable the study of surface interactions with various proteins and lipids.[314-316] In comparison to other nanostructure analysis techniques, the major advantage of this method is the possibility to be applied in an aqueous environment which is very helpful for the investigation of living organisms at room or physiological temperature. For example, the visualization of plasma protein molecules under aqueous conditions was possible.[317]

Furthermore, AFM images can be obtained without surface treatment, vacuum or coating which may damage or alter the materials surface.[318] A major drawback of the atomic force microscope is the quite small maximum image size of 15 x 15 µm, where variations in the surface may be invisible, and time required for obtaining high quality images can be significant. AFM is not only used for imaging, but also for manipulation of molecules.[319]

AFM, TEM and SEM are powerful techniques to understand surface morphology and topography. However, they are not suitable to give any quantitative information about surface composition.

2.4.2 Quantification methods on surfaces

2.4.2.1 Radiolabeling, XPS, ToF-SIMS and ATR-FTIR

In order to enable interactions of the material with the surrounding tissue and offer suitable functionality for specific applications, appropriate surface analytical techniques are crucial to reveal important surface properties of the biomaterial. Here, it is essential to perform a detailed chemical surface analysis, whereas the applied methods not only deliver different chemical and physical surface characteristics but are also often quite different in terms of their lateral and depth resolution.

While the use of radiolabeling ligands gives information about the bulk of the coating, X-ray Photoelectron Spectroscopy (XPS) and Time-of-Flight Secondary Ion Mass Spectrometry (ToF-SIMS) only measure surface-near regions of materials. For both setups, the penetration depth depends on the experimental composition and the material characteristics.

Until now, only few papers were published on radiolabeling of fibers. For example, the radiolabeled peptide sequence GRGDY was used to determine sufficient peptide surface density for fibroblast spreading, focal contact and stress fiber formation.[273, 320] Results were confirmed by SEM images and fluorescence micrographs. However, in this study it is assumed that a homogeneous peptide distribution was obtained by controlling the peptide concentration in the reaction buffer. An evenly peptide distribution was expected and could only be approved by cell experiments. In contrast, other research groups studied the influence of other radiolabeled adhesion peptides on cell adhesion.[274, 321-322] Furthermore, Tewson et al labeled asbestos fibers with ^{68}Ge[323] and the effects of labeling on the bioactivity of the fibers were evaluated. Radiolabeled fibers kept their ability to stimulate cells to more than 95%. So far, the radiolabeling technique was not determined for application on electrospun fibers and the studies using the method for fibrous structures are quite old, respectively. Scanning the literature does not lead to more updated findings for radiolabeling meshes derived from electrospinning.

Several reviews are published describing the method of XPS extensively.[280, 324-326] The use for surface characterization and quantification is quite established in the field of 1D structures as well as in the area of fiber surfaces underlining the fact that this technique suits excellently for fibrillary surfaces. For example, poly(L-lactic acid)-co-

poly(ε-caprolactone) (P(LLA-CL)) nanofiber meshes were coated with collagen after air plasma treatment and were investigated by XPS.[327] Ramakrishna's group examined core-shell structures of nanofibers in which the release of fluorescein isothiocyanate-conjugated bovine serum albumin (fitcBSA) in the core is further analyzed by XPS. They encapsulated fitcBSA as model protein along with PEG inside PCL nanofibers via coaxial electrospinning technique.[328]

Most studies applying Tof-SIMS were conducted on flat surfaces.[274, 329] Fibers are challenging to analyze due to their round shape and insulating nature. There are only a few studies performing fiber surface analysis via ToF-SIMS. For example, Uyar et al. used it to describe the presence and the lateral distribution of cyclodextrins in the outer molecular layers of polystyrene nanofibers. Additionally, ToF-SIMS is often applied in combination with XPS results due to its increased surface sensitivity for obtaining information about the lateral resolution. For instance, Michel et al. used XPS to quantify the amount of three different proteins with varying sizes adsorbed to the surfaces while by ToF-SIMS, the protein conformation could be detected.[330] Here, ToF-SIMS identifies significant, but very low protein adsorption indicating the higher sensitivity of this method compared to XPS.

The chemical analysis obtained with Fourier transform infrared spectroscopy with attenuated total reflection (ATR-FTIR) is a combination of layers on the substrate surface and deeper regions. The interpretation of IR spectra by subtraction of the original substrate spectrum from the spectrum of protein-adsorbed substrates has become a common technique of quantification, often combined with the use of internal standards.[331] However, it has to be kept in mind that all the published data concern relative values and that they are evaluated in relation to unmodified materials. There are practically no publications which measured absolute values for modified materials with ATR-FTIR. Nevertheless, this method is an attractive tool for studying protein adsorption.[332-333] or to evaluate the successful grafting of fibers.[334-335]

However, the majority of studies using the described methods were performed on flat surfaces. Due to the high surface to area ratio and the challenging structure of fibers, only limited data are available concerning fibrillary scaffolds. Generally, a combination of different methods is recommended to address the quantification of ligands from different perspectives.

2.4.2.2 Surface sensitive quantification

On surface functionalized polymers, the grafted layers usually have a thickness of less than ten nanometers, compared to some hundred nanometers penetration depth of many analytical methods used for surface characterization. ToF-SIMS, ATR-FTIR, XPS and radiolabeling are suitable methods to understand the chemical composition of a biomaterial qualitatively and semi-quantitatively. Nevertheless, these methods do not exclusively determine the number of ligands available for cells at the surface of the material. For the functionality of a biomaterial, the determination of the composition, structure, orientation and spatial distribution of all chemical species and biomolecules present on the biomaterials surface is very important. Since the surface structure may be different in comparison to the bulk composition, surface-sensitive techniques are required. Surface plasmon resonance (SPR), quartz crystal microbalance (QCM), and surface acoustic wave (SAW) are methods which allow surface sensitive, fully quantitative measurements without labeling. Additionally, the enzyme linked immunosorbent assay (ELISA) and the colorimetric assay will be shortly introduced as promising but semi-quantitative methods for analyzing the surface of biomaterials. Furthermore, cell adhesion assays are commonly used to confirm biocompatibility.

Surface plasmon resonance

The surface plasmon resonance (SPR) method can optically monitor biological interactions between ligands immobilized on a metal surface and a binding partner in a liquid environment.[336] Surface plasmons (SPs) are free accumulated electrons in gold which oscillate at the interface of two media. If excited by incident light, they create evanescent electromagnetic fields which lead to a transfer of energy from the source to the SPs. Subsequently, the resonance signal of reflected light can be calculated from the reflection angle.[337-338] For immobilization and quantification experiments, changes in the refractive index at the solvent-surface interface are detected and correlated with the adsorption of mass on the surface.[338] The change of the refractive index arises from the binding of molecules to the surface and a resulting mass change. It is possible to measure an interaction in real-time and no labeling or sample preparation is required.[336] Although the method is described as appropriate for quantification of ligands on functionalized biomaterials, it is limited to very thin model surfaces on noble metals like gold or silver and is only suitable for biomaterials which

can be prepared as ultrathin films.[338] The sensitivity of SPR greatly depends on the distance to the sensor surface; for biological molecules larger than the evanescent field, the method shows lower sensitivity with increasing distance from the surface.[337] As described by Netsuwan et al., the penetration depth of surface plasmon fields is about 100-200 nm,[339] thus nanostructured films or fibers on the metal surface of SPR chips should be at a nanoscale range to maintain the sensitivity of the method.

SPR has been demonstrated as useful technique for the establishment of biosensors as well as for characterization of any biological ligand interaction, like proteins, oligonucleotides, lipids and other small molecules. In several publications, the technique was used for an affinity comparison and binding kinetic analysis of peptide displaying bacteriophages on biosensors[340] and for the quantification of cytokines which are related to wound healing, by attaching specific antibodies to a binding layer on SPR sensors.[341] Electrospun fibers are reported to be used for sensor applications because of their large surface, by which reactivity and sensitivity of sensors can be improved. Furthermore, the huge surface area provides more contact surface for analyte adsorption compared with film-based sensors. As shown in literature, polymers can be electrospun directly on the gold surface of SPR chips.[339, 342]

However, a quantification of ligands on modified fiber surfaces is not possible with this method since it does not provide absolute values. The quantification is only possible for immobilized analytes and additional methods are needed for final quantification of biomolecules.

Quartz crystal microbalance

Quartz crystal microbalance (QCM) is an acoustic wave technique for surface-sensitive detection of small mass uptakes on the surface of an oscillating piezoelectric quartz crystal.[343-344] The measuring principle consists in propagation of the acoustic wave along the sensor where a solid substrate can be deposited. In most setups, a liquid is pumped over the coated sensor surface and the immobilized substrate interacts with an analyte added to the fluid. An additional mass binding on the surface results in a resonance frequency shift of the quartz crystal sensor. It is possible to observe mass deposition in real time without the need to add enzymes, radioactivity or other labeling techniques.[344] Alterations of the viscoelastic properties of the adsorbed films caused by conformational changes during adsorption can also be detected.[345] The films

coated on the quartz crystal have to be very thin since the distance of the interacting molecules to the coating has an influence on the accuracy of measurements; typically used coatings have a thickness between 1 nm and 10 µm. Due to the small frequency of around 5-20 MHz, QCM has a rather low sensitivity.[346] The method is suitable for the characterization of adsorbed thin layers of fluids or gases, biospecific binding of DNA or protein-protein-measurements, sensors for environmental monitoring and chemical and biochemical analysis through modification of the electrodes by different coatings. Even a quantitative characterization of cell interactions and measuring of binding kinetics are possible. Furthermore, cell adhesion could be followed in real-time using QCM on surfaces.[347]

In literature, the use of fiber materials in the context of QCM is solely mentioned as sensors modified with electrospun biomaterials. All authors used electrospun nanofibers to improve sensitivity, selectivity and the time response of newly developed devices.[348] They argued that nanostructured materials are appropriate for the application as biosensor because of their large surface area, the high porosity and the interconnected porous structures; this is why nanofiber-based QCM sensors show an improved sensing performance.[349] With such sensors, it is possible to create self-assembled monolayers (SAMs) and to examine interactions by subsequently immobilizing proteins, antibodies or other biological molecules.[344, 350] One group was able to monitor modifications of QCM sensors coated with polyvinyl alcohol (PVA) nanofibers by plasma polymerization with allylamine monomer; each step could be observed by measuring the frequency shifts. Nevertheless, the authors did not use the sensor for quantification of polymer functionalization but for recognition and quantification of certain biomolecules, for example bovine serum albumin (BSA) as model protein.[351]

Finally, it can be concluded that the surface sensitive method of QCM is appropriate for quantification of ligands which attach to surfaces of electrospun fibers and can be used to determine cell adhesion on such surfaces as well. The method provides values of the frequency shift which show corresponding mass alterations but nevertheless the results are relative values and need other methods to give a quantitative statement about the surface and immobilized molecules.

Surface acoustic wave

Another possibility for a surface sensitive quantification is the surface acoustic wave (SAW) technology. A SAW is a mechanical wave which is horizontally polarized propagating along a piezoelectric substrate. This acoustic wave is produced by an interdigitated transducer (IDT), using an additional guiding layer on the surface. The propagation of the wave is restricted to the surface without penetrating into the liquid phase pumped over the piezoelectric crystal.[352] That is an important fact because the most binding events occur near the biosensor surface. The method shows a higher sensitivity than QCM because of the higher frequency (150 MHz, Love wave) and two signals are detected: The phase signal shift shows mass changes on the sensor surface during the measurement; a shift in the amplitude signal is related to structural changes and viscoelastic characteristics.[353] However, ultrathin films on e.g. gold layers of the SAW surface are required which makes the application of this method quite complex in the field of biomaterials. It is also important for the development of new applications that it is possible to immobilize materials by coupling reactions to develop functional layers which bind target analytes to specific recognition ligands.

Since 2010, only few publications emerged about the use of electrospinning nanofibers for SAW sensors. Many authors referred to the huge specific area and the high porosity of electrospun fibers to create ultrasensitive sensors.[354-357] They all found that the thickness was a limiting factor of improving the sensitivity and they were able to adapt the spinning conditions to deposit fibers directly on the sensor.

The SAW technology is mainly used for analysis of association and dissociation kinetics of immobilized analytes. Binding processes could be measured by real mass changes on the surface and the method is known to be very sensitive achieving a detection limit of <50 pg cm^{-2}.[353] Neverthless, no publication reported about quantification of chemical or physical functionalizations of fibers. Probably, the porous and fibrous structure could falsify the results of SAW measurements due to the high porosity; interaction between the gold layer and the adjacent medium or analyte could disturb the quantification. Applying an additional coating may prohibit this unspecific binding.

Enzyme-linked immunosorbent assay

Most surface sensitive ligand quantification techniques such as SAW and SPR cannot easily be transferred to standard biomaterials, and specialized sensors are required. Moreover, it is only possible to apply these techniques on ultrathin coatings. The enzyme-linked immunosorbent assay (ELISA) is a well-studied, surface sensitive method that measures the binding of an antibody to an antigen. The primary antibody selectively binds with high affinity to antigens such as proteins or peptides which are immobilized on a surface. This antibody is detected by a secondary antibody linked to an enzyme. By adding an enzymatic substrate, a visible signal occurs which is measured photometrically. ELISA is a semi-quantitative method since evaluation is only possible together with a standard curve produced with known concentrations of antigens. The orientation and conformation of the observed species plays an important role. If the antibody binding site within the protein is sterically blocked, attachment may not be possible, leading to serious underestimation of the adsorbed amount of protein.

For example, Goodfriend et al. used ELISA to investigate the fibrin and platelet adsorption on a PLLA stent.[358] Another group analyzed the influence of the PEG concentration on the amount of the immobilized model protein fibronectin together with a fibronectin antibody. Moreover, it was found that PEG can regulate the extent, the conformation and specific bioactivity of the adsorbed fibronectin.[147] Amin et al. investigated the production of ECM components, including collagen, fibronectin, laminin, osteonectin, osteopontin and vitronectin of osteoblasts on the surface of PLGA and PLA scaffold and quantified them via ELISA.[359]

Extensive characterization has been performed on films; however, the characterization and quantification of fibers is challenging since they present a complex 3D network with pores, a huge surface area and inaccessible areas.

Colorimetric assays

Several approaches exist for determination of the protein concentration on cell culture media including Bradford assay,[360-361] Lowry assay,[362-363] and Biuret reaction.[364-365] However, these methods are designed to verify the protein concentration in solution and not proteins bound to surfaces. For investigations of surface protein adsorption, usually the remaining protein in solution was measured followed by calculation of the adsorbed amount by mass balance.[366] This may lead to an overestimation since it

cannot be distinguished between covalently bound or physically adsorbed proteins. The bicinchoninic acid (BCA) assay is an effective approach to directly determine the amount of protein attached to the surface.[367] It contains Cu^{2+} ions which are reduced by adsorbed proteins to Cu^{+}. This reacts with BCA to a purple complex measured at a wavelength of 562 nm. In case of the BCA assay, the chromophore occurs through a secondary reaction not involving the protein itself.

Besides proteins, functional groups can be determined with the colorimetric approach. Most assays detect carboxyl and amino groups on polymer surfaces by ion exchange mechanisms. For instance, Chua et al. functionalized poly(ε-caprolactone-*co*-ethyl ethylene phosphate) (PCLEEP), a biodegradable copolymer, with poly(acrylic acid) (PAA) to investigate how a functional nanofiber scaffold with surface-galactose ligands influences the spheroid formation, the functional maintenance and the attachment of rat hepatocytes in culture.[368] The amount of PAA grafting on the scaffolds was determined by a colorimetric method using Toluidine Blue O (TBO) staining. TBO is a positively charged dye and reacts with carboxyl groups forming a stable electrostatic complex in alkaline solution. After dissolution in acetic acid, the TBO molecules are detached and measured. The number of functional groups is calculated under the assumption of a stoichiometrical reaction with TBO. Other groups used the principle of desorbing a dye in a secondary solution to make quantitative statements.[369-370] The performance of measurements is also possible by *in situ* quantification of the dye bound to the polymer[371] and by analyzing the decrease of absorbance of the dye solution.[372] It might happen that the bulk dye concentration is so high compared to the absorbance that a change in concentration is not measurable.

Regarding the sensitivity of colorimetric assays, it must be said that adsorption and desorption rely on electrostatic interactions, that means that the reactions are pH dependent and for adequate characterization, equimolar amounts of dye molecules must be bound. Moreover, these assays are not able to elucidate protein conformation and might be disturbed by interfering components. It is challenging to measure fibers by colorimetrical assays due to the high surface area to volume ratio. All colorimetric methods are used in conjugation with a standard curve. The generation of such curves may be difficult; hence, these tests are often more suitable for qualitative rather than for quantitative analyses. In principle, fluorescence-based assays offer higher sensitivity, wider dynamic range and lower background signals than absorbance-based assays.

Cell experiments

With cell adhesion experiments, it is not possible to measure a precise number of ligands bound to the surface. However, it is important to correlate quantification results obtained by the previously mentioned physicochemical methods with biological experiments to analyze the effect of immobilized ligands on vitality, proliferation, spreading and cell adhesion. The most straightforward way is to analyze the cell number after detachment. Furthermore, the DNA amount can be evaluated to determine cell numbers. PicoGreen and Hoechst 33258 are two commonly used fluorescence dyes for double strand DNA, which become fluorescent upon binding with nucleic acids. Many colorimetric methods have been developed for determination of cell numbers such as the 3-(4,5-dimethylthiazol-2-yl)-2,5-diphenyltetrazolium bromide (MTT) or 3-(4,5-dimethylthiazol-2-yl)-5-(3-carboxymethoxyphenyl)-2-(4-sulfophenyl)-2H-tetrazolium (MTS) assay, which measure the metabolic activity of cells. The advantage of these colorimetric assays is that cells do not need to be detached since they cannot be dissolved from rough or porous materials in some cases. In literature, cells were used as a proof for cytotoxicity,[373] biocompatibility,[374] and to determine the success of surface modification approaches.[375-376] Cells might be the most sensitive criterion to measure changes in bioactivity of the surface, because instrumentation techniques often show much higher detection limits. However, a detailed surface analysis cannot be obtained by investigation of cell adhesion, proliferation and spreading. Since each technique has its own strength and weakness, more than one method is typically required for a detailed characterization and quantification of a biomaterial. Cell experiments should be always conducted and correlated with results from other methods.

2.4.3 Summary of quantification methods on surfaces

XPS and ToF-SIMS are currently the most widely used techniques in the compositional characterization of biomaterials particularly after applying thin coatings and surface modification. The majority of studies were conducted on flat surface and an application of many methods to analyze surfaces of thin fibers is challenging due to the high ratio of total analytical area to the actually analyzed fiber surface. Another drawback of most methods is that only relative values can be measured. A combination of different techniques could be an approach to describe the fibers characteristics.

3 Development of a polymer functionalized α-TCP cement with enhanced mechanical properties

This chapter is expected to be reused in a publication manuscript, where L. Wistlich will hold first authorship. The manuscript is however not submitted or published by the time of the submission of this thesis.

3.1 Introduction

To overcome the limitations of CPCs such as their brittle mechanical behavior and slow resorption *in vivo,* natural or synthetic polymers can be added to the system to create scaffolds with the advantages of both components.[377] As mentioned in **chapter 2**, the bioceramic polymer composites based on self-setting mineral bone cements are less explored compared to polymer modified Portland cements in civil engineering. While set cements or sintered scaffolds can be easily modified with biocompatible polymers such as PLA, PGA or PLGA post-setting by impregnation with a polymer solution, the direct formation of a hydrogel phase in the cement matrix during hardening is challenging and requires water soluble monomers, which are able to crosslink during setting. This can be achieved for example by radical polymerization of HEMA,[378] acrylamide,[77] degradable PEG-PLLA-methacrylate monomers[379] or by a polycondensation of six-armed NCO-sP(EO-*stat*-PO) prepolymers.[47] The latter shows the advantage that the stimulus for hydrogel formation stems from an aqueous environment of the cement paste, whereas water initially hydrolyzes isocyanates to amines followed by the formation of a urethane network which was described earlier in detail.

In the following section of the thesis, a new polymer-modified cement composite was developed which is based on the application of commercially available star-shaped polymers. Here, a three-armed star-shaped prepolymer with functional isocyanate groups at the end of the polymer chains was established (Aquapol[380]) consisting of three arms of an ethylene and propylene oxide co-polymer with isocyanate groups at the end of the polymer chains.[381] Such molecules are known to crosslink in an aqueous environment with the formation of mechanically strong hydrogel networks due to a higher density of functional NCO groups.[232, 382] These prepolymers were used for modifications of both an α-TCP based biocement and a fast setting calcium aluminate cement known from civil engineering with the focus on an analysis of the resulting mechanical properties of the formed composites.

3.2 Materials and methods

Preparation of the cement powder. α-$Ca_3(PO_4)_2$ (α-TCP) powder was prepared by heating a mixture of $CaHPO_4$ (Mallinckrodt-Baker, Griesheim, Germany) and $CaCO_3$ (Merck, Darmstadt, Germany) in a molar ratio of 2:1 for 5 h at 1400°C followed by quenching to room temperature. The same procedure was done for β-$Ca_3(PO_4)_2$ (β-TCP) at 1100°C for 5 h. The sintered cake was crushed by pestle and mortar and passed through a 125 µm pore size sieve. Milling of the product was performed in a planetary ball mill (PM400 Retsch, Haan, Germany) at 200 rpm for 2 h for α-TCP or for 10 min for β-TCP using 500 ml agate jars, with four agate balls (30 mm) and a 125 g load of powder per jar.

Cement paste formulation. For mechanical testing, cement pastes were formed by mixing α-TCP with 2.5 % Na_2HPO_4 solution on a glass slab for about 30 s at a powder to liquid ratio (PLR) of 3.0 g/ml. Polymer modified cements were fabricated by adding 28 wt% three-armed star-shaped NCO-sP(EO-*stat*-PO) (Aquapol with a molecular weight of 6 kDa, kindly provided by Paul Hartmann, Heidenheim, Germany) to the α-TCP powder, followed by mixing and setting of this paste by 1 ml Na_2HPO_4 solution.

Mechanical testing. Cement pastes were transferred into cuboid silicon rubber forms to fabricate samples for either compressive strength (12 x 6 x 6 mm) or 3-point bending strength (30 x 6 x 5 mm) testing. For determination of diametral tensile strength, cylindrical molds (diameter 13 mm, height 8 mm) and for tensile strength, dumbbell-shaped silicon molds (62 x 18 / 6 x 1.5 mm) were used. Samples were allowed to set for 1 hour, 24 h and 7 d at 37°C in a water bath. Half-wet specimens were measured in axial compression (compression and 3-point bending test), radial compression (diametral test) or in tension (tensile test) at a crosshead speed of 1 mm/min using a static mechanical testing machine Zwick 1440 (Zwick, Ulm, Germany) and a 10 kN load cell. The compressive and the tensile strength was calculated by dividing the force by the cross-sectional area of the sample. The bending strength BS was calculated according to

$$BS\ (MPa) = 3 * F * \frac{L_1 - L_2}{b * h^2} \quad (1)$$

where $F_{(max)}$ is the standard force (failure load), L_1 (L_2) is the distance between the outer (inner) rolls, b is the width and h is the height of the samples.

The diametral tensile strength DTS was estimated by

$$DTS\ (MPa) = 2 * \frac{F}{d*\pi*t} \quad (2)$$

where $F_{(max)}$ is the standard force (failure load), d is the diameter and t is the height of the sample.

Characterization methods. The reaction of NCO-groups with water was analyzed by Fourier Transform Infrared Spectroscopy with Attenuated Total Reflection (ATR-FTIR; Nicolet is10, Thermo Scientific, Waltham, MA) in a range from 400 to 4000 cm^{-1} with a spectral resolution of 4 cm^{-1}. X-ray diffraction (XRD) patterns of 7 d set cements were recorded by using monochromatic CuK_a radiation (D5005, Siemens, Karlsruhe, Germany) in a 2Theta range from 2θ = 20-40° with a step size of 0.02° and a normalized count time of 3 s per step. The phase composition was established by means of JCPDS reference patterns for α-TCP (powder diffraction files (PDF) Ref. 29-0359) and hydroxyapatite (PDF Ref. 09-0432). A crossbeam scanning electron microscope CB 340 (Zeiss, Oberkochen, Germany) was used to examine the surfaces of the composite monoliths. Samples were imaged using an acceleration voltage of 5 kV.

Analysis of variance (ANOVA): ANOVA was examined by means of SigmaPlot (Systat Software GmbH, Erkrath, Germany) using 1-way or 2-way ANOVA depending on the raw data. In order to calculate the statistical significance, a post hoc Tukey test was performed.

3.3 Results and discussion

3.3.1 Mechanical properties

Initially, the mixing ratio between Aquapol and α-TCP was evaluated with regard to the paste workability. With lower amounts of α-TCP, the paste could be stirred easily but shear-thinning resulted in free-flowing mixtures. Increasing amounts of water were added to the paste in ratios of paste to liquid of 1.5:1, 1:1, 1:3 and 1:5 g/ml. **Figure 7** shows the first approaches resulting in very soft and porous specimens.

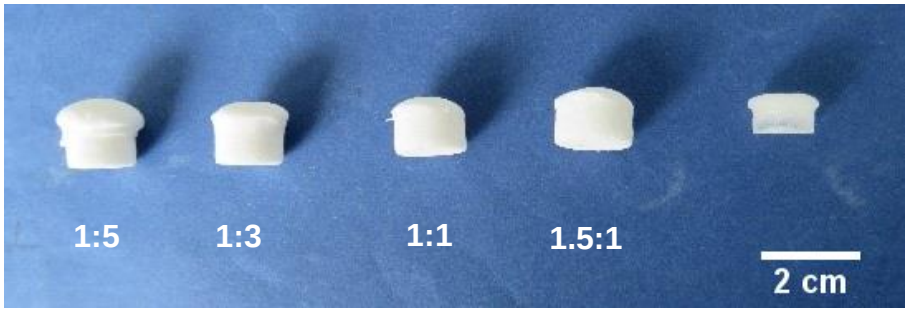

Figure 7: Preliminary testing led to smooth and porous samples which were expanded in height. They were prepared with differing amounts of α-TCP and varying addition of aqueous phase. From left to right, the mineral addition was increased as indicated in a paste to liquid ratio whereas the aqueous phase decreased from left to right. On the right, as an example, a sample without α-TCP addition is shown, which built a pure hydrogel due to the NCO-sP(EO-*stat*-PO) crosslinking.

It was also observed that with a lower mineral content, more CO_2 was produced during crosslinking of isocyanates with aqueous solution followed by expanding of samples in their molds. By adding the 2.5-fold quantity of α-TCP related to Aquapol and by using Na_2HPO_4 as setting liquid, the foaming could be reduced to a minimum. In concretes, usually the addition of anti-foaming agents is necessary[59, 383] which could be avoided in this system by adjusting the ratio of paste and liquid to a value of 2:1. A possible explanation for this phenomenon might be the denser packing of the cement particles in the paste which reduces the space for foaming and secondly, Ca^{2+} released from α-TCP during setting might have reacted with CO_2 to form calcium carbonate. The capacity for the later reaction is clearly depending on the amount of added α-TCP such that pastes with higher mineral load are expected to bind more CO_2 as precipitate.

On the other side, a foaming of samples could be advantageous for the use in biological systems, since such pores can serve as a pathway for a supply of bone cells with liquids and nutrients for an enhanced bone healing.[384] Na_2HPO_4 was used as setting regulator because it is known that the addition of phosphate ions leads to a shorter setting time of α-TCP to hydroxyapatite.[129] The paste to liquid ratio was fixed to 2:1 to produce specimens with proper hardness which showed also elastic properties while reducing foaming of specimens.

For mechanical testing, the samples were measured initially and after storage at 37°C in a water bath for 24 h and 7 d compared to references manufactured from α-TCP and Na_2HPO_4 solution alone in a powder-to-liquid ratio (PLR) of 2 g/ml. The content of α-TCP was higher in the references because samples with a lower PLR of 1.43 g/ml which would be comparable to the PLR of the test specimens (and in relation to the corresponding paste to liquid ratio from functionalized samples) did not set fast enough until an initial time point of 1 h after preparation. The compressive, 3-point bending, diametral tensile and tensile strength were measured to show differences between specimens without and with the addition of Aquapol. In **Figure 8**, the stress strain curves of samples and references are shown, whereas in **Figure 9**, the calculated strengths of references are demonstrated (except the conventional tensile test).

In **Figure 8A**, the compressive stress strain diagram shows that the specimens with Aquapol addition did not break at a particular point but were elongated until the measurement ended at 60% deformation. By examination of the samples, it could be observed that they did not rupture vertically but longitudinally and thus parallel to the compression plates. That means that at a certain time point (at about 40% deformation), the cement composite finally failed not only through forces from above but mainly through forces inside the specimens by failure of the material itself. In comparison, the measured compressive stresses of the references showed their highest points at about 8-10 MPa with a strain of only 1-2%. The calculated strengths are shown in **Figure 9A**; the reference samples deformed under compression until failure at an initial compressive stress of 0.3 MPa increasing to about 10 MPa after a storage time of 7 d in a water bath at 37°C.

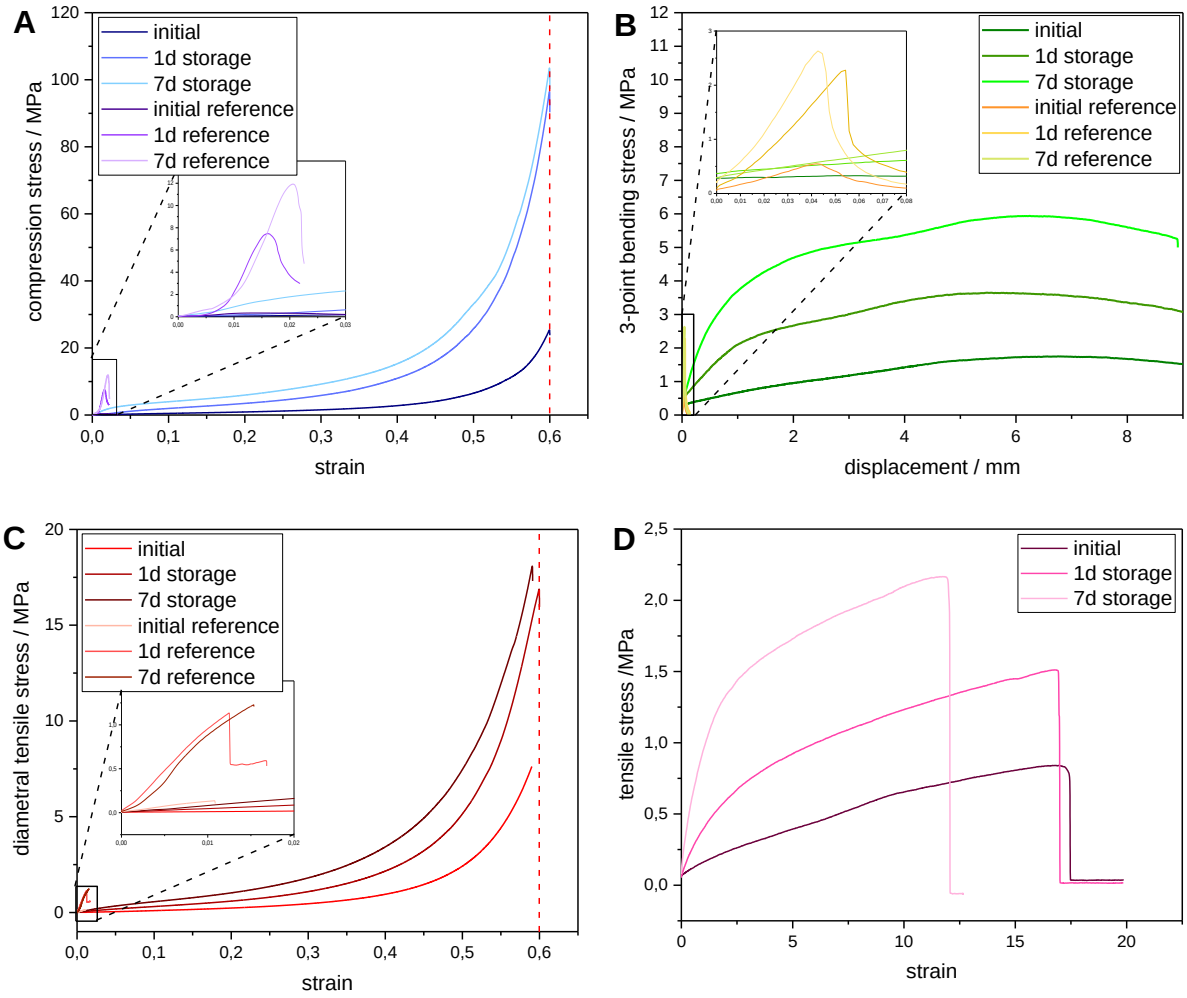

Figure 8: Mechanical testing of samples containing Aquapol. **A** shows the results of the compressive test, **B** the 3-point bending strength. **C** reveals the diametral tensile test and **D** the common tensile test. Aquapol modified samples contained 2 g polymer-cement paste and 1 ml Na_2HPO_4. (n = 10 for compressive, n = 8 for bending and n = 4 for diametral and tensile tests)

For determination of elasticity or flexural strength, a 3-point bending test was performed (**Figure 8B, Figure 9B**). Here, the references turned out to be very brittle in comparison to samples with polymer addition which showed an elastic behavior with no certain failure point. The slope in the linear part of the stress strain curve is defined as elastic modulus (Young's modulus) which reached a higher value for stiffer materials. This was also observed in **Figure 9B** where the references showed a higher elastic modulus than functionalized samples which are much more ductile.

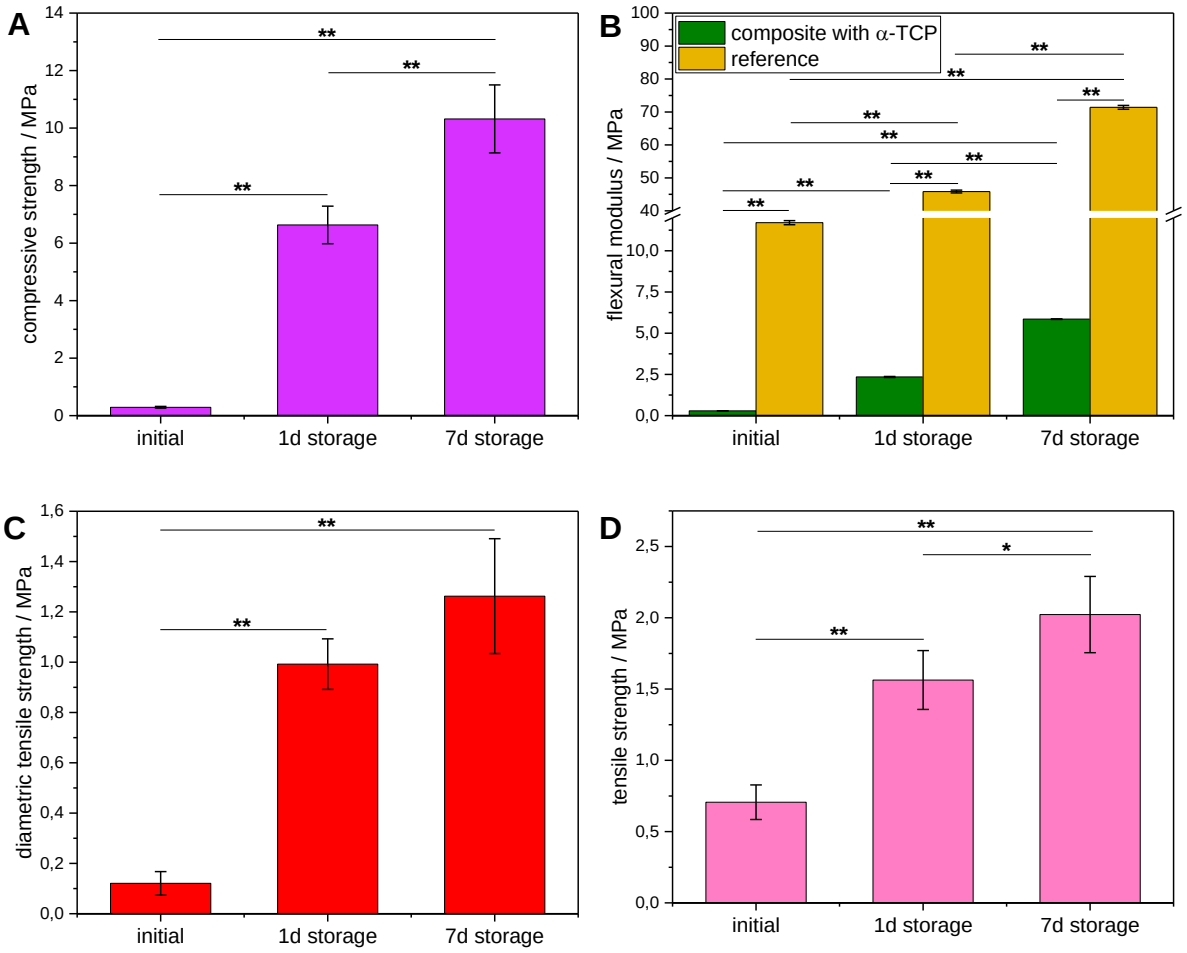

Figure 9: Mechanical testing of reference samples without Aquapol. **A** shows the results of the compressive test, **B** the flexural modulus which was calculated out of the slope of the linear part of the 3-point bending curve. Here, the values were compared with results from samples with Aquapol addition displayed in **Figure 8B**. **C** reveals the diametral tensile test of references and **D** the tensile test for specimens with Aquapol addition calculated from **Figure 8D**. All reference samples were prepared with a PLR of 3.0 g/ml. Level of significance of 1-way and 2-way ANOVA: ** means $p < 0.01$, * means $p < 0.05$. (n = 10 for compressive, n = 8 for bending and n = 4 for diametral and tensile tests)

To evaluate the tensile properties, different tests were applied. Because it was not possible to measure tensile strength of the brittle reference in a conventional tensile test, a diametral tensile test setup was applied (**Figure 8C, Figure 9C**). For samples with polymer functionalization, a common tensile test was used (**Figure 8D**, **Figure 9D**). The results are in good agreement with the literature,[385] e.g. Feldman et al. found DTS values between 1.7 and 3.1 MPa for concretes modified with polypropylene (PP) fibers.[386] Furthermore, Al-Zahrani et al.[387] examined tensile strengths of 1.1-3.2 MPa after 3 days of storage using polymer and cement based repair mortar.

Another reference test using non-active β-TCP instead of the reactive α-TCP filler also revealed a very flexural behavior when combined with Aquapol. However, the 3-point bending stresses (**Figure 10A**) for β-TCP containing samples were significantly lower in comparison to the α-TCP containing samples for all three tested time points. The measured stresses of β-TCP specimens were not able to exceed 1 MPa also after storage of 7 days due to the absence of a cement setting reaction in these specimens. Calculating the flexural moduli of all samples revealed significant higher values for α-TCP containing samples (**Figure 10B**). The reason for that is the different setting behavior of the ceramic materials: α-TCP shows a setting reaction to calcium deficient hydroxyapatite in an aqueous medium at neutral pH. For crystalline β-TCP, the setting reaction in water is very slow[388-389] and after 7 days, the samples behaved more like a particle filled hydrogel rather than a polymer modified concrete.

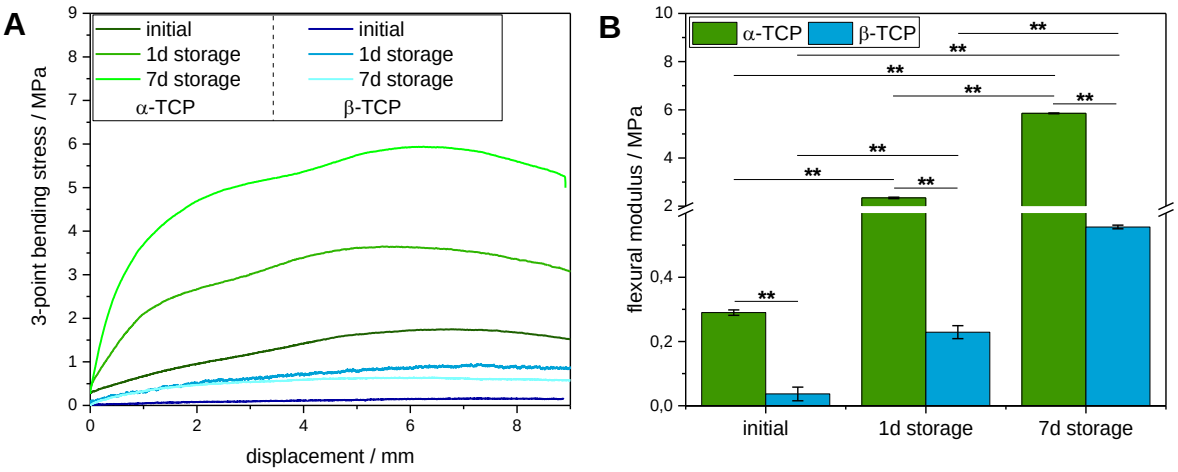

Figure 10: Comparison of the 3-point bending stress (**A**) and flexural modulus (**B**) of α-TCP and β-TCP samples containing Aquapol after a storage time of 7 d. All samples were prepared containing 2 g polymer-cement paste and 1 ml Na_2HPO_4. Level of significance of 1-way and 2-way ANOVA: ** means $p < 0.01$. (n = 6)

Comparing the resulting compressive and flexural strength to literature, a quite high compressive strength of 39.5 MPa after 28 days and 45.0 MPa after 90 days of storage at room temperature was noticed by Aggarwal et al. for an another polymer-cement system using an epoxy based polymer or an acrylic emulsion for modification of an ordinary Portland cement.[64] The developed Aquapol-HA-system showed lower 3-point bending strength but was at the same time very elastic and reached a compressive

stress of about 100 MPa until the end of measurement although some cracks could be observed on the surface of the specimens. Indeed, this value was achieved already after 24 hours during storage at higher temperatures. Regarding the flexural strength evaluated by 3-point bending strength shown by Aggarwal et al., the values were 7.8 MPa (unmodified) and about 9 MPa (polymer-modified) after 28 days. In contrast, the system from this thesis achieved a strength of about 2 MPa without polymer addition whereas the functionalized samples showed again a very flexural behavior. Another approach was developed by Wang et al.[390] mixing a calcium phosphate cement powder and methacrylate modified dextran (Dex-MA) to create an improved CPC with a faster setting time and enhanced mechanical properties. They achieved a compressive strength of about 98.3 MPa by addition of Dex-MA which is comparable to our system. Unfortunately, no flexural strength was measured to compare the systems in detail. A disadvantage of the Dex-MA system is the mandatory use of an APS/TEMED initiator, which is not necessary for the examined system from this thesis as the isocyanate crosslinking is stimulated by the aqueous environment in the cement paste alone and needs no further reaction partners.

3.3.2 Characterization of the system by terms of XRD, FT-IR and SEM

Figure 11 depicts FT-IR spectra of the cement paste mixed with the sodium phosphate solution after several time points, which revealed the disappearance of the isocyanate peak already after 30 min. This reaction was more rapidly for the three-armed prepolymers than observed with the six-armed NCO-sP(EO-*stat*-PO) component by Schamel and co-workers[47] and shown by A. Rücker.[391] The fast hydrolysis is a hint that the component may non-toxic *in vitro* and *in vivo* similar to the six-armed NCO-sP(EO-*stat*-PO) and in contrast to commonly used hydrophobic isocyanate compounds.[392] The fast initial setting of the polymer cement composite is advantageous for its potential use as highly flexible tile adhesive.

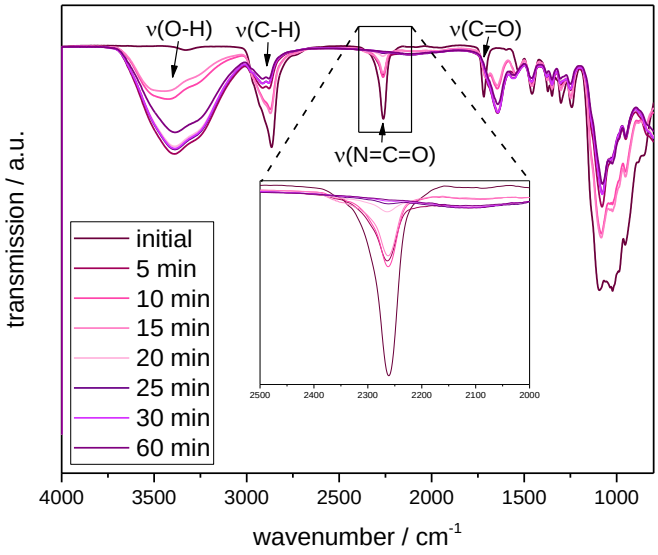

Figure 11: FT-IR analysis. Conversion of the NCO peak in samples with α-TCP and Aquapol addition initially and after various time points after mixing 2 g polymer-cement paste and 1 ml Na_2HPO_4. Prominent absorption bands of functional groups are indicated.

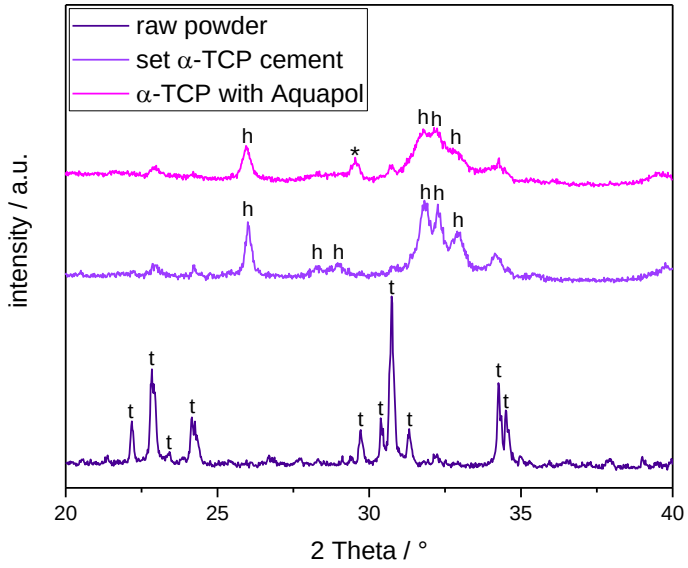

Figure 12: X-ray diffraction (XRD) patterns of α-TCP raw powder in comparison to set cements without and with the addition of Aquapol in the liquid phase after a setting time of 7 d. The most significant diffraction peaks correspond to α-TCP (t) and hydroxyapatite (HA, h). The peak * originates from the sample holder. Samples were prepared containing 2 g polymer-cement paste and 1 ml Na_2HPO_4.

X-ray diffraction patterns were determined to show differences which occurred by adding the polymeric compound Aquapol. As evident in **Figure 12**, both cements showed an adequate conversion of α-TCP; the addition of the polymer had almost no influence on the HA formation which is also known in literature.[393] An interpenetrating network (IPN) of polymer and cement powder was examined before in our group using a dual setting system consisting of α-TCP and HEMA.[76] Here, the polymer addition had an influence on α-TCP setting demonstrated by examination of samples after 24 h and after 7 d setting, and by Rietveld refinement analysis a degree of conversion of a-TCP of about 80% was revealed when 70% of HEMA was added. For further investigation of the introduced system, a quantitative analysis of α-TCP conversion should be performed and furthermore, the content of polymer should be varied.

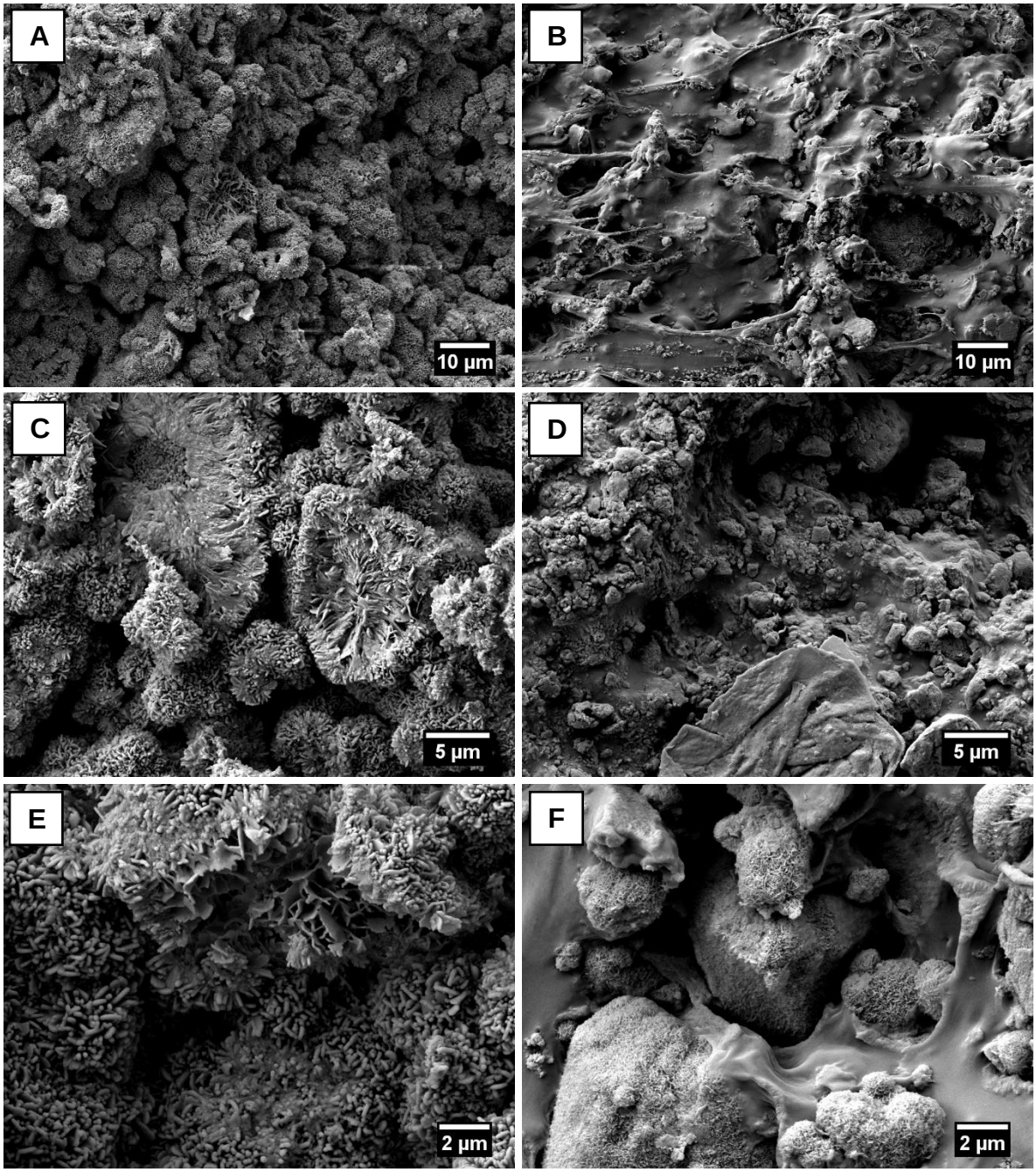

Figure 13: Scanning electron microscope (SEM) images of set cement samples made from α-TCP without Aquapol (**A, C, E**) or with Aquapol addition (**B, D, F**) after storage for 7 days at 37°C in a water bath. Magnification: **A, B** 2000x, **C, D** 5000x, **E, F** 10000x. Samples were prepared containing 2 g polymer-cement paste and 1 ml Na_2HPO_4.

Figure 13 displays SEM images of samples without and with polymeric addition. Needle-like and plate-like crystals in a size range of 0.5 to 1 µm built up in the reference cement (**Figure 13A, C, E**), which is typical for HA formed by α-TCP hydrolysis.[32, 394] The modification with Aquapol (**Figure 13B, D, F**) led to a decreased crystal size of HA; furthermore, a polymeric matrix could be observed, which filled the pores of the cement structure.[390] These findings were already demonstrated before for a matrix formed of HEMA and a-TCP[76, 378] and these structures are very similar to polymer bridges built in polymer modified concrete.[395-396]

3.4 Conclusion

In this section, the development of a new polymer-cement system from an isocyanate-functionalized prepolymer and a fast setting calcium phosphate cement powder is introduced. The setting reaction of both components formed interpenetrating networks (IPNs) of a polyurethane hydrogel and a matrix of entangled HA crystals resulting in a material with hard but elastic properties. Possible applications of such a material are either self-setting and load bearing bone implants or in civil engineering, e.g. as a tile adhesive. A similar application was shown in **chapter 4**, using the prepolymer additive for application as bone adhesive. Clearly, the material developed in this chapter is only a proof of principle and it would be necessary to optimize the system by varying the amounts of polymer or the ratio of the cement paste to liquid content. However, crucial properties of fresh mortar and concrete such as workability, air entrainment by pore formation and an accelerated setting behavior are already fulfilled by the new system; additionally, an adequate strength, deformability, and elasticity were achieved after setting.[59]

As shown above, promising results were obtained by using a bone cement, which is however not suitable for technical application. Hence, a transfer of these findings to a commercially available masonry cement was tested by combining calcium aluminate cement with Aquapol. The results are presented in **Figure 14**.

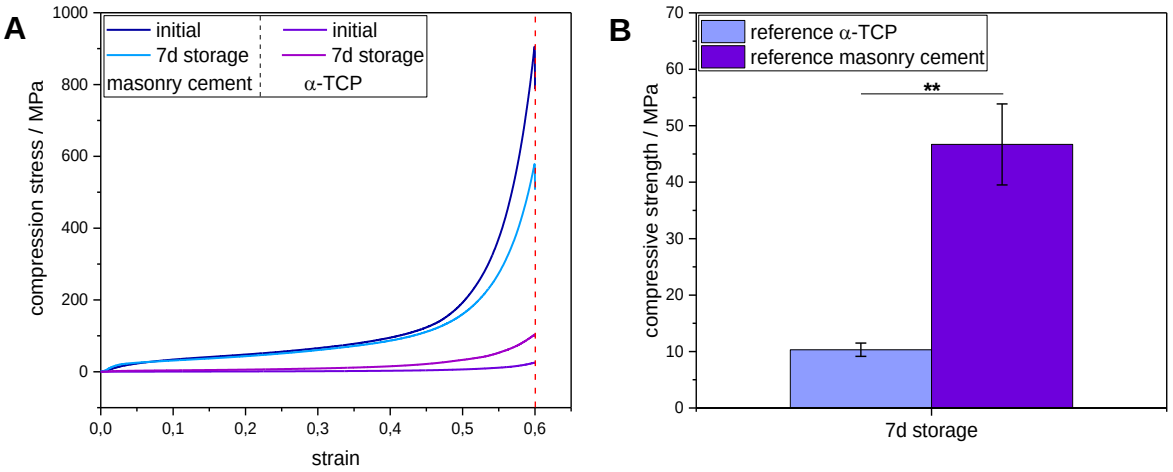

Figure 14: Comparison of the polymer-cement systems using Aquapol together with α-TCP or a commercially available masonry cement. **A** shows the comparison of Aquapol-functional cement mixtures, **B** the differences of the references. Samples were prepared containing 2 g polymer-cement paste and 1 ml Na_2HPO_4 whereas the reference was made from a PLR of 3 g/ml. Level of significance of 1-way ANOVA: ** means $p < 0.01$. (n = 6)

These results revealed that the mixture of NCO-functionalized prepolymers and cements was more resistant against higher compressive stresses than the system with α-TCP. Additionally, the 3-point bending test of the references without addition of Aquapol showed significant higher strengths for the commercially available cement system. These preliminary results should be considered in future experiments.

The use of reactive and water-soluble isocyanates building a hydrogel and forming an IPN together with cement powder is a novel approach and seems to be useful for the development of enhanced mortar and concrete.

4 Development of a bone adhesive by addition of NCO-sP(EO-*stat*-PO)

Many results of the following section were adapted from the research article “A Bone Glue with Sustained Adhesion under Wet Conditions” where L. Wistlich holds 1st authorship. She performed all experiments and wrote the whole manuscript by herself, except the preliminary mechanical, IR-spectroscopic and microscopic analysis of a similar system using different ceramic fillers, which were performed by A. Rücker who wrote her dental doctoral thesis on the basis of these results. M. Schamel helped with answering questions, while A.C. Kübler, U. Gbureck und J. Groll were involved in supervision and proof-reading of the mansucript.

4.1 Introduction

4.1.1 Development of a new bone adhesive

Many experimental bone adhesives suffer from a quite low adhesion to bone due to the wet environment in the human body.[87] Approaches to solve this problem include the use of sandcastle or frog glue[397] derived from natural materials or by means of DOPA moieties which are known to reveal a better adhesion in wet environment. Because many bone glues fail regarding the fixation of wet bone surfaces, the objective introduced in this chapter mainly deals with enhancing the hydrolytic stability of the interface between bone and adhesive material.

Here, an alternative material approach is introduced which exploited hydrophilic NCO-sP(EO-*stat*-PO) molecules as reactive additives applied to a matrix consisting of a photochemically curable polyethylene glycol dimethacrylate (PEGDMA) matrix.[398] Polyurethanes bearing isocyanate moieties often serve as adhesive reagent for wet surfaces in technical applications such as wood.[399-400] Compared to isocyanate groups applied for technical tasks, the prepolymers in the current thesis reveal a quite low cytotoxicity *in vitro* and *in vivo*[401] because of the high molecular weight. Only 2 wt% of the whole polymer are occupied by the NCO groups at the endings of the polymer chains, which are rapidly reacting in a moist environment due to their hydrophilic nature. The crosslinking reaction of NCO-sP(EO-*stat*-PO) in water has been described in **chapter 2**.

4.1.2 Previous results with different ceramic fillers

The composition of bone adhesives is based on the use of ceramic fillers together with polymers from dental resins.[402] In this case, hydrophilic PEGDMA was chosen as dimethacrylate compound because this polymer is known to react for example with camphorquinone (CQ) and amine-bearing molecules followed by radical polymerization and to build up a highly branched network after photochemical curing with light.[403-404] For first experiments, amounts of 1 wt% CQ and 1 wt% N,N,N',N'-tetramethylethylenediamine (TEMED) as photoinitiator system were chosen. Further functionalization was achieved by the addition of different ceramic fillers such as struvite ($MgNH_4PO_4 \cdot 6H_2O$), newberyite ($MgHPO_4 \cdot 3H_2O$) or gypsum ($CaSO_4 \cdot 2H_2O$) to the polymeric phase, which should lead to an enhanced porosity after implantation due

to their quite high solubility. This could also result in the release of ions facilitating the ingrowth of bone cells leading to bone matrix regeneration.[28, 405]. 20-40 wt% NCO-sP(EO-*stat*-PO) was added as further ingredient, which is able to crosslink with protic functional groups like amines, thiols and hydroxyl moieties in a polyaddition reaction as already described in **chapter 2.3**. This reaction runs simultaneously with the radical photopolymerization of PEGDMA. An interpenetrating network structure is built where the isocyanates were expected to additionally facilitate bone adhesion through partial reaction with protic groups at the bone surface.[406]

The reactions were analyzed by FT-IR spectroscopy and the results showed a reaction degree of the methacrylate moieties of approximately 50-60% after 120 s irradiation similar to studies on dental resins consisting of bifunctional methacrylates according to Sideridou et al.[407] Additionally, hydrolysis of isocyanate moieties was observed by FT-IR analysis resulting in quantitative reaction after 60 min immersion in PBS (**Figure 15A**). At the same time, the partial dissolution of the mineral filler particles in PBS buffer could be proved by XRD (**Figure 15B**).[406]

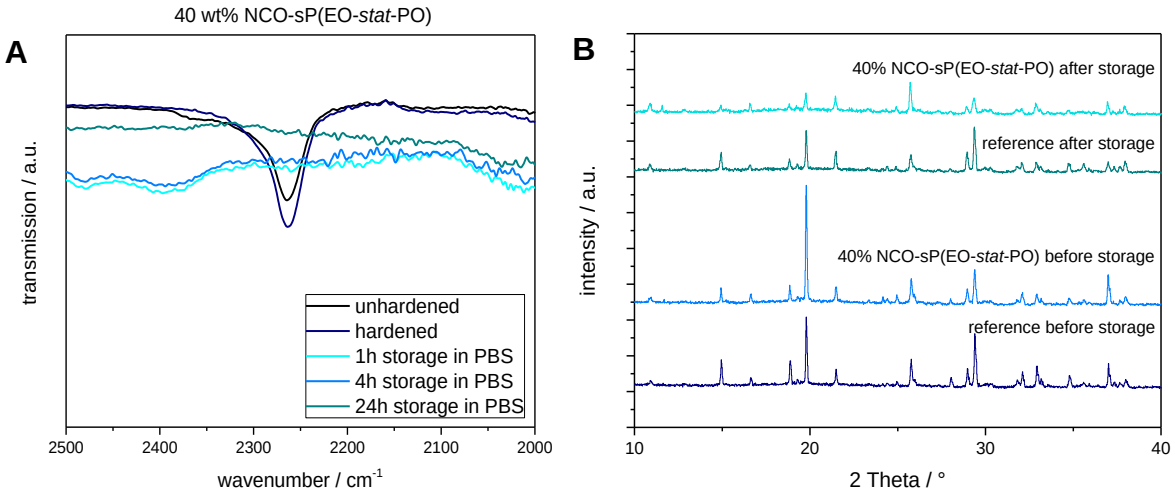

Figure 15: FT-IR and XRD measurements. **A**) Isocyanate peak of the adhesives with 40 wt% NCO-sP(EO-*stat*-PO) with newberyite filler during the storage period of 24 h. **B**) X-ray diffraction patterns of the samples with newberyite as filler before and after 7 d of storage in PBS. All diffraction peaks correspond to newberyite (powder diffraction file (PDF) No.: 35-0780). (Reprinted from [391]. Copyright (2017) with permission from John Wiley and Sons)

To determine the failure mode of bone adhesives on bovine bones, samples without additive and with 20 wt% and 40 wt% NCO-sP(EO-*stat*-PO) were examined macroscopically and microscopically. In **Figure 16**, a cohesive failure was assessed

since distinct residues from adhesive materials could be observed on the surface of bone after performing the shear bonding test in comparison to the reference bone piece where no residues were visible. (**Figure 16A**) This suggested an adhesive mode of failure of samples without NCO-sP(EO-*stat*-PO) addition. In **Figure 16A, C** and **E**, it could be demonstrated by stereomicroscopy that specimens with 40 wt% NCO-sP(EO-*stat*-PO) built a thick layer of adhesive compared to the reference (**Figure 16A, B, D**) and to samples with 20 wt% additive as well. This was confirmed by SEM investigations, where significant residues of bone glue were apparent on the surface of NCO-functionalized samples (**Figure 16G**) in comparison to those without addition of the functional prepolymers (**Figure 16F**).

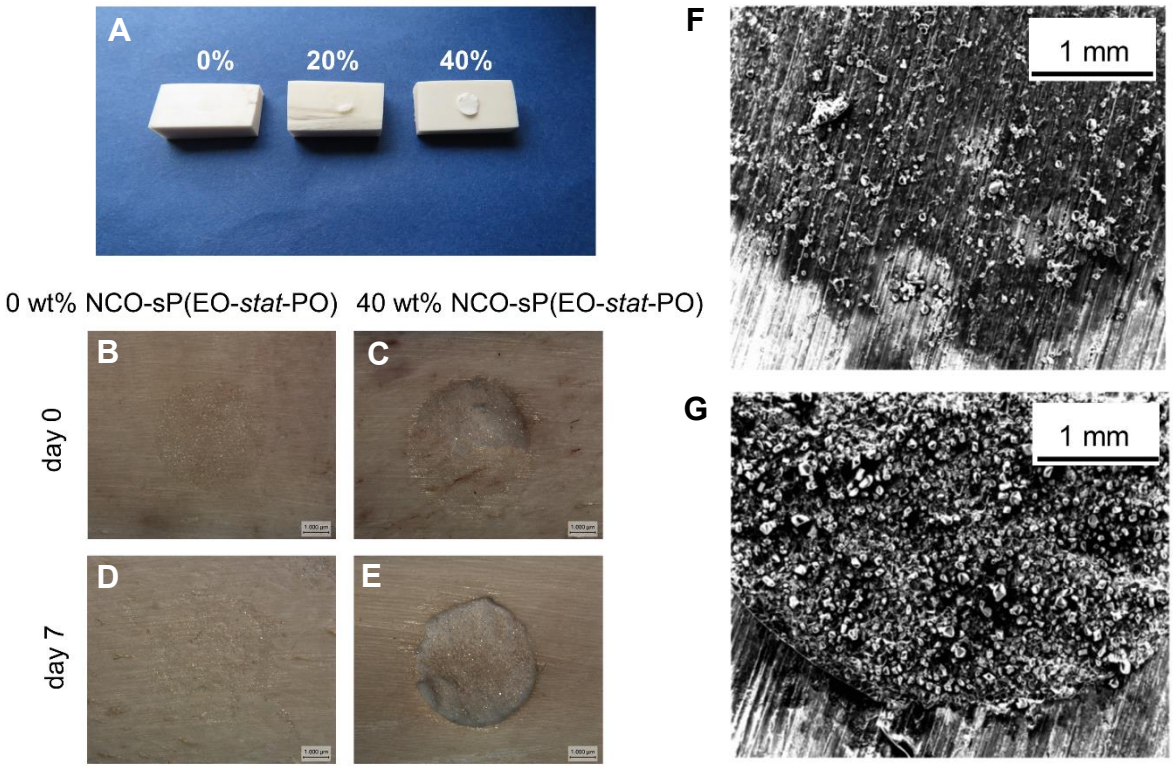

Figure 16: Macroscopic and microscopic analysis of the interface. Bone surfaces of adhesives with newberyite filler and varying contents of NCO-sP(EO-*stat*-PO) were examined after 7 d storage in PBS and shear testing. The adhesive areas of the reference sample and a sample with 20 or 40 wt% NCO-sP(EO-*stat*-PO) are shown as example in **A**. **B**-**E**) Interface micrographs of samples with newberyite as mineral filler without addition of NCO-sP(EO-*stat*-PO) and with 40 wt% NCO-sP(EO-*stat*-PO) before and after 7 d of storage in PBS. **F**, **G**) Scanning electron micrograph of a 0% (reference) and a 40 wt% NCO-sP(EO-*stat*-PO) containing sample with newberyite filler after storage for 7 d in PBS and subsequent shear testing. (Reprinted from [391]. Copyright (2017) with permission from John Wiley and Sons)

4.1.3 Subsequent tests regarding reproducibility and cytocompatibility of the developed system

In this chapter, the new bone adhesive system consisting of a PEGDMA matrix building an IPN together with NCO-sP(EO-*stat*-PO) as functional additive was examined further regarding cytocompatibility, whereas based on these results, the composition of the bone glue was modified concerning the amount of TEMED which was added to the initiator system. This was followed by investigation of the mechanical properties such as 3-point bending strength and adhesive strength on bovine bone of the altered formulation. Furthermore, other prerequisites described by Farrar[87] (shown in **Table 1** in **chapter 2.2**) were evaluated such as working and setting time, shelf-life and clinical applicability which might be influenced by the functional additive NCO-sP(EO-*stat*-PO).

4.2 Materials and methods

Bone adhesive preparation. 10 mmol poly(ethylene glycol) dimethacrylate (PEGDMA) were used as matrix for the polymeric phase. Samples with increased bonding strength were prepared by dissolving 20 wt% NCO-sP(EO-*stat*-PO) in the liquid PEGDMA. Subsequently, this solution was merged with 0.338 mmol (1 wt%) D,L-camphorquinone (CQ) as radical initiator and stirred until complete dissolution. When TEMED was supplementary used as an activator, 0.483 mmol (1 wt%) or 0.048 mmol (0.1 wt%) was added and stirred again. Newberyite was prepared as described before[391] and was sieved <125 µm before use and mixed with polymeric phase in a powder-to-liquid ratio (PLR) of 1.1:1 g/ml.

Sample preparation. For 3-point bending strength testing, bone adhesives were filled in cuboid silicone rubber molds (3 x 4 x 25 mm) and subsequently polymerized with an LED hand lamp (Bluephase100, Ivoclar Vivadent, Ellwangen, Germany). The samples were exposed to light of 385-515 nm for 30 s and this process was repeated three times. Afterwards, the samples were removed and irradiated from the bottom for additional 30 s to achieve an overall polymerization time of 120 s. The test rods were either examined directly after crosslinking or stored in phosphate buffered saline (PBS) for 24 h or 7 d at 37°C and investigated after this storage time. The 3-point bending test was performed during axial bending at a crosshead speed of 5 mm/min using a static mechanical testing machine Zwick 1440 (Zwick, Ulm, Germany) and a 10 kN load cell. The bending strength (BS) was calculated according to

$$BS\ [MPa] = \frac{3\ F_{max} * l}{2 * b * h^2} \qquad (1)$$

where F_{max} is the failure load, l is the span length, b is the width and h is the height of the samples.

Preparation of bone disks and adhesion tests. First, the diaphysis of bovine femurs obtained from a local butcher was divided into 2.5 cm thick slices using a bone saw which were then cut into 0.5-1.0 cm thick pieces with a belt-saw Bizerba FK 22 (Balingen, Germany). By mechanical treatment with 80 grit wet sandpaper, the bone pieces were grinded to a final size of about 1 cm x 2 cm x 0.5 cm and stored in PBS until use to prevent drying. The bone disk was placed in a poly(methyl methacrylate) cavity fixed with a silicone rubber matrix with a bore hole of 6 mm diameter x 5 mm height, and a metal plate. The liquid bone adhesive was applied in the resulting hole

and cured with the LED lamp four times for 30 s as mentioned above. To determine the shear strength of the bone adhesive joints, the static mechanical testing machine Zwick 1440 with a 2.5 kN load cell was used; the shear strengths were tested after 1 h dry storage as well as after 1 d and 7 d storage in PBS at 37°C. The test settings were 1 N for the initial preload and a cross-head speed of 1 mm/min.

***In vitro* cytocompatibility.** Cytocompatibility was determined according to DIN EN ISO 10993-5 and 10993-12. Therefore, disk-shaped samples with a diameter of 15 mm and a height of 2 mm were produced as described above. Bone adhesives with newberyite filler, 1 wt%, 0.1 wt% or 0 wt% TEMED and 20 wt% NCO-sP(EO-*stat*-PO) as well as pure hydrogels from 20 wt% NCO-sP(EO-*stat*-PO) prepared with H_2O were examined using mouse fibroblasts L929 CC1 (ATCC, Wesel, Germany) and human fetal osteoblast cell line hFOB 1.19 (LGC Standards, Wesel, Germany). Fibroblasts were cultured in Dulbecco's modified Eagle's medium (DMEM) supplemented with 1% penicillin and streptomycin, 1% 4-(2-hydroxyethyl)-1-piperazineethanesulfonic acid (HEPES) buffer (1M solution) and 10% FCS and incubated according to the manufacturer's instructions in a humidified 5% CO_2 incubator at 37°C. Osteoblasts were cultured in DMEM supplemented with 1% penicillin and streptomycin, 0.3 mg/ml geneticin (G-418 sulfate) and 10% FCS and incubated a humified 5% CO_2 incubator at 34°C. Cytocompatibility tests were performed on bone adhesives with newberyite filler and different amounts of TEMED (0 wt% and 0.1 wt%) without and with 20 wt% NCO-sP(EO-*stat*-PO). Samples were transferred in a 24-well plate (Nunc, Wiesbaden, Germany) in quadruplicate and washed three times with sterile PBS. After disinfection with 1 ml ethanol for 5 min, the specimens were washed with PBS twice. The samples were incubated in DMEM for 48 h, the eluate was separated and used undiluted for cell tests. Cells were seeded in a 48-well plate (Nunc, Wiesbaden, Germany) in triplicate with an initial cell density of 50,000 cells/ml. Vekoplan KT polyvinyl chloride (PVC) plates (König GmbH, Wendelstein, Germany) and polystyrene (PS) surfaces of the cell culture plates were used as controls. The eluate was incubated on samples for 48 h, followed by evaluation of L929 fibroblast cell number using a cell counter CASY 1 (Roche, Mannheim, Germany). After cell cultivation for 3, 7 and 10 d, hFOB 1.19 cell numbers were counted. The cell proliferation reagent WST-1 (Roche Diagnostics, Mannheim, Germany) was applied to determine the cell activity of both cell types. Therefore, WST-1 was mixed with cell culture medium in a ratio of 1:10. Then, this

mixture was added onto the cells and after incubation at 37°C for 30 min, the absorption of the supernatant was measured by means of a Tecan Spark 20M plate reader (Tecan, Crailsheim, Germany) at 450 nm. Both cell activity and cell number were normalized to PS as reference.

Analysis of variance (ANOVA). ANOVA was examined by means of SigmaPlot (Systat Software GmbH, Erkrath, Germany) using 1-way, 2-way, or 3-way ANOVA depending on the raw data. For calculation of the statistical significance, a post hoc Tukey test was performed.

4.3 Results and discussion

As mentioned above, the aim of this project was to develop a system using isocyanate-terminated six-armed star-shaped prepolymers (NCO-sP(EO-*stat*-PO)) as functional additive to improve the adhesion of a photo-curable PEGDMA matrix to wet bone. *In vivo*, the bone surface will in addition be contaminated with fats and proteins which may have a detrimental effect on the adhesion ability. An IPN was formed by simultaneous polyaddition of NCO-sP(EO-*stat*-PO) and radical polymerization of PEGDMA. The functional NCO groups within this network will contribute to bone adhesion by interacting partially with protic groups (e.g., thiols, amines, hydroxyl groups) at the surface of the bone. Adhesives containing these components were examined regarding their mechanical properties with a 3-point bending test and a shear bonding strength test on bovine bone. Cell tests with two different cell lines showed cytocompatibility of the samples. In literature, Farrar mentioned some prerequisites[87] which were also tested in this chapter.

4.3.1 Investigation of cytocompatibility

Adhesives with newberyite filler were found to have superior mechanical properties[391, 406] and hence were used to determine cytocompatibility. This is important since compounds containing low molecular weight isocyanates are known to be harmful or toxic when transferred into the human body.[392] Isocyanates react fast with protic groups and in general, low molecular weight compounds have a high mobility *in vivo* and are able to be incorporated by cells. An advantage of the isocyanate functional prepolymers from this thesis is that the NCO groups only occupy less than 2 wt% of the molecule and due to the high molecular weight of 12 kDa, the migration into tissue and cells is limited. NCO-sP(EO-*stat*-PO) show a very fast hydrolysis to amine groups and subsequently a crosslinking reaction building urea bridges and a three-dimensional network; therefore, remaining isocyanates are fixed inside the system and are not able to be released into the environment. This point is very important for a feasible application in the human body.

4.3.1.1 Preliminary tests

In preliminary cell tests, attachment and survival of L929 fibroblasts and human fetal osteoblastic cells (hFOB 1.19) was examined on samples containing 1 wt% CQ, 1 wt% TEMED and 20 wt% NCO-sP(EO-*stat*-PO) to prove their cytocompatibility. At first, some issues occurred regarding the sterilization of the samples. After washing in PBS, drying at 37°C, and also after gamma sterilization, the specimens remained stable, but after incubation in the cell culture medium at 37°C, the samples disintegrated (**Figure 17**). Therefore, it was very difficult to seed cells on the surface and first results showed cell apoptosis on specimens in comparison to the reference surface polystyrene.

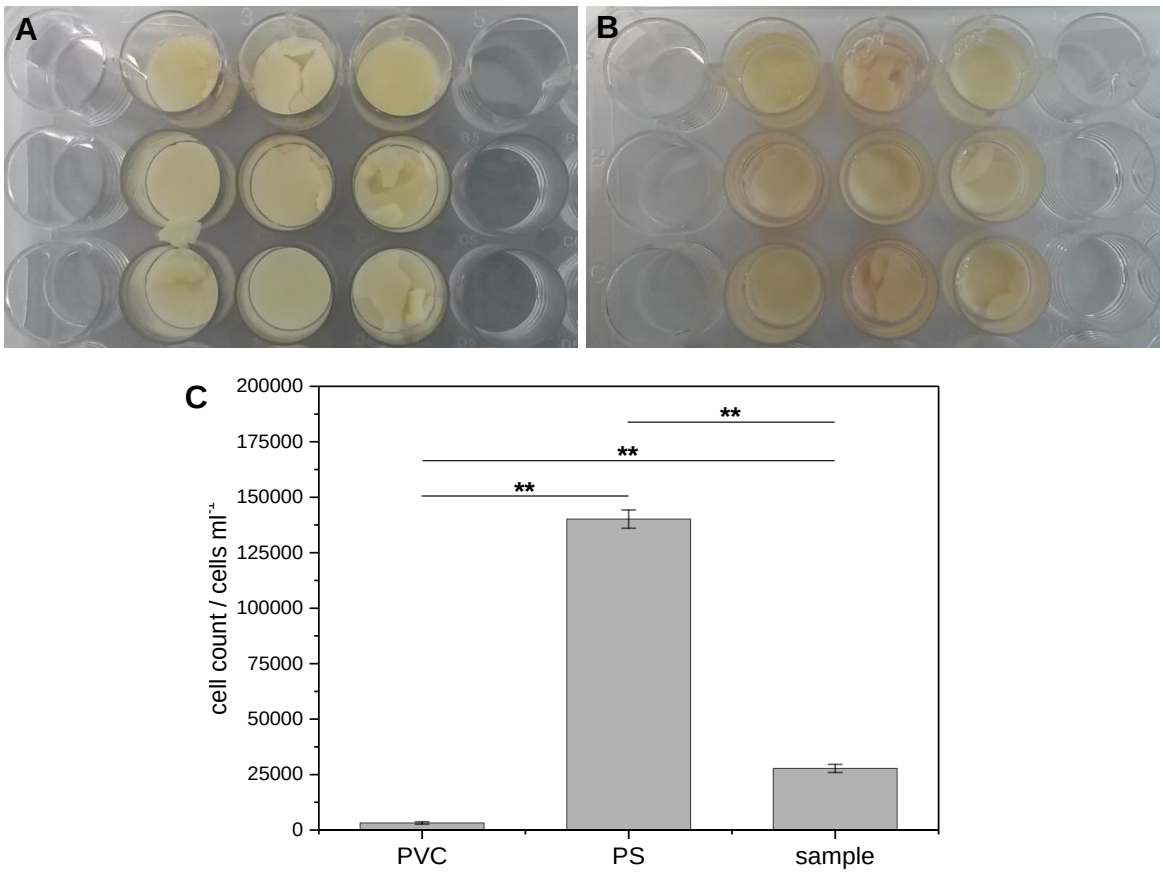

Figure 17: Samples after immersion in cell culture medium in 24-well plates and cell seeding with hFOB 1.19. The behavior of disks after 3 days (**A**) and after 10 days of cell culture (**B**) is shown. **C**) Preliminary results of cell growth of L929 fibroblasts in eluate medium of samples containing 1 wt% CQ, 1 wt% TEMED and 20 wt NCO-sP(EO-*stat*-PO). PVC serves as a negative control where no cell attachment should occur. PS is the positive control which is a hydrophobic surface and on which cells show a good attachment via unspecific protein adsorption. Level of significance of 1-way ANOVA: ** means $p < 0.01$. ($n = 3$)

As described in a guideline of Rutala et al., an oxidation of polyethylene depending on the ionizing radiation could appear.[408] This may be the reason for the disintegration of the bone adhesive samples after immersion in medium. Hence, a reason for apoptosis of hFOB 1.19 is that probably residual cytotoxic monomers or additives are released from the samples because of incomplete polymerization.

Therefore, the experimental set-up was changed into using an eluate test instead of seeding cells directly on the samples. Furthermore, the component has to be found which may be the reason for cell apoptosis. In **Figure 17**, it was only demonstrated that the whole sample act toxic for cells.

4.3.1.2 Investigations with different TEMED concentrations

More detailed examinations of the *in vitro* cytocompatibility revealed that the component with the highest cell toxicity must be TEMED[409] since diminishing the TEMED concentration from 1 wt to 0.1 wt% led to an increase of cell number and activity to more than 80% compared to the reference PS (100%). This value describes a specified requirement that a surface can be termed as “cytocompatible” according to ISO standard. Cytocompatibility was demonstrated for the pure hydrogel of NCO-sP(EO-*stat*-PO) which showed even higher cell numbers and activity, for PEGDMA with the CQ/TEMED initiator system and furthermore for the complete system of bone adhesive (**Figure 18**).

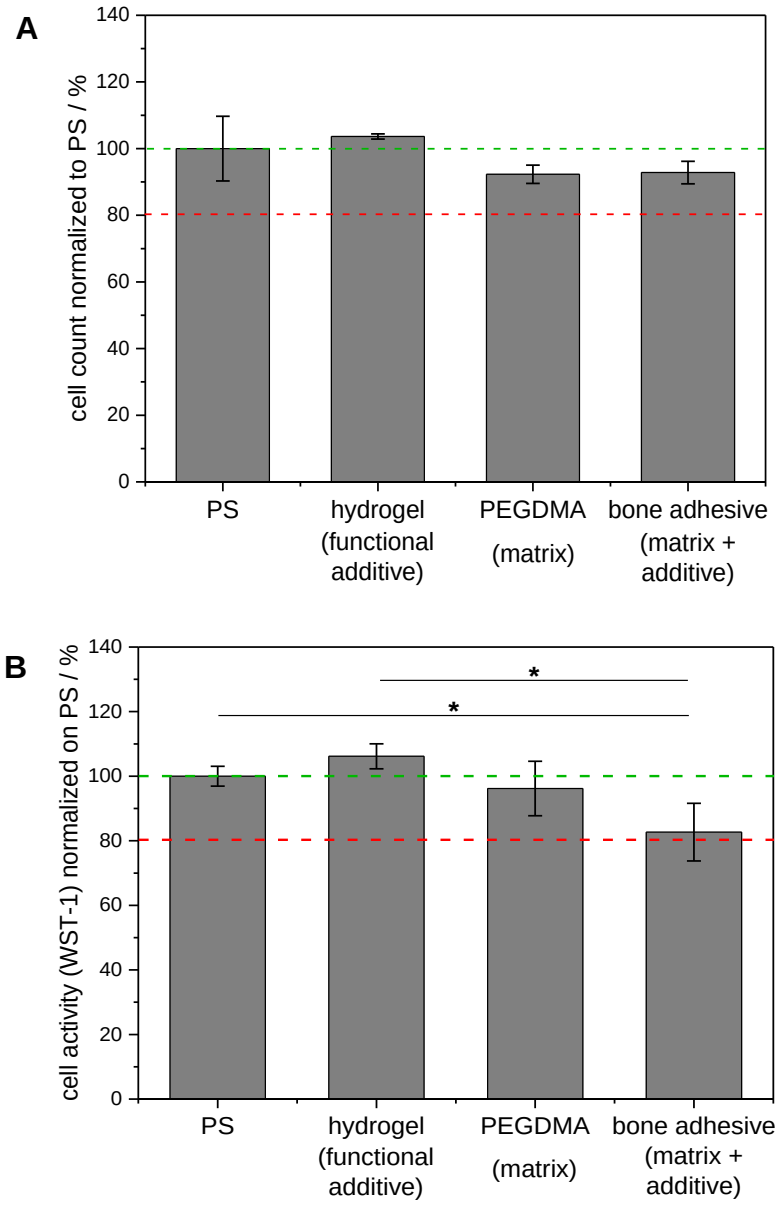

Figure 18: Cytocompatibility tested with L929 mouse fibroblasts. Cell number (**A**) and cell activity (**B**) according to WST-1 test of a 20 wt% NCO-sP(EO-*stat*-PO) hydrogel as functional additive and bone adhesives with and without 20 wt% NCO-sP(EO-*stat*-PO) using newberyite as filler and PEGDMA as matrix according to DIN EN ISO 10993-5 and -12. Samples were prepared with 0.1 wt% TEMED. Cells were cultured in a 100% DMEM eluate from the samples for 48 h. Level of significance of 1-way ANOVA: * means $p < 0.05$. (n = 3) (Reprinted from [391]. Copyright (2017) with permission from John Wiley and Sons)

Because the *in vitro* experiments with L929 fibroblasts showed promising results, the eluate test was repeated with the cell line hFOB 1.19 to reveal proper cytocompatibility also towards bone cells. This was done by incubation of samples prepared without and with 20 wt% NCO-sP(EO-*stat*-PO) and with 0 wt% and 0.1 wt% TEMED addition in cell culture medium. hFOB 1.19 were cultivated with 100% eluate for 3, 7 and 10 d and cell

count and activity were measured (**Figure 19**). It could be demonstrated that all samples achieved almost 80% and therefore showed a good or even better cell activity and cell count after 10 days of cell culture in comparison to PS as reference surface.

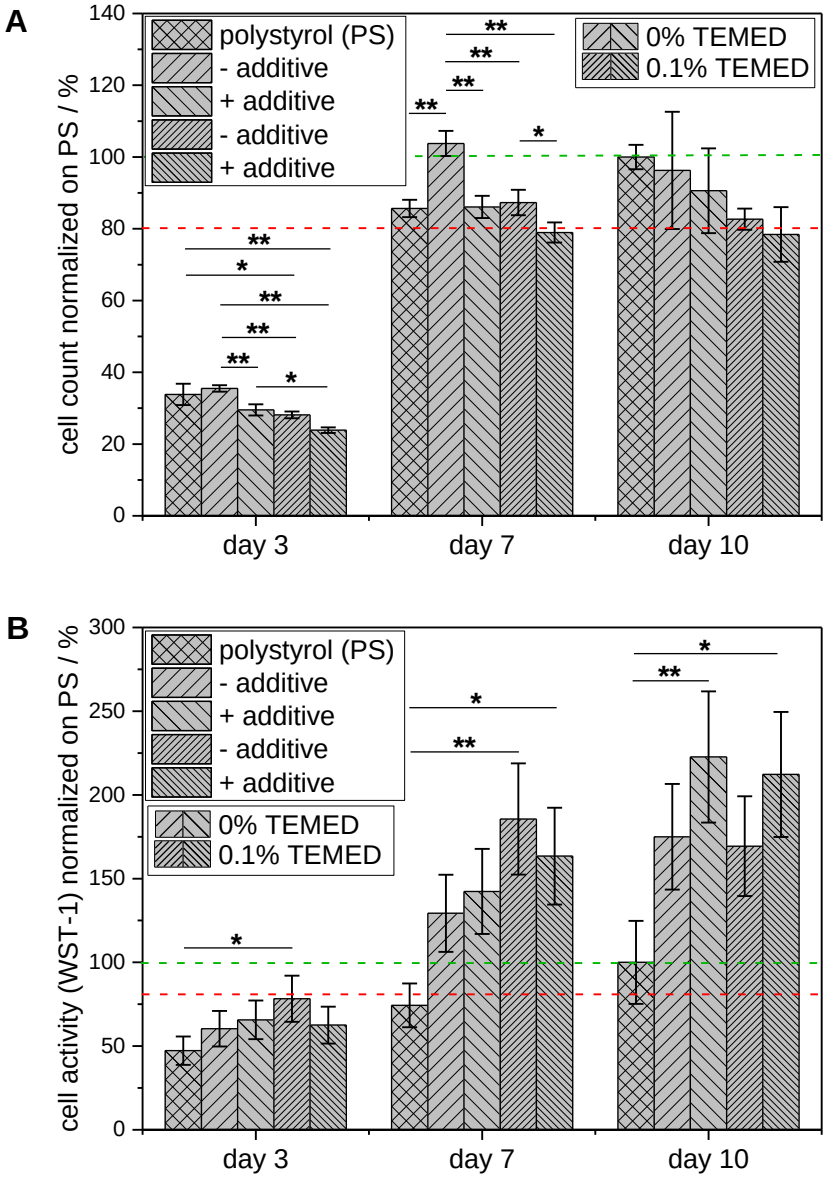

Figure 19: Cell number (**A**) and cell activity (**B**) of hFOB 1.19 cells according to WST-1 test of bone adhesives with and without 20 wt% NCO-sP(EO-*stat*-PO) with newberyite as filler using eluate testing. Samples were prepared with 0 wt% or 0.1 wt% TEMED. Cells were cultured in 100% DMEM eluate from the samples for 3, 7, and 10 d. Level of significance of 1-way and 3-way ANOVA: * means $p < 0.05$, ** means $p < 0.01$. (n = 3) The statistical significance is indicated between different TEMED concentrations and different NCO-sP(EO-*stat*-PO) contents, not between time points. (Reprinted from [391], Copyright (2017) with permission from John Wiley and Sons)

In summary, these findings demonstrated a good cytocompatibility of the NCO-sP(EO-*stat*-PO) additive and pointed out the crucial influence of TEMED on cell tolerance using it in a system together with CQ.

4.3.2 Mechanical testing: 3-point bending strength and shear bonding strength on bovine bone of samples with different TEMED amounts

Since the decrease of the TEMED amount used in the bone adhesives may also affect other material parameters, 3-point bending strength and shear bonding strength tests were repeated for samples with 0 wt% and 0.1 wt in comparison to 1 wt% TEMED addition. The outcomes are displayed in **Figure 20** and show the even higher bending strengths which were achieved by adding no TEMED or the lower TEMED concentration for initial time points. For the samples without NCO-sP(EO-*stat*-PO) the strength increased significantly from 5 MPa to 11 MPa while for samples with 20 wt% NCO-sP(EO-*stat*-PO) only an improvement of about 1 MPa could be observed. After storage in PBS for 1 and 7 days at 37°C the bending strength of all samples was in the range of 1 to 2 MPa (**Figure 20A**). The possible reason for this unambiguous decrease might be the water uptake and swelling of the crosslinked NCO-sP(EO-*stat*-PO) hydrogel on one side[235-236] and the dissolution of newberyite from the polymerized PEGDMA matrix on the other side.[410]

Regarding the bonding strength on bovine bone (**Figure 20B**), it could be noticed that for all samples, the bone glue without TEMED was superior in comparison to the samples with 0.1 wt% and 1 wt% TEMED. Initially, the shear bonding strength was higher for samples without NCO-sP(EO-*stat*-PO) addition and with lower TEMED content, but after storage in PBS, the samples with the functional additive showed bonding strengths of approximately 0.2-0.6 MPa whereas the samples without NCO-sP(EO-*stat*-PO) lost their adhesiveness to bone. This effect was more evident after 7 d of PBS storage.

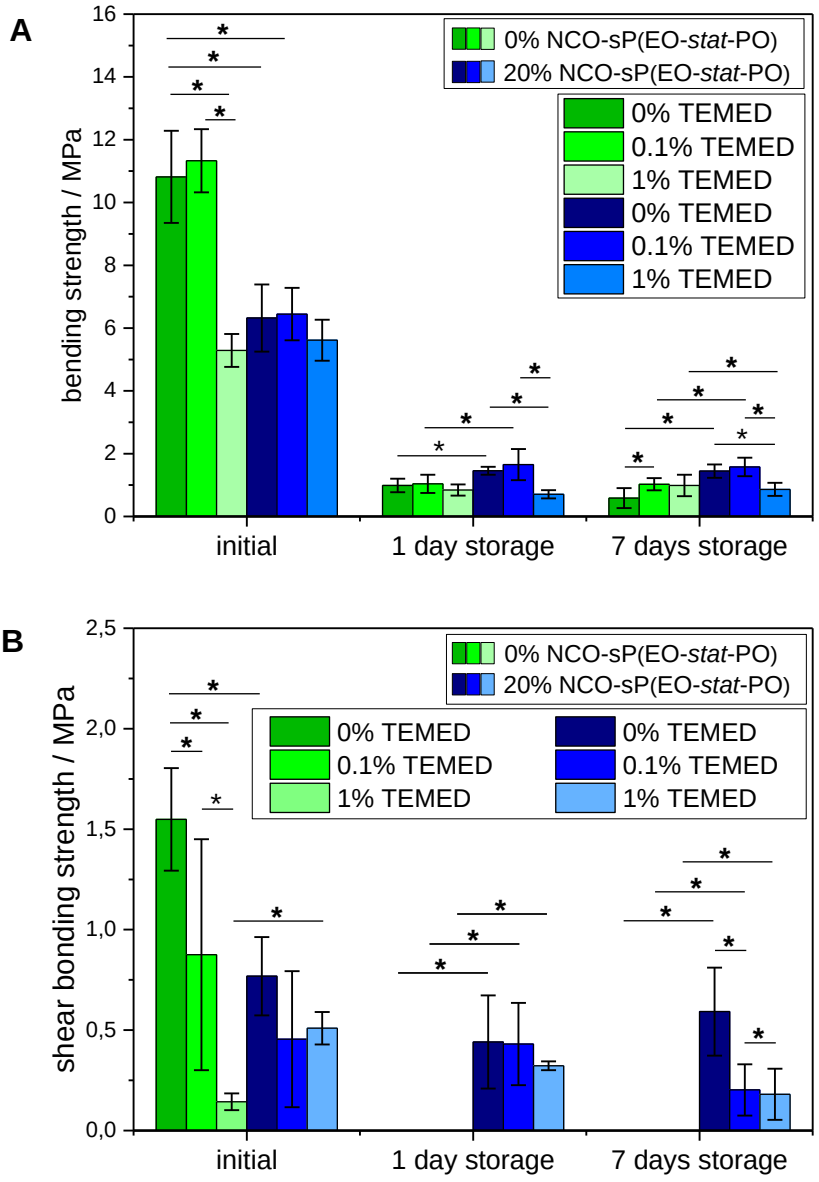

Figure 20: Mechanical testing with 0 wt%, 0.1 wt% and 1 wt% TEMED. Bending (**A**) and bonding strength (**B**) of newberyite samples without and with NCO-sP(EO-*stat*-PO) with different TEMED concentrations. Level of significance of 3-way ANOVA: * means $p<0.05$ ($n = 6$ for bending strength, $n = 5$ for shear bonding strength). The statistical significance is indicated between different TEMED concentrations and different NCO-sP(EO-*stat*-PO) contents, not between time points. (Reprinted from [391], Copyright (2017) with permission from John Wiley and Sons)

The enhancement of adhesive strengths to bovine bone after one week could originate from polymer swelling in aqueous surrounding which extends the contact surface. Another reason might be tensions inside the material due to shrinkage during the polymerization reaction. Weber and Chapman[99] reported that in general, it is very delicate to quantify adhesion forces on bone and that values under 0.2 MPa indicate a

bonding strength which is too low and inappropriate for *in vivo* applications.[411] In the aforementioned experiments, the values lay above this threshold, and for lower TEMED amounts the bonding strength was even higher. For clinical researchers dealing with bone adhesives, the paramount demand is the transient adherence of small bone debris, and not necessarily the adhesion for a longer time which could be achieved through fixation with screws and plates.

In comparison to other adhesive materials like cyanoacrylates[119, 412] or functionalized PMMA cements,[125, 413] the developed bone glues prepared from newberyite, PEGDMA and NCO-sP(EO-*stat*-PO) showed lower bonding strengths. However, it is difficult to compare values from literature due to differences in testing and aging regimes (e.g. dry vs. wet storage of samples) or varying storage times not exceeding 24 h. Here, the samples were kept for up to one week in PBS at 37°C to mimic the wet environment in the human body and the specimens did not lose their adhesion to bovine bone. In literature, Brauer et al.[114] could show for bone adhesives consisting of cyanoacrylates with ethyl or butyl moieties a higher adhesive strength of 4.7 MPa and a storage time for 30 d. Bou-Francis and Ghanem calculated for commercially available adhesives containing cyanoacrylates or PMMA cements adhesion strengths of approximately 2.5 MPa.[414] They investigated the samples in dry and wet state with different measuring configurations on femoral bovine bone demonstrating a decrease of strength, when specimens were transferred from dry to wet environment. Here, the storage time did not exceed 24 h in water at 37°C.

Apart from that, using cyanoacrylates implicates toxicity of monomers and could build a physical barrier between the bone pieces; this makes these adhesives inadequate for the use *in vivo*.[113] Natural fibrin glues were also used in literature before, but they exhibited very low bonding strengths of 0.01 to 0.2 MPa regardless of whether stored in dry or wet conditions.[100] Bhagad et al.[415] could reveal a new approach by exploiting phosphoserines from caddisfly adhesive silk which is a natural gluing material together with copolymers. In this way, they were able to develop a bioresorbable system and to enhance the bonding strength by Ca^{2+} crosslinking. In another study, ceramic fillers like HA and TCP were mixed together with gelatin and alginate by Cohen et al.[416] This led to an enhancement of adhesive strength from 8.4 to 18.1 kPa using it in soft tissue; in general, these values did not achieve the postulated threshold at all but are in the range of soft tissue bonding strength.

4.3.3 Investigations of clinical applicability of bone adhesives

As described by Farrar,[87] besides mechanical stability, stable adhesion and shear force in a wet environment, there are many additional requirements for bone adhesives including an appropriate working time to fill the bone adhesive into gaps, a fast setting time and preferably a non-exothermic curing reaction. Additionally, shelf-life, the ability to sterilize the material without toxic by-products and a cost-effective use play an important role.

The bone glue developed here already fulfills some prerequisites as it is possible to prepared it quickly at room temperature, it is biocompatible and ready to use after preparation without addition of other reagents. A practical *ex vivo* application is shown in **Figure 21A** and **B**, where the adhesive was used to fix a porcine jawbone fracture. In contrast to adhesives which cure by chemical reactions as 2-component systems, photochemical hardening of adhesives expands the time frame for the surgeon to arrange bone pieces in the right position, and the hardening procedure occurs on demand by irradiation. Another advantage of the adhesive is the relatively low viscosity which makes it easier to apply the paste and to ensure an appropriate wetting on the bone surface without spreading all over the sample.

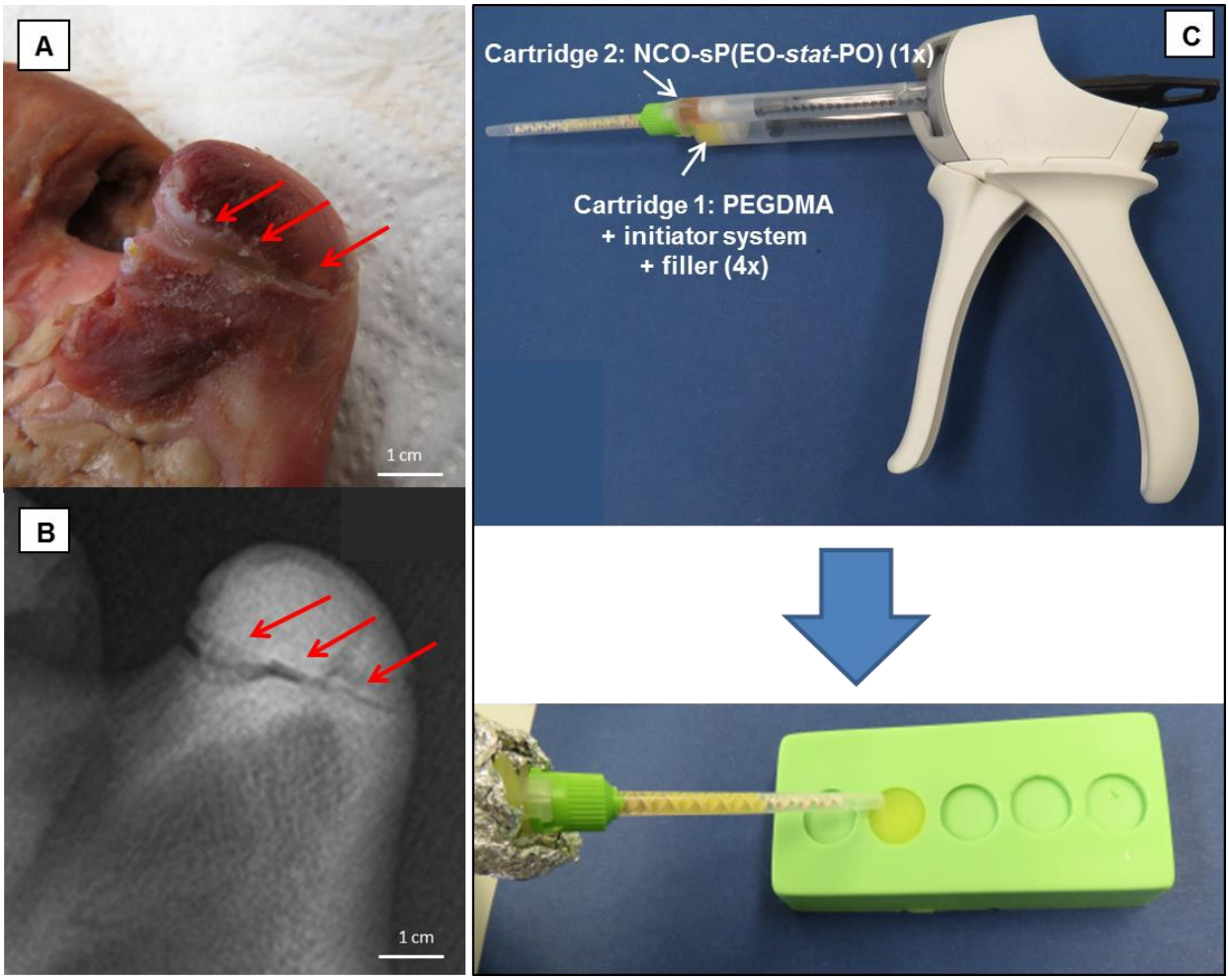

Figure 21: *Ex vivo* testing for demonstrating clinical applicability. **A**) Photograph and **B**) X-ray image of fixing of a porcine jawbone by using a bone adhesive with 20% NCO-sP(EO-*stat*-PO). **C**) Bone adhesive filled in a double cartridge syringe. One cartridge contained PEGDMA + initiator system + newberyite filler, the second cartridge included NCO-sP(EO-*stat*-PO). The mixing ratio was 4:1. (Reprinted from [391], Copyright (2017) with permission from John Wiley and Sons)

Concerning the shelf life of the engineered adhesives and moreover to ensure a proper working time for the surgeon, a storage of at least 8 months could be demonstrated for pastes without NCO-sP(EO-*stat*-PO) addition when preserved under light protection. Here, it was still possible to fabricate adhesive specimens which showed the same appearance and properties as samples prepared from freshly mixed pastes. Nevertheless, mixtures functionalized with the isocyanate prepolymers hardened within 2 d in the cartridge which could be explained by reaction of NCO-groups with water. This might either stem from the PEGDMA or from crystal water released from the newberyite filler. A possible solution for this problem is shown in **Figure 21C**. Here, a double cartridge delivery system (MedMix, Switzerland) was used to separate the

two parts of PEGDMA system with filler and NCO-sP(EO-*stat*-PO) during storage. Both components were then directly mixed during extruding and application. Thereby, the storage time could be prolonged to at least 23 d under light protection at 4°C; until this time point, the pastes remained workable.

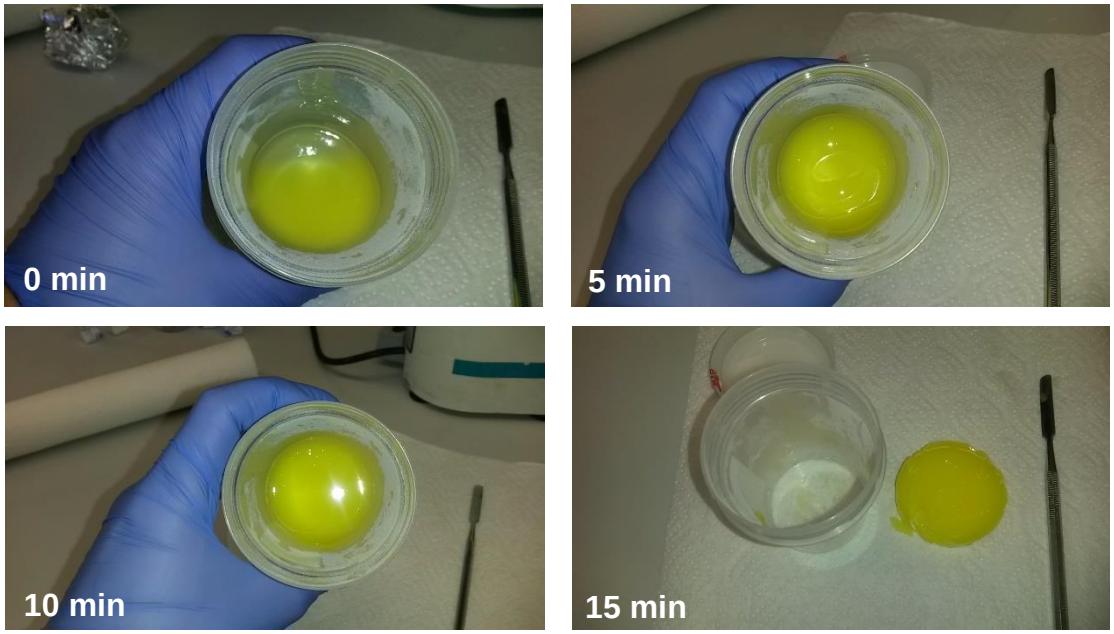

Figure 22: Time frame of hardening of the adhesive paste without NCO-sP(EO-*stat*-PO) addition. After 15 min, the sample is cured by light and could be removed from the beaker.

As examined before in previous works,[406] the viscosity of adhesives predominantly depends on the sort of filler and not on functional additives like NCO-sP(EO-*stat*-PO); also particle size distribution may contribute. Here, newberyite revealed an improved texture in comparison to other ceramic fillers like gypsum or struvite.[391] As an important clinical parameter, the working time was examined by preparing the paste with newberyite filler followed by storage without light protection at room temperature (**Figure 22**). For the samples without NCO-sP(EO-*stat*-PO), the working time was 15 min in comparison to 6 min for modified pastes with addition of the functional additive. Both time frames are adequate for a surgeon to prepare the fracture fixation and are found to be much slower as for fibrin adhesives.[88] The yellow color of the sample originates from camphorquinone which has not yet completely reacted because of lack of selective hardening by a light source with defined wave lengths.

4.4 Conclusion

In this part of the thesis, the high reactivity and bonding strength of isocyanate adhesives was exploited in a wet environment. Here, NCO-sP(EO-*stat*-PO) served as functional prepolymer added to a polymerizable PEGDMA matrix to build up interpenetrating networks of both components. The simultaneous crosslinking of both matrices led to an enhanced shear bond stability on cortical bovine bone after a storage time of 7 d in PBS buffer at 37°C. Furthermore, by seeding different cell types on photochemically crosslinked samples, cytocompatibility could be proved and the usability for clinical utilization was shown as well.

The developed bone glues meet clinical demands such as an appropriate adhesive strength in a wet surrounding as well as a sufficient working time and shelf-life. Concerning the formation of the IPN, the system might be further improved by a chemical crosslinking of both networks.[417] For instance, a mixture of methacrylate and isocyanate moieties in one compound is thought to promote a better stability of the whole system and additionally an enhanced adhesion strength. Another approach could be a further functionalization of the organic system with chelating moieties (e.g., bisphosphonates)[418] for divalent calcium or magnesium ions to stabilize the interface between the polymeric compounds and ceramic fillers and therefore to achieve ameliorated mechanical characteristics. A third method is linked to an enhanced degradation rate of the organic compound.[88-89] Here, crosslinkable methacrylate ester groups might be coupled with hydroxyl moieties from resorbable polyglycolides or polylactides. In literature, examination of poly(methacrylic-*co*-lactic) acid disintegration showed that an enhanced degradation over the time frame of 14 weeks was provoked by a higher number of lactic units present in the molecule. If samples carried more poly(ethylene oxide) moieties, the mass loss was down-regulated.[419]

As conveyed in literature, no standardized norms exist how to comprise and evaluate the adhesive strength of bone glues. Furthermore, the structure of the experimental set-up varies over a broad range.[414, 420] For example, MacDonald et al. performed a shear pull-out test using bone from the femur of dogs and achieved a shear strength of about 5 MPa.[421] Recently, Bou-Francis and Ghanem tested commercially available bone glues by using lap shear and butt joint test configurations.[414] Besides these shear strength testing regimes, also resistance to tensile strength should be further considered in testing bone adhesives. In addition, bone surfaces might be pretreated

before adhesion, e.g. by etching[422], roughening[100] or grinding.[423-424]. Another important point is the kind of bone used for testing, which could differ concerning the animal species (bovine, porcine)[99, 425] or if the used part of bone is of cortical or spongy nature.[100] Additionally, the aging requirements such as storage time or storage medium have to be considered for future experiments.[87, 120] Here, the development of standardized testing and aging regimes for bone adhesives is highly encouraged in future works.

5 Immobilization of antibodies and other proteins on electrospun fiber surfaces

Many results of the following section were adapted from the research article “Multimodal Bioactivation of Hydrophilic Electrospun Nanofibers Enables Simultaneous Tuning of Cell Adhesivity and Immunomodulatory Effects” where L. Wistlich holds first authorship. She performed all experiments and wrote the whole manuscript by herself, except the fluorescence experiments, which were performed by K.H. Heffels who showed these results in his doctoral thesis. J. Kums helped performing the experiments regarding the binding measurements of the fusion proteins at their institute and supported with evaluation of results. A. Rossi assisted with preparation of the electrospun fibers, while H. Wajant und J. Groll were involved in supervision and proof-reading of the mansucript.

5.1 Introduction

5.1.1 Experiments with multimodal functionalization of electrospun fibers using fluorescent dyes

The method to functionalize electrospun meshes exploiting different functional groups on their surface performed in this chapter was examined before.[427] Here, NCO-sP(EO-*stat*-PO) was used as a functional additive for rendering hydrophobic PLGA fibers to hydrophilic ones and various functionalization possibilities of these electrospun fibers were demonstrated.

As mentioned in **chapter 2.3.2**, NCO-sP(EO-*stat*-PO) migrates to the surface of the fibers during solution electrospinning with PLGA via surface segregation and is available for covalent crosslinking with molecules carrying protic groups like thiols or amines present in the electrospinning solution before the process (1). A second possibility for modification exists via reactive isocyanate groups which can be found on the fibers directly after electrospinning. These are able to react with sensitive moieties which are present in an aqueous solution. The incubation of the mesh in such a solution leads to covalent coating of the fiber surface with the reactive substances (2). To immobilize additional molecules on the fiber surface, the present isocyanates are hydrolyzed by treatment with water or by time via reaction with air humidity and the resulting amines are available for further modification.[381] For instance, amino groups can be treated with active ester moieties (3).

All mentioned functionalization steps were performed without the need of an additional crosslinker and were proved by means of fluorescent dyes and the strong biocytin-streptavidin interaction[428] recording fluorescence images.[426-427] For step (1), biocytin was used which was mixed into the spinning solution, for step (2), Alexa Fluor 568 cadaverine was added which is reactive against isocyanates and revealed a red fluorescence. As step (3), Alexa Fluor 488 succinimidyl ester was applied which interacts with amines showing a green fluorescence. Biocytin was detected after the process by addition of streptavidin (SA) labeled beads visible in optical images. The protocol and the results of fluorescence can be found in **Figure 23.**

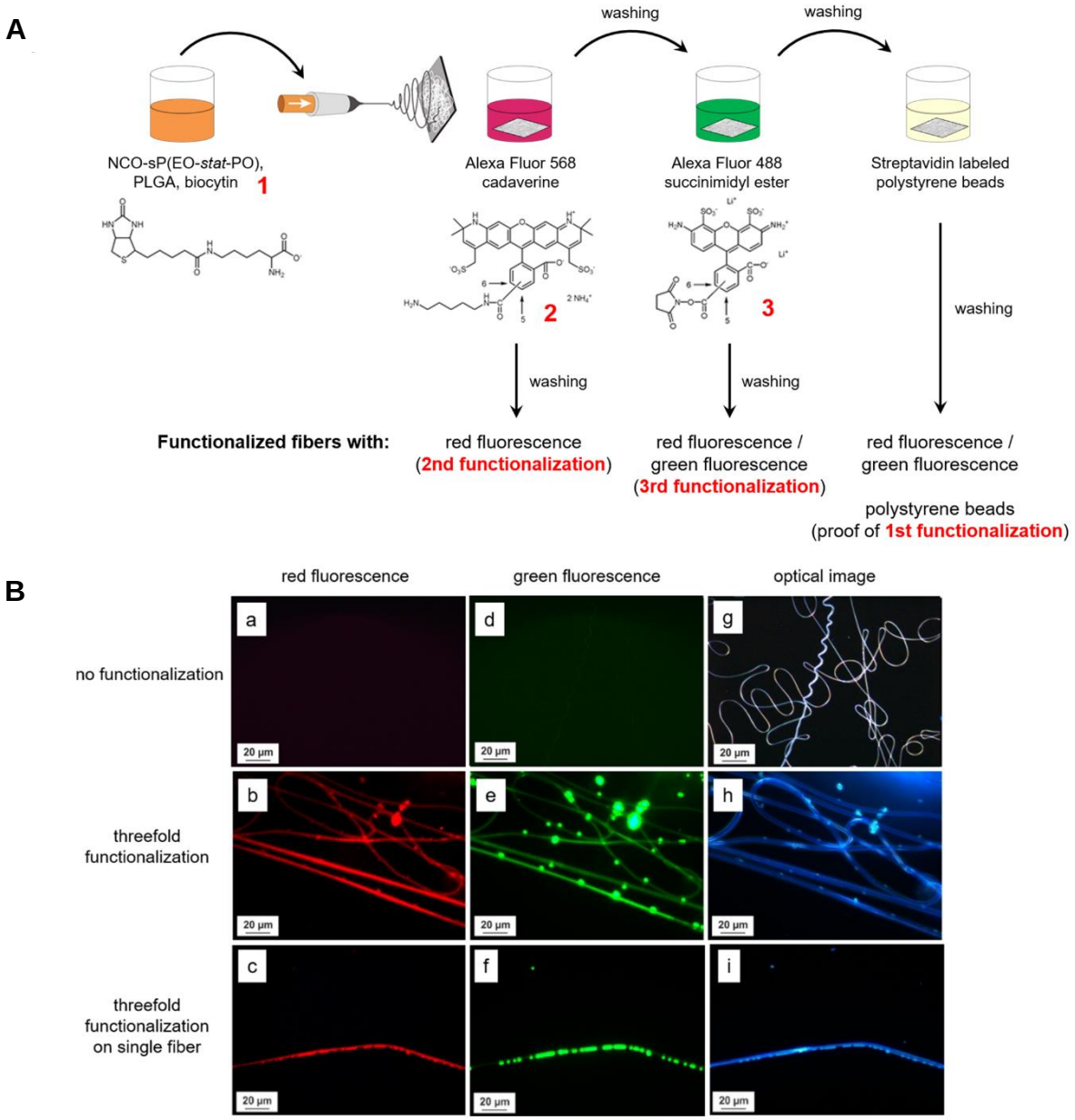

Figure 23: Threefold functionalization with biocytin and fluorescent dyes. **A**) Working protocol of immobilization of different components on electrospun fibers. The first functionalization occurred by adding biocytin to the spinning solution; the second functionalization was done by Alexa Fluor 568 cadaverine; the third functionalization happened with Alexa Fluor 488 NHS ester. To demonstrate the success of the first functionalization, binding of SA beads was evaluated. **B**) Results of fluorescent staining. Top row: Control images of NCO-sP(EO-*stat*-PO) / PLGA fibers without any staining. Panels **a**-**c** represent the red and panels **d**-**f** the green fluorescence. Panels **g**-**i** show the optical images. The exposure time of panels **a** and **d** was 20 000 ms. Triple functionalization with Alexa Fluor 488 succinimidyl ester, Alexa Fluor 568 cadaverine, and SA-labeled polystyrene beads is shown in the middle and bottom row. The exposure time of panels **b** and **c** was 1000 ms. Panels **e** and **f** had an exposure time of 20 000 ms. In the bottom row, one single fiber is depicted to better show the fluorescence. (Reprinted from [426], Copyright (2017) with permission from John Wiley and Sons)

5.1.2 Transfer of fluorescence results to a biological application

In order to find a possible biological application for the above-mentioned threefold surface modification examined via fluorescent dyes, the use of peptide sequences and larger proteins was focused. It is known that the cell attachment mediating peptide sequence RGD can easily be added to the spinning solution as described earlier and after the electrospinning process, it is present on the fiber surface promoting cell attachment.[46, 429-430]

In general, the biofunctionalization of textiles should facilitate the examination and the control of cell behavior on such fiber meshes in the nanometer range. Thereby, the most important challenge is the interaction of biomaterials with the surrounding tissue after having transferred them into the body. Inflammation processes could be provoked which might lead to the rejection of non-endogenous substances triggered by the immune system.[8-9] It would be advantageous to regulate the immune answer of the body in a way, that an urgent reaction is prevented and rejection of biomaterials is avoided; consecutively, the healing opportunities would be enhanced after implantation of a scaffold.

As found in literature, several approaches exist for influencing the immune system by biomaterials.[163] Different strategies were developed for manipulating inflammatory pathways via morphology of implants[431] or by means of altering the surface chemistry.[162] Additionally, electrospun meshes functionalized with various molecules such as proteins, growth factors or antibacterial drugs gained more attention. For example, Smith et al. studied the biocompatibility of electrospun blends of polydioxanone (PDO) and elastin for benefitting the *in situ* regeneration.[432] Both innate and required immune responses were tested and elastin was found to be biological active causing cell-mediated immunosuppression. Holan et al. used Cyclosporine A (CsA) as immunosuppressive drug blending it with PLA and fabricating nanofibers.[433] CsA remained pharmacologically active and was released over 96 h influencing local suppression of inflammatory reactions by down-regulation of proinflammatory cytokines like interleukins IL-2 and IL-17. In another study, the movement of neutrophils migrating through electrospun meshes fabricated with PCL was examined.[434] These immune cells are known to be the first answer against foreign cells. By means of IL-8 as chemotactic attractant, neutrophils were able to penetrate electrospun fibers similar to ECM. Recently, galectin-1, an immunosuppressive

protein, was co-electrospun with PDO and then seeded with macrophages.[435] It could be demonstrated, that the cell production of immunomodulating cytokines, for example IL-6, decreased.

By now, only few publications dealt with immunomodulatory effects targeting the early immune response which originate from the innate immune system after implantation of a biomaterial as well as specific cell communication being responsible for remodeling and tissue regeneration. As a new approach, reactive NCO-sP(EO-*stat*-PO) molecules were used as an additive for solution electrospinning with PLGA and were immobilized with neutralizing antibodies tending to the master cytokine tumor necrosis factor (TNF) in order to attenuate proinflammatory reactions by cells adherent to electrospun meshes. This modification of fibers was accomplished by a multimodal immobilization procedure exploiting the findings from experiments with fluorescent dyes. In a first functionalization step, cell adhesion mediating RGD peptide was added to the electrospinning solution before starting the process. Then, for a second functionalization, reactive isocyanates on the surface of meshes were used to immobilize various antibodies and mixtures of them for immunomodulation. Here, neutralizing antibodies against TNF and the fibroblast growth-factor-inducible 14 molecule (Fn14) were applied. An antagonist of tumor necrosis factor, the human monoclonal antibody Humira®, avoids TNF binding to its receptor.[436] 5B6, a recombinant antibody targeting Fn14, was the second protein used for immobilization.

The tumor necrosis factor (TNF) is a multifunctional cytokine of the immune system, which is involved in local or systemic inflammatory reactions in the human body and which is mainly released by macrophages but also from other cell types like mast cells. One of the main functions of TNF is regulating the activity of different immune cells and tissue homeostasis.[437-438] Together with its corresponding receptor Fn14,[439] TWEAK which is another member of the TNF superfamily plays an important role in the immune system as well: it is able to excite the differentiation and proliferation of progenitor cells and to provoke the formation of proinflammatory or angiogenic proteins, which is important for wound healing and tissue homeostasis but could also lead to chronic development of diseases, when malfunctioning.[440]

It would be highly advantageous to modify electrospun mesh surfaces with antagonists of both mentioned systems (TNF or TWEAK and their receptors) to regulate the

reaction of the body against non-endogenous materials and to control inflammation processes via damping of TNF / TNF receptor or TWEAK / Fn14 pathways.[436, 441-443]

5.2 Materials and methods

For convenience, the pharmaceutical manufactured drug Humira® is stated as "Humira" without the registration sign ® in the following chapters.

Electrospinning. For preparing the electrospinning solution, 5 wt% NCO-sP(EO-*stat*-PO) was dissolved in dry DMSO. If the peptide sequence CGRGDS was used for functionalization during the process, it was dissolved in DMSO before and this solution was added to the NCO-sP(EO-*stat*-PO). After stirring for 10 min, acetone was added for achieving a DMSO to acetone volume ratio of 1:5. The solution was vortexed briefly and 24.5 wt% PLGA was added and stirred until full dissolution. For electrospinning, the polymer solution was fed through a flat-tip stainless steel spinneret with a flow rate of 0.5 ml/h. The tip of the needle was connected to a high-voltage power supply (Voltcraft® Laboratory Power Supply, Conrad Electronic SE, Hirschau, Germany) applying a high voltage of 13 kV. As grounded collector, a rotating drum (diameter 60 mm, length 100 mm) with a rotation speed of 120 rpm was used and the distance between the collector and the needle tip was set to 15 cm.

Incubation with proteins and antibodies. After the electrospinning process, the freshly spun meshes were cut into 1 x 1 cm pieces and rinsed with different antibody solutions or compositions of them as described for each experiment. After overnight incubation and removing of residual solution, RPMI medium supplemented with 10% fetal calf serum (FCS) was added for 1.5 h to finish the reaction and to occupy the remaining binding sites. The samples were washed 5 times with phosphate buffered saline (PBS) and then incubated with corresponding *Gaussia princeps* luciferase (GpL) fusion proteins self-cloned by Prof. Wajant and co-workers. The binding of the GpL fusion proteins was used to indirectly detect and quantify functional antibody molecules. The washing step with PBS was repeated and each mesh was cut into 4 pieces. After transferring the samples to a UV-transparent 96-well plate (Greiner FLUOTRAC™ 200 96-well plates black medium binding), the activity of GpL was measured by a Luciferase Assay Kit (New England Biolabs GmbH, Frankfurt am Main, Germany) in a Luminometer (Lucy 2, Anthos Labtec Instruments, Wals/Salzburg, Austria). In experiments where low physiological relevant concentrations of TNF have been used, the control meshes were incubated after blocking with FCS for 1 h with Humira solution as a minor modification to absolutely assure that differences in the TNF-inhibitory effect between PBS and Humira meshes are due to immobilized Humira

and not affected by micro traces originating from unspecifically bound Humira antibody which was resistant against washing.

Cell culture experiments. L929 murine fibroblasts CC1 (ATCC, Wesel, Germany) were seeded in a 24-well culture plate (Nunc, Wiesbaden, Germany) in triplicate onto the RGD modified meshes using 50,000 cells per well in 1 ml Dulbecco's modified Eagle's medium (DMEM) supplemented with 10% FCS, 1% penicillin/streptomycin and 1% HEPES buffer (1M solution). For fixation, the nonwoven mats were stuck in cell crowns (MINUCELLS and MINUTISSUE, Bad Abbach, Germany) at a distance of 1.25 mm from the bottom. After incubation for 3−4 d at 37°C in a 5% CO_2 humidified atmosphere, a live/dead staining was performed**.** Calcein AM (life technologies, Germany) show living cells by green fluorescence, while dead cells exhibit a red fluorescence from ethidium homodimer-1 (Sigma Aldrich, Germany). Fluorescence images were recorded with the Axio Imager M1 (Carl Zeiss, Germany).

Interleukin 8 (IL-8) specific enzyme-linked immunosorbent assay (ELISA). After overnight incubation with TNC-scTNF(143N/145R) or Humira, the specimens were rinsed 5 times with PBS and again clamped into cell crowns. For showing an enhanced IL-8 answer of cells, 250,000 HT1080-Bcl2-TNFR2 cells were seeded on samples in triplicate in RPMI medium supplemented with 10% FCS and 1% penicillin/streptomycin. After 3 to 4 h of cell culture, the fiber mats were converted into a 12-well cell culture plate and cells were cultured for another 24 h at 37°C. In the second approach showing an inhibited IL-8 production, 225,000 HT1080-Bcl2-TNFR2 cells were grown in triplicate with the above-mentioned medium for 24 h. Functionalized meshes fixed in cell crowns were added onto the cells and stimulation of cells with 800 µl fresh medium containing 1, 5 or 10 ng/ml GpL-FLAG-TNC-TNF followed. After collection of the supernatants, these were evaluated for IL-8 with a commercially available ELISA kit (BD OptEIA^{TM}, BD Biosciences, San Diego, CA) according to the manufacturer's instructions. After adding the relevant substrate for the reaction from the kit showing a light green color, the binding was followed by a dark green color change indicating a successful production of IL8.[444] A scheme of the ELISA reaction is demonstrated in **Figure 24**.

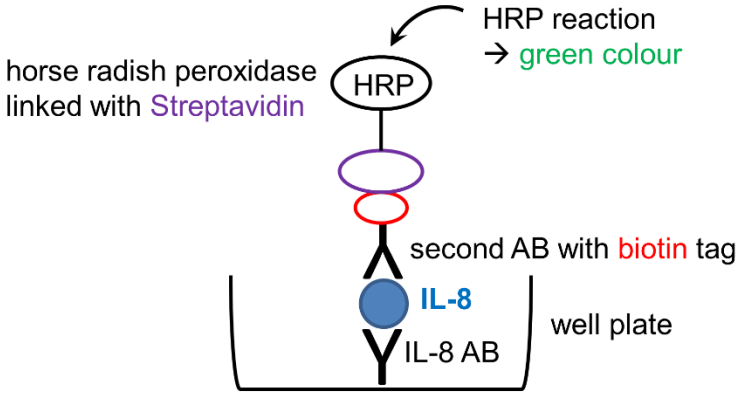

Figure 24: Illustration of sandwich ELISA reaction in a well plate. IL-8 is caught by the antibody immobilized on the well plate surface. Subsequently, a second antibody binds and leads via a biotin-streptavidin interaction to enzyme coupling of horse radish peroxidase (HRP). When the HRP reacts with its chromogenic substrate, a color change from light to dark green occurs.

Scanning electron microscopy. For the examination of cell adhesion and morphology, cells adherend to meshes were fixed and dried and two different SEM devices (Zeiss DSM940, Oberkochen, Germany and FIB-SEM CB 340, Carl Zeiss, Jena, Germany) were used for visualization.

Analysis of Variance (ANOVA): ANOVA was examined by means of SigmaPlot (Systat Software GmbH, Erkrath, Germany) using 1-way, 2-way or 3-way ANOVA depending on the raw data. In order to calculate the statistical significance, a post hoc Tukey test was performed.

5.3 Results and discussion

Aim of the experiments described in this chapter was to examine the possibility of immobilizing proteins such as members of the TNF superfamily or TNF antagonists on electrospun fiber surfaces and the subsequent biological investigation of such modified nonwovens. Furthermore, a multimodal functionalization should be achieved by using different functionalization steps with various biological molecules. For this purpose, the meshes were fabricated using PLGA as backbone polymer and NCO-sP(EO-*stat*-PO) as functional prepolymer. In this case, a one-step procedure was performed without any need of further chemical crosslinking.

5.3.1 Preliminary tests

A simple attempt to prove the immobilization of proteins on the surface of electrospun fibers was the incubation of the nonwovens with different antibody solutions in PBS overnight. The binding of the antibodies was proved by a luminescence reaction. The immobilization was done by covalent crosslinking of free amino, thiol and hydroxyl groups with isocyanate moieties on the nonwovens' surface. This interaction was indirectly detected by binding the specific substrate of the antibodies, the so-called GpL-FLAG-TNC-TNF. This construct is composed of the tumor necrosis factor sequence which bears a GpL-FLAG-TNC domain. *Gaussia princeps* luciferase (GpL) which leads to a light emission by catalyzing the reaction of coelenterazine to coelenteramide is coupled with the octapeptide FLAG used for purification purposes. TNC, a short domain derived from tenascin C, is generally exploited to support the trimeric assembly of TNF super family members.[445] In this way, successful binding of the antibodies to the electrospun fibers is detected by an interaction with different domains of the used substrate resulting in a luminescence reaction when coelenterazine is present. This light reaction can be measured by the quantification of relative light units (RLU) via a plate reader (**Figure 25**).

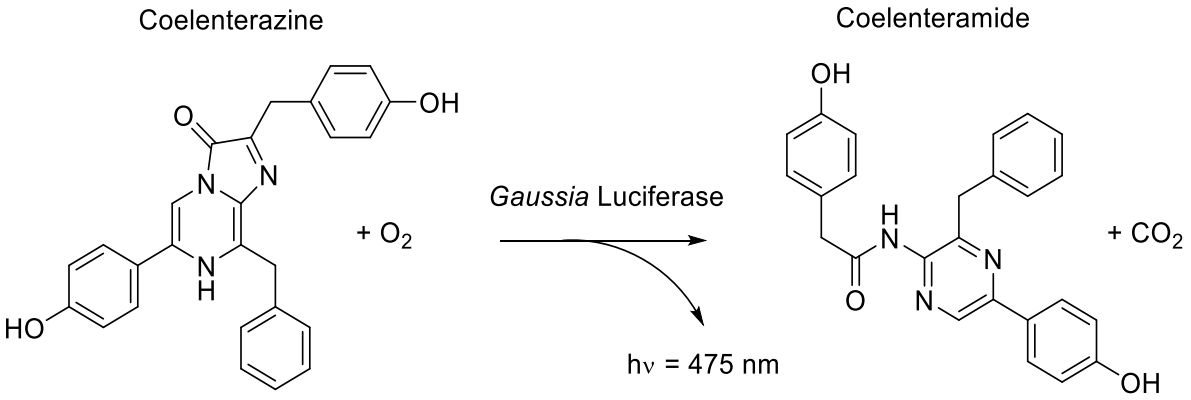

Figure 25: Conversion reaction of the enzyme *Gaussia princeps* Luciferase (GpL). Coelenterazine is transferred to coelenteramide resulting in a light emission.[446-447]

5.3.1.1 Immobilization of different antibodies

For a first experiment to test the possibility of an interaction between the fiber mesh and an antibody in general, solutions of three different antibodies were prepared: a CD20 antibody (Rituximab), a TNF antibody (Humira) and a FLAG antibody. Rituximab is a human IgG1 antibody directed against the B-cell specific CD20 protein present on the cell surface[448] and was used as negative control which shows no binding of GpL-FLAG-TNC-TNF. Humira is a human IgG1 antibody against TNF which is generally used for several clinical application.[441] *In vivo*, it avoids the binding of TNF to the corresponding receptors TNFR1 and TNFR2 and serves here as the protein for examination of immobilized fibers. M2 is an antibody against FLAG that recognizes the sequence on antigens. The FLAG tag is an octapeptide with a size of about 1 kDa and is often used to label proteins.[449]

After the electrospinning process, round pieces of 10 mm in diameter were produced from the electrospun meshes with a puncher and placed in a 48-well plate for incubation. Subsequently, in each case, 500 µl of antibody solution (50 µg/ml for Humira and Rituximab, 10 µg/ml for M2) were pipetted on the nonwoven pieces in triplicate and incubated overnight at 4°C. Afterwards, the antibody solution was removed and 900 µl RPMI medium containing 10% FCS was added to stop the reaction. After washing with PBS, the GpL-FLAG-TNC-TNF solution was added at a concentration of 500 ng/ml and the meshes were incubated for about 1 hour. The washing steps with were repeated and the nonwovens were quartered and placed in a UV-well plate. 50 µl RPMI medium with 0.5% FCS and 10 µl *Gaussia* substrate were

added, the UV plate was shaken in the plate reader and the device determined the RLU. In addition, the following control experiment was carried out: On the one hand, the nonwovens were incubated only with RPMI medium in order to prove that the used medium did not influence the measurement and did not show any light emission. On the other hand, only the fusion protein GpL-FLAG-TNC-TNF was incubated to see whether the light detection on the nonwovens works, since the molecule is also able to adhere to the nonwovens.

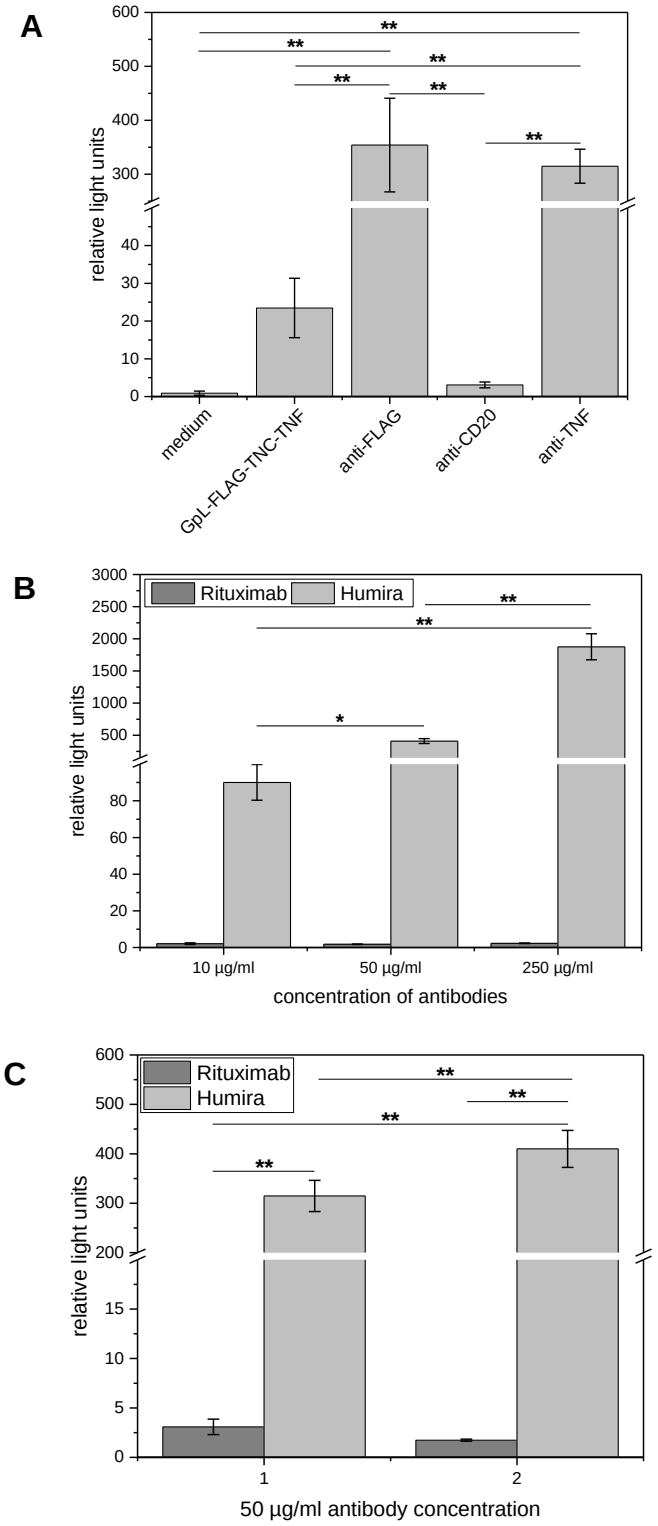

Figure 26: Control experiments. **A**) Examination of fiber meshes immobilized with GpL-FLAG-TNC-TNF substrate in contrast to meshes incubated with RPMI medium and comparison of three different antibodies immobilized on electrospun fiber meshes. **B**) Comparison of three different antibody concentrations of Rituximab and Humira (10, 50 and 250 µg/ml). **C**) Comparison between the two measurements using Rituximab as negative control and Humira as reactive antibody. 50 µg/ml of antibody was used, respectively. Level of significance of 1-way and 2-way ANOVA: * means $p < 0.05$; ** means $p < 0.01$. (n = 3)

As shown in **Figure 26A**, for the examined fibers incubated with medium, the amount of RLU was very low which means that hardly any light emission was observed. In comparison, GpL-FLAG-TNC-TNF substrate showed significant higher values. As expected, the medium showed no unspecific binding on the fiber surface and therefore had no effect on the light emission. However, the incubation reaction worked since it was possible to bind proteins like GpL-FLAG-TNC-TNF detected by the positive luminescence reaction. Comparing the mean values of the mesh pieces incubated with the three different antibodies, it is shown that GpL-FLAG-TNC-TNF does not interact with Rituximab (anti-CD20), but strongly with the TNF antibody Humira and also with M2, the anti-FLAG antibody, which was detected with the same fusion protein. The interaction with M2 is on the same level as with anti-TNF; however, a higher standard deviation could be observed. In summary, it is possible to immobilize different antibodies on electrospun fibers detecting them via the fusion protein GpL-FLAG-TNC-TNF resulting in a luminescence reaction. Because Humira, which is clinically applied in the human body, seemed to be more promising for subsequent investigations, for example inflammation processes, this approach was pursued in the following experiments.

In order to find out whether it is possible to bind more antibodies to the surface of the nonwovens visible in higher values of the RLU, electrospun fibers were incubated with 3 different concentrations of the antibodies Rituximab and Humira, respectively. In **Figure 26B**, it is shown that the extent of light reaction increases with higher concentrations of applied antibody. That means, that the applied concentration of the antibody does directly affect the amount of bound substrate. GpL-FLAG-TNC-TNF hardly binds to the CD20 antibody, and the corresponding RLU showed very low values.

Considering both experiments in direct comparison (**Figure 26C**), it could be observed that the second approach led to significant higher RLU values. This might due to the variation of the time frame passing by after the electrospinning process. In the first attempt, 45 min after electrospinning, the meshes were rinsed with the antibody solution. In the second experiment, the incubation was done directly after electrospinning.

In conclusion, it could be assumed that incubation immediately after spinning leads to a higher antibody density on the surface of the fibers. More isocyanate groups are

available directly after the process and a longer period of time after spinning leads to proceeded crosslinking on the surface of the fibers which is in contact with humidity from environment. As stated by Groll and Möller,[229] not more than 20 min should be elapsed after contact of the NCO-sP(EO-*stat*-PO) electrospun mesh with an aqueous solution. Crosslinking by exposition of fibers to humidity from air might be not that fast but as demonstrated, has an influence on the immobilization capacity of the mesh. Additionally, it was evaluated that a higher concentration of the antibody solution results in a more extensive luminescence reaction.

5.3.1.2 Binding assays with Rituximab and Humira

In the following experiments, the immobilization of the antibodies Humira and Rituximab was examined in detail. Because the meshes were found to be electrically charged directly after the spinning process and remained partially adherent to different surfaces, preparing the fibers for examination was linked to some difficulties. First, a puncher was used to get circular pieces of mesh, but it turned out that cutting of the meshes into squares and placing them directly in the 24-well plate for incubation was easier in handling. Also, the transfer to 96-well UV plates for examination of light reaction was easier and even more uniform pieces could be obtained by cutting 4 quarters out of one mesh piece.

In order to determine an upper limit for immobilization on electrospun fiber surfaces, solutions with various increasing concentrations of antibodies were added to freshly spun meshes and incubated overnight. Accordingly, the luminescence reaction of was measured, the mean values were calculated and plotted against the applied concentrations of antibody solutions to show the functional immobilization of Humira. In **Figure 27A**, it could be observed that the values of Rituximab were near zero, as expected. In contrast, with Humira, more molecules could be immobilized on the surface of the nonwovens with an increasing number of antibodies at a constant GpL-FLAG-TNC-TNF concentration with antibody-saturating effect. If the concentration of Humira antibody was lower than 0.5 mg/ml, the detection of GpL-FLAG-TNC-TNF and therefore antibody immobilization showed a linear behavior. Comparing the two measurements in **Figure 27**, the slope of the linear zone was found to be higher in **B** than in **A**. This might be due to variations in the electrospinning process. As mentioned earlier, amongst others, temperature and air humidity play a significant role for the

properties of the fiber mesh regarding the texture of the fiber surface and also fiber diameter which might influence the number of immobilized molecules.[450] However, it was not possible to avoid these influences because of a missing climate chamber for the electrospinning device.

The immobilization limit was not reached by the use of 2 mg/ml Humira, which was the highest used concentration in **Figure 27A**. The results of two individual tests revealed that the maximum of immobilization lay at about 2.5 mg/ml; in this range, the results became uneven and the standard deviations reached higher levels (**Figure 27B**).

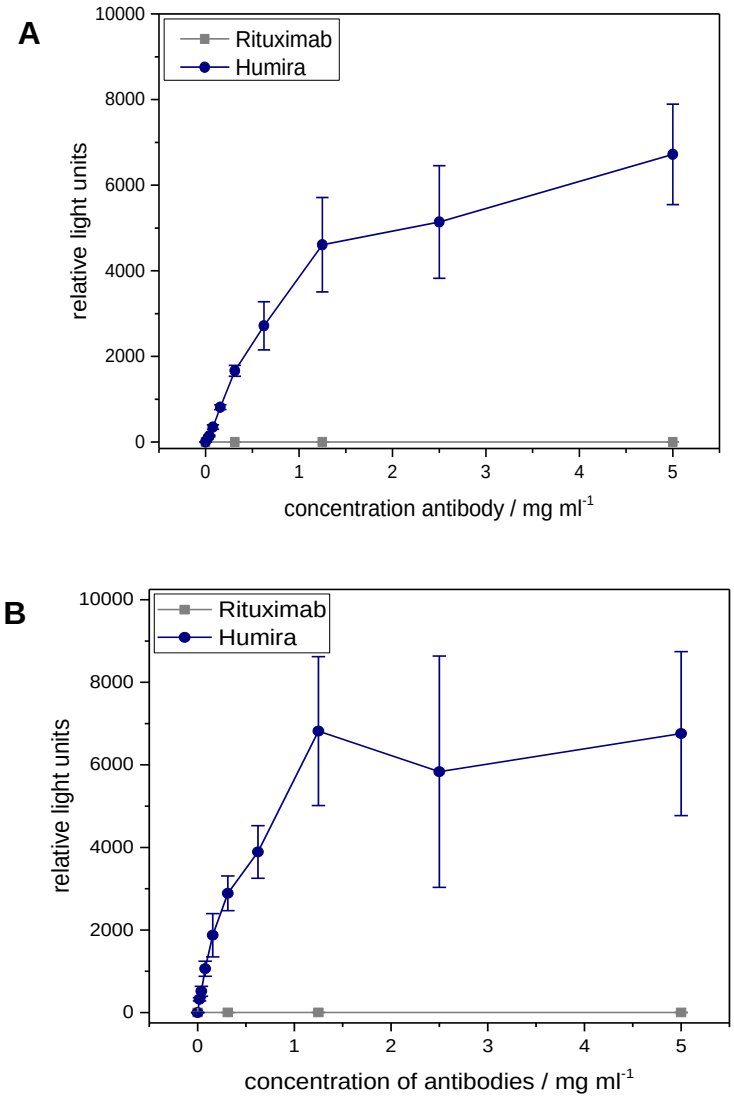

Figure 27: Dilution series of Rituximab as control antibody and Humira as TNF antagonist. Freshly spun fiber meshes were incubated with solutions containing different concentrations of antibody. These were indirectly detected by use of the substrate GpL-FLAG-TNC-TNF. **A** and **B** reveal individual experiments.

5.3.1.3 SEM examination

For ongoing attempts, it was important to know whether cells are able to interact with the immobilized proteins. In preliminary experiments, which are not shown here, an interaction between antibodies immobilized on electrospun fibers and cells could not be proved due to the hydrophilicity and lack of protein sequences on the surface. Furthermore, the shrinkage of the nonwovens after cell culture incubation at 37°C stated a problem. To further investigate such shrunk fibers, the meshes were freeze-dried and examined by SEM microscopy (**Figure 28**). It was clearly visible that the fiber diameter broadened, and the fibers were much closer together than before the storage in the incubator showing a thickness of about 2 µm (**Figure 28A**). In addition, the fibers were fused in some areas. Hardly any cells were recognizable (**Figure 28B-D**).

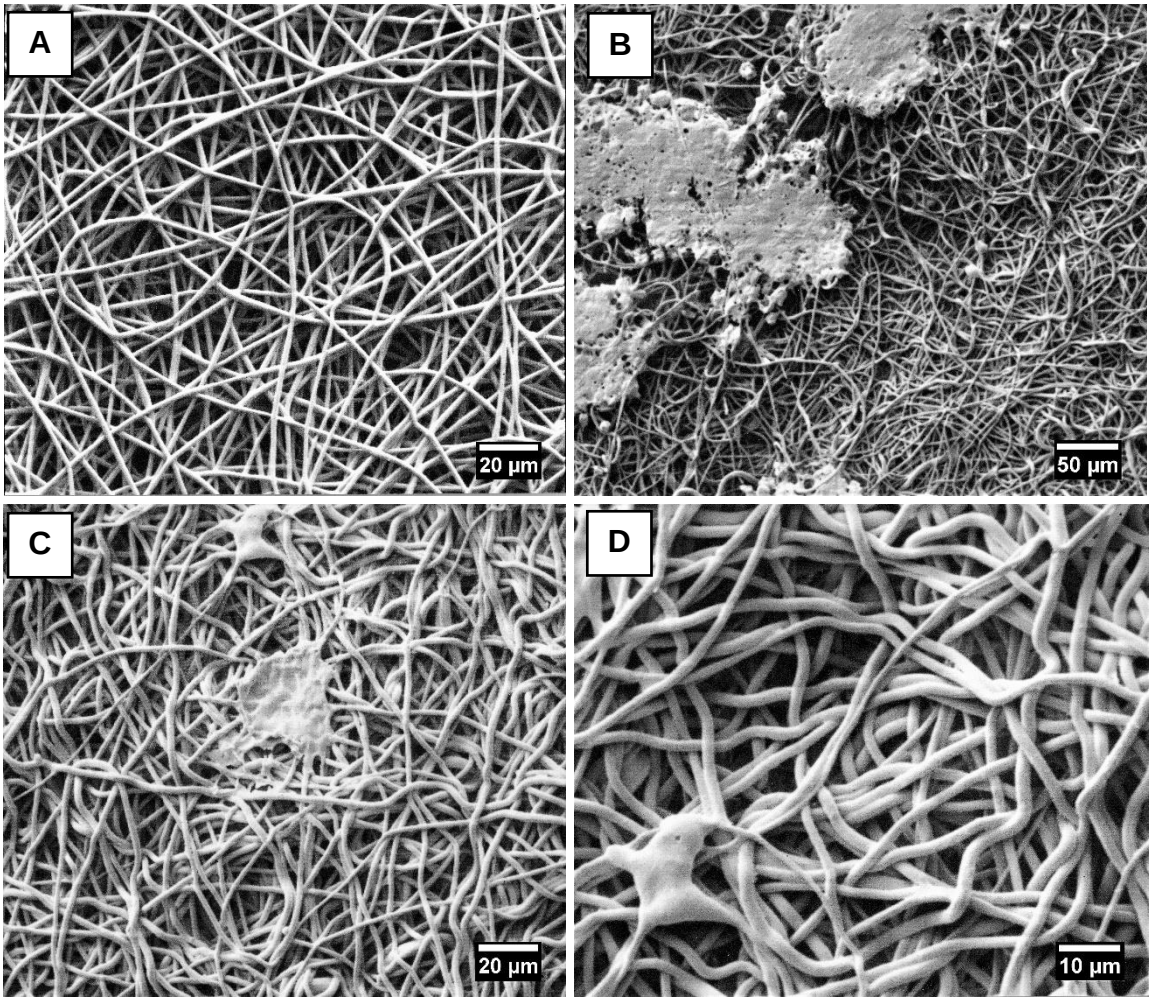

Figure 28: SEM images of fibers before and after incubation at 37°C. **A** shows the electrospun fibers without any treatment, **B-D** reveal shrunk fibers after seeding of cells and storage in the incubator at 37°C in different magnifications. Hardly any cells are visible.

In general, it could be concluded that the cutting of the meshes in squares led to a better handling during the experiment. However, it was problematic that the nonwoven pieces shrank during incubation at 37°C. Simultaneously, the fiber diameter got wider because of swelling, which seemed to be a common occurrence concerning the hydrogel layer on the fiber surface.[236] Anyway, the shrinkage was avoided by application of cell crowns in following cell tests.

Furthermore, it was important to perform some preliminary experiments to investigate the influence of the antibody immobilization on cells cultivated on electrospun fibers. As known from literature, the surface of PLGA fibers decorated with NCO-sP(EO-*stat*-PO) shows hydrophilic properties and therefore, cell attachment is avoided.[242] By specific biofunctionalization with peptide sequences, the surface becomes attractive for cells because of cell-mediation via biochemical signals.[45, 157, 451] This was commonly described for the cell-mediating peptide sequence RGD[452] which was used for following experiments.

5.3.1.4 Modification of fibers with the peptide sequence RGD

To subsequently increase the cell-scaffold interaction, an additional functionalization of fibers with the RGD peptide sequence derived from fibronectin, shown in **Figure 29**, was performed before immobilization of proteins or antibodies.

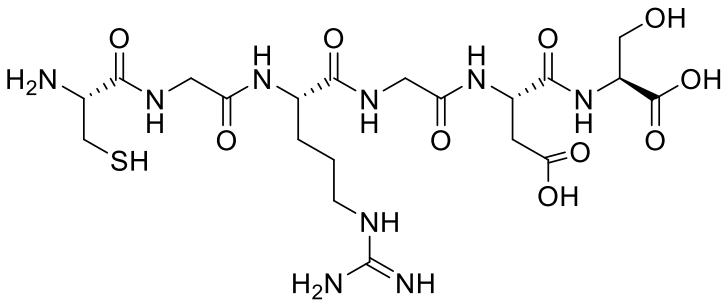

Figure 29: The cell-mediating peptide sequence consisting of the tripeptide Arg-Gly-Asp.[429] Here, the sequence CGRGDS is used to exploit the amino acid cysteine for covalent binding to the isocyanates in the spinning solution. G (glycine) and S (serine) serve as spacers.

Initially, it was supposed that the addition of the RGD peptide to the nonwovens might state a problem because isocyanate groups present on the surface after electrospinning would be occupied with RGD and thus a smaller number of antibodies and proteins would be able to bind to the surface after incubation. Moreover, it was tested whether the cells were able to grow on electrospun meshes which have been treated with antibody, since these proteins might cover or hinder the RGD sequences on the surface and thus avoid cell adhesion. In order to prevent the shrinkage of the nonwovens in the cell experiment and to ensure that the cells remain on the meshes, cell crowns were used to keep the fibers in shape.

For a first control experiment, a concentration of 350 µg/ml Humira was selected and the antibody binding to an RGD functionalized mesh was examined. The meshes were incubated with GpL-FLAG-TNC-TNF and the light reaction was measured.

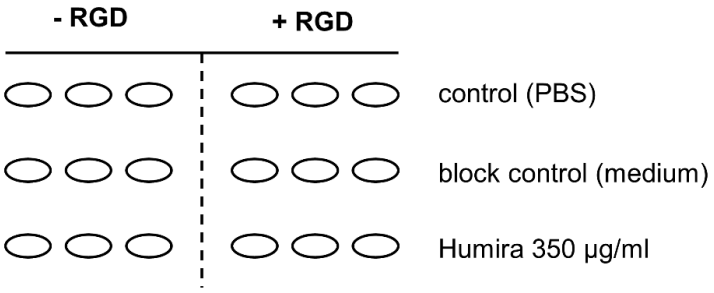

Figure 30: 48-well plates were prepared with mesh pieces and incubated with the mentioned solutions overnight in triplicate. The experiments were performed with fibers without and with RGD functionalization.

The experiment was performed as demonstrated in **Figure 30**. The block control was incubated with Humira for validating free binding sites.

When meshes were spun with addition of RGD, 10 µl of 2% trifluoroacetic acid (TFA) solution was added to DMSO to achieve a higher charge density and therefore an increased conductivity of the jet.[427, 453] The spinning process did not work well, hence, the flow rate was reduced to 0.2 ml/h. This, together with the addition of TFA, led to thinner fibers and thus to a larger fiber surface.[427, 454]

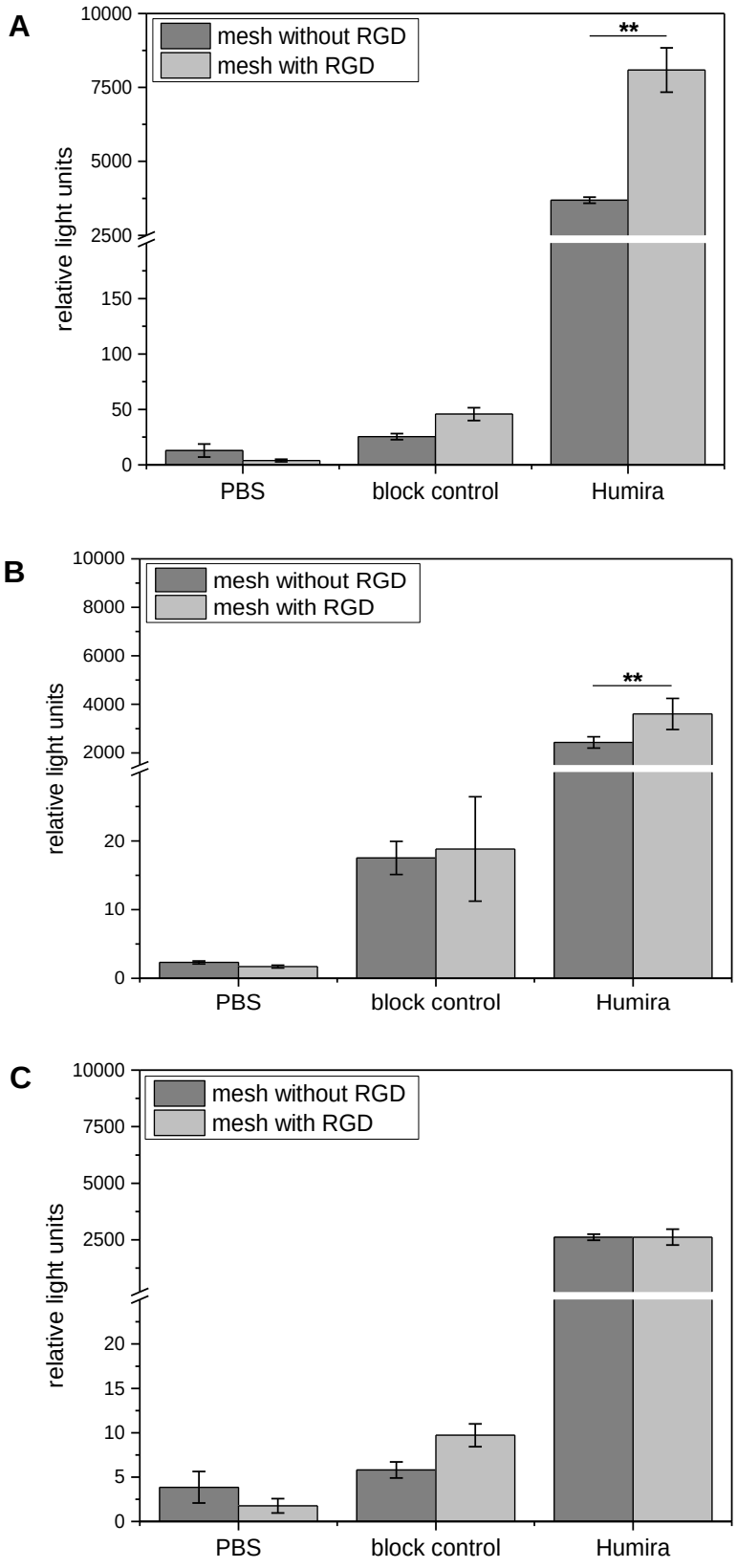

Figure 31: Three individual experiments (**A**, **B**, **C**) with 350 µg/ml Humira in comparison to fibers treated with PBS or block control. Level of significance of 1-way ANOVA (shown due to adequate visualization): ** means $p < 0.01$. (n = 3)

After the luminescence measurement the nonwovens without and with RGD addition were compared against each other. **Figure 31A** clearly shows that both untreated negative control and block control revealed little luminescence compared to meshes with immobilized Humira. With RGD, about twice the amount of substrate was bound via the TNF fusion protein to Humira functionalized fibers compared to the nonwovens without RGD. This indicates that the binding of the antibody is not disturbed by RGD addition; even more substrate molecules were detected which means that there is either an interaction between the proteins themselves or that the higher surface area of the RGD functionalized fibers plays a role for the antibody binding.

In a second experimental set, no TFA was added to the spinning solution to avoid irregular jet formation during the spinning process due to additional charges by TFA. Though, the flow rate had to be altered again to 0.2 ml/h instead of 0.5 ml/h. A reason for that might be influences on the electrospinning process, provoked by ambient parameters like temperature and air humidity. **Figure 31B** shows a similar result as **A**: Untreated fibers and block control revealed little luminescence, whereas both nonwovens functionalized with Humira, without or with RGD, resulted in a distinct light reaction. However, the difference between fibers without and with RGD was not that high as in the first attempt.

Nonetheless, to demonstrate the influence of RGD on the occupancy level of electrospun PLGA / NCO-sP(EO-*stat*-PO) fibers and to reveal the reproducibility, the experiment was repeated without TFA using a flow rate of 0.5 ml/h which was working this time. As demonstrated in **Figure 31C**, the controls showed a barely perceptible luminescence. There was hardly any difference between the non-woven fabrics without and with RGD addition which is also shown statistically with no significance. From this point, it can be concluded that the immobilized RGD has no influence on the antibody binding. There are free binding sites available bearing isocyanate which are not occupied by RGD or by crosslinking of NCO-sP(EO-*stat*-PO) molecules.

When comparing the three experiments, it was obvious that the binding of the antibody to the meshes without RGD was relatively uniform, which has already been proved in previous experiments. However, binding to the RGD-functionalized fibers was relatively irregular. Since in the first two experiments the fibers were thinner by adjusting the flow rate[189] or by adding experiments TFA, it could be assumed that more antibody molecules have bound due to the higher surface. Only in the last

experiment, the same flow rate was used for both types of mesh. Overall, it could be concluded from these experiments that the functionalization of the fiber meshes with RGD had little effect on the surface and that hindering of binding sites by the peptide sequence does not state a problem here.

5.3.2 Influence of RGD on antibody immobilization

To clearly reveal if a previous functionalization of electrospun fibers with RGD prevents the binding of antibodies, fibers without and with RGD peptide were electrospun as previously described and again incubated with two different concentrations of Humira (350 and 500 mg/ml) to show a possible influence of the amount of applied antibody (**Figure 32**). Again, the values revealed comparable results for meshes without RGD and meshes with RGD functionalization, as already shown. By using a higher concentration of antibody in the incubation solution, no significant difference was visible as well; therefore, it was assumed that Humira binds on both meshes and thus the further functionalization of the mesh with RGD was not significantly altering antibody binding.

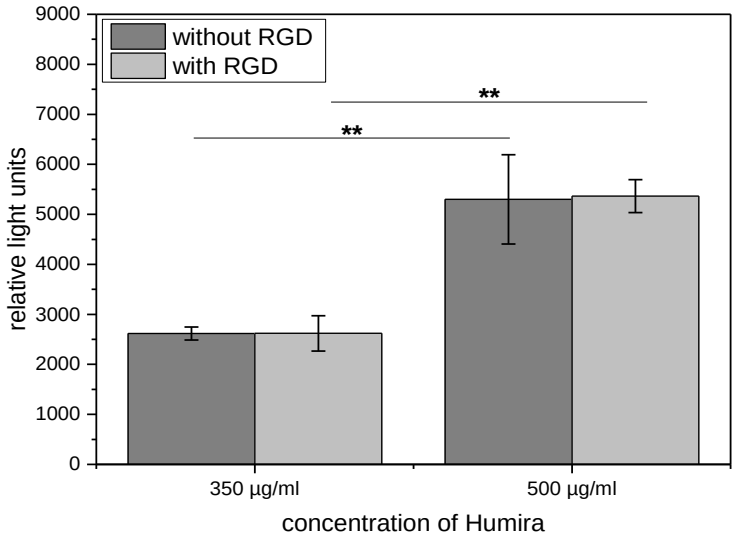

Figure 32: Comparison of two different concentrations of Humira without and with RGD. The pure meshes are shown in light grey, the pre-functionalized RGD meshes in dark grey. Level of significance of 1-way and 2-way ANOVA: ** means $p < 0.01$. (n = 3)

It was shown in literature, that a multiple functionalization of electrospun fibers modified with NCO-sP(EO-*stat*-PO) is possible because of crosslinking ability of the macromers with protic groups.[45] A demonstration was done by Rossi et al. using several peptide sequences and adding them directly into the spinning solution to transfer them to the surface of electrospun fibers.[226] For a dual functionalization with antibody and the peptide sequence RGD during separate procedure steps, some questions had to be answered in the next chapters regarding the introduced meshes:

- The binding behavior of antibodies without and with RGD was examined using a binding curve with increasing concentrations of Humira. Does RGD and antibody influence each other?
- An IL-8 specific ELISA was performed to show pro- or anti-inflammatory answers of cells. Is cell stimulation possible with this dual functionalization?
- How long does the antibody stay on the mesh after the immobilization process?
- Is a triple modification with different antibodies and different detection systems possible as well?

5.3.2.1 Binding behavior of RGD and antibodies shown in an immobilization curve

To reveal the functionality of the Humira after the immobilization on the fibers for different concentrations, a binding experiment was performed. For this purpose, PBS solutions with increasing concentrations of Humira antibody were used for incubation of freshly spun meshes applying a constant antibody-saturation amount of GpL-FLAG-TNC-TNF (**Figure 33**).

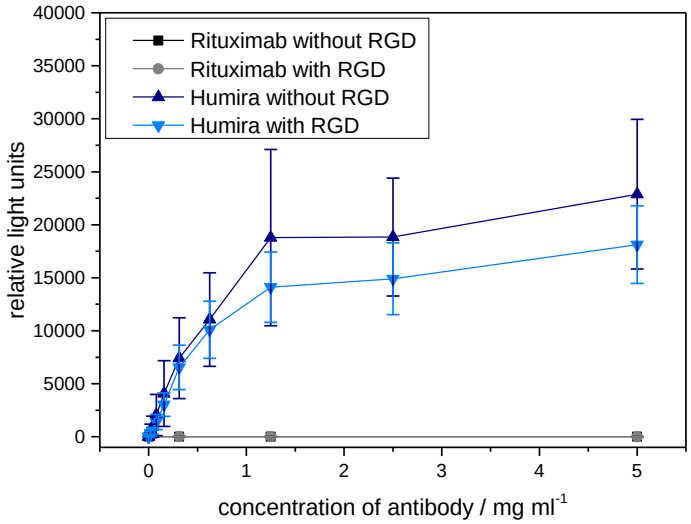

Figure 33: Freshly spun meshes without RGD or pre-functionalized with RGD were incubated with indicated concentrations of anti-CD20 antibody Rituximab and anti-TNF Humira antibodies in PBS overnight at 4°C. After blocking of remaining binding sites by treatment with serum supplemented with 10% FCS, meshes were incubated with 500 ng/ml GpL-FLAG-TNC-TNF. After removal of unbound molecules, immobilized GpL-FLAG-TNC-TNF molecules were quantified using BioLux Gaussia Luciferase Assay Kit (n = 3). (Reprinted from [426]. Copyright (2017) with permission from John Wiley and Sons)

As demonstrated, ascending amounts of immobilized Humira led to the detection of more GpL-FLAG-TNC-TNF fusion protein which bound to the electrospun mesh. Considering lower amounts of Humira under 0.5 mg/ml, it was visualized that the rise of GpL-FLAG-TNC-TNF molecules and therefore the immobilization of Humira showed an almost linear behavior. When the amount of antibodies became higher, a saturation of binding sites was noticed at about 2.5 mg/ml Humira. Fibers which bear the RGD modification revealed lower amounts of GpL-FLAG-TNC-TNF and thus lower immobilization rate of Humira than fibers without RGD on their surface. Significant differences were determined at increased concentrations of antibody which could be explained by the fact that several binding sites, which were potentially available for Humira functionalization, were already occupied by RGD due to the pre-functionalization of fibers by mixing the peptide sequence into the spinning solution.

5.3.2.2 Comparison between different RGD types and different amounts of RGD

As demonstrated, it was possible to immobilize antibodies on functional fiber scaffolds. If cell culture should be performed on such modified meshes, it is important to pre-functionalize the meshes with the cell-mediating peptide sequence RGD. However, this leads to a decrease of available binding sites because a certain number of isocyanate groups on the surface of the fibers are occupied with RGD molecules. Here, altering the amount of RGD is thought to be a key parameter to tune the availability of binding sites on electrospun meshes. Therefore, experiments with various amounts of RGD were performed; furthermore, two kinds of RGD from different companies were tested (jpt, Berlin, Germany or Gene-Cust, Ellange, Luxembourg).

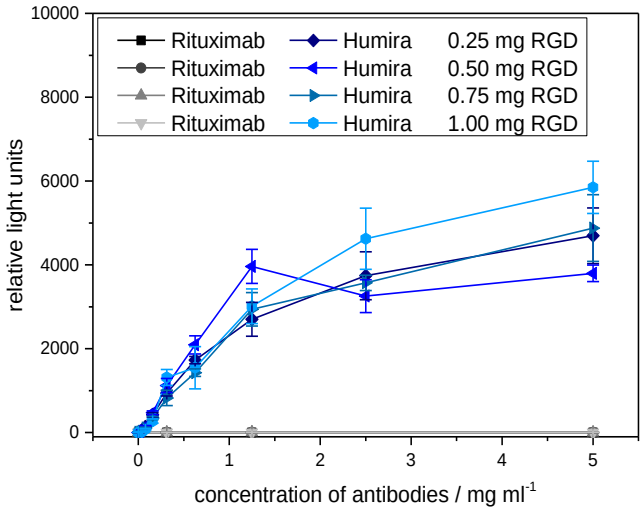

Figure 34: Immobilization of various concentrations of Humira and Rituximab with different amounts of 0.25 mg, 0.5 mg, 0.75 mg and 1.0 mg RGD (jpt) added to the spinning solution.

As evident in **Figure 34**, the binding curves show a very similar behavior. As expected, the detection of antibodies with GpL-FLAG-TNC-TNF fusion protein led to very small values near the zero line for the reference antibody Rituximab, whereas Humira was demonstrated to result in a uniform curve excluding the meshes with pre-functionalization applying 0.5 mg RGD. For fibers using 0.25 mg and 0.75 mg RGD, the binding curve was found to be on the same level, and the highest immobilization rate of Humira was achieved by the scaffold with 1.0 mg RGD. This leads to the suggestion that higher values were reached with more RGD on the surface which cannot be explained until now.

Another experiment was done to compare different RGD peptides from a German company (jpt) and a manufacturer from Luxemburg (GeneCust). Several companies offer custom-made peptides which show huge variations in prices and delivery times. In this case, the peptide sequence originating from GeneCust was cheaper with a shorter delivery time.

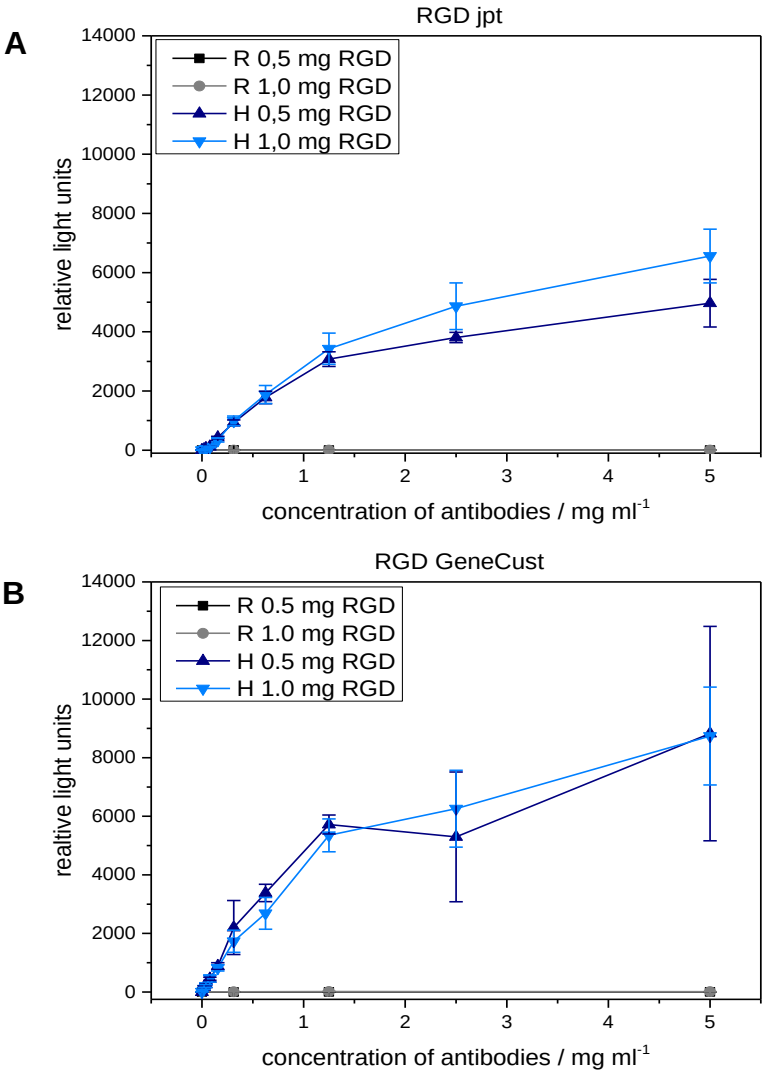

Figure 35: Immobilization of Humira and Rituximab on meshes pre-functionalized with 0.5 mg and 1.0 mg RGD from different manufacturers. **A**) RGD from jpt, Berlin, Germany. **B**) RGD from GeneCust, Ellange, Luxembourg. Rituximab is stated as R, Humira as H.

Again, the assumption, that more pre-functionalized RGD present on the fiber surface leads to less antibody immobilization, could not be verified. As shown in **Figure 35A** and **B**, no difference was visible between the binding curves; however, more antibody was immobilized on scaffolds with more RGD. Noticeably, the binding curves with RGD

from jpt were uniform without fluctuations of the curve, but with the peptide sequence from GeneCust, higher amounts of relative light units could be achieved.

Another binding assay was performed using four different amounts of RGD from both manufacturers. The summarized results are shown in **Figure 36**.

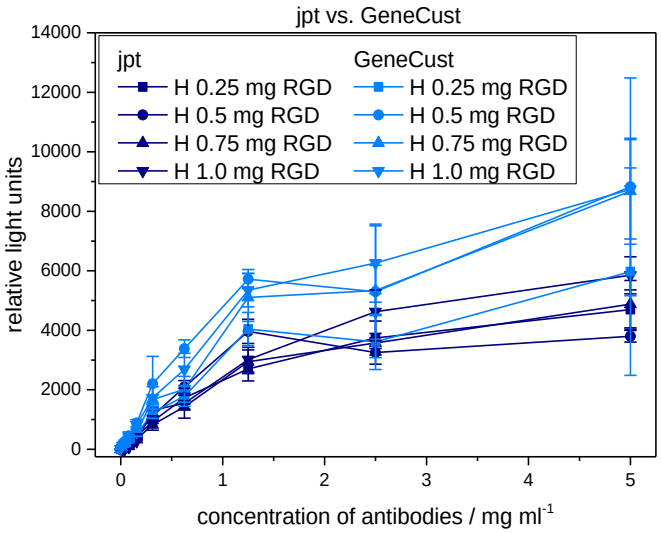

Figure 36: Functionalization of electrospun meshes with Humira pre-modified with 0.25 mg, 0.5 mg, 0.75 mg and 1.0 mg RGD from different companies. In dark blue, the modification with RGD from jpt, Berlin, Germany is shown, the light blue shows the modification with RGD from GeneCust, Ellange, Luxembourg. Humira is stated as H.

With RGD from GeneCust for pre-functionalization of electrospun fibers, higher amounts of immobilized antibody were achieved but also higher standard deviations occurred. A certain chronology of the immobilization rate of antibodies could not be recognized with RGD from jpt. However, the highest amount of antibody binding was observed with 1.0 mg RGD pre-functionalization. By using RGD from GeneCust, the lowest maximum value of Humira immobilization was achieved by applying the lowest level of 0.25 mg RGD, for higher amounts of peptide sequence, no clear difference was visible.

For the following experiments, RGD from jpt was used due to more uniform results.

5.3.2.3 Is it possible to perform cell experiments?

Important for an interaction of electrospun fibers and cells is the adherence of cells to anchor points or to a hydrophobic surface via unspecific protein absorbance. Therefore, cells need to stay on the fibers for some time to enable adherence. However, electrospun fibers out of PLGA and the functional additive NCO-sP(EO-*stat*-PO) reveal a hydrophilic surface which leads to a cell-repellent environment. To render the surface cell-friendly again and to create a specific biofunctionalization of the fibers, a second modification with the cell-mediating peptide sequence RGD is necessary before incubation with antibody to perform tests with cell seeding.

For examination of cytocompatibility of the electrospun meshes functionalized with antibodies and to study if an interference of cell growth due to the immobilized proteins occurred, a live/dead staining was performed. Therefore, L929 mouse fibroblasts were seeded on meshes and cultivated for 4 days at 37°C. As a positive control, a PLGA fiber mesh was used for general determination of L929 cell culture because a hydrophobic surface was established showing unspecific protein adsorption and an improved cell adherence. A dense cell layer with mainly living cells could be observed (**Figure 37**). However, some dead cells were detected, which could be attributed to the fact that the cell layer was already too dense after 4 days and the nutrients in the medium were running low.

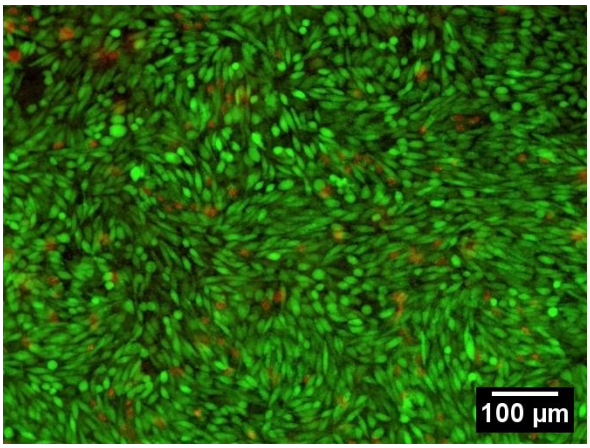

Figure 37: PLGA control for examination of L929 fibroblasts. Due to the highly hydrophobic surface, proteins are able to adhere unspecifically and cells build a dense cell layer. Living cells are visible in green, dead cells in red (live/dead staining). (Reprinted from [426]. Copyright (2017) with permission from John Wiley and Sons)

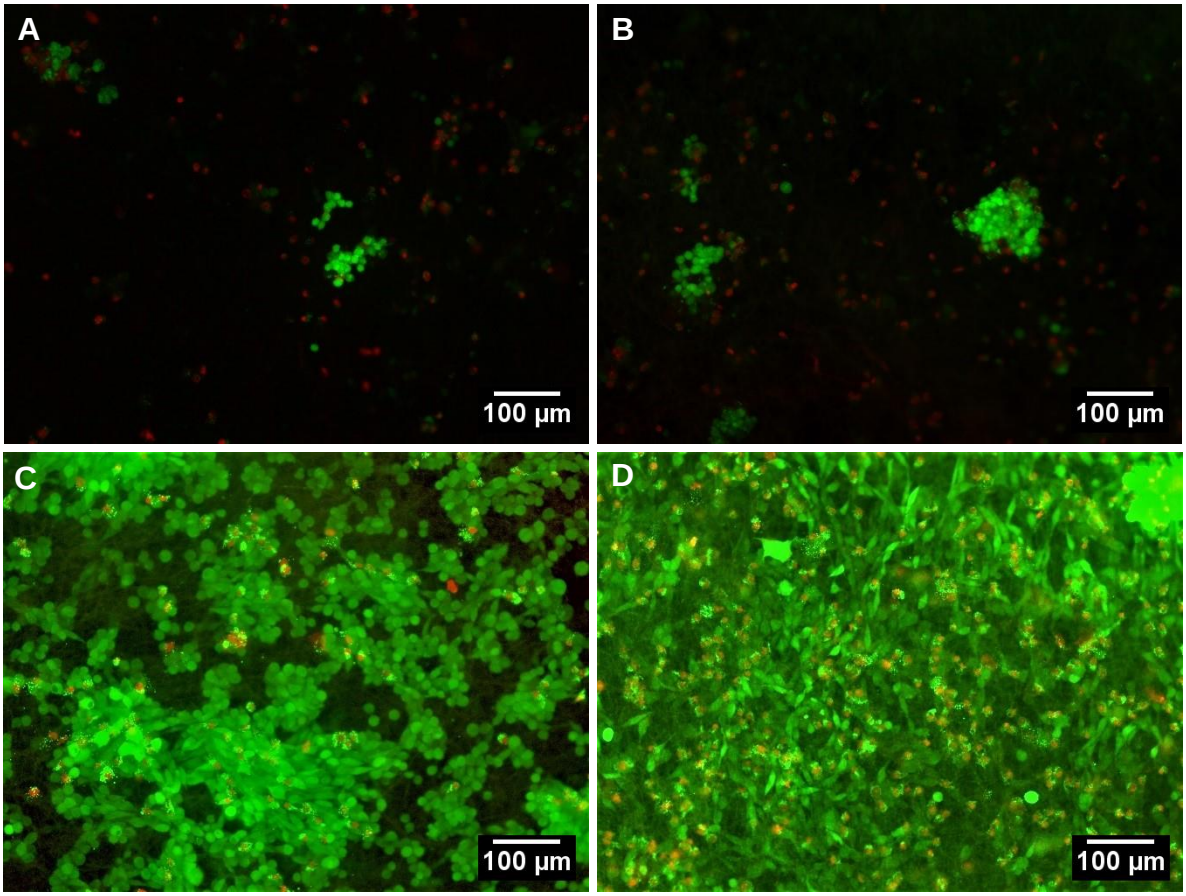

Figure 38: Upper row: Growth of L929 fibroblast on NCO-sP(EO-*stat*-PO) / PLGA meshes incubated with PBS (**A**) or with 350 µg/ml antibody solution (**B**). Lower row: Growth of L929 fibroblast on NCO-sP(EO-stat-PO) / PLGA meshes pre-functionalized with RGD peptide sequence and incubated with PBS (**C**) or with Humira antibody (**D**). (Reprinted from [426]. Copyright (2017) with permission from John Wiley and Sons)

A mesh spun with PLGA and NCO-sP(EO-*stat*-PO) was used as a negative control. Cell growth should be inhibited on the surface of these fibers, since it is hydrophilic due to the properties of the functional prepolymers. In comparison, functional meshes were examined, which had been incubated overnight with 350 µg/ml Humira (**Figure 38**).

Both nonwovens incubated with PBS or with antibody solution showed barely any cells growing on the surface after 4 days; the cells were agglomerated in clusters suggesting a poor cell status (**Figure 38A, B**). These results were expected and revealed that NCO-sP(EO-*stat*-PO) macromers were present on the surface and a colonization of cells was prevented. This is also clearly visible on the pretreated fibers which were incubated with Humira.

In addition, it should be investigated how cells behave on an RGD functionalized nonwoven treated with antibodies (**Figure 38C, D**). When RGD molecules are present on the fiber surface, cells recognize this sequence and the growth was strongly improved on such surfaces although these show hydrophilic properties by additional use of NCO-sP(EO-*stat*-PO). Here, it could be observed that a uniform cell layer was present on the meshes. A comparable number on cells occurred with and without antibodies. In comparison to the surface of pure PLGA, the cells showed a less dense layer because only a certain number of anchors were present on the RGD-NCO-sP(EO-*stat*-PO) modified fibers available whereas the interaction between fibroblasts and the hydrophobic PLGA consists in unspecific adsorbed proteins.[46] This might explain the differences regarding the density of the cell layer.

The cell test was carried out as desired, the cells grew very well on PLGA as positive control, whereas on the PLGA / NCO-sP(EO-*stat*-PO) meshes without and with antibody functionalization hardly any cells were apparent. Both results are comparable to the controls, from which it can be concluded that the antibodies have little effect on the growth of cells on the RGD-functionalized meshes.

5.3.3 Long-time experiment

The results demonstrated above led to the question whether the antibody molecules remain on the fiber surface for a longer time frame. Thus, an immobilization experiment was performed over a month. The fiber meshes were incubated overnight with PBS as negative control and with 500 µg/ml Humira as positive control. After washing with PBS, the meshes were stored at 4°C on a shaker in PBS and the light reaction of incubated meshes was measured after day 1, 4, 6, 8, 15 and 29, respectively. In **Figure *39***, the corresponding results are shown.

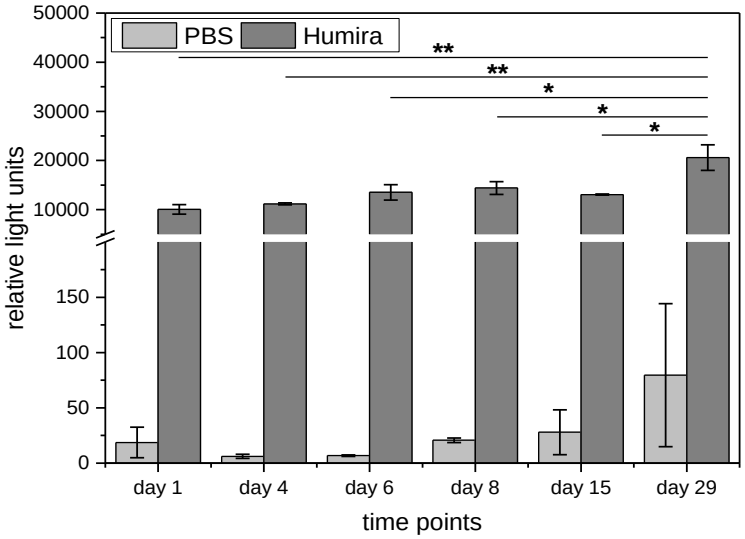

Figure 39: Long-time experiment. The mesh pieces were prepared by incubation with 500 µg/ml of Humira and PBS as negative control and the light reaction was measured after different time points. Level of significance of 1-way ANOVA (for easier visualization): ** means $p < 0.01$, * means $p < 0.05$. ($n = 2$)

The amount of relative light units remained nearly at the same value or even showed an increase, until after one month the highest amount was reached. This indicates that the antibodies remained on the fibers and were not washed off by shaking in PBS. The increasing RLU values could be attributed to diversities of the examined mesh pieces which was evident due to higher standard deviations.

5.3.4 Competition experiment

Additionally, it was analyzed if Humira binding is influenced by a high number of other immobilized antibodies. In this case, Rituximab was used. The incubation of meshes was determined either with 500 µg/ml Humira® or with 500 µg/ml Humira® together with an excess of 3 mg/ml Rituximab for blocking available binding sites present on the fiber surface which otherwise would be available for Humira binding.

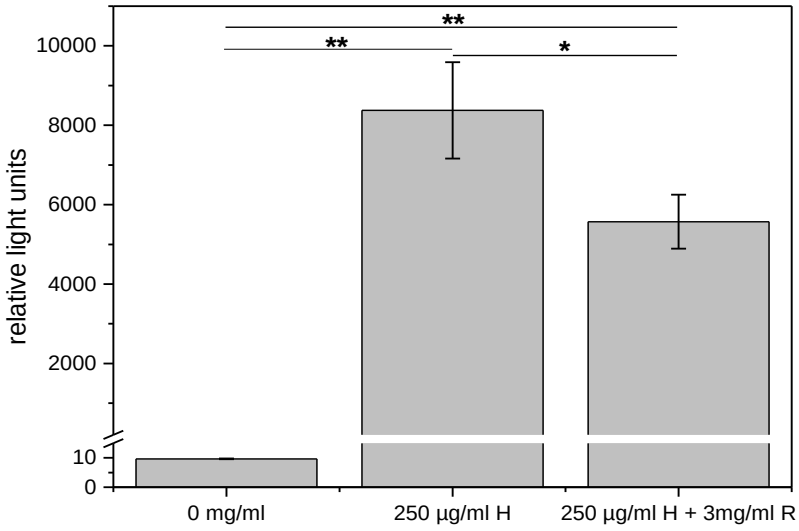

Figure 40: Competition of Humira (H) and Rituximab (R). Meshes were either incubated with PBS or 250 µg/ml Humira or a mixture of 250 µg/ml Humira and 3 mg/ml Rituximab as blocking agent. After washing the relative light units (RLU) were detected. Level of significance of 1-way ANOVA: ** means $p < 0.01$, * means $p < 0.05$. (n=3)

As evident in **Figure 40**, a significant decrease of RLU values was found when Humira was incubated together with Rituximab. This demonstrated that a high amount of Rituximab led to a decrease of binding sites for Humira but nevertheless, there were some isocyanate groups available for a quantifiable light reaction originating from Humira binding. This is another hint that the number of binding sites is restricted or that a higher immobilization rate is avoided by steric hindrance of the antibodies against each other.

5.3.5 Two- and threefold functionalization with different antibodies

Another investigation was done to analyze a possible influence between different antibodies on each other when they are used for functionalization at the same time and coexist on the same mesh. For this purpose, diverse antibodies were utilized (**Figure 41**). Again, Rituximab served as negative control. The functionality of the antibody Humira was detected by binding of GpL-FLAG-TNC-TNF as mentioned above and another antibody called 5B6 was used which is an antagonist specifically directed against Fn14 and which was also measured in an indirect way by binding Fn14(ed)-TNC-FLAG-GpL. This is a luciferase fusion protein of Fn14 produced genetically which bears the extracellular domain of the receptor.[455]

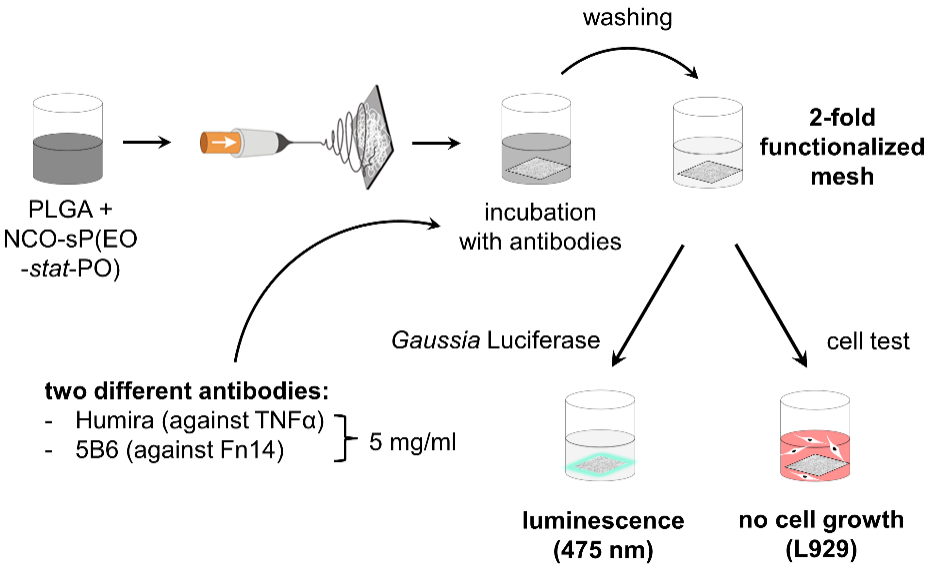

Figure 41: Double functionalization. Scheme of the functionalization process. Two different antibodies used as a mixture were immobilized on freshly electrospun scaffolds and examined regarding their luminescence. Additionally, a cell test was performed suggesting no cell growth. (Reprinted from [426]. Copyright (2017) with permission from John Wiley and Sons)

To achieve a threefold functionalization on electrospun fibers, the same combination of two antibodies was used together with a pre-functionalization of the mesh via the sequence CGRGDS by adding the peptide directly into the spinning solution before the process (**Figure 42**).

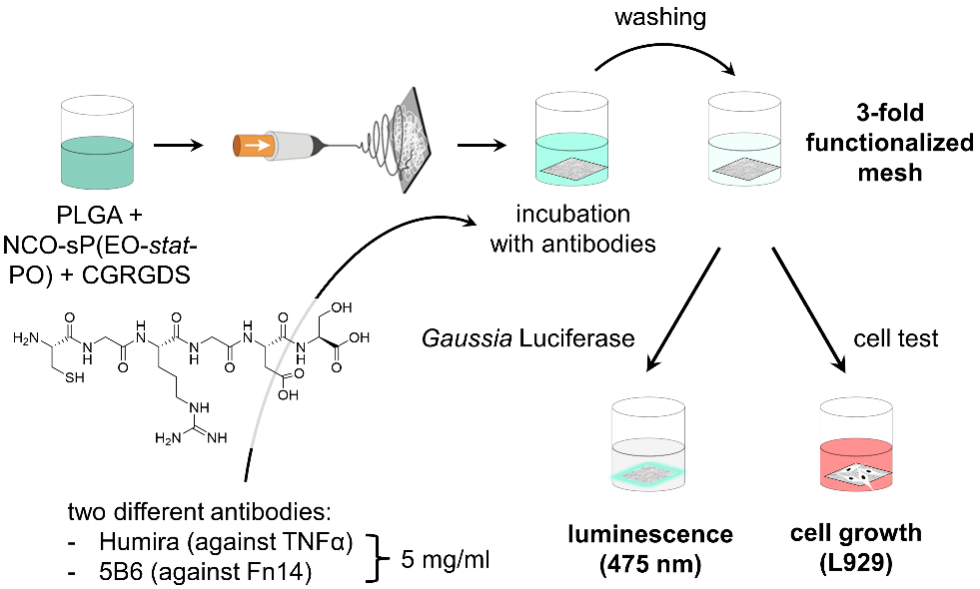

Figure 42: Triple functionalization using two antibodies and the RGD peptide sequence. Scheme of the functionalization process. Two different antibodies used as a mixture were immobilized on freshly electrospun scaffolds with RGD and examined regarding their luminescence. In addition, a cell test was performed. (Reprinted from [426]. Copyright (2017) with permission from John Wiley and Sons)

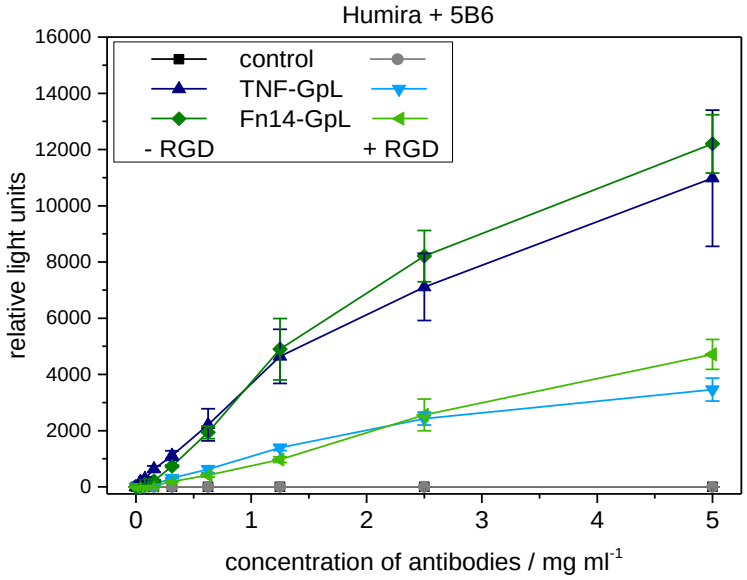

Figure 43: Comparison of two- and threefold functionalization. Binding curves of fibers functionalized with antibodies. Dark-colored curves: Meshes were treated with different concentrations of an equimolar mixture of Humira and 5B6. Light-colored curves: Meshes were treated with RGD and with different concentrations of an equimolar mixture of Humira and 5B6. Indirect detection was done by using 500 ng/ml GpL-FLAG-TNC-TNF (Humira) or 500 ng/ml Fn14(ed)-TNC-FLAG-GpL. (n = 3) (Reprinted from [426]. Copyright (2017) with permission from John Wiley and Sons)

As demonstrated in **Figure 43** (dark-colored curves), hardly any difference could be observed between detection substrates GpL-FLAG-TNC-TNF and Fn14(ed)-TNC-FLAG-GpL by measuring meshes which were immobilized with a mixture of the antibodies Humira and 5B6. From this fact, it could be concluded that the modification of electrospun fibers with both antibodies occurred in the same order of magnitude which leads to an efficient two-fold functionalization of scaffolds happening within one step.

As obvious, the values of RLU without and with addition of RGD differ from each other. For pre-functionalized RGD meshes, the luminescence reaction leads to significantly lower signal (**Figure 43**, light-colored curves) measured as relative light units than for meshes without RGD functionalization. This appearance could be explained by the fact that less binding sites for antibody immobilization are present on the surface of fibers if they are functionalized with RGD before because the peptide sequence occupies free isocyanate groups during electrospinning. As expected from measurements with only Humira as immobilizing agent, the binding sites are not abundantly available on the electrospun fiber mesh. Nevertheless, both antibodies were immobilized at the same rate also on RGD functionalized meshes.

5.3.5.1 Twofold / threefold functionalization – Cell test

To control cell growth on the two- and threefold functionalized fibers, a live/dead staining was performed. In **Figure 44A** and **B**, it is visible that no difference occurred between meshes incubated with PBS or the antibody mixture consisting of Humira and 5B6; barely no cells adhered due to the surface properties. In conclusion, this means that the functionalization of electrospun fiber meshes with an antibody mixture did not lead to an influence on cell behavior.

However, the pre-functionalization of meshes with the cell-mediating sequence RGD resulted in adequate cell adherence of L929 fibroblasts without influence of antibodies on the behavior of cells. Both meshes showed a uniform cell layer (**Figure 44C** and **D**) which was not as dense as for PLGA meshes but led to a specific biofunctionalization mediated by RGD functionalization.

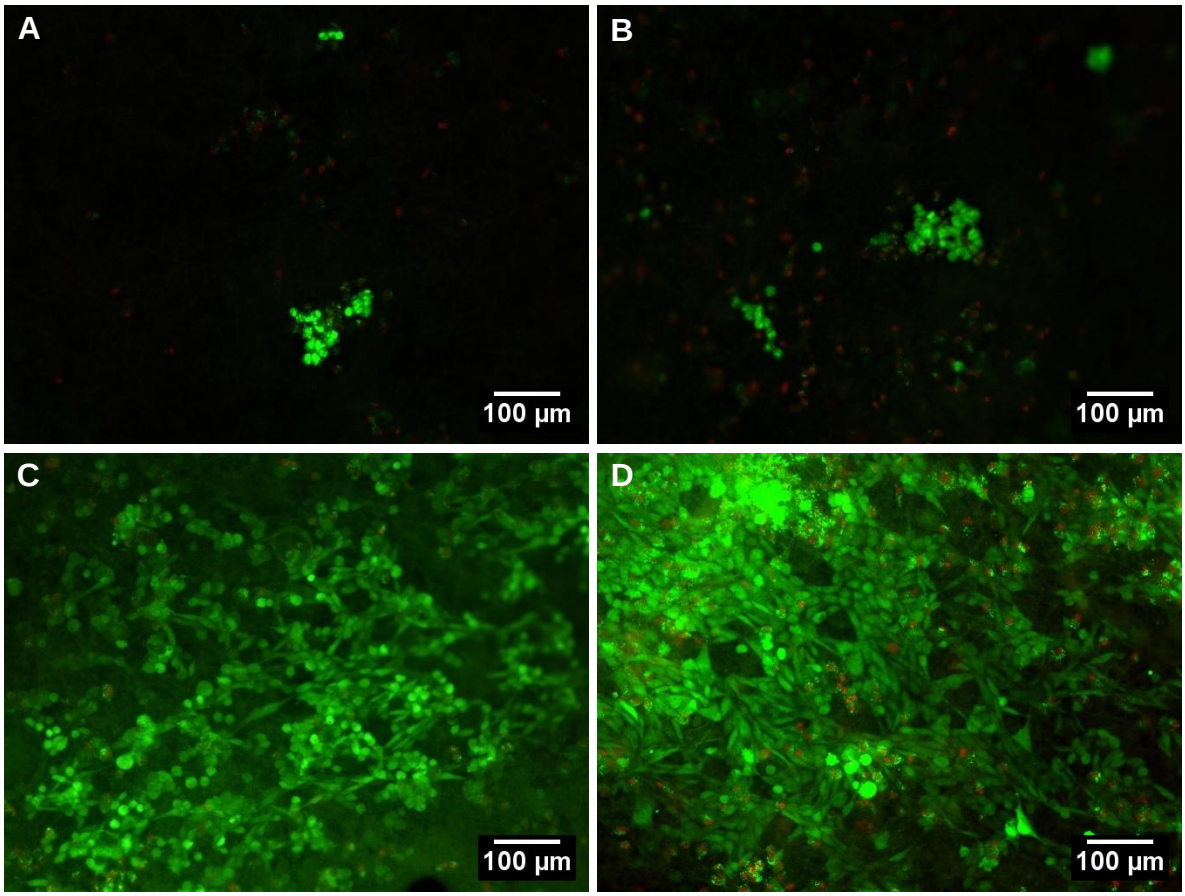

Figure 44: Upper row: Growth of L929 fibroblast on NCO-sP(EO-*stat*-PO) / PLGA meshes incubated with PBS (**A**) or with antibody mixture (**B**). Lower row: Growth of L929 fibroblast on NCO-sP(EO-*stat*-PO) / PLGA meshes pre-functionalized with RGD peptide sequence and incubated with PBS (**C**) or with antibody mixture (**D**). (Reprinted from [426]. Copyright (2017) with permission from John Wiley and Sons)

In conclusion, no interference by antibodies appeared by seeding cells on functionalized fiber meshes which is in good agreement with the cell test done with only Humira as immobilized antibody (see **chapter 5.3.2.3**).

5.3.5.2 IL-8 specific ELISA – pro-inflammatory response

For the performance of a specific IL-8 ELISA, a type of HT1080 fibrosarcoma cell line[456] was used to produce IL-8 via stimulation of the TNF receptor 2.[457] Two properties of these HT1080-Bcl2-TNFR2 cells were important for the experiments: They show an overexpression of Bcl2 (B-cell lymphoma 2) protein which is responsible for regulation of apoptosis and leads to a less distinctive cell death; on the other side, they overexpress TNFR2 which is a receptor for TNF and not commonly present in this cell type. The procedure of the IL-8 ELISA is shown in the Materials and Methods section.

First, the pro-inflammatory answer of cells was evaluated by the use of TNC-scTNF (143N/145R) as a model protein which is a trimeric fusion protein sequence of a single chain TNF.[458] Amino acids in position 143 and 145 are changed which leads to binding of this protein only to TNF receptor 2 resulting in a down-regulation of an TNFR1 dependent cytokine storm *in vivo*.[459]

For the stimulation of TNFR2, meshes were functionalized with RGD during electrospinning and then incubated with a solution of TNC-scTNF (143N/145R) immediately after the process to achieve a second immobilization of the protein on the electrospun fibers. After extraction of molecules which were not bound to the fiber surface, HT1080-Bcl2-TNFR2 cells were seeded onto the meshes and incubated overnight at 37°C. The functionality of TNC-scTNF (143N/145R) immobilized on the mesh was tested by measuring the IL-8 content in the supernatant which is formed by the cells after the activation of the TNFR2 (**Figure 45A**).

As clearly visible from **Figure 45B**, a significant difference occurred between the fibers incubated with PBS as control mesh and those which were treated with TNC-scTNF (143N/145R). This means that cells could be cultured on functionalized meshes and, at the same time, were able to interact with proteins immobilized on electrospun meshes. The adherence of cells was strong enough for those interactions which was proved by performing live/dead staining demonstrated earlier and SEM images (**chapter 5.3.5.4**).

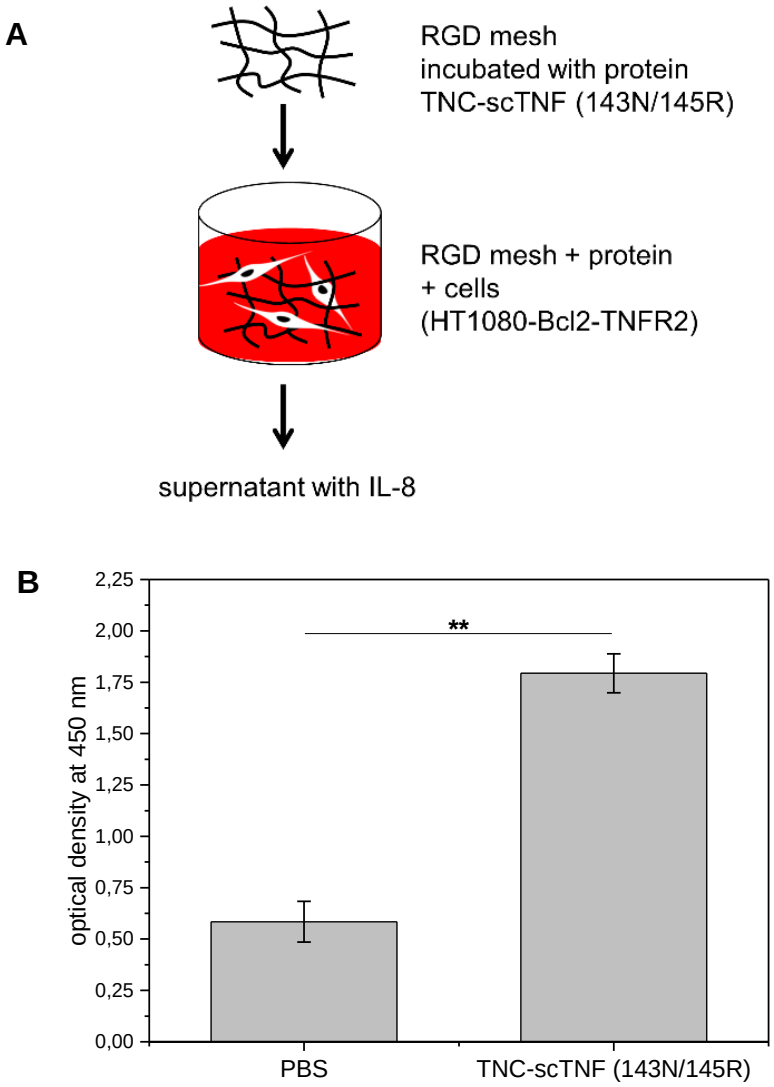

Figure 45: Pro-inflammatory IL-8 ELISA. **A**) Scheme of the reaction. After immobilization of TNC-scTNF (143N/145R), cells were seeded, and the supernatant was collected and examined regarding the IL-8 amount. **B**) TNFR2 stimulatory activity of TNC-scTNF (143N/145R)-functionalized electrospun meshes. Electrospun fibers were treated with PBS or immobilized with TNC-scTNF (143N/145R). After washing, meshes were transferred in 100 µL medium to HT1080-Bcl2-TNFR2 cells and after overnight incubation, IL-8 production of the cells was measured by ELISA. Level of significance of 1-way ANOVA: ** means $p < 0.01$. (n=3) (**B** was reprinted from [426]. Copyright (2017) with permission from John Wiley and Sons)

5.3.5.3 IL-8 specific ELISA – anti-inflammatory response

By modification of the meshes with the TNF antibody Humira, the surface of the electrospun fibers were able to attenuate pro-inflammatory reactions of the human body because immobilized Humira could retain TNF from binding to its receptors. This assumption was examined by using cell culture medium supplemented with GpL-

FLAG-TNC-TNF which was added to Humira modified fibers. After an incubation time of 2 h, the medium was transferred to HT1080-Bcl2-TNFR2 cells for stimulation.

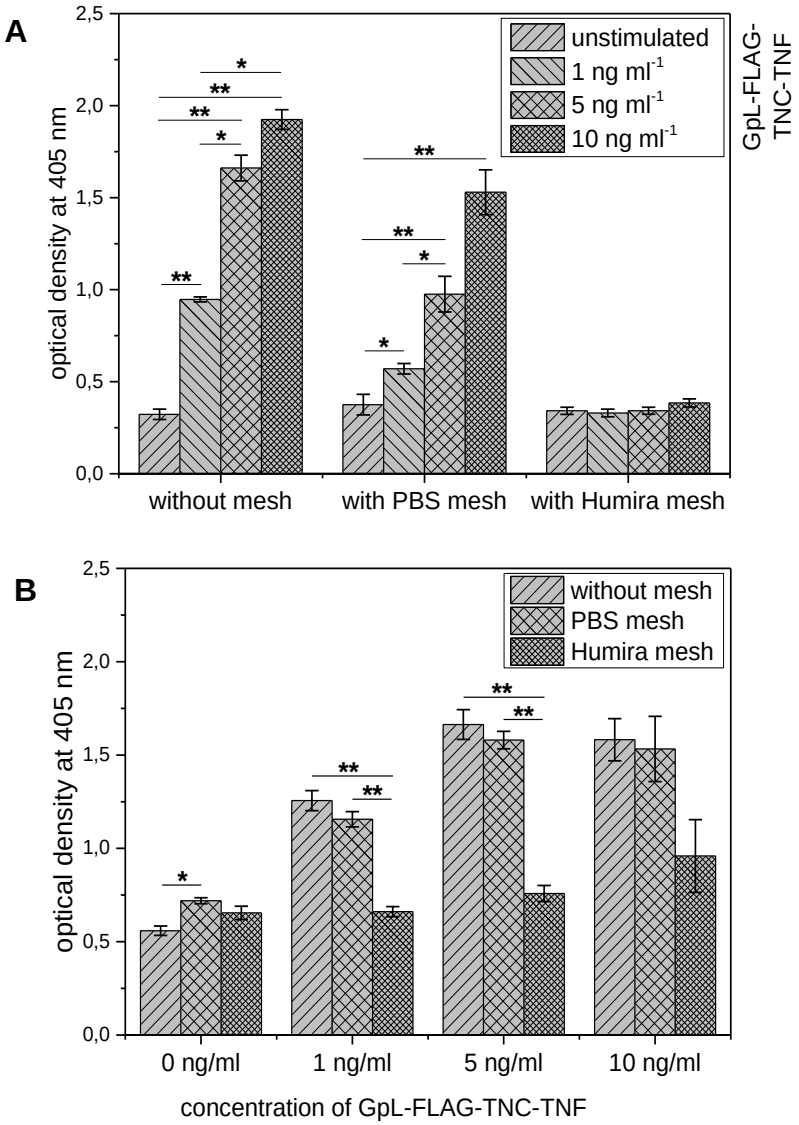

Figure 46: A) Inhibition of TNF activity by electrospun meshes functionalized with Humira antibody. The fibers treated with PBS or solution of Humira antibody were incubated with 200 µL of 1, 5 or 10 ng/ml GpL-FLAG-TNC-TNF solution in cell culture medium or in 200 µL control medium. After 24 h, 100 µL of the mesh supernatants were transferred to HT1080-Bcl2-TNFR2 cells and after overnight incubation, IL-8 production of the cells was measured by ELISA. Significant differences in IL-8 induction by supernatants of different GpL-FLAG-TNC-TNF concentrations for the same mesh type are shown. An additional experiment highlighting significant differences between different types of meshes at a given concentration of GpL-FLAG-TNC-TNF is shown in **B**. Level of significance of 3-way ANOVA: *, $p < 0.05$; **, $p < 0.01$ (n = 2). (reprinted from [426], Copyright (2017) with permission from John Wiley and Sons)

In **Figure 46**, the IL-8 measurement in the supernatants of cells is demonstrated. For control meshes without modification of antibody, it was found that the amount of IL-8 production showed the same increasing levels as for cell culture medium supplemented with GpL-FLAG-TNC-TNF without contact to an electrospun mesh. Nevertheless, the introduction of Humira immobilized on fibers and extraction and transfer of supernatants from these meshes to HT1080-Bcl2-TNFR2 cells led to significantly dampened IL-8 formation; thus, the anti-inflammatory effect of modified meshes was clearly verified by TNF depletion of the immobilized antibody.

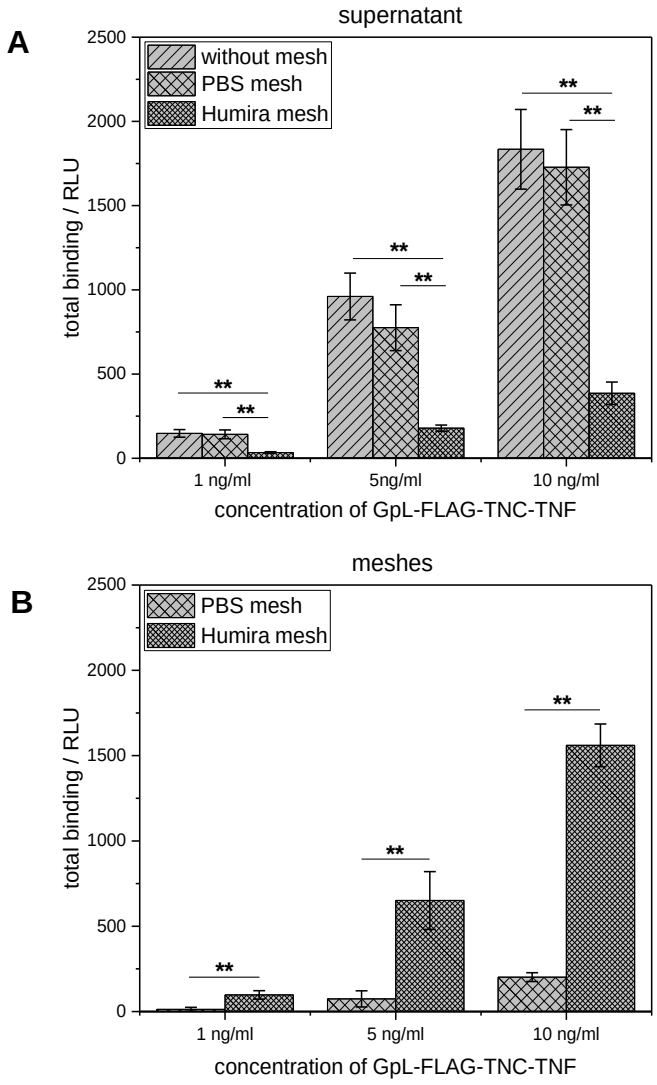

Figure 47: TNF depletion by electrospun meshes functionalized with Humira. After incubating the meshes of **Figure 46** for 2 h in 200 µL control medium or 200 µL GpL-FLAG-TNC-TNF medium, the activity of *Gaussia princeps* luciferase of an aliquot of 50 µL was measured and multiplicated with 4 to obtain total GpL activity of the supernatants (**A**). Complementary, the GpL activity of the washed meshes was measured (**B**). Level of significance of 2- and 3-way ANOVA: ** means $p < 0.01$. (n = 2) (Reprinted from [426]. Copyright (2017) with permission from John Wiley and Sons)

Additionally, the activity of *Gaussia princeps* luciferase was measured both bound on the electrospun fibers and present in the relevant supernatants from cell culture which were used to trigger cells. The results turned out to be in consistence with the significant retardant impact of fibers immobilized with Humira antibody which were incubated with GpL-FLAG-TNC-TNF containing medium and showed an alteration of IL-8 production (**Figure 46**). As visualized in **Figure 47**, the amount of GpL-FLAG-TNC-TNF fusion protein present in the cell culture medium decreased in the consistent way as the value increased bound to functionalized fibers. This is an evidence for a potent depletion of the proinflammatory molecule from the supernatant.

5.3.5.4 SEM investigation

For further examination of the cell behavior on functionalized meshes, scanning electron microscope images were recorded. In **Figure 48**, SEM pictures show the appearance of two different cell types on electrospun fiber meshes which were incubated with PBS or protein solution. As protein, TNC-scTNF(143N/147R) was used here.

For both cell types, L929 mouse fibroblasts and HT1080-Bcl2-TNFR2, similar results could be demonstrated. The cells showed an excellent adherence independently from the solution, PBS or protein, which was used for preincubation. In addition to the results from live/dead staining, this is another proof that the antibodies and proteins used for these experiments do not disturb the cell adherence.

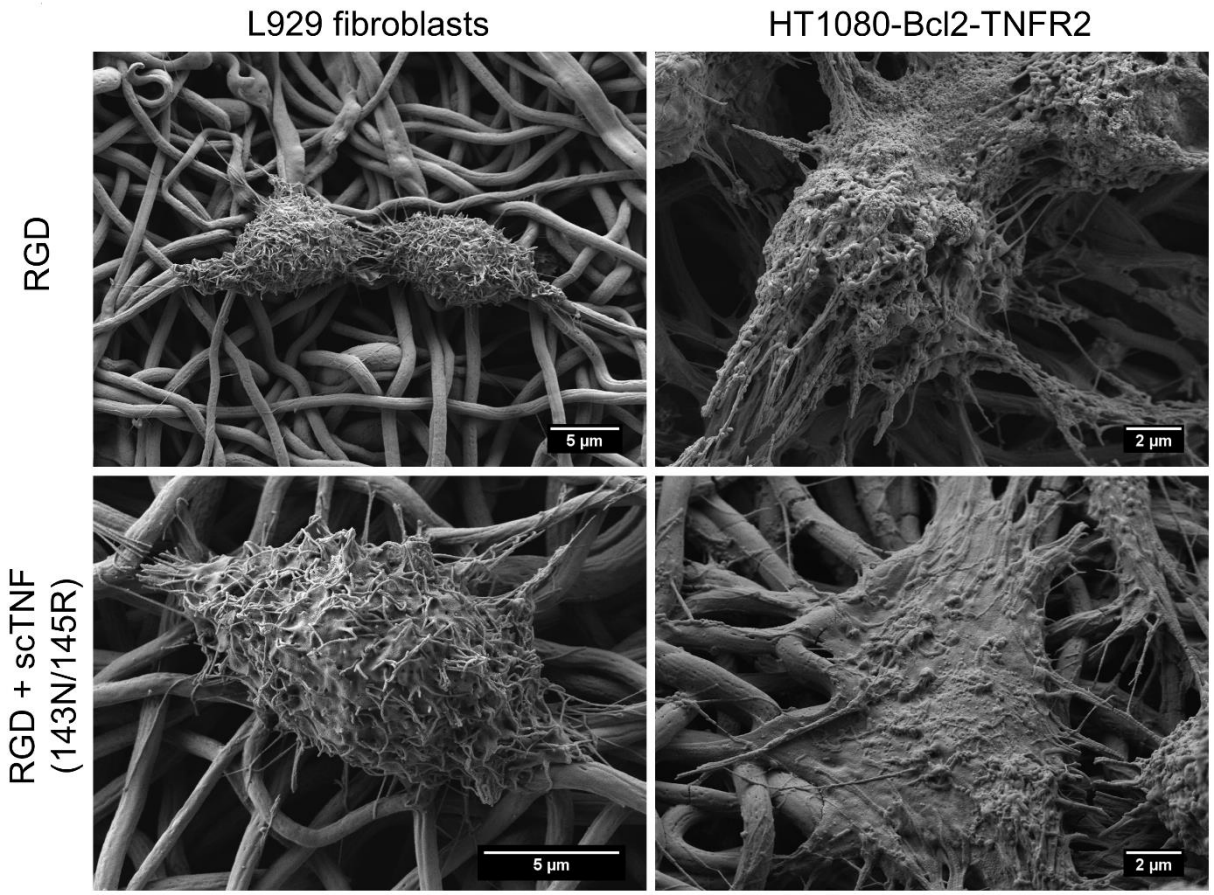

Figure 48: Scanning electron microscope (SEM) images of RGD functionalized fibers without and with addition of TNC-scTNF (143N/145R) solution which were cultured with L929 mouse fibroblasts or HT1080-Bcl2-TNFR2 cells. (Reprinted from [426]. Copyright (2017) with permission from John Wiley and Sons)

5.3.6 Immobilization of TNC-scTNF(mu) (221N/223R)

In a last experiment, it was tested if HT1080-Bcl2-TNFR2 cells were also able to adhere to mesh pieces if a TNFR2 specific reagent is present on the fiber surface independently from RGD peptide functionalization. The protein applied here is a TNFR2 specific fusion protein (TNC-scTNF(mu) (221N/223R)) which was already used in above mentioned experiments in the human variant.[459] Here, the murine type (also called STAR2)[460] was added to test an additional type of protein from varying host organisms. The results are shown in **Figure 49.**

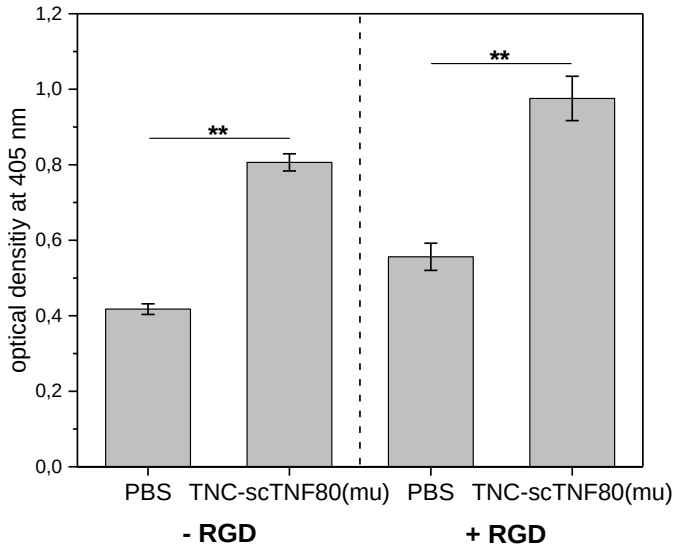

Figure 49: IL-8 ELISA of electrospun fiber meshes incubated with PBS or immobilization with the peptide TNC-scTNF80(mu) (221N/223R) without and with pre-functionalization with RGD peptide. Level of significance of 1-way ANOVA: ** means $p < 0.01$.

As clearly revealed, cells were able to interact with TNC-scTNF80(mu) (221N/223R) which was immobilized on the fibers before seeding of HT1080-Bcl2-TNFR2. This effect was observed also on meshes which were not functionalized with RGD peptide during electrospinning which means that there is an interaction of cells and peptide despite the hydrophilic properties of the fibers. The difference is not that huge but significant. Further approaches should be evaluated regarding these findings for development of an anti-inflammatory wound dressing material.

5.4 Conclusion

In this chapter, it could be demonstrated that the developed crosslinker free method of fiber functionalization is suitable for covalent binding of proteins on the surface of electrospun fibers consisting of PLGA and the prepolymer NCO-sP(EO-*stat*-PO) which leads to selective enrichment at and bioactivation of the fiber surface. The method was first proved by the use of fluorescent dyes[426-427] but was additionally transferred to an application as antibody bearing scaffold which was altered into a cell-adhesive surface by pre-functionalization with the RGD peptide sequence. Here, it was possible to immobilize one or two antibodies together with RGD at the same time which resulted in a threefold modification of the surface in two steps.

Different amounts of RGD were directly compared concerning the detection values of immobilized antibody. The hypothesis, that it would be possible to tune the number of immobilized antibodies by adjusting the RGD amount, could not be confirmed. In most cases, a higher amount of used RGD peptides led to a higher immobilization level of Humira. Further investigations must be done in future to find out more about the variations of peptide sequences.

It was shown that two different cell types, L929 mouse fibroblasts and HT1080 cells, could be cultivated on such modified scaffolds, however, the RGD peptide is needed for an adequate cell growth on the Humira functionalized meshes; without RGD, the cell adherence is not possible in these experiments.

Furthermore, cells were able to interact with proteins which are present of RGD modified fiber surfaces and in this way, IL-8 production of cells was influenced by up- or downregulation. By showing this influence on cell behavior and impact on cytokine pathways, corresponding fiber meshes could be imagined as wound dressings with immunomodulatory functionality.

6 Quantification of cell mediating peptide sequences on different surfaces produced with NCO-sP(EO-*stat*-PO)

6.1 Introduction

6.1.1 Quantification approach using Super Resolution Microscopy

The visualization of biological structures, ranging from single molecules to complete organisms, by means of newly developed fluorophores is a widely used method to label biomolecules, enzyme substrates or cellular objects.[461-462] Amongst a wide variety of detection methods, fluorescent structures can be depicted very accurately using the dSTORM method (super-resolution imaging by direct stochastic optical reconstruction microscopy). For this technique, photoactivatable or "switchable" fluorophores are used, which cause a temporary separation of the fluorescence emission.[463] dSTORM is applied for single molecule localization experiments, e.g. the distribution of proteins in cells, giving information about both molecular structures or quantitative results. It is a non-invasive fluorescence imaging technique and belongs to recent imaging technologies which are able to display absolute protein quantities present in subcellular compartments in both fixed and living cells.[464-465] Standard fluorescent dyes such as Alexa Fluor or ATTO dyes are commonly used which can reversibly switch between a fluorescent and non-fluorescent state under light irradiation. In this way, even cellular nanostructures are visualized in high resolution. The connection and disconnection of the fluorophores takes place by adding the thiol buffer β-mercaptoethylamine (MEA) which interacts with the fluorescent dye photoswitching between the active and the non-active state.[466] The cycling of fluorophores between the ground state and the excited singlet state is dependent on the redox properties, presence or absence of thiols and oxygen and pH value of the solution.[467] Thiols are known to work as a triplet quencher in an oxygen-free environment and to transfer fluorophores from the triplet into a stable nonfluorescent OFF state to ensure single-molecule localization. Oxygen leads to a recovery of the fluorescent ON state.[463, 468]

In a recent application of dSTORM, Seibel et al.[469] proposed the method to examine the adhesion properties of human cell surface glycoproteins concerning their modification after translation. Here, distribution and trafficking of membrane proteins or visualization of clusters were investigated via super resolution imaging by labeling of galectin with Alexa Fluor 647 in fixed cells. Furthermore, for analyzing the distribution of different cell components, dSTORM was applied to the visualization of mitochondria and tubulin,[470] mRNA,[471] and viruses or neuron proteins.[472]

Since dSTORM was successfully investigated for visualization and distribution of glycans present on plasma membranes,[473] it was supposed that this method is also applicable to NCO-sP(EO-*stat*-PO) modified electrospun mesh surfaces to analyze the arrangement of immobilized proteins on these materials as discussed in the following **chapter 6.3.1**.

6.1.2 Quantification approach using 2-mercaptopyridine

The immobilization of bioactive peptide sequences to biomaterials' surfaces is a popular method to improve their interaction with the surrounding biological environment. However, the identification and quantification of these peptides is challenging, as explained in the **chapter 2.4**. Therefore, an approach was developed which turned out to be a convenient and sensitive assay to detect small numbers of bioactive molecules like RGD as a fibronectin derived sequence,[430] on high-specific surface materials like electrospun fiber meshes. This new development is thought to be beneficial for determining the optimal concentration of biomolecules and for occupying a functional surface to enhance cell adhesion and proliferation.

Here, the UV-detectable 2-mercaptopyridine (also known as 2-thiopyridine) was bound to the peptide sequence serine-glycine-arginine-glycine-aspartate-serine (SGRGDS) via a cysteine disulfide bridge (SGRGDSC-thiopyridine). This molecule was used in the same way as the common RGD sequence (CGRGDS) and was mixed directly with the electrospinning solution. During the process, it crosslinked with NCO-sP(EO-*stat*-PO) followed by segregation to the fiber surface. Afterwards, 2-mercaptopyridine was cleaved by addition of *tris*(2-carboxy-ethyl) phosphine (TCEP) as a reducing agent for disulfide bridges. The quantification of the released 2-mercaptopyridine occurred photometrically, whereas the rearranging reaction of 2-mercaptopyridine and 2-thiopyridone due to thione-thiol tautomerism[474] and their UV absorption maxima were taken in account (**Figure 50**).

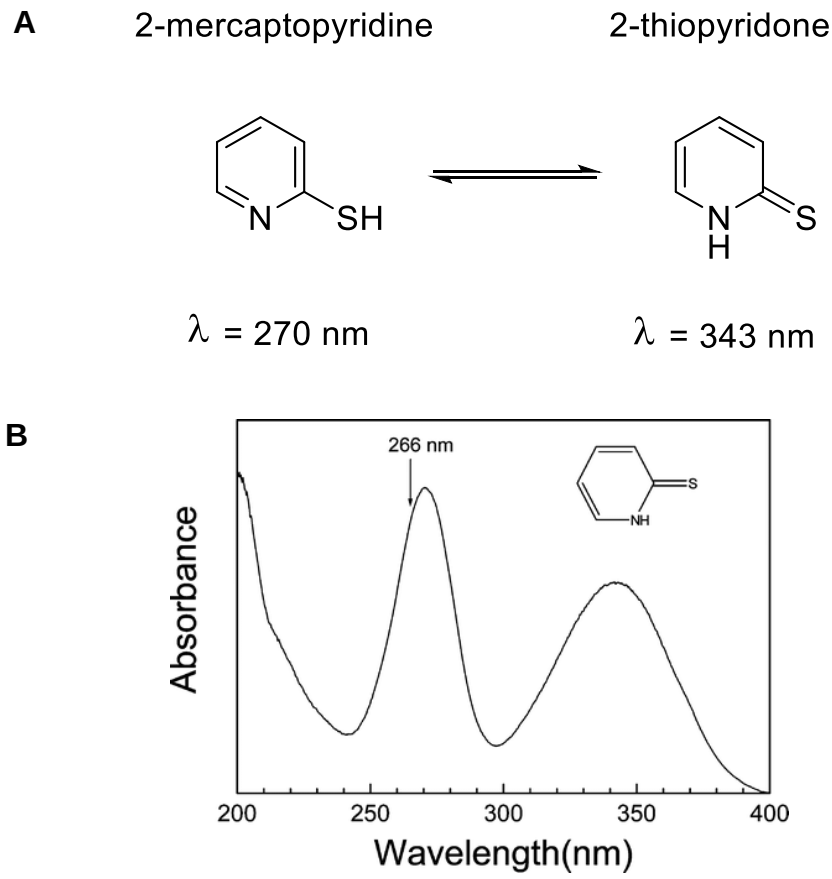

Figure 50: Thione-thiol tautomerism of 2-mercaptopyridine. **A** shows the rearrangement of 2-mercaptopyridine and its tautomer 2-thiopyridone. In **B**, an absorption spectrum is revealed with UV maxima at λ = 270 nm (2-mercaptopyridine) and λ = 343 nm (2-thiopyridone). Here, the substance was solved in water. (Reprinted with permission from [475]. Copyright (2011) American Chemical Society)

Because it was found that the absorption maximum of 2-mercaptopyridine at 270 nm revealed a stronger signal when solved in the neutral TCEP solution,[476] this wavelength was chosen for subsequent measurements.

The practicability of the described method on eletrospun fiber meshes was already proved before.[476] Aim of the following experiments in this chapter was the application of this method to quantify RGD sequences in a smaller scale comparing coated flat surfaces (2D) and electrospun fibers attached to cover slips (3D). Furthermore, the approach using 2-mercaptopyridine as detecting agent was applied to longer peptides. The RGD sequence used before consists of only 6 amino acids whereas for example a peptide sequence originating from collagen type IV exhibits a length of 14 amino acids. Collagen IV also belongs to the natural components of the extracellular matrix revealing cell adhesive properties.[477-478] Rossi et al. described that collagen in

combination with other basement membrane components led to cell adhesion of different cell types.[226] Quantification of this larger peptide chain could strengthen the reliability of this method and may lead to an advancement regarding the quantification of different basement membrane peptides.

6.2 Materials and methods

Coating of 2D substrates. Glass slides (diameter 15 mm, Marienfeld, Lauda-Königshofen, Germany) were cleaned with isopropanol and ultrasonicated with acetone, H_2O and isopropanol for 10 min at 40°C, respectively. The glass surface was activated by nitrogen plasma. Subsequently, aminosilylation was performed in an exsiccator by use of (3-aminopropyl) trimethoxysilane (Sigma Aldrich, Germany). The coating of glass substrates was done as described before.[230] Briefly, prepolymers NCO-sP(EO-*stat*-PO) were dissolved in dry THF and H_2O was added in a ratio of 1:9 (THF/H_2O) to achieve a prepolymer concentration of 10 mg/ml. For spin-coating, the substrates were placed on the device under vacuum, covered with solution and subsequently accelerated to 2500 rpm with an acceleration time of 5 s. The device operated for 40 s. The glass slides were labeled with an ethanol- and water-resistant pen. These samples were used for subsequent electrospinning to fix the fibers on the coating. If not electrospun, the coated glass slides were stored overnight at room temperature to complete the crosslinking. For experiments with peptide addition, the desired amount was mixed with water and added to NCO-sP(EO-*stat*-PO) dissolved in THF.[155] For preparation of samples which were used for quantification of RGD on flat surfaces, CGRGDS (CGRGDS (jpt, Berlin, Germany) or SGRGDS-Cys-thiopyridine (jpt, Berlin, Germany) was added to the solution in molar ratios of 2:1, 5:1 and 10:1 peptide to prepolymer.

Electrospinning: Directly after coating, the samples were transferred to the electrospinning device and fixed on the drum with double-sided adhesive tape. NCO-sP(EO-*stat*-PO) was dissolved in dry dimethyl sulfoxide (DMSO) and stirred for 10 min. The solution was diluted with acetone (DMSO – acetone ratio 1:5 V/V), briefly mixed and finally PLGA was added and stirred until the solution was homogenous. The polymer content of the solution was 5 wt% for NCO-sP(EO-stat-PO) and 24.5 wt% for PLGA. Polymer solutions were fed at 0.5 ml/h through a flat-tip stainless steel spinneret connected to a high-voltage power supply (Voltcraft® Laboratory Power Supply, Conrad Electronic SE, Hirschau, Germany) and a high voltage of 13 kV was applied to the spinning solution. The collection distance between spinneret and grounded collector was 14-15 cm. The non-woven meshes were collected on a rotating drum as grounded collector (diameter 60 mm, length 100 mm) with a rotation speed of 120 rpm.

Samples for quantification using Alexa Fluor dyes and microscopy. After various processing times of electrospinning, the process was stopped, and the glass slides were removed from the drum by cutting the edges with a scalpel. These samples were stored overnight at room temperature to complete the crosslinking reaction. After 12 h, the glass slides were incubated with PBS to crosslink any remaining isocyanate groups to amines. Subsequently, Alexa Fluor 647 NHS ester (50 µg/ml in PBS; Life Technologies, Germany) was added. The samples were incubated for 2 h in the dye solution and washed at least 6 times with PBS to remove residual Alexa Fluor 647. Another approach was the incubation of samples with immobilized 2-mercaptopyridine-modified RGD with *tris*(2-carboxyethyl) phosphine hydrochloride (TCEP, Sigma Aldrich, Germany) solution ($3.018x10^{-5}$ mol/ml in 0.1M NaOH, pH 7.4) to remove the UV-detectable group. Afterwards, the free thiol group was thought to be available for the reaction with Alexa Fluor 647 maleimide (50 µg/ml in PBS; Life Technologies, Germany). After washing, the samples were measured by means of a fluorescence microscope Axioimager M1 (Zeiss, Germany) and a confocal laser scanning microscopy (Leica TCS SP8, Wetzlar, Germany). Additionally, samples were observed with a confocal laser scanning microscope LSM 700 (Zeiss, Germany). For dSTORM microscopy, a self-made setup was used which was constructed around an inverted fluorescence microscope IX71 (Olympus, Germany) together with a laser, lenses and a dichroic beam splitter. The experimental setup was described before.[463]

Quantification using 2-mercaptopyridine. Samples were prepared with addition of different amounts of peptide sequences into DMSO, solved and subsequently added to NCO-sP(EO-*stat*-PO) and stirred for 10 min as described above. The electrospinning process took place for 7.5, 15, 30 and 60 min. The quantification protocol was adapted from [476].

RGD Quantification. For quantification of samples in 2D (flat NCO-sP(EO-*stat*-PO)-coated surfaces) and 3D (NCO-sP(EO-*stat*-PO)-coated substrates with electrospun fibers), RGD was detected via the UV-active molecule 2-mercaptopyridine. Therefore, samples were prepared as described above and transferred into 24-well plates. After washing with 300 µl TCEP ($3.018x10^{-5}$ mol/ml in 0.1M NaOH, pH 7.4) overnight on a shaker under light protection, the solution was removed from samples and measured with a plate reader (Tecan Spark 20 or Tecan Infinite 200, Tecan Trading AG, Männedorf, Switzerland) at 270 nm. The samples were washed 3 times with water and

300 µl 1M NaOH was added to solve the specimens during overnight incubation under light protection. After 24 h, TCEP powder was solved in the NaOH solution in a concentration of $3.018x10^{-5}$ mol/ml to achieve a pH value of 7.4. The samples were incubated on a shaker for another hour and the absorbance of the supernatant was measured with both Tecan readers at 270 nm.

Quantification of collagen sequences. After electrospinning as described above using different amounts of collagen sequences CGEFYFDLRLKGDK as reference and SGEFYFDLRLKGDK-Cys(2-Thiopyiridine) as quantification reagent (both jpt, Berlin, Germany), meshes were cut into pieces (4 x 6 cm) and weighed. Pieces were transferred into petri dishes (94 x 16 mm) and washed with H_2O overnight on the shaker under light protection. After 24 h, water was removed from the samples and mixed with a defined quantity of water with the same amount of TCEP (in 0.2M NaOH, pH 7.4) and the absorbance was measured with two different Tecan reader at 270 nm. Remaining samples were rinsed with 2 ml TCEP solution ($3.018x10^{-5}$ mol/ml, in 0.1M NaOH, pH 7.4) and shaken overnight at room temperature under light protection. The solution was removed and used for absorbance measurements at 270 nm. The meshes were washed three times with water and afterwards were solved in 1M NaOH. After 24h, TCEP was added to samples to achieve a pH value of 7.4, solved and after another hour of incubation, the supernatants were measured again by means of a plate reader at 270 nm.

Analysis of Variance (ANOVA): ANOVA was examined by means of SigmaPlot (Systat Software GmbH, Erkrath, Germany) using 1-way or 2-way ANOVA depending on the raw data. In order to calculate the statistical significance, a post hoc Tukey test was performed.

6.3 Results and discussion

6.3.1 Quantification of molecules using super resolution microscopy

6.3.1.1 Fluorescence and confocal images

The aim of these experiments was to visualize NCO-sP(EO-*stat*-PO) molecules on the fiber surface by labeling them with Alexa Fluor 647 NHS ester. In order to ensure that all isocyanate groups reacted to amino groups, meshes were cut into pieces and stored in PBS buffer overnight. After incubation and visualization of the meshes by means of the ZEISS fluorescence microscope, it was found that the samples incubated with Alexa Fluor 647 (**Figure 51B** and **D**) had a strong red fluorescence in comparison to those incubated with PBS only (**Figure 51A** and **C**) revealing no fluorescence. This indicates a successful incubation process.

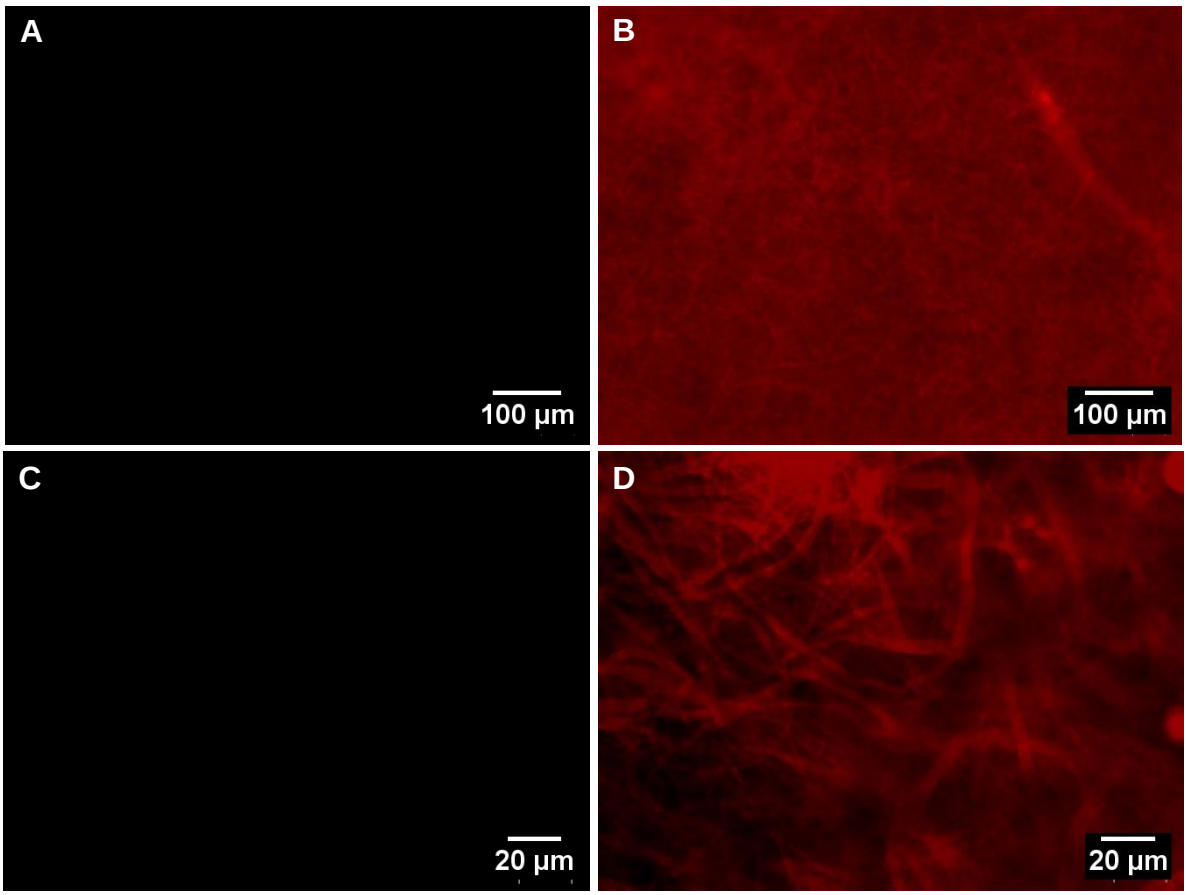

Figure 51: Meshes incubated with PBS as control (**A, C**) and with Alexa Fluor 647 NHS ester (**B, D**). Two different magnifications are shown. The exposure time was 2500 ms.

With confocal microscopy (**Figure 52**), it was additionally possible to detect the strong red fluorescence in comparison to a non-functionalized fiber mesh.

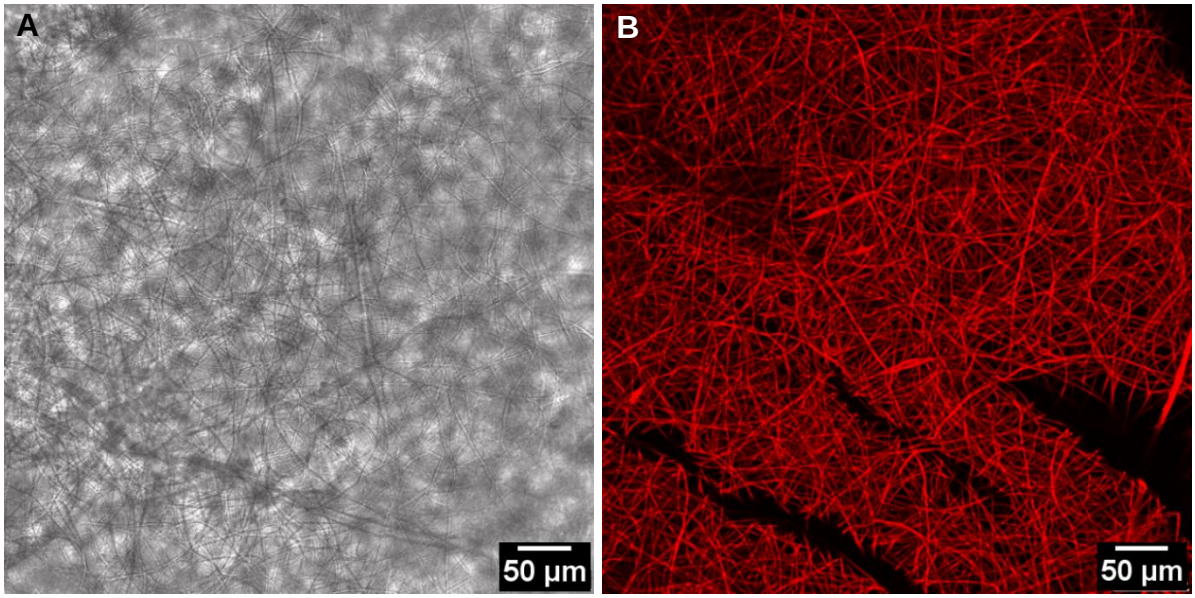

Figure 52: Fiber meshes were observed via a confocal microscope. In **A**, a control image of the nonwovens is shown which was recorded with transmitted light. In **B**, the laser was switched on and the red fluorescence of the fibers originating from Alexa Fluor 647 immobilization is demonstrated.

6.3.1.2 Imaging with dSTORM microscopy

Subsequently, the visualization of fiber meshes was tested via dSTORM microscopy to examine the distribution of NCO-sP(EO-*stat*-PO) on the mesh surfaces. Here, after isocyanate hydrolysis, amino-functional scaffolds were used to detect them via the fluorescent NHS ester.

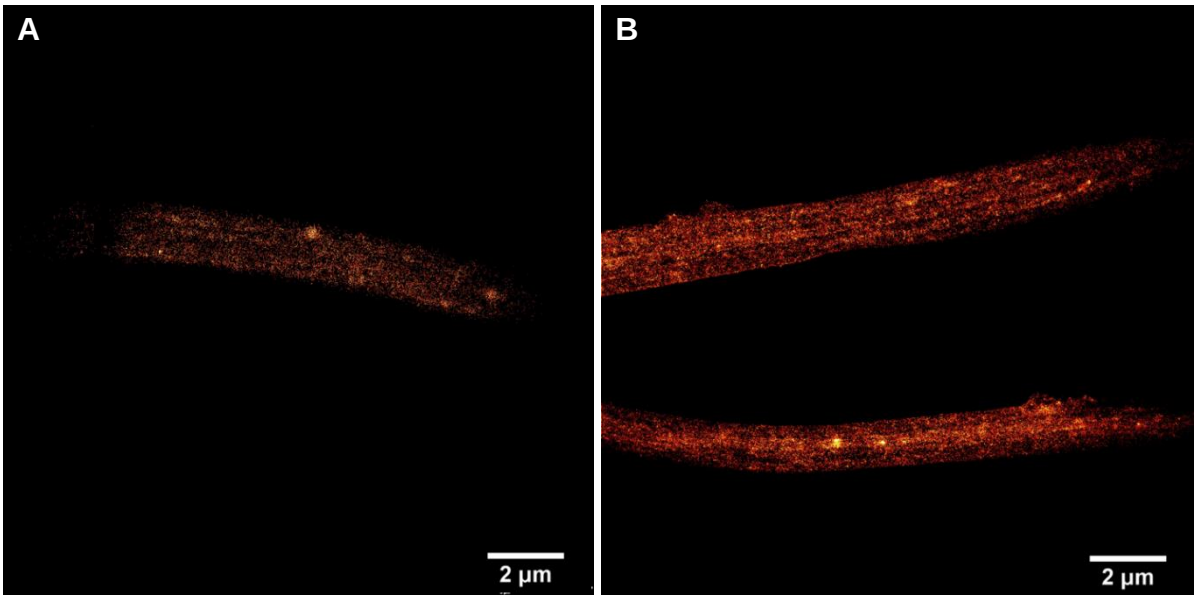

Figure 53: 2D dSTORM images showing two different areas (**A** and **B**) of electrospun fibers labeled with fluorescent dye.

Figure 53 shows fibers at the edge of the mesh pieces with a thickness of about 1 µm which is in good agreement with results from scanning electron microscopy (SEM).[46] The dye occupancy appeared homogeneously but the fluorescent molecules seemed to be distributed within the fiber. This is probably a result of an excessive label density and background caused by a high fiber density on the surface after prolonged electrospinning. This problem was solved by a reduction of the processing time to collect only a small number of fibers on the cover slips. In addition, 3D imaging was thought to be helpful to analyze whether the dye molecules are located within the whole fiber volume or only on top of the fibers.

In order to improve focusing during data acquisition, single electrospun fibers were fixed on NCO-sP(EO-*stat*-PO) coated cover slips to improve the adhesion of fibers via a crosslinking reaction. As a result, demonstrated in **Figure 54**, apparent double wall structures were observed for some fibers whereas other fibers showed a homogenous distribution of dye localization. Furthermore, the diameter of several fiber areas was measured showing variations of the thickness of fibers. The double wall structures could be a hint that Alexa Fluor 647 is mainly located in the walls of the fibers and is not migrating into the fiber which means that NCO-sP(EO-*stat*-PO) remained predominantly on the surface during the electrospinning process.

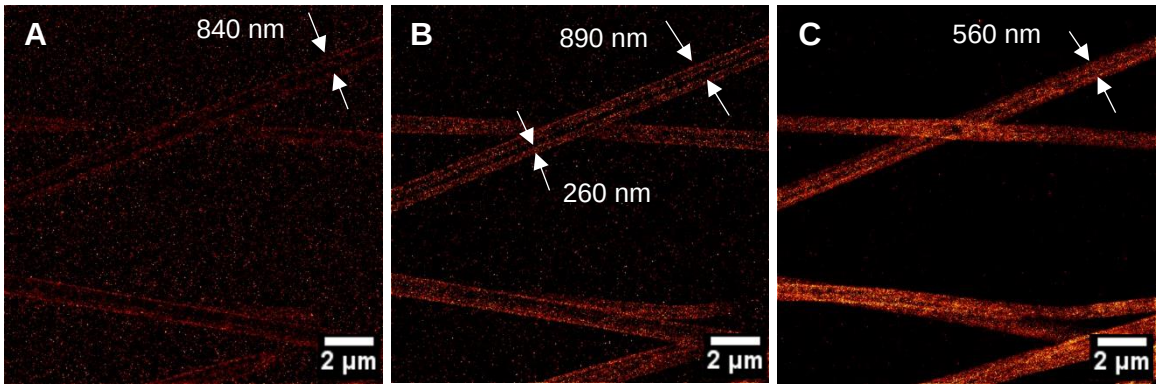

Figure 54: dSTORM image in 2D without coating. Fiber diameters are indicated with arrows. **A**, **B** and **C** show different sections. (adapted from measurements done by M.Sc. Saskia Kutz, Department of Biotechnology and Biophysics, Würzburg)

6.3.1.3 Approaches for quantification

The electrospinning time was further reduced from 10 min to about 7 min to achieve more isolated fibers for the following examination. Additionally, the established method of quantification using the UV-detectable 2-mercaptopyridine as modifying agent for peptide sequences[476] was transferred to 2D glass substrates. Therefore, SGRGDSC-thiopyridine functionalized fibers on glass cover slips were stored at room temperature after electrospinning to complete the crosslinking of isocyanates and functionalized peptide. Then, the samples were washed in TCEP solution ($3.018*10^{-5}$mol/ml in 0.1M NaOH, pH 7.4) to cleave the disulfide bridge within the molecule. Thiol moieties are known to interact with SH-reactive Alexa Fluor 647 maleimide [479] Therefore, resulting free thiol groups might interact with this dye which was detected by confocal microscopy.

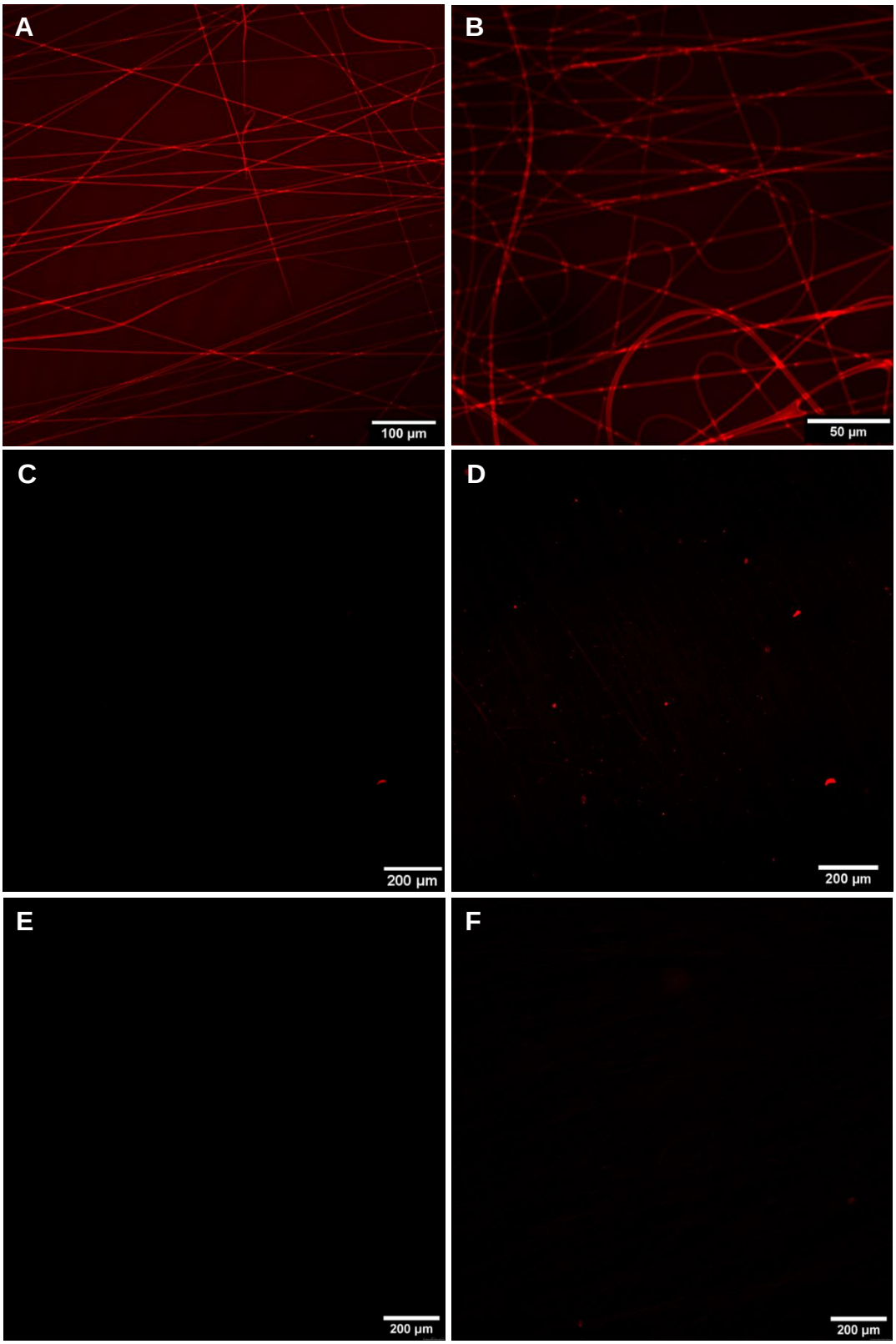

Figure 55: Confocal images of samples labeled with Alexa Fluor 647 NHS ester (**A, B**) or maleimide (**C, D**) in comparison to controls washed with PBS buffer (**E, F**). The successful immobilization of the dye is demonstrated in different magnifications. In **C** and **E**, the same adjustments were used as for Alexa Fluor 647 NHS ester, in **D** and **F** a higher laser power and higher gain was adjusted. Images were recorded with the Leica TCS SP8 (Wetzlar, Germany).

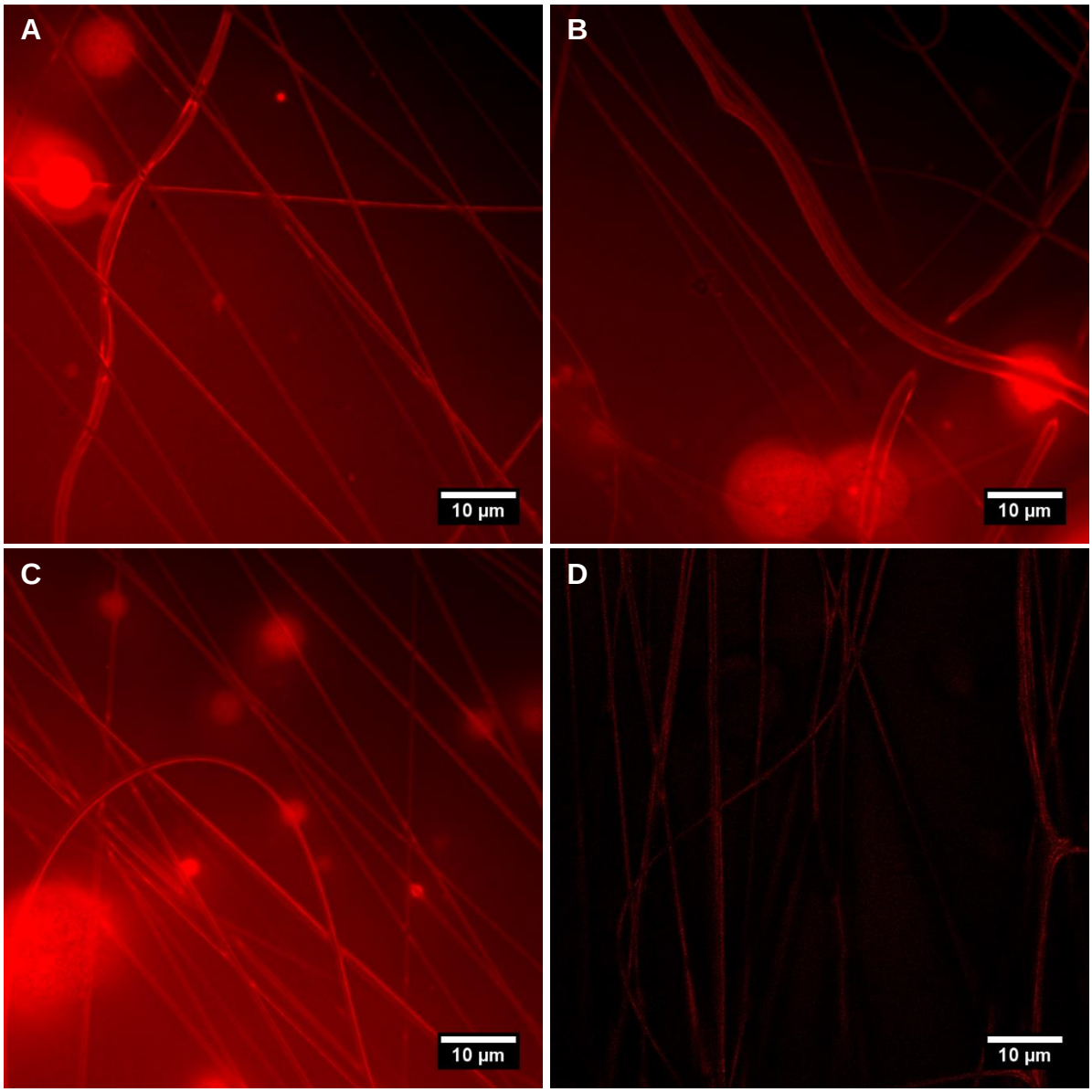

Figure 56: Confocal microscopy with the confocal laser scanning microscope LSM 700 (Zeiss, Germany). The images show various areas of the fiber meshes. In **A**, **B** and **C**, fibers were labeled with Alexa Fluor 647 NHS ester. **D** is the control washed with PBS buffer only.

In **Figure 55A** and **B**, the successful binding of Alexa Fluor 647 NHS ester and the resulting strong red fluorescence is demonstrated in comparison to PBS washed samples (**Figure 55E** and **F**). The distribution of fluorescent dye over the whole fiber diameter was observed again revealing a stronger fluorescence at intersections of two fibers. Additionally, some apparent double wall structures were present. Samples with immobilized Alexa Fluor 647 maleimide on free thiol groups resulting from disulfide cleavage via TCEP (**Figure 55C** and **D**) revealed only some fluorescent “dots” but no

labeling of the whole fiber. This is either due to an insufficient cleavage of the disulfide bridges or a failed reaction of thiols with the fluorescent dye.

Similar results were obtained with the Zeiss LSM microscope (**Figure 56**). Some fibers showed apparent double walls, and some artefacts were visible because of the strong labeling quantity. In comparison, in the control meshes, where the fibers were treated with PBS buffer, hardly any red fluorescence could be detected.

Nevertheless, with these samples, dSTORM microscopy was not possible due to the absence of a fluorescent image since the activation of the dye with the MEA buffer was not working. For the successful quantification of functional RGD on fiber surfaces, another method should be used which is introduced in **chapter 6.3.2**.

6.3.2 RGD quantification of 2D flat surfaces compared to 3D electrospun fibers

Since the established method of using 2-mercaptopyridine for quantification of surface-bound RGD led to reliable results in former experiments,[476] this approach was transferred from the dense electrospun meshes to a functional coated glass substrate where only few electrospun fibers were collected as 3D model. Subsequently, these samples were compared with coatings on a flat surface which represented the 2D status.

For the coating, glass slides were treated via aminosilylation and coated with NCO-sP(EO-*stat*-PO) solution which was functionalized with RGD peptide bearing the UV-cleavable group 2-mercaptopyridine. For electrospinning, cover slips were coated with NCO-sP(EO-*stat*-PO) without RGD to enable crosslinking with electrospun fibers. These fibers were spun from a solution containing the functional peptide. The surfaces were thought to be compared to each other regarding the available number of RGD molecules. Therefore, varying densities of RGD on 2D or 3D surfaces were prepared, as demonstrated in **Figure 57**.

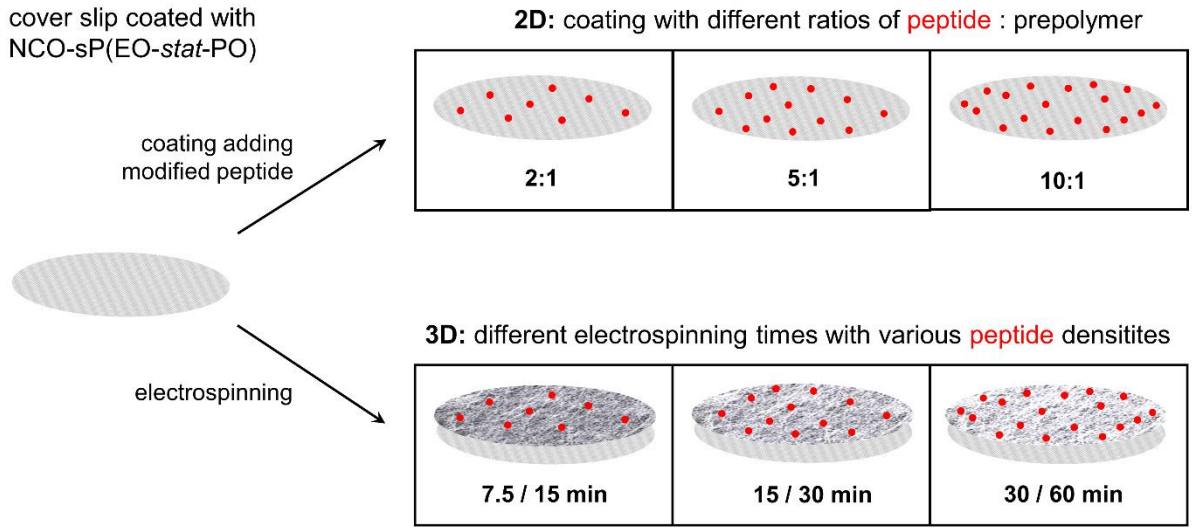

Figure 57: Working protocol of RGD quantification experiments for comparison of 2D vs. 3D surfaces. Different ratios of peptide to prepolymer and varying working times are indicated.

Initially, a calibration curve was obtained to show the correlation between the number of peptides and the measured absorbance. Increasing amounts of 2-mercaptopyridine and the functionalized peptide were solved in TCEP solution ($3.018x10^{-5}$ mol/ml, in 0.1M NaOH, pH = 7.4) and UV absorbance was obtained by means of a plate reader. Since former experiments were performed with the plate reader Tecan Infinite 200, the following experiments were done with this device. To compare the outcomes of diverse plate readers, additionally, a Tecan Spark 20M was used. The resulting calibration curves for both machines are shown in **Figure 58**.

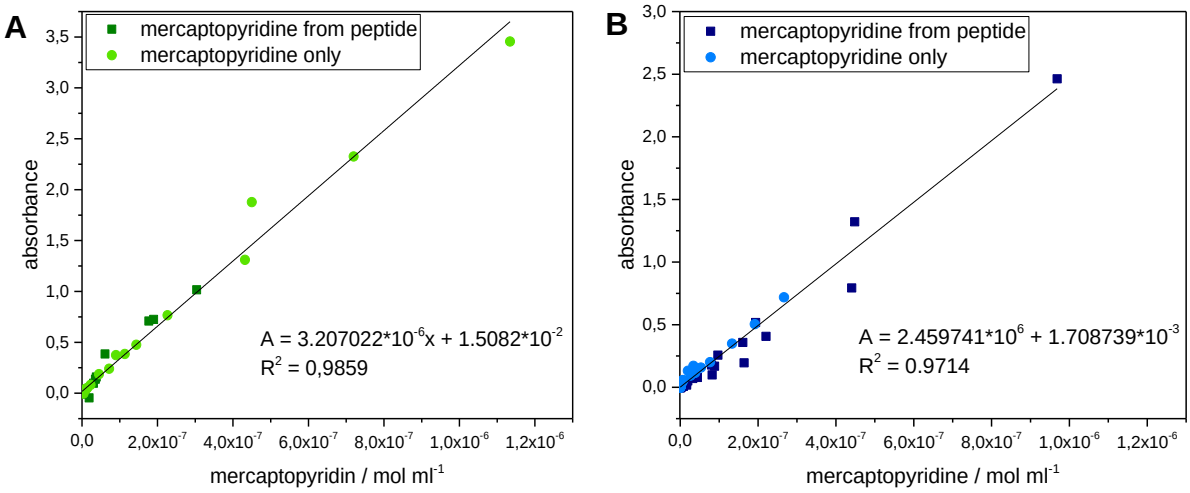

Figure 58: Calibration curves of modified RGD peptide measured with different Tecan plate readers at a wavelength of 270 nm. **A** shows the curve established with the Tecan Spark 20M, **B** shows the curve from the Tecan Infinite 200. For the measurements, peptides were solved in neutral TCEP solution ($3.018x10^{-5}$ mol/ml, in 0.1M NaOH, pH 7.4).

Comparing values from pure 2-mercaptopyridine and the cleaved one from the peptide, it could be observed that the concentrations were in good agreement to each other and led to a linear correlation between the applied concentration and the measured absorption.

These standard curves were used for the following experiments to calculate the amount of RGD molecules on different surfaces indirectly by measuring equivalent values of 2-mercaptopyridine cleaved from the peptide.

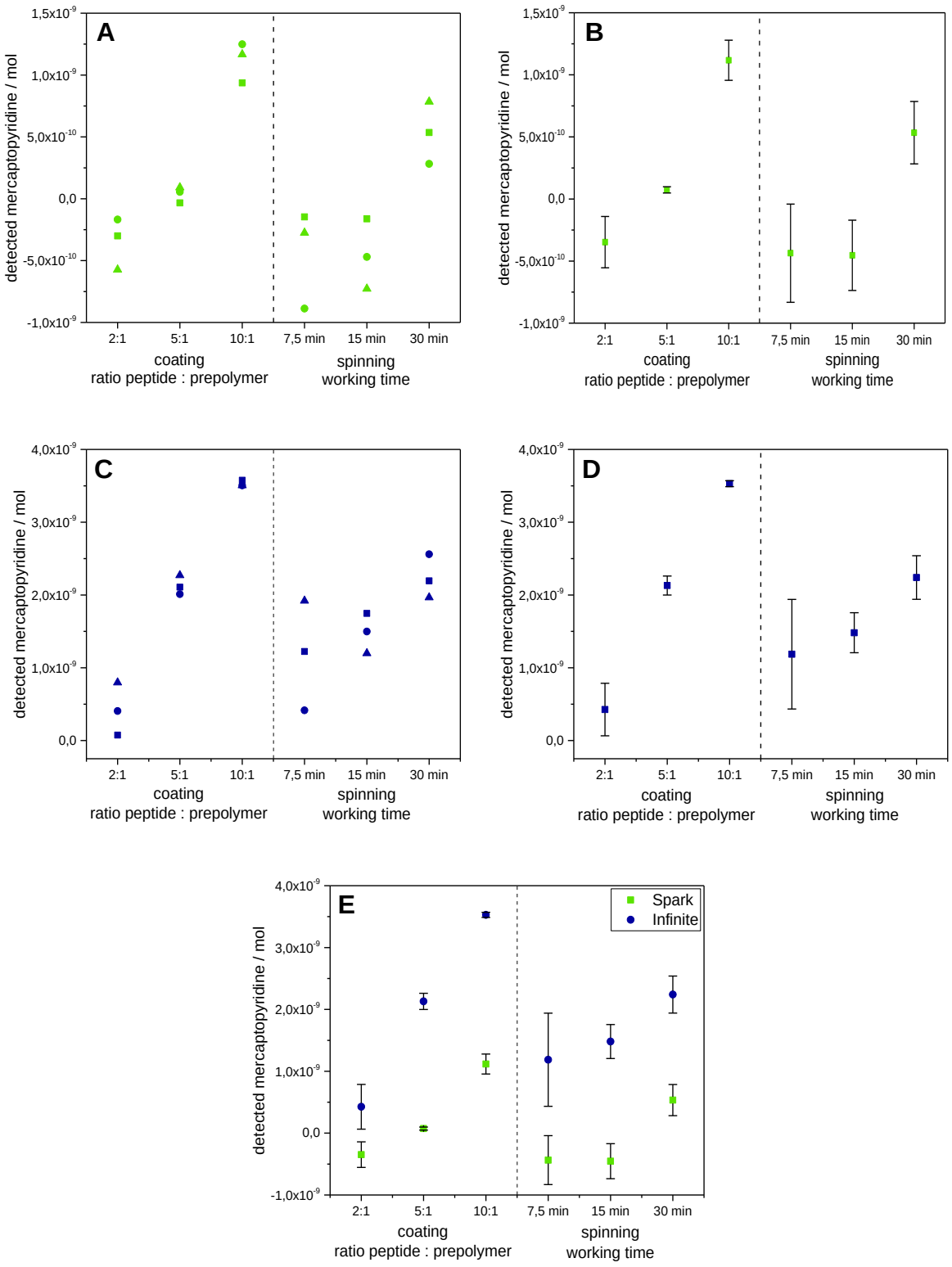

Figure 59: First quantification experiment performed with coatings using different ratios of functional RGD (stated as peptide) to NCO-sP(EO-*stat*-PO) (stated as prepolymer) in comparison to varying dense fiber meshes achieved by different working times of electrospinning attached to cover slips. Experiments with Tecan Spark 20M are marked in green, the ones using Tecan Infinite 200 are shown in blue. **A** and **C** depict the single values from three samples, **B** and **D** reveal the mean value and standard deviation. In **E**, the results from both devices are compared. (n = 3)

In **Figure 59**, the first results of RGD quantification on the 2D vs. 3D level are shown. For better visualization, all performed calculations are demonstrated and marked in green and blue showing the results of different devices. First, the single values are presented in **A** and **C** plotted against the molar amount of 2-mercaptopyridine which was figured out of the linear fit from **Figure 58**. Furthermore, the mean values were determined as shown in **B** and **D**. In **Figure 59E**, both devices were compared regarding the results. It is revealed that the outcomes of the Tecan Spark 20M and the Tecan Infinite 200 are similar. The values showed a linear behavior, when the different ratios of peptide to prepolymers used for the flat coatings and the increasing working times of electrospinning are plotted against the detected 2-mercaptoyridine concentration. Concerning the comparison between the two devices, it is clearly demonstrated that the measurement with the plate reader Tecan Infinite 200 yielded higher values which are located above the zero line; these results are much more convenient than data with negative outcomes. Here, the negative values resulted from a very low absorption of the samples. Absorption data from the bottom end of the calibration curve are commonly not reliable. Additionally, the absorption of the pure TCEP solution revealed a higher value than the measured value of the sample followed by negative results when this blank value was subtracted.

Hence, only results from the Tecan Infinite 200 are shown below.

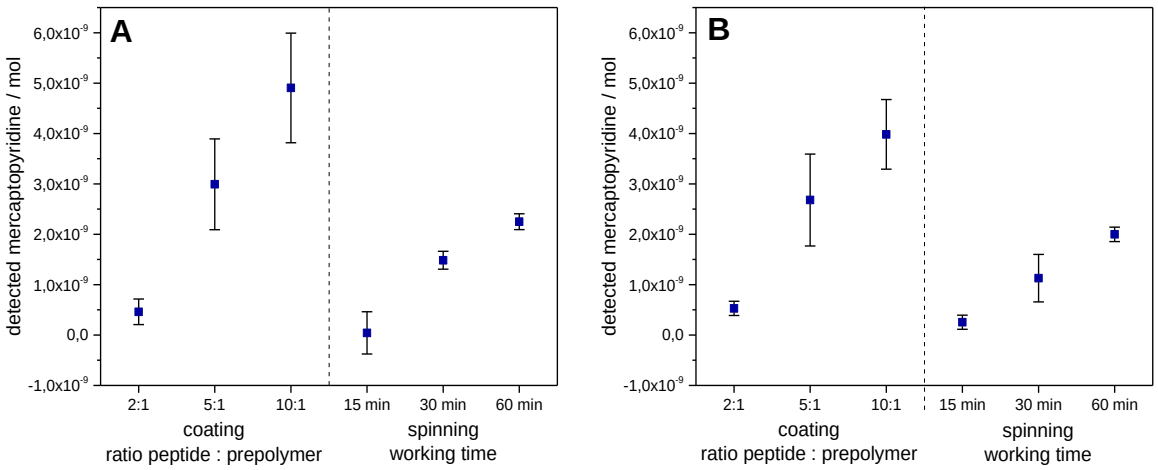

Figure 60: Further experiments regarding RGD quantification of 2D vs. 3D surfaces. Again, different ratios of functional RGD (stated as peptide) to NCO-sP(EO-*stat*-PO) (stated as prepolymer) in comparison were used. For electrospinning, longer working times were chosen. Experiments were performed using the plate reader Tecan Infinite 200. **A** and **B** reveal individual experiments. (n = 3)

Figure 60 shows that for longer electrospinning times, the values were similar for both experiments. However, the extension of the spinning duration did not result in higher molar amounts of 2-mercaptopyridine. A reason for this phenomenon might be a variation of the electrospinning process due to influences from air humidity and temperature. Another explanation could be the density of the fiber mesh. 2-mercaptopyridine molecules might be caught between the dense packed fibers, which result from a longer electrospinning time, and therefore were not available in the supernatant for UV detection.

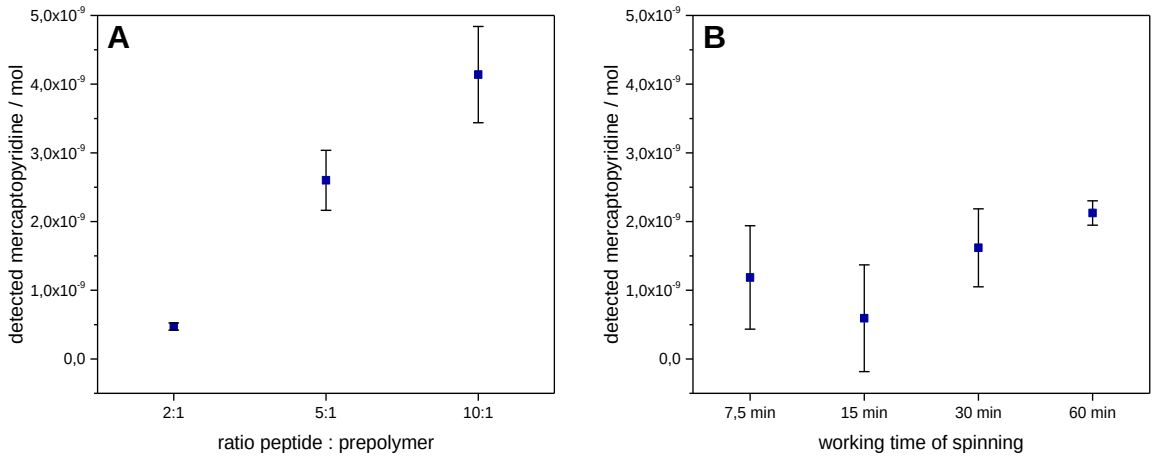

Figure 61: Comparison of all RGD quantification experiments of 2D flat surfaces (**A**) with varying ratios of RGD to NCO-sP(EO-*stat*-PO) and 3D electrospun fibers with increasing time periods (**B**) using the UV-reactive molecule 2-mercaptopyridine. (n = 3)

Figure 61 gives a summary of all experiments calculating the mean values and standard deviations. Regarding the results of the RGD quantification on flat surfaces, it could be concluded that there was a linear correlation between the applied peptide being available on the coating and the molar amount of detected 2-mercaptopyridine. Nevertheless, it was not possible to calculate the certain number of detected UV-cleaved molecules because the coating was formed by spin rotation where several drops are applied on the glass substrate, but parts of the solution are removed from the surface by spinning. Thus, no relation could be established between the applied and the detected amount of 2-mercaptopyridine.

For electrospun 3D surfaces, an evaluation of the accurate 2-mercaptopyridine quantity could not be performed as well because it cannot be clarified how many percent of electrospun fibers are present on the coverslips stuck on the rotating collector. However, a linear relation between rising spinning times and molar concentration of detected 2-mercaptopyridine was evaluated.

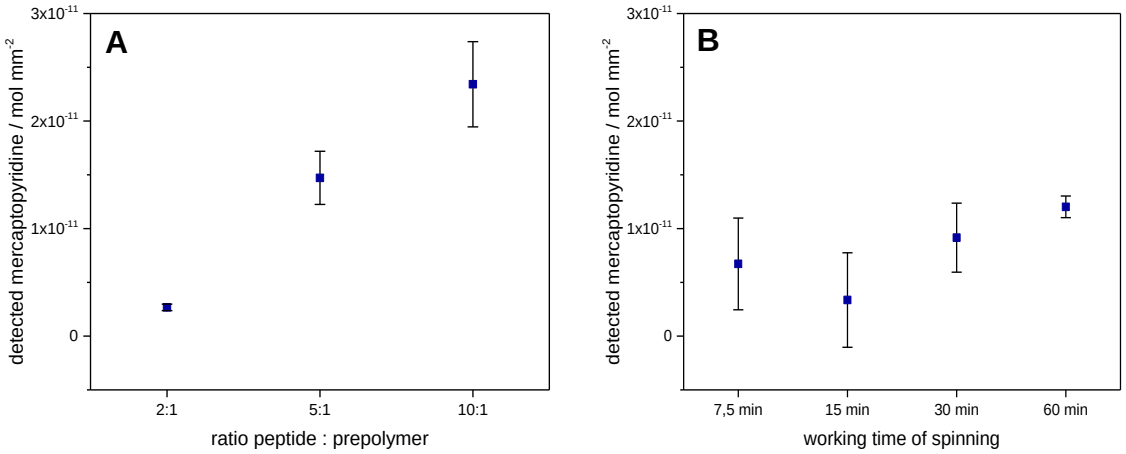

Figure 62: Quantification of 2-mercaptopyridine on flat coatings with different ratios of peptide to NCO-sP(EO-*stat*-PO) **(A**) and on 3D electrospun surfaces with increasing time periods of electrospinning (**B**) in relation to mm^2 of surface. (n = 3)

Another calculation is shown in **Figure 62** determining the results in mol per mm^2 surface. As demonstrated here, the linear trends for both surfaces remain the same revealing lower values as demonstrated in **Figure 61** which can be explained by the relation to 1 mm^2. For 3D surfaces in comparison to 2D flat coatings, molar concentrations of detected 2-mercaptopyridine were lower. A reason for that might be that for preparation of these fibers a peptide to prepolymer ratio of 1:1 was used for the electrospinning solution.[46] When considering flat coatings with a ratio of 2:1, the resulting molar concentrations of 2-mercaptopyridine were found to be higher on electrospun surfaces. Therefore, it might be concluded, that in general a smaller amount of RGD peptide is needed to cover electrospun fibers than for 2D coatings, where an excess of coating solution must be used, and a certain amount of coating solution gets lost during the process.

6.3.3 Quantification of collagen peptide sequences on electrospun fiber surfaces

In this section, the quantification of longer peptide sequences was evaluated for the first time using 2-mercaptopyridine. Therefore, a peptide derived from collagen IV (CGEFYFDLRLKGDK) was used consisting of the residues 531-543. Here, the UV-detectable group 2-mercaptopyridine was bound to the peptide via a terminal cysteine functionalization (SGEFYFDLRLKGDK-Cys(2-Thiopyiridine)); this is going to be stated as thiopyridine-collagen in the following section.

The calibration curves were determined using 2-mercaptopyridine as pure substance and, in this case, the modified collagen sequence. The samples were measured with the previously mentioned Tecan plate readers Spark 20M and Infinite 200. The resulting curves are in good correlation to the ones derived from 2-mercaptopyridine functionalized RGD (**Figure 63**).

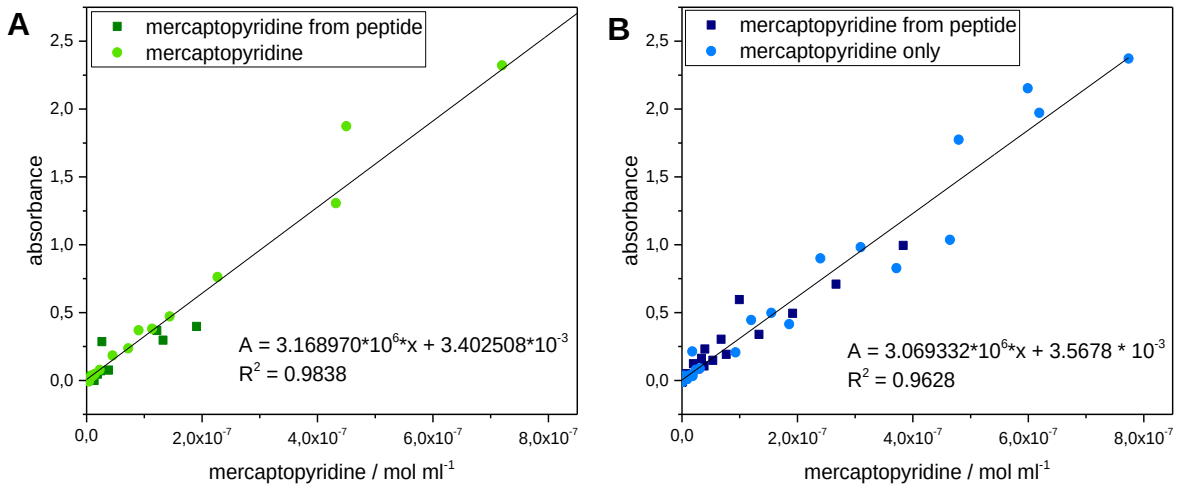

Figure 63: Calibration curves of 2-mercaptopyridine from peptide and from the pure reagent. **A** shows the resulting linear slope received from the plate reader Tecan Spark 20M, **B** reveals the results from the Tecan Infinite 200. For the measurements, peptides were solved in neutral TCEP solution (3.018×10^{-5} mol/ml, in 0.1M NaOH, pH 7.4).

The calculation of collagen IV was done by measuring the absorbance and calculating the mol/ml from of the calibration curve. The amount of 2-mercaptopyridine (mol) was then correlated to the theoretical calculated value estimated from the weight of the samples and the molecular weight of the reagent resulting in %.

In the beginning, some problems occurred, because the absorption of pure TCEP solution showed similar results than those of the measured samples. After calculating the mol/ml of 2-mercaptopyridine from the standard curve, the values turned out to be very low in the range of 10-20% of detected 2-mercaptopyridine in comparison to the introduced 2-mercaptopyridine (100%) measured with both devices (data not shown). Thus, meshes were stored for at least 48-96 hours before evaluating them to guarantee a complete crosslinking between NCO-SP(EO-*stat*-PO) and immobilized peptide.

On the other hand, during preparation of the calibration curve, it was already found that the modified collagen IV was not soluble in the TCEP solution at a pH of 7.4. This was also the case for varying batches of the peptide. In a solution test, it was demonstrated that the thiopyridine-collagen did not solve in PBS buffer and TCEP solution, but was soluble in 0.1M NaOH. Therefore, the mesh pieces were first rinsed with 0.1M NaOH before solving TCEP powder for achieving the desired pH value and for cleavage of 2-mercaptopyridine. An overview of all experiments is shown in **Figure 64**.

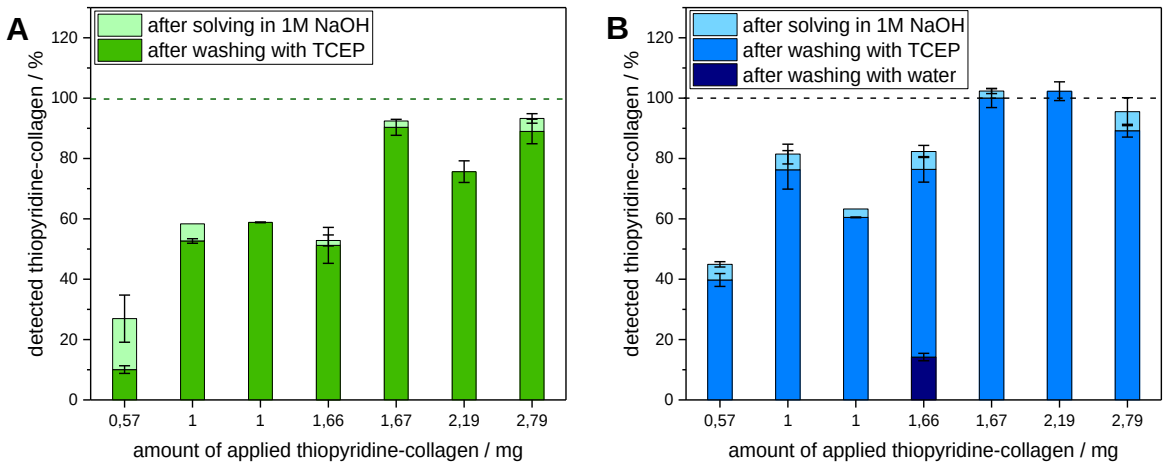

Figure 64: Summary of the experiments quantifying collagen IV via thiopyridine on the surface of electrospun fibers. Different amounts of modified collagen were added to the electrospinning solution and thiopyridine was detected after incubating with the cleaving agent TCEP. **A** was measured with the Tecan Spark 20M, **B** was measured with the Tecan Infinite 200. (n = 3)

As demonstrated, the amount of applied collagen influenced the outcomes of the experiments: when a higher quantity of collagen was used, the value of 2-mercaptopyridine, which was found after the quantification process, increased. Here, it can be noticed that the measurements with the Tecan Infinite 200 led to higher yields than the Tecan Spark20.

On closer inspection, it gets clear that results varied because of problems with the sample preparation. For one sample using 1 mg thiopyridine-collagen, meshes were incubated with 0.1M NaOH for about 60 min and afterwards, TCEP powder was added to achieve a pH value of 7.4. Here, PLGA present in the fibers was solved and NCO-sP(EO-*stat*-PO) polymers remained as transparent cohesive structure. This can be explained by the high pH value of the base and the long incubation time. In a second experiment, which was done one day later with samples from the same batch, higher values were obtained for the Infinite 200 device. In this case, the incubation with 0.1M NaOH was done for only 5 min. However, in the end, not the complete number of collagen was found.

When using 1.67 or 2.19 mg functionalized collagen, in both cases, approximately 100% yield of 2-mercaptopyridine, and therefore collagen IV, could be detected with the Tecan Infinite 200, whereas with the Tecan Spark 20M only about 75% and 92% of 2-mercaptopyridine were found. This leads to the assumption that there are differences regarding the measurements done with different plate readers.

The experiments were repeated using 1.66 mg thiopyridine-collagen and adding a washing step with H_2O before the whole procedure in order to show if non-crosslinked collagen could be removed by water. Here, not all collagen molecules were found and a great number of UV-active 2-mercaptopyridine could be detected in the washing water after incubation for 24 hours in measurements with the Tecan Infinite 200. This result is not explainable because it was proven that modified collagen IV was not soluble in PBS buffer and therefore unsolvable in aqueous liquids at all. Some reactions must occur with collagen in water. This could be a partial solution of the collagen IV sequence; in literature, the peptide sequence was used for example for coating issues in an aqueous solution.[156-157] Another problem arose with these meshes, since after electrospinning, the mesh stuck to the collector drum and could not be removed easily as a result of high air humidity during the spinning process. This could lead additionally to varying fiber properties. A solution for that might be the use

of a climate chamber for electrospinning so that the air humidity could be kept on a constant value.

For a higher quantity of 2.79 mg thiopyridine-collagen, similar results were obtained for both devices. Almost 100% of 2-mercaptopyridine were found after the procedure; however, the yield of the Tecan Spark 20M was lower than for the Infinite 200. Here, after solving the fibers with 1M NaOH, a small number of molecules could be detected. By using a lower amount of 0.5 mg modified collagen, the results lay under 50% for both devices.

A last general discussion point might be the changed amino acid within the peptide sequences CGEFYFDLRLKGDK and SGEFYFDLRLKGDK which is functionalized with 2-thiopyiridine via a disulfide bond. The cysteine is substituted by a serine in the quantification peptide. The reason for that is a possible bridging of disulfide bonds which would lead to changes within the molecule. Thus, the cleavage of 2-mercaptopyridine for quantification might be avoided. As known from literature, NCO-sP(EO-*stat*-PO) show a crosslinking with nucleophiles like thiols, amines and hydroxy groups,[391] whereby thiol moieties lead to the best and fastest reaction followed by amines and hydroxy groups revealing moderate reaction kinetics.[382] This means for the used peptide sequences that the reference bearing a cysteine at the N-terminus might lead to a better interaction with NCO-sP(EO-*stat*-PO) than that of the modified peptide which carries a serine with a hydroxyl group. Therefore, the results obtained from the modified peptide sequence might be underestimated and the actual values are probably higher than measured. This problem is thought to be solved by the use of a more suitable detecting agent which also interacts with peptide sequences without building a disulfide bond.

6.4 Conclusion

The method to visualize single molecules via dSTORM microscopy was established for cell surface glycans which could be detected and quantified by super-resolution imaging before. However, it was not possible to transfer the technique to NCO-sP(EO-*stat*-PO) molecules and immobilized RGD sequences on the surface of fibers. One problem might be the autofluorescence of fibers which could lead to disruption of the sensitive dSTORM method. If the whole background flashes it gets difficult to see the blinking of single molecules. Hence, another approach had to be developed to detect and quantify functional molecules on fiber surfaces.

Regarding the quantification of active peptide sequences on electrospun meshes with the UV-detectable molecules 2-mercaptopyridine, it was possible to transfer the procedure to a smaller scale of sample preparation where a comparison of 2D and 3D surfaces was possible as well. However, differences between two applied plate readers were found indicating that the values for one device are always lower than for the other which could be a sign for calibration errors.

Additional experiments need to be done to evaluate more points for linear fitting regarding the calibration curves for both surfaces, 2D and 3D. For electrospinning, the time points should be fixed, and a way of calculation might be determined to get more evident results for the real surface of fibers in order to develop a better evaluation of RGD molecules on the fiber surface independent from the glass area they are fixed on.

In summary, the quantification of longer peptide sequences, in this case collagen type IV, led to promising results. In many approaches, the applied amount of thioypyridine-collagen could be found again after the procedure. This means that the method provides quantitative results also by using longer amino acid chains in comparison to the shorter sequence RGD. A few drawbacks occurred by using a washing step with H_2O before the treatment with TCEP solution. In general, it was tested if the modified collagen was solvable in aqueous solutions like PBS buffer. Therefore, 2-mercaptopyridine should not be detected in the washing water. On the other hand, a partial dissolution could take place leading to the low results.

Generally, it could be demonstrated, that measurements with the Tecan Infinite 200 provided higher results as using the Tecan Spark 20M. In future, it must be examined

why the outcomes showed this variation, and an additional calibration of the devices should be determined.

A last question might be, if the modified collagen is destroyed by the solution in 0.1M or 1M NaOH since not all 2-mercaptopyridine molecules could be detected after chemical treatment with the base. Regarding the RGD sequence used for quantification issues, a neutral solution of TCEP and 0.1M NaOH is applied to the mesh to cleave disulfide bonds. It was shown that the modified collagen did not solve in the TCEP solution and therefore, the solution step using 0.1M NaOH and the subsequent neutralization of the solution with TCEP was necessary.

For future experiments, it is important to evaluate the correlation between the detected and the applied quantities of 2-mercaptopyridine. In the performed measurements, with higher numbers of thiopyridine-collagen, more UV-detectable molecules were found. However, it was expected, that independent of the inserted amount of modified peptide sequence, 100% of 2-mercaptopyridine results for every approach. Thus, the experiments with lower numbers of thiopyridine-collagen should be repeated.

Finally, a successful transfer of the quantification method from short peptide sequences to longer amino acid chains and small peptides like collagen IV was demonstrated. It was revealed that the method is suitable for quantitative detection of peptide sequences independent of the chain length of these peptides. Longer peptide sequences or even proteins should be tested as well with this method.

7 Summary – Zusammenfassung

7.1 Summary

The aim of this thesis was the application of the functional prepolymer **NCO-sP(EO-*stat*-PO) for the development of new biomaterials**. The thesis was divided into three topics: the first was the investigation of the influence of star-shaped polymers on the **mechanical properties of biocements and bone adhesives**. 3-armed star-shaped macromers were used as an additive for a mineral bone cement, and the influence on the mechanical properties was studied. Additionally, a previously developed bone adhesive was examined regarding cytocompatibility. The second topic was the examination of **novel functionalization steps which were performed on the surface of electrospun fibers modified with NCO-sP(EO-*stat*-PO)**. This established method of functionalizing electrospun meshes was advanced regarding the modification with proteins and antibodies which was then demonstrated in a biological application. Two different kinds of antibodies were immobilized on the fiber surface in a consecutive manner and the influence of these proteins on the cell behavior was investigated. The final topic involved the **quantification of surface-bound peptide sequences**. By functionalization of the peptides with the UV-reactive molecule 2-mercaptopyridine it was possible to quantify this compound via UV measurements by cleavage of disulfide bridges and indirectly draw conclusions about the number of immobilized peptides.

In the field of mineral biocements and bone adhesives, NCO-sP(EO-*stat*-PO) was able to influence the setting behavior and mechanical performance of mineral bone cements based on calcium phosphate chemistry. The addition of NCO-sP(EO-*stat*-PO) resulted in a pseudo-ductile fracture behavior due to the formation of a hydrogel network in the cement, which was then mineralized by nanosized hydroxyapatite crystals following cement setting. Besides the application to calcium phosphate bone cements, also a commercially available aluminum silicate cement from civil engineering could be modified accordingly.

In addition, it could be shown that the use of the functional additive NCO-sP(EO-*stat*-PO) is beneficial for adjusting specific material properties of bone adhesives. Here, the cross-linking behavior of the prepolymer in an aqueous medium was exploited to form an interpenetrating network (IPN) together with a system of photochemically curing poly(ethylene glycol) dimethacrylate (PEGDMA) matrix. This could be used for the development of a bone adhesive with an improved adhesion to bone in a wet

environment. In this thesis, the developed bone adhesive was further investigated in terms of possible influences of the initiator systems. In addition, the material system was tested for cytocompatibility by using different cell lines. This is considered to be the basis for further cell-material interaction studies and *in vivo* tests.

Moreover, the preparation of electrospun fiber meshes by means of solution electrospinning consisting of poly(lactide-*co*-glycolide) (PLGA) as a backbone polymer and NCO-sP(EO-*stat*-PO) as functional additive is an established method for the application of the meshes as a replacement of the native extracellular matrix (ECM). In general, these fibers reveal diameters in the nanometer range, are protein and cell repellent due to the hydrophilic properties of the prepolymer and show a specific biofunctionalization by immobilization of peptide sequences. Here, the isocyanate groups of the additive presented on the fiber surface after electrospinning were used to carry out various functionalization steps, while retaining the properties of protein and cell repellency. The modification of the electrospun fibers involved the immobilization of various antibodies and proteins, which are analogs or antagonists of tumor necrosis factor (TNF), and the indirect detection of these by interaction with a light-producing enzyme. Here, a multimodal modification of the fiber surface with RGD to mediate cell adhesion and two different antibodies could be achieved. After culturing the special cell line HT1080, the pro- or anti-inflammatory response of cells could be detected by IL-8 specific ELISA measurements. In future, these immobilized antibody constructs might be used as immunomodulatory surfaces for incorporation into the body and for a prevention of an immunologic rejection of transplants.

Furthermore, the quantification of molecules on the surface of electrospun fibers was investigated. Based on earlier results, in which a UV-spectrometrically active molecule was used to detect the quantification of the peptide sequence RGD, it was tested whether the detection by means of super-resolution microscopy would be possible. For this purpose, experiments were performed with short amino acid sequences such as fluorescence labeled RGD for quantification by means of fluorescence microscopy. In addition, it was shown that short peptides can also be quantified in a small scale on flat functional substrates (2D) such as hydrogel coatings from NCO-sP(EO-*stat*-PO), and modified electrospun fibers produced from PLGA and NCO-sP(EO-*stat*-PO) (3D).

In addition, a collagen sequence was used to prove that a successful quantification can be carried out as well for longer peptide chains. This is another indication that the established method can be used generically for many peptide sequences.

These studies have revealed that NCO-sP(EO-*stat*-PO) can serve as a functional additive for many applications and should be considered for further studies on the development of novel biomaterials. The rapid crosslinking reaction, the resulting hydrogel formation and the biocompatibility are to be mentioned as positive properties, which makes the prepolymer interesting for future applications.

7.2 Zusammenfassung

Ziel der Arbeit war die Anwendung von funktionalen Präpolymeren des Typs **NCO-sP(EO-*stat*-PO) für die Entwicklung von neuen Biomaterialien**. Die Arbeit wurde in drei Themengebiete aufgeteilt: Als erstes wurde untersucht, welchen Einfluss sternförmige Polymere auf die **mechanischen Eigenschaften von Biozementen und Knochenadhäsiven** haben. Beispielsweise wurden 3-armige, sternförmige Macromere als **Additive für einen mineralischen Knochenzement** verwendet und untersucht, wie sich dessen mechanische Eigenschaften ändern. Außerdem wurde ein kürzlich entwickelter **NCO-sP(EO-*stat*-PO) haltige Knochenklebers** auf seine Zytokompatibilität. getestet. Ein zweites Ergebniskapitel beinhaltete die **Modifikation von elektrogesponnenen Polymerfasern mit NCO-sP(EO-*stat*-PO)** basierend auf einer etablierten Methode. Es wurde untersucht, welche weiteren **neuen Funktionalisierungen auf solchen Oberflächen** vorgenommen werden können. Diese Modifizierungsschritte wurde in einer biologischen Anwendung demonstriert, hierbei wurden verschiedene Antikörper aufeinanderfolgend auf der Faseroberfläche gebunden und der Einfluss dieser Proteine auf das Verhalten von Zellen, die auf diese Oberflächen gesät wurden, untersucht. Als letztes wurde die **Quantifizierung von oberflächengebundenen Peptidsequenzen** demonstriert. Mittels Funktionalisierung der Peptide mit dem UV-reaktiven Molekül 2-Mercaptopyridin konnte durch Spaltung von Disulfidbrücken diese Verbindung mit UV-Messungen quantifiziert und indirekt Rückschlüsse auf die Anzahl der immobilisierten Peptide gezogen werden.

Es konnte beispielsweise durch den Zusatz von NCO-sP(EO-*stat*-PO) das Abbindeverhalten und die mechanischen Eigenschaften von mineralischen Knochenzementen aus Calciumphosphat moduliert werden. Der Zusatz von 3-armigem, sternförmigem NCO-sP(EO-*stat*-PO) führte dabei zu einem pseudoduktilem Bruchverhalten durch die Bildung eines Hydrogelnetzwerks im Zement, das anschließend durch die Zementreaktion mit nanoskaligem Hydroxylapatit mineralisiert wurde. Neben der Anwendung für Knochenzemente auf Calciumphosphat-Basis konnte auch ein kommerziell verfügbarer Aluminiumsilikat-Bauzement entsprechend modifiziert werden.

Im Bereich mineralischer Knochenzemente und Adhäsive konnte ebenso gezeigt werden, dass das funktionale Additiv NCO-sP(EO-*stat*-PO) zur Einstellung der Eigenschaften verwendet werden kann. Hierbei wurde das Quervernetzungsverhalten

des Präpolymers im wässrigen Medium ausgenutzt, um basierend auf einem System einer photochemisch härtenden Polyethylenglykoldimethakrylat (PEGDMA) Matrix interpenetrierende Netzwerke (IPNs) zu bilden. Dieses konnte etwa für die Entwicklung eines Knochenklebers mit verbesserter Haftung auf Knochen im feuchten Milieu ausgenutzt werden. Im Rahmen der Arbeit wurde das kürzlich entwickelte Knochenadhäsiv im Hinblick auf den Einfluss des Initiatorsystems untersucht. Außerdem wurde die Zytokompatibilität des Materialsystems anhand verschiedener Zelltypen getestet. Damit wurde der Grundstein für weiterführende Zell-Material-Interaktionsstudien und In-vivo-Studien gelegt.

Die Herstellung von elektrogesponnenen Faservliesen mittels Solution Electrospinning aus Polylactid-*co*-Glycolid (PLGA) als Gerüst-bildendem Polymer und NCO-sP(EO-*stat*-PO) als funktionalem Additiv ist eine etablierte Methode, um diese Vliese zur Nachbildung nativer Extrazellulär-Matrix anzuwenden. Die Fasern weisen hierbei einen Durchmesser im Nanometer-Bereich auf, sind protein- und zellabweisend durch die hydrophilen Eigenschaften des Präpolymers und können durch Immobilisierung von Peptidsequenzen eine spezifische Biofunktionalisierung erhalten. Hierbei wurden die Isocyanat-Gruppen des Additivs auf der Faseroberfläche ausgenutzt, um verschiedenste Funktionalisierungsschritte unter Beibehaltung der protein- und zellabweisenden Eigenschaften auszuführen. Die Modifizierung der elektrogesponnenen Fasern beinhaltete die Immobilisierung von verschiedenen Antikörpern und Proteinen, welche Analoga oder Antagonisten des Tumornekrosefaktors (TNF) darstellen, sowie den indirekten Nachweis dieser über die Interaktion mit einem Licht produzierenden Enzym. Hierbei konnte eine multimodale Modifizierung der Faseroberfläche mit RGD-Sequenzen zur Vermittlung der Zelladhäsion und zwei verschiedenen Antikörpern erreicht werden. Nach Kultivierung der speziellen Zelllinie HT1080 konnte die pro- oder antiinflammatorische Antwort von Zellen mittels IL-8 spezifischem ELISA nachgewiesen werden. Diese Konstrukte mit immobilisierten Antikörpern könnten in Zukunft als immunmodulierende Oberflächen zur Einbringung in den Körper und Verhinderung der immunologischen Abstoßung von Transplantaten verwendet werden.

Eine weitere Fragestellung war der Quantifizierung von Molekülen auf der Oberfläche von elektrogesponnen Fasern gewidmet. Basierend auf früheren Ergebnissen, in welchen für den Nachweis der Quantifizierung der Peptidsequenz RGD ein UV-aktives

Molekül genutzt wurde, wurde getestet, ob ein Nachweis mittels hochauflösender Mikroskopie möglich wäre. Hierzu wurden Versuche mit kurzen, fluoreszenzmarkierten RGD-Aminosäuresequenzen zur fluoreszenzmikroskopischen Quantifizierung durchgeführt. Es konnte gezeigt werden, dass sich kurze Peptide auch im kleinen Maßstab auf flachen funktionalen Substraten (2D) wie Hydrogel-Beschichtungen aus NCO-sP(EO-*stat*-PO) als auch auf modifizierten elektrogesponnenen Fasern aus PLGA und NCO-sP(EO-*stat*-PO) (3D) quantifizieren lassen. Außerdem wurde eine Kollagen-Sequenz als längere Peptidkette herangezogen, um zu beweisen, dass auch hier eine erfolgreiche Quantifizierung durchgeführt werden kann. Die Ergebnisse zeigen, dass die etablierte Methode generisch für eine Vielzahl von Peptidsequenzen verwendet werden kann.

Durch diese Untersuchungen konnte gezeigt werden, dass NCO-sP(EO-*stat*-PO) als funktionales Additiv für viele Anwendungen dienen kann und für weitere Untersuchungen zur Entwicklung von Biomaterialien berücksichtigt werden sollte. Die schnelle Quervernetzungsreaktion, die resultierende Hydrogelbildung und die Biokompatibilität sind hierbei als positive Eigenschaften zu nennen, die das Präpolymer für zukünftige Anwendungen interessant macht.

8 References

[1] D.F. Williams, presented at the European Society for Biomaterials, Chester, England, **1987**.
[2] D. Williams, *The Williams Dictionary of Biomaterials Liverpool, UK: Liverpool*. **1999**, University Press.
[3] J. Park, R.S. Lakes, *Biomaterials: an introduction*, Springer Science & Business Media, **2007**.
[4] D.F. Williams, *Biomaterials* **2009**, *30*, 5897.
[5] D.F. Williams, *Biomaterials* **2008**, *29*, 2941.
[6] D.F. Williams, *Biomaterials* **2014**, *35*, 10009.
[7] R. Sridharan, A.R. Cameron, D.J. Kelly, C.J. Kearney, F.J. O'Brien, *Mater. Today* **2015**, *18*, 313.
[8] B.D. Ratner, S.J. Bryant, *Annu. Rev. Biomed. Eng.* **2004**, *6*, 41.
[9] J.M. Anderson, *Annu. Rev. Mater. Res.* **2001**, *31*, 81.
[10] P. Parida, A. Behera, S.C. Mishra, *Int. J. Adv. Appl. Sci.* **2012**, *1*, 125.
[11] T. Fujisato, T. Sajiki, Q. Liu, Y. Ikada, *Biomaterials* **1996**, *17*, 155.
[12] U. Nöth, L. Rackwitz, A. Heymer, M. Weber, B. Baumann, A. Steinert, N. Schütze, F. Jakob, J. Eulert, *J. Biomed. Mater. Res., Part A* **2007**, *83*, 626.
[13] E. Khor, L.Y. Lim, *Biomaterials* **2003**, *24*, 2339.
[14] J. Meinhart, M. Fussenegger, W. Höbling, *Ann. Plast. Surg.* **1999**, *42*, 673.
[15] Q. Ye, G. Zünd, P. Benedikt, S. Jockenhoevel, S.P. Hoerstrup, S. Sakyama, J.A. Hubbell, M. Turina, *Eur. J. Cardiothorac. Surg.* **2000**, *17*, 587.
[16] G. Kogan, L. Šoltés, R. Stern, P. Gemeiner, *Biotechnol. Lett.* **2007**, *29*, 17.
[17] K. Fukui, A. Kaneuji, T. Sugimori, T. Ichiseki, K. Kitamura, T. Matsumoto, *J. Arthroplasty* **2011**, *26*, 45.
[18] E.J. Hollick, D.J. Spalton, P.G. Ursell, M.V. Pande, S.A. Barman, J.F. Boyce, K. Tilling, *Ophthalmology* **1999**, *106*, 49.
[19] J. Wang, D. Fonn, T.L. Simpson, *Invest. Ophthalmol. Visual Sci.* **2003**, *44*, 1070.
[20] G. Lewis, *J. Biomed. Mater. Res.* **1997**, *38*, 155.
[21] W.J. Li, K.G. Danielson, P.G. Alexander, R.S. Tuan, *J. Biomed. Mater. Res., Part A* **2003**, *67*, 1105.
[22] J. Guan, K.L. Fujimoto, M.S. Sacks, W.R. Wagner, *Biomaterials* **2005**, *26*, 3961.
[23] A.J. Lasprilla, G.A. Martinez, B.H. Lunelli, A.L. Jardini, R. Maciel Filho, *Biotechnol. Adv.* **2012**, *30*, 321.
[24] B.D. Boyan, Z. Schwartz, *Nat. Rev. Rheumatol.* **2011**, *7*, 8.
[25] M. Kamitakahara, C. Ohtsuki, T. Miyazaki, *J. Biomater. Appl.* **2008**, *23*, 197.
[26] K. Köster, E. Karbe, H. Kramer, H. Heide, R. König, *Langenbecks Arch. Surg.* **1976**, *341*, 77.
[27] H. Yuan, H. Fernandes, P. Habibovic, J. De Boer, A.M. Barradas, A. De Ruiter, W.R. Walsh, C.A. Van Blitterswijk, J.D. De Bruijn, *Nat. Rev. Rheumatol.* **2011**, *7*, 1.
[28] B.M. Holzapfel, J.C. Reichert, J.-T. Schantz, U. Gbureck, L. Rackwitz, U. Nöth, F. Jakob, M. Rudert, J. Groll, D.W. Hutmacher, *Adv. Drug Delivery Rev.* **2013**, *65*, 581.
[29] H.R. Ramay, M. Zhang, *Biomaterials* **2004**, *25*, 5171.

[30] M. Navarro, A. Michiardi, O. Castano, J. Planell, *J. R. Soc., Interface* **2008**, *5*, 1137.
[31] J.S. Temenoff, A.G. Mikos, *Biomaterials* **2000**, *21*, 2405.
[32] J. Zhang, W. Liu, V. Schnitzler, F. Tancret, J.-M. Bouler, *Acta Biomater.* **2014**, *10*, 1035.
[33] S.-B. Yang, J. Wang, C.-S. Liu, *J. Inorg. Mater.* **2013**, *28*, 85.
[34] M. Vallet-Regí, J.M. González-Calbet, *Prog. Solid State Chem.* **2004**, *32*, 1.
[35] E. Vorndran, U. Klammert, A. Ewald, J.E. Barralet, U. Gbureck, *Adv. Funct. Mater.* **2010**, *20*, 1585.
[36] M.-P. Ginebra, T. Traykova, J.A. Planell, *J. Controlled Release* **2006**, *113*, 102.
[37] U. Klammert, U. Gbureck, E. Vorndran, J. Rödiger, P. Meyer-Marcotty, A.C. Kübler, *J. Craniomaxillofac. Surg.* **2010**, *38*, 565.
[38] M. Castilho, C. Moseke, A. Ewald, U. Gbureck, J. Groll, I. Pires, J. Teßmar, E. Vorndran, *Biofabrication* **2014**, *6*, 015006.
[39] E. Vorndran, M. Klarner, U. Klammert, L.M. Grover, S. Patel, J.E. Barralet, U. Gbureck, *Adv. Eng. Mater.* **2008**, *10*.
[40] N. Ostrowski, A. Roy, P.N. Kumta, *ACS Biomater. Sci. Eng.* **2016**, *2*, 1067.
[41] B. Kanter, A. Vikman, T. Brückner, M. Schamel, U. Gbureck, A. Ignatius, *Acta Biomater.* **2018**.
[42] F. Wu, J. Wei, H. Guo, F. Chen, H. Hong, C. Liu, *Acta Biomater.* **2008**, *4*, 1873.
[43] G. Mestres, M.-P. Ginebra, *Acta Biomater.* **2011**, *7*, 1853.
[44] G. Mestres, M. Abdolhosseini, W. Bowles, S.-H. Huang, C. Aparicio, S.-U. Gorr, M.-P. Ginebra, *Acta Biomater.* **2013**, *9*, 8384.
[45] P. Gasteier, A. Reska, P. Schulte, J. Salber, A. Offenhäusser, M. Moeller, J. Groll, *Macromol. Biosci.* **2007**, *7*, 1010.
[46] D. Grafahrend, K.-H. Heffels, M.V. Beer, P. Gasteier, M. Möller, G. Boehm, P.D. Dalton, J. Groll, *Nat. Mater.* **2011**, *10*, 67.
[47] M. Schamel, J. Groll, U. Gbureck, *Mater. Sci. Eng., C* **2017**, *75*, 471.
[48] P.D. Tennis, H.M. Jennings, *Cem. Concr. Res.* **2000**, *30*, 855.
[49] C. Shi, A.F. Jiménez, A. Palomo, *Cem. Concr. Res.* **2011**, *41*, 750.
[50] G. Zhang, P. Wang, L. Xu, H. Li, L. Yu, *Adv. Cem. Res.* **2017**, *29*, 147.
[51] S.V. Dorozhkin, *J. Mater. Sci.* **2008**, *43*, 3028.
[52] S.V. Dorozhkin, *Int. J. Mater. Chem.* **2011**, *1*, 1.
[53] M. Nabiyouni, T. Brückner, H. Zhou, U. Gbureck, S.B. Bhaduri, *Acta Biomater.* **2017**.
[54] R. Krüger, J. Groll, *Biomaterials* **2012**, *33*, 5887.
[55] M. Geffers, J. Groll, U. Gbureck, *Materials* **2015**, *8*, 2700.
[56] C. Canal, M. Ginebra, *J. Mech. Behav. Biomed. Mater.* **2011**, *4*, 1658.
[57] J.A. Manson, *Mater. Sci. Eng.* **1976**, *25*, 41.
[58] Y. Ohama, *Adv. Cem. Based Mater.* **1997**, *5*, 31.
[59] Y. Ohama, *Cem. Concr. Compos.* **1998**, *20*, 189.
[60] D. Silva, V. John, J. Ribeiro, H. Roman, *Cem. Concr. Res.* **2001**, *31*, 1177.
[61] C. Giraudeau, J.B. D'Espinose De Lacaillerie, Z. Souguir, A. Nonat, R.J. Flatt, *J. Am. Ceram. Soc.* **2009**, *92*, 2471.
[62] Y. Ohama, *Handbook of polymer-modified concrete and mortars: properties and process technology*, William Andrew, **1995**.
[63] Z. Su, J. Larbi, J. Bijen, *Cem. Concr. Res.* **1991**, *21*, 983.
[64] L. Aggarwal, P. Thapliyal, S. Karade, *Constr. Build. Mater.* **2007**, *21*, 379.
[65] D. Nguyen, L. Devlin, P. Koshy, C. Sorrell, *J. Mater. Sci.* **2014**, *49*, 923.
[66] H. Kuehn, B. Rothenhaeusser, V. Kiesel, A. Wichmann, *Redispersible polymer powders*. **2002**, Google Patents.

[67] L. De Lorenzis, R. Tepfers, *J. Compos. Constr.* **2003**, *7*, 219.
[68] U.S. Camli, B. Binici, *Constr. Build. Mater.* **2007**, *21*, 1431.
[69] S.M. Abtahi, M. Sheikhzadeh, S.M. Hejazi, *Constr. Build. Mater.* **2010**, *24*, 871.
[70] B. Han, Y. Wang, S. Dong, L. Zhang, S. Ding, X. Yu, J. Ou, *J. Intell. Mater. Syst. Struct.* **2015**, *26*, 1303.
[71] W.-C. Chen, C.-P. Ju, J.-C. Wang, C.-C. Hung, J.-H.C. Lin, *Dent. Mater.* **2008**, *24*, 1616.
[72] R.M. Khashaba, M. Moussa, C. Koch, A.R. Jurgensen, D.M. Missimer, R.L. Rutherford, N.B. Chutkan, J.L. Borke, *Int. J. Biomater.* **2011**, *2011*.
[73] T.E. Douglas, J. Schietse, A. Zima, S. Gorodzha, B.V. Parakhonskiy, D. KhaleNkow, R. Shkarin, A. Ivanova, T. Baumbach, V. Weinhardt, *J. Biomed. Mater. Res., Part A* **2018**, *106*, 822.
[74] S.V. Dorozhkin, *Materials* **2009**, *2*, 221.
[75] R.A. Perez, H.-W. Kim, M.-P. Ginebra, *J. Tissue Eng.* **2012**, *3*, 2041731412439555.
[76] T. Christel, M. Kuhlmann, E. Vorndran, J. Groll, U. Gbureck, *J. Mater. Sci. Mater. Med.* **2013**, *24*, 573.
[77] L.A. Dos Santos, R.G. Carrodeguas, A.O. Boschi, A.C. De Arruda, *Artif. Organs* **2003**, *27*, 412.
[78] E. Rigo, L. Dos Santos, L. Vercik, R. Carrodeguas, A. Boschi, *Lat. Am. Appl. Res.* **2007**, *37*, 267.
[79] H. Schierle, J. Hausamen, *Unfallchirurg* **1997**, *100*, 330.
[80] J. Wiltfang, *HNO* **2002**, *50*, 800.
[81] H.K. Uhthoff, P. Poitras, D.S. Backman, *J. Orthop. Sci.* **2006**, *11*, 118.
[82] N. Diwersi, R. Babst, B. Link, *Oper. Orthop. Traumatol.* **2016**, *28*, 402.
[83] E.T. Daif, *J. Craniofac. Surg.* **2014**, *25*, e526.
[84] S. Aykut, K. Öztürk, Ç. Özcan, M. Demiroğlu, A.U. Gürün, E. Özden, *Ulus. Travma Acil Cerrahi Derg.* **2015**, *21*, 279.
[85] H. Xu, Z. Xue, H. Ding, H. Qin, Z. An, *PloS one* **2015**, *10*, e0140037.
[86] C. Hudson, A. Pozzi, D. Lewis, *Vet. Comp. Orthop. Traumatol.* **2009**, *22*, 175.
[87] D.F. Farrar, *Int. J. Adhes. Adhes.* **2012**, *33*, 89.
[88] C. Heiss, R. Schnettler, *Unfallchirurg* **2005**, *108*, 348.
[89] C. Heiss, N. Hahn, P. Pokinskyj, S. Wenisch, J.-P. Stahl, C. Meyer, R. Schnettler, *Biomed. Tech.* **2004**, *49*, 163.
[90] D.M. Sidle, C.S. Maas, *Arch. Facial Plast. Surg.* **2008**, *10*, 316.
[91] H.H. Chao, D.F. Torchiana, *J. Card. Surg.* **2003**, *18*, 500.
[92] W. Fürst, A. Banerjee, *Ann. Thorc. Surg.* **2005**, *79*, 1522.
[93] C. Heiss, R. Kraus, D. Schluckebier, A.-C. Stiller, S. Wenisch, R. Schnettler, *Eur. J. Trauma* **2006**, *32*, 141.
[94] M. Donkerwolcke, F. Burny, D. Muster, *Biomaterials* **1998**, *19*, 1461.
[95] R. Bitton, E. Josef, I. Shimshelashvili, K. Shapira, D. Seliktar, H. Bianco-Peled, *Acta Biomater.* **2009**, *5*, 1582.
[96] S.H. Song, H. Kyung, S.-H. Oh, N. Kang, *J. Craniofac. Surg.* **2014**, *25*, 919.
[97] H. Kyung, S.H. Song, N. Kang, S.-H. Oh, *J. Craniofac. Surg.* **2013**, *24*, 1781.
[98] H.-S. Jeong, M.-S. Moon, H.-K. Lee, K.-S. Kim, *J. Craniofac. Surg.* **2010**, *21*, 75.
[99] S.C. Weber, M.W. Chapman, *Clin. Orthop. Relat. R.* **1984**, *191*, 249.
[100] R. Chivers, R. Wolowacz, *Int. J. Adhes. Adhes.* **1997**, *17*, 127.
[101] C.J. Dunn, K.L. Goa, *Drugs* **1999**, *58*, 863.
[102] G. Giebel, M. Rimpler, *Biomed. Tech.* **1981**, *26*, 35.
[103] C.-C. Ho, S.-J. Ding, *J. Biomed. Nanotechnol.* **2014**, *10*, 3063.

[104] S.K. Madhurakkat Perikamana, J. Lee, Y.B. Lee, Y.M. Shin, E.J. Lee, A.G. Mikos, H. Shin, *Biomacromolecules* **2015**, *16*, 2541.
[105] S.A. Burke, M. Ritter-Jones, B.P. Lee, P.B. Messersmith, *Biomed. Mater.* **2007**, *2*, 203.
[106] H. Shao, K.N. Bachus, R.J. Stewart, *Macromol. Biosci.* **2009**, *9*, 464.
[107] B.D. Winslow, H. Shao, R.J. Stewart, P.A. Tresco, *Biomaterials* **2010**, *31*, 9373.
[108] B. Hoffmann, E. Volkmer, A. Kokott, P. Augat, M. Ohnmacht, N. Sedlmayr, M. Schieker, L. Claes, W. Mutschler, G. Ziegler, *J. Mater. Sci. Mater. Med.* **2009**, *20*, 2001.
[109] C.R. Matos-Pérez, J.D. White, J.J. Wilker, *J. Am. Chem. Soc.* **2012**, *134*, 9498.
[110] K. Huang, B.P. Lee, D.R. Ingram, P.B. Messersmith, *Biomacromolecules* **2002**, *3*, 397.
[111] S.C. Woodward, J.B. Herrmann, J.L. Cameron, G. Brandes, E.J. Pulaski, F. Leonard, *Ann. Surg.* **1965**, *162*, 113.
[112] D.M. Toriumi, M. Raslan, M. Friedman, E. Tardy, *Arch. Otolaryngol., Head Neck Surg.* **1990**, *116*, 546.
[113] F.J. Papatheofanis, *J. Biomed. Mater. Res.* **1989**, *23*, 661.
[114] G. Brauer, J. Kumpula, D. Termini, K. Davidson, *J. Biomed. Mater. Res.* **1979**, *13*, 593.
[115] U. Kandalam, A. Bouvier, S. Casas, R. Smith, A. Gallego, J. Rothrock, J. Thompson, C.-Y. Huang, E. Stelnicki, *Int. J. Oral Max. Surg.* **2013**, *42*, 1054.
[116] J.C. Esteves, J.M. Monteiro, A.M. Aranega, W. Betoni Junior, C.K. Sonoda, *J. Oral Implantol.* **2014**, *40*, 411.
[117] M.A. Akcal, O. Poyanli, K. Unay, I. Esenkaya, B. Gokcen, A.S. Fıratlıgil, *J. Orthop. Surg. Res.* **2014**, *9*, 1.
[118] J.J. Sohn, T.M. Gruber, J.L. Zahorsky-Reeves, G.W. Lawson, *J. Am. Assoc. Lab. Anim. Sci.* **2016**, *55*, 199.
[119] E. Hochuli-Vieira, E. Pinto, A.C. Basso, V.A. Pereira-Filho, S. Saska, M.S. Monnazzi, *Dent. Traumatol.* **2017**, *33*, 261.
[120] K. Endres, R. Marx, J. Tinschert, D.C. Wirtz, C. Stoll, D. Riediger, R. Smeets, *Biomed. Eng. Online* **2008**, *7*, 16.
[121] R. Smeets, R. Marx, A. Kolk, S. Said-Yekta, M.B. Grosjean, C. Stoll, J. Tinschert, D.C. Wirtz, D. Riediger, K. Endres, *J. Oral Maxillofac. Surg.* **2010**, *68*, 3028.
[122] R. Smeets, K. Endres, G. Stockbrink, H. Hanken, B. Hermanns-Sachweh, R. Marx, M. Heiland, M. Blessmann, K.D. Wolff, A. Kolk, *J. Biomed. Mater. Res., Part A* **2013**, *101*, 2058.
[123] H.J. Erli, R. Marx, O. Paar, F.U. Niethard, M. Weber, D.C. Wirtz, *Biomed. Eng. Online* **2003**, *2*, 15.
[124] T. Sakai, S. Morita, K.i. Shinomiya, A. Watanabe, N. Nakabayashi, K. Ishihara, *J. Biomed. Mater. Res., Part A* **2000**, *52*, 128.
[125] H.-J. Jiang, J. Xu, Z.-Y. Qiu, X.-L. Ma, Z.-Q. Zhang, X.-X. Tan, Y. Cui, F.-Z. Cui, *Materials* **2015**, *8*, 2616.
[126] D.S. Brauer, E. Gentleman, D.F. Farrar, M.M. Stevens, R.G. Hill, *Biomed. Mater.* **2011**, *6*, 045007.
[127] X. Cui, W. Huang, Y. Zhang, C. Huang, Z. Yu, L. Wang, W. Liu, T. Wang, J. Zhou, H. Wang, *Mater. Sci. Eng., C* **2017**, *73*, 585.
[128] M. Bohner, *J. Mater. Chem.* **2007**, *17*, 3980.
[129] M. Bohner, U. Gbureck, J. Barralet, *Biomaterials* **2005**, *26*, 6423.
[130] E.A. Abou Neel, V. Salih, P.A. Revell, A.M. Young, *Adv. Eng. Mater.* **2014**, *16*, 218.

[131] L.M. Grover, U. Gbureck, D. Farrar, J. Barralet, presented at the Key Engineering Materials, **2006**.
[132] Y. Yu, J. Wang, C. Liu, B. Zhang, H. Chen, H. Guo, G. Zhong, W. Qu, S. Jiang, H. Huang, *Colloids Surf., B* **2010**, *76*, 496.
[133] M. Waselau, V.F. Samii, S.E. Weisbrode, A.S. Litsky, A.L. Bertone, *Am. J. Vet. Res.* **2007**, *68*, 370.
[134] L.V. Gulotta, D. Kovacevic, L. Ying, J.R. Ehteshami, S. Montgomery, S.A. Rodeo, *Am. J. Sports Med.* **2008**, *36*, 1290.
[135] J.F. Mano, R.A. Sousa, L.F. Boesel, N.M. Neves, R.L. Reis, *Compos. Sci. Technol.* **2004**, *64*, 789.
[136] J. Santerre, K. Woodhouse, G. Laroche, R. Labow, *Biomaterials* **2005**, *26*, 7457.
[137] P.W. Fedak, E. Kolb, G. Borsato, D.E. Frohlich, A. Kasatkin, K. Narine, N. Akkarapaka, K.M. King, *Ann. Thorc. Surg.* **2010**, *90*, 979.
[138] P.W. Fedak, T.M. Kieser, A.M. Maitland, M. Holland, A. Kasatkin, P. LeBlanc, J.K. Kim, K.M. King, *Ann. Thorc. Surg.* **2011**, *92*, 1444.
[139] P.W. Fedak, A. Kasatkin, *Surg. Innov.* **2011**, *18*, NP8.
[140] K.J. Schreader, I.S. Bayer, D.J. Milner, E. Loth, I. Jasiuk, *J. Appl. Polym. Sci.* **2013**, *127*, 4974.
[141] S. Sahan, P. Hosseinian, D. Ozdil, M. Turk, H.M. Aydin, *J. Biomater. Tissue Eng.* **2017**, *7*, 401.
[142] F. Witte, N. Hort, C. Vogt, S. Cohen, K.U. Kainer, R. Willumeit, F. Feyerabend, *Curr. Opin. Solid State Mater. Sci.* **2008**, *12*, 63.
[143] N. Huebsch, D.J. Mooney, *Nature* **2009**, *462*, 426.
[144] B.D. Ratner, *J. Biomed. Mater. Res., Part A* **1993**, *27*, 837.
[145] J.M. Harris, *Poly (ethylene glycol) chemistry: biotechnical and biomedical applications*, Springer Science & Business Media, **2013**.
[146] P. Kingshott, S. McArthur, H. Thissen, D.G. Castner, H.J. Griesser, *Biomaterials* **2002**, *23*, 4775.
[147] E. Tziampazis, J. Kohn, P.V. Moghe, *Biomaterials* **2000**, *21*, 511.
[148] M.C. Lensen, V.A. Schulte, M. Diez, in *Biomaterials-Physics and Chemistry*, Edt: InTech, **2011**.
[149] G.L. Kenausis, J. Vörös, D.L. Elbert, N. Huang, R. Hofer, L. Ruiz-Taylor, M. Textor, J.A. Hubbell, N.D. Spencer, *J. Phys. Chem. B* **2000**, *104*, 3298.
[150] Z. Harris, S. Zalipsky, *Poly(ethylene Glycol)*, American Chemical Society, Washington, DC**1997**.
[151] S.J. Hollister, *Nat. Mater.* **2005**, *4*, 518.
[152] H. Shin, S. Jo, A.G. Mikos, *Biomaterials* **2003**, *24*, 4353.
[153] L. Perlin, S. MacNeil, S. Rimmer, *Soft Matter* **2008**, *4*, 2331.
[154] S. VandeVondele, J. Vörös, J.A. Hubbell, *Biotechnol. Bioeng.* **2003**, *82*, 784.
[155] J. Groll, J. Fiedler, E. Engelhard, T. Ameringer, S. Tugulu, H.A. Klok, R.E. Brenner, M. Moeller, *J. Biomed. Mater. Res., Part A* **2005**, *74*, 607.
[156] J. Salber, S. Gräter, M. Harwardt, M. Hofmann, D. Klee, J. Dujic, H. Jinghuan, J. Ding, S. Kippenberger, A. Bernd, *Small* **2007**, *3*, 1023.
[157] D. Grafahrend, K.H. Heffels, M. Möller, D. Klee, J. Groll, *Macromol. Biosci.* **2010**, *10*, 1022.
[158] B.G. Sengers, M. Taylor, C.P. Please, R.O. Oreffo, *Biomaterials* **2007**, *28*, 1926.
[159] A. Schober, U. Fernekorn, S. Singh, G. Schlingloff, M. Gebinoga, J. Hampl, A. Williamson, *Eng. Life Sci.* **2013**, *13*, 352.
[160] M.L. Tanzer, *J. Orthop. Sci.* **2006**, *11*, 326.
[161] Z. Ma, M. Kotaki, R. Inai, S. Ramakrishna, *Tissue Eng.* **2005**, *11*, 101.

[162] S. Franz, S. Rammelt, D. Scharnweber, J.C. Simon, *Biomaterials* **2011**, *32*, 6692.
[163] A. Vishwakarma, N.S. Bhise, M.B. Evangelista, J. Rouwkema, M.R. Dokmeci, A.M. Ghaemmaghami, N.E. Vrana, A. Khademhosseini, *Trends Biotechnol.* **2016**, *34*, 470.
[164] P.S. Hume, J. He, K. Haskins, K.S. Anseth, *Biomaterials* **2012**, *33*, 3615.
[165] S. Chakraborty, I.-C. Liao, A. Adler, K.W. Leong, *Adv. Drug Delivery Rev.* **2009**, *61*, 1043.
[166] A. Formhals, *Process and apparatus for preparing artificial threads*. **1934**, Google Patents.
[167] J. Doshi, D.H. Reneker, *J. Electrost.* **1995**, *35*, 151.
[168] D.H. Reneker, I. Chun, *Nanotechnology* **1996**, *7*, 216.
[169] S. Koombhongse, W. Liu, D.H. Reneker, *J. Polym. Sci., Part B: Polym. Phys.* **2001**, *39*, 2598.
[170] A.L. Yarin, S. Koombhongse, D.H. Reneker, *J. Appl. Phys.* **2001**, *89*, 3018.
[171] A.L. Yarin, S. Koombhongse, D.H. Reneker, *J. Appl. Phys.* **2001**, *90*, 4836.
[172] S. Agarwal, J.H. Wendorff, A. Greiner, *Adv. Mater.* **2009**, *21*, 3343.
[173] S. Agarwal, A. Greiner, J.H. Wendorff, *Adv. Funct. Mater.* **2009**, *19*, 2863.
[174] K. Shalumon, J.-P. Chen, *Curr. Pharm. Des.* **2015**, *21*, 1979.
[175] H. Yoshimoto, Y. Shin, H. Terai, J. Vacanti, *Biomaterials* **2003**, *24*, 2077.
[176] J.-H. Jang, O. Castano, H.-W. Kim, *Adv. Drug Delivery Rev.* **2009**, *61*, 1065.
[177] M.S. Lee, T. Ahmad, J. Lee, H.K. Awada, Y. Wang, K. Kim, H. Shin, H.S. Yang, *Biomaterials* **2017**, *124*, 65.
[178] J. Wang, M. Windbergs, *Eur. J. Pharm. Biopharm.* **2017**, *119*, 283.
[179] S.A. Sell, M.J. McClure, K. Garg, P.S. Wolfe, G.L. Bowlin, *Adv. Drug Delivery Rev.* **2009**, *61*, 1007.
[180] S. Heydarkhan-Hagvall, K. Schenke-Layland, A.P. Dhanasopon, F. Rofail, H. Smith, B.M. Wu, R. Shemin, R.E. Beygui, W.R. MacLellan, *Biomaterials* **2008**, *29*, 2907.
[181] A. Greiner, J.H. Wendorff, *Angew. Chem. Int Ed. Engl.* **2007**, *46*, 5670.
[182] K. Pawlowski, H. Belvin, D. Raney, J. Su, J. Harrison, E. Siochi, *Polymer* **2003**, *44*, 1309.
[183] X. Wang, C. Drew, S.-H. Lee, K.J. Senecal, J. Kumar, L.A. Samuelson, *Nano Lett.* **2002**, *2*, 1273.
[184] S. Ji, Y. Li, M. Yang, *Sens. Actuators, B* **2008**, *133*, 644.
[185] S. Sell, C. Barnes, M. Smith, M. McClure, P. Madurantakam, J. Grant, M. McManus, G. Bowlin, *Polym. Int.* **2007**, *56*, 1349.
[186] R. Gopal, S. Kaur, Z. Ma, C. Chan, S. Ramakrishna, T. Matsuura, *J. Membr. Sci.* **2006**, *281*, 581.
[187] V. Thavasi, G. Singh, S. Ramakrishna, *Energy Environ. Sci.* **2008**, *1*, 205.
[188] Z.-M. Huang, Y.-Z. Zhang, M. Kotaki, S. Ramakrishna, *Compos. Sci. Technol.* **2003**, *63*, 2223.
[189] N. Bhardwaj, S.C. Kundu, *Biotechnol. Adv.* **2010**, *28*, 325.
[190] A. Rogina, *Appl. Surf. Sci.* **2014**, *296*, 221.
[191] D. Han, P.-I. Gouma, *Nanomedicine* **2006**, *2*, 37.
[192] A. Baji, Y.-W. Mai, S.-C. Wong, M. Abtahi, P. Chen, *Compos. Sci. Technol.* **2010**, *70*, 703.
[193] J. Lannutti, D. Reneker, T. Ma, D. Tomasko, D. Farson, *Mater. Sci. Eng., C* **2007**, *27*, 504.
[194] D. Reneker, A. Yarin, E. Zussman, H. Xu, *Adv. Appl. Mech.* **2007**, *41*, 43.
[195] T.J. Sill, H.A. von Recum, *Biomaterials* **2008**, *29*, 1989.

[196] W.-E. Teo, R. Inai, S. Ramakrishna, *Sci. Technol. Adv. Mater.* **2011**, *12*, 013002.
[197] Q.P. Pham, U. Sharma, A.G. Mikos, *Tissue Eng.* **2006**, *12*, 1197.
[198] S. De Vrieze, T. Van Camp, A. Nelvig, B. Hagström, P. Westbroek, K. De Clerck, *J. Mater. Sci.* **2009**, *44*, 1357.
[199] S.A. Sell, P.S. Wolfe, K. Garg, J.M. McCool, I.A. Rodriguez, G.L. Bowlin, *Polymers* **2010**, *2*, 522.
[200] Q. Jiang, N. Reddy, S. Zhang, N. Roscioli, Y. Yang, *J. Biomed. Mater. Res., Part A* **2013**, *101*, 1237.
[201] G.P. Huang, S. Shanmugasundaram, P. Masih, D. Pandya, S. Amara, G. Collins, T.L. Arinzeh, *J. Biomed. Mater. Res., Part A* **2015**, *103*, 762.
[202] T. Liu, W.K. Teng, B.P. Chan, S.Y. Chew, *J. Biomed. Mater. Res., Part A* **2010**, *95*, 276.
[203] F. Zhang, B. Zuo, Z. Fan, Z. Xie, Q. Lu, X. Zhang, D.L. Kaplan, *Biomacromolecules* **2012**, *13*, 798.
[204] J.H. Kim, C.H. Park, O.J. Lee, J.M. Lee, J.W. Kim, Y.H. Park, C.S. Ki, *J. Biomed. Mater. Res., Part A* **2012**, *100*, 3287.
[205] N. Bhattarai, Z. Li, D. Edmondson, M. Zhang, *Adv. Mater.* **2006**, *18*, 1463.
[206] E. Pabjańczyk-Wlazło, I. Krucińska, M. Chrzanowski, G. Szparaga, A. Chaberska, B. Kolesińska, A. Komisarczyk, M. Boguń, *Fibres Text. East. Eur.* **2017**.
[207] Y. Ji, K. Ghosh, X.Z. Shu, B. Li, J.C. Sokolov, G.D. Prestwich, R.A.F. Clark, M.H. Rafailovich, *Biomaterials* **2006**, *27*, 3782.
[208] K.Y. Lee, L. Jeong, Y.O. Kang, S.J. Lee, W.H. Park, *Adv. Drug Delivery Rev.* **2009**, *61*, 1020.
[209] C. Pillai, W. Paul, C.P. Sharma, *Prog. Polym. Sci.* **2009**, *34*, 641.
[210] A.C. Mendes, K. Stephansen, I.S. Chronakis, *Food Hydrocolloids* **2017**, *68*, 53.
[211] M.M. Demir, I. Yilgor, E. Yilgor, B. Erman, *Polymer* **2002**, *43*, 3303.
[212] E. Kiliç, A. Yakar, N.P. Bayramgil, *J. Mater. Sci. Mater. Med.* **2018**, *29*, 8.
[213] C. Yao, X. Li, K. Neoh, Z. Shi, E. Kang, *J. Membr. Sci.* **2008**, *320*, 259.
[214] A. Cipitria, A. Skelton, T. Dargaville, P. Dalton, D. Hutmacher, *J. Mater. Chem.* **2011**, *21*, 9419.
[215] W.K. Son, J.H. Youk, T.S. Lee, W.H. Park, *Polymer* **2004**, *45*, 2959.
[216] Z. Song, S.W. Chiang, X. Chu, H. Du, J. Li, L. Gan, C. Xu, Y. Yao, Y. He, B. Li, *J. Appl. Polym. Sci.* **2018**, *135*.
[217] F. Yang, R. Murugan, S. Wang, S. Ramakrishna, *Biomaterials* **2005**, *26*, 2603.
[218] H. Cho, S.K. Madhurakkat Perikamana, J. Lee, J. Lee, K. Lee, C.S. Shin, H. Shin, *ACS Appl. Mater. Interfaces* **2014**, *6*, 11225.
[219] E.D. Boland, G.E. Wnek, D.G. Simpson, K.J. Pawlowski, G.L. Bowlin, *J. Macromol. Sci., Part A* **2001**, *38*, 1231.
[220] Y. You, B.M. Min, S.J. Lee, T.S. Lee, W.H. Park, *J. Appl. Polym. Sci.* **2005**, *95*, 193.
[221] X. Xin, M. Hussain, J.J. Mao, *Biomaterials* **2007**, *28*, 316.
[222] C.N. Riggin, F. Qu, D.H. Kim, J. Huegel, D.R. Steinberg, A.F. Kuntz, L.J. Soslowsky, R.L. Mauck, J. Bernstein, *Ann. Biomed. Eng.* **2017**, *45*, 2348.
[223] F. Danhier, E. Ansorena, J.M. Silva, R. Coco, A. Le Breton, V. Préat, *J. Controlled Release* **2012**, *161*, 505.
[224] H.K. Makadia, S.J. Siegel, *Polymers* **2011**, *3*, 1377.
[225] A. Lancuški, F. Bossard, S. Fort, *Biomacromolecules* **2013**, *14*, 1877.
[226] A. Rossi, L. Wistlich, K.-H. Heffels, H. Walles, J. Groll, *Adv. Healthcare Mater.* **2016**, *5*, 1939.

[227] J.M. Ren, T.G. McKenzie, Q. Fu, E.H. Wong, J. Xu, Z. An, S. Shanmugam, T.P. Davis, C. Boyer, G.G. Qiao, *Chem. Rev.* **2016**, *116*, 6743.
[228] W. Wu, W. Wang, J. Li, *Prog. Polym. Sci.* **2015**, *46*, 55.
[229] J. Groll, M. Moeller, *Method. Enzymol.* **2010**, *472*, 1.
[230] J. Groll, T. Ameringer, J.P. Spatz, M. Moeller, *Langmuir* **2005**, *21*, 1991.
[231] D. Irvine, A. Mayes, L. Griffith-Cima, *Macromolecules* **1996**, *29*, 6037.
[232] H. Götz, U. Beginn, C.F. Bartelink, H.J. Grünbauer, M. Möller, *Macromol. Mater. Eng.* **2002**, *287*, 223.
[233] C.D. Heyes, J. Groll, M. Möller, G.U. Nienhaus, *Mol. BioSys.* **2007**, *3*, 419.
[234] A. Dhanasingh, J. Salber, M. Moeller, J. Groll, *Soft Matter* **2010**, *6*, 618.
[235] A. Dhanasingh, J. Groll, *Soft Matter* **2012**, *8*, 1643.
[236] P.D. Dalton, C. Hostert, K. Albrecht, M. Moeller, J. Groll, *Macromol. Biosci.* **2008**, *8*, 923.
[237] M. Hütten, A. Dhanasingh, R. Hessler, T. Stöver, K.-H. Esser, M. Möller, T. Lenarz, C. Jolly, J. Groll, V. Scheper, *PloS one* **2014**, *9*, e104564.
[238] J. Groll, E.V. Amirgoulova, T. Ameringer, C.D. Heyes, C. Röcker, G.U. Nienhaus, M. Möller, *J. Am. Chem. Soc.* **2004**, *126*, 4234.
[239] J. Groll, Z. Ademovic, T. Ameringer, D. Klee, M. Moeller, *Biomacromolecules* **2005**, *6*, 956.
[240] E.V. Amirgoulova, J. Groll, C.D. Heyes, T. Ameringer, C. Röcker, M. Möller, G.U. Nienhaus, *ChemPhysChem* **2004**, *5*, 552.
[241] J. Groll, W. Haubensak, T. Ameringer, M. Moeller, *Langmuir* **2005**, *21*, 3076.
[242] K. Bruellhoff, J. Fiedler, M. Möller, J. Groll, R.E. Brenner, *Int. J. Artif. Organs* **2010**, *33*, 646.
[243] A.M. Greiner, P. Hoffmann, K. Bruellhoff, S. Jungbauer, J.P. Spatz, M. Moeller, R. Kemkemer, J. Groll, *Macromol. Biosci.* **2014**, *14*, 1547.
[244] S. Sinn, M. Eichler, L. Müller, D. Bünger, J. Groll, G. Ziemer, F. Rupp, H. Northoff, J. Geis-Gerstorfer, F.K. Gehring, *Sensors* **2011**, *11*, 5253.
[245] J. Groll, J. Fiedler, K. Bruellhoff, M. Moeller, R.E. Brenner, *Int. J. Artif. Organs* **2009**, *32*, 655.
[246] J. Fiedler, J. Groll, E. Engelhardt, P. Gasteier, C. Dahmen, H. Kessler, M. Moeller, R.E. Brenner, *studies* **2011**, *3*, 4.
[247] G. Böhm, J. Groll, K.-H. Heffels, N. Heussen, P. Ink, H.P. Alizai, U.P. Neumann, R. Schnabel, U. Mirastschijski, *J. Biomater. Appl.* **2018**, 0885328218759043.
[248] X.Y. Sun, R. Shankar, H.G. Börner, T.K. Ghosh, R.J. Spontak, *Adv. Mater.* **2007**, *19*, 87.
[249] K. Klinkhammer, J. Bockelmann, C. Simitzis, G.A. Brook, D. Grafahrend, J. Groll, M. Möller, J. Mey, D. Klee, *J. Mater. Sci. Mater. Med.* **2010**, *21*, 2637.
[250] G. Böhm, Y. Ushakova, H.P. Alizai, T. Braunschweig, C. Lente, K.-H. Heffels, J. Groll, U.P. Neumann, K. Junge, *Eur. Surg. Res.* **2011**, *47*, 118.
[251] M. Bartneck, K.-H. Heffels, Y. Pan, M. Bovi, G. Zwadlo-Klarwasser, J. Groll, *Biomaterials* **2012**, *33*, 4136.
[252] M. Bartneck, K.-H. Heffels, M. Bovi, J. Groll, G. Zwadlo-Klarwasser, *Mater. Sci. Eng., C* **2013**, *33*, 5109.
[253] T. Simón-Yarza, A. Rossi, K.-H. Heffels, F. Prósper, J. Groll, M.J. Blanco-Prieto, *Tissue Eng., Part A* **2015**, *21*, 1654.
[254] H.S. Yoo, T.G. Kim, T.G. Park, *Adv. Drug Delivery Rev.* **2009**, *61*, 1033.
[255] Q. Cheng, B.L.-P. Lee, K. Komvopoulos, Z. Yan, S. Li, *Tissue Eng., Part A* **2013**, *19*, 1188.
[256] L. Grøndahl, J.Z. Luk, in *Biointerfaces*, Edt, **2014**.

[257] Z. Wang, B. Sun, M. Zhang, L. Ou, Y. Che, J. Zhang, D. Kong, *J. Bioact. Compat. Polym.* **2013**, *28*, 154.
[258] S. Regis, S. Youssefian, M. Jassal, M.D. Phaneuf, N. Rahbar, S. Bhowmick, *J. Biomed. Mater. Res., Part A* **2014**, *102*, 1697.
[259] T. Brueckner, A. Eberl, S. Heumann, M. Rabe, G.M. Guebitz, *J. Polym. Sci., Part A: Polym. Chem.* **2008**, *46*, 6435.
[260] L. Meng, O. Arnoult, M. Smith, G.E. Wnek, *J. Mater. Chem.* **2012**, *22*, 19412.
[261] S. Turmanova, M. Minchev, K. Vassilev, G. Danev, *J. Polym. Res.* **2008**, *15*, 309.
[262] M. Mori, Y. Uyama, Y. Ikada, *J. Polym. Sci., Part A: Polym. Chem.* **1994**, *32*, 1683.
[263] R.-Q. Kou, Z.-K. Xu, H.-T. Deng, Z.-M. Liu, P. Seta, Y. Xu, *Langmuir* **2003**, *19*, 6869.
[264] Z. Ma, M. Kotaki, T. Yong, W. He, S. Ramakrishna, *Biomaterials* **2005**, *26*, 2527.
[265] P. Viswanathan, E. Themistou, K. Ngamkham, G.C. Reilly, S.P. Armes, G. Battaglia, *Biomacromolecules* **2014**, *16*, 66.
[266] M.B. Taskin, R. Xu, H. Gregersen, J.V. Nygaard, F. Besenbacher, M. Chen, *ACS Appl. Mater. Interfaces* **2016**, *8*, 15864.
[267] A.M. Nicolini, T.D. Toth, J.-Y. Yoon, *Colloids Surf., B* **2016**, *145*, 830.
[268] B.K. Mann, J.L. West, *J. Biomed. Mater. Res.* **2002**, *60*, 86.
[269] S.P. Palecek, J.C. Loftus, M.H. Ginsberg, D.A. Lauffenburger, A.F. Horwitz, *Nature* **1997**, *385*, 537.
[270] M.L. Condic, P.C. Letourneau, *Nature* **1997**, *389*, 852.
[271] D.J. Irvine, K.-A. Hue, A.M. Mayes, L.G. Griffith, *Biophys. J.* **2002**, *82*, 120.
[272] G. Maheshwari, G. Brown, D.A. Lauffenburger, A. Wells, L.G. Griffith, *J. Cell Sci.* **2000**, *113*, 1677.
[273] S.P. Massia, J.A. Hubbell, *Anal. Biochem.* **1990**, *187*, 292.
[274] J.A. Neff, P. Tresco, K. Caldwell, *Biomaterials* **1999**, *20*, 2377.
[275] M. Arnold, M. Schwieder, J. Blümmel, E.A. Cavalcanti-Adam, M. López-Garcia, H. Kessler, B. Geiger, J.P. Spatz, *Soft Matter* **2009**, *5*, 72.
[276] E.A. Cavalcanti-Adam, A. Micoulet, J. Blümmel, J. Auernheimer, H. Kessler, J.P. Spatz, *Eur. J. Cell Biol.* **2006**, *85*, 219.
[277] E.A. Cavalcanti-Adam, T. Volberg, A. Micoulet, H. Kessler, B. Geiger, J.P. Spatz, *Biophys. J.* **2007**, *92*, 2964.
[278] J.A. Deeg, I. Louban, D. Aydin, C. Selhuber-Unkel, H. Kessler, J.P. Spatz, *Nano Lett.* **2011**, *11*, 1469.
[279] M. Jassal, S. Sengupta, S.B. Warner, S. Bhowmick, *Text. Res. J.* **2013**.
[280] J.M. Goddard, J.H. Hotchkiss, *Prog. Polym. Sci.* **2007**, *32*, 698.
[281] Z. Ma, Z. Mao, C. Gao, *Colloids Surf., B* **2007**, *60*, 137.
[282] R. Vasita, G. Mani, C.M. Agrawal, D.S. Katti, *Polymer* **2010**, *51*, 3706.
[283] K.E. Park, K.Y. Lee, S.J. Lee, W.H. Park, presented at the Macromolecular Symposia, **2007**.
[284] D.M. Campos, K. Gritsch, V. Salles, G.N. Attik, B. Grosgogeat, *Biores. Open Access* **2014**, *3*, 117.
[285] M. Endo, K. Takeuchi, S. Igarashi, K. Kobori, M. Shiraishi, H.W. Kroto, *J. Phys. Chem. Solids* **1993**, *54*, 1841.
[286] S. Zhan, D. Chen, X. Jiao, C. Tao, *J. Phys. Chem. B* **2006**, *110*, 11199.
[287] Z.L. Wang, *J. Phys. Chem. B* **2000**, *104*, 1153.
[288] J.M. Petroski, Z.L. Wang, T.C. Green, M.A. El-Sayed, *J. Phys. Chem. B* **1998**, *102*, 3316.
[289] P. Fili, J. Lausmaa, J. Musialek, K. Mazanec, *Biomaterials* **2001**, *22*, 2131.

[290] G.E. Fantner, H. Birkedal, J.H. Kindt, T. Hassenkam, J.C. Weaver, J.A. Cutroni, B.L. Bosma, L. Bawazer, M.M. Finch, G.A. Cidade, D.E. Morse, G.D. Stucky, P.K. Hansma, *Bone* **2004**, *35*, 1013.
[291] M. Esposito, J. Lausmaa, J.M. Hirsch, P. Thomsen, *J. Biomed. Mater. Res.* **1999**, *48*, 559.
[292] M.S. Sader, A. Balduino, A. Soares Gde, R. Borojevic, *Clin. Oral. Implants Res.* **2005**, *16*, 667.
[293] J. Li, Y. Dou, J. Yang, Y. Yin, H. Zhang, F. Yao, H. Wang, K. Yao, *Mater. Sci. Eng., C* **2009**, *29*, 1207.
[294] B. Inanc, Y.E. Arslan, S. Seker, A.E. Elcin, Y.M. Elcin, *J. Biomed. Mater. Res. A* **2009**, *90*, 186.
[295] H.-J. Jin, J. Chen, V. Karageorgiou, G.H. Altman, D.L. Kaplan, *Biomaterials* **2004**, *25*, 1039.
[296] J. Chen, G.H. Altman, V. Karageorgiou, R. Horan, A. Collette, V. Volloch, T. Colabro, D.L. Kaplan, *J. Biomed. Mater. Res. A* **2003**, *67*, 559.
[297] H. Backdahl, G. Helenius, A. Bodin, U. Nannmark, B.R. Johansson, B. Risberg, P. Gatenholm, *Biomaterials* **2006**, *27*, 2141.
[298] W.Y. Chuang, T.H. Young, C.H. Yao, W.Y. Chiu, *Biomaterials* **1999**, *20*, 1479.
[299] Y.W. Wang, Q. Wu, G.Q. Chen, *Biomaterials* **2004**, *25*, 669.
[300] S. Megelski, J.S. Stephens, D.B. Chase, J.F. Rabolt, *Macromolecules* **2002**, *35*, 8456.
[301] K. Zhang, L.L. Zhang, X.S. Zhao, J. Wu, *Chem. Mater.* **2010**, *22*, 1392.
[302] M. Endo, Y.A. Kim, T. Hayashi, K. Nishimura, T. Matusita, K. Miyashita, M.S. Dresselhaus, *Carbon* **2001**, *39*, 1287.
[303] C.J. Buchko, L.C. Chen, Y. Shen, D.C. Martin, *Polymer* **1999**, *40*, 7397.
[304] N. Durán, P.D. Marcato, G.I.H. De Souza, O.L. Alves, E. Esposito, *J. Biomed. Nanotechnol.* **2007**, *3*, 203.
[305] S.P. Chandran, M. Chaudhary, R. Pasricha, A. Ahmad, M. Sastry, *Biotechnol. Prog.* **2006**, *22*, 577.
[306] G. Binnig, C.F. Quate, C. Gerber, *Phys. Rev. Lett.* **1986**, *56*, 930.
[307] R. Chen, C. Huang, Q. Ke, C. He, H. Wang, X. Mo, *Colloids Surf., B* **2010**, *79*, 315.
[308] D.H. Reneker, W. Kataphinan, A. Theron, E. Zussman, A.L. Yarin, *Polymer* **2002**, *43*, 6785.
[309] J. Miller, S. Veeramasuneni, J. Drelich, M. Yalamanchili, G. Yamauchi, *Polym. Eng. Sci.* **1996**, *36*, 1849.
[310] M. Salerno, L. Giacomelli, G. Derchi, N. Patra, A. Diaspro, *Biomed. Eng. Online* **2010**, *9*, 59.
[311] N.E. Zander, K.E. Strawhecker, J.A. Orlicki, A.M. Rawlett, T.P. Beebe, *J. Phys. Chem. B* **2011**, *115*, 12441.
[312] U. Stachewicz, A.H. Barber, *Langmuir* **2011**, *27*, 3024.
[313] C.M. Franz, P.H. Puech, *Cell. Mol. Bioeng.* **2008**, *1*, 289.
[314] D.J. Wold, C.D. Frisbie, *J. Am. Chem. Soc.* **2001**, *123*, 5549.
[315] C. Jeppesen, J.Y. Wong, T.L. Kuhl, J.N. Israelachvili, N. Mullah, S. Zalipsky, C.M. Marques, *Science* **2001**, *293*, 465.
[316] J.Y. Wong, T.L. Kuhl, J.N. Israelachvili, N. Mullah, S. Zalipsky, *Science* **1997**, *275*, 820.
[317] C. Werner, H.J. Jacobasch, *Int. J. Artif. Organs* **1999**, *22*, 160.
[318] S.O. Vansteenkiste, M.C. Davies, C.J. Roberts, S.J.B. Tendler, P.M. Williams, *Prog. Surf. Sci.* **1998**, *57*, 95.
[319] O. Custance, R. Perez, S. Morita, *Nat. Nanotechnol.* **2009**, *4*, 803.

[320] S.P. Massia, J.A. Hubbell, *J. Cell Biol.* **1991**, *114*, 1089.
[321] P.D. Drumheller, J.A. Hubbell, *Anal. Biochem.* **1994**, *222*, 380.
[322] B.K. Brandley, R.L. Schnaar, *Anal. Biochem.* **1988**, *172*, 270.
[323] T. Tewson, M. Francsechini, R. Scheule, A. Holian, *Int. J. Radiat. Appl. Instrum., Part A* **1991**, *42*, 499.
[324] C.S. Fadley, *Prog. Surf. Sci.* **1984**, *16*, 275.
[325] C. Gualandi, C.D. Vo, M.L. Focarete, M. Scandola, A. Pollicino, G. Di Silvestro, N. Tirelli, *Macromol. Rapid Commun.* **2013**, *34*, 51.
[326] B.L. Henke, E.M. Gullikson, J.C. Davis, *At. Data Nucl. Data Tables* **1993**, *54*, 181.
[327] W. He, Z. Ma, T. Yong, W.E. Teo, S. Ramakrishna, *Biomaterials* **2005**, *26*, 7606.
[328] Y. Zhang, X. Wang, Y. Feng, J. Li, C. Lim, S. Ramakrishna, *Biomacromolecules* **2006**, *7*, 1049.
[329] A. Henss, M. Rohnke, S. Knaack, M. Kleine-Boymann, T. Leichtweiss, P. Schmitz, T. El Khassawna, M. Gelinsky, C. Heiss, J. Janek, *Biointerphases* **2013**, *8*, 31.
[330] R. Michel, S. Pasche, M. Textor, D.G. Castner, *Langmuir* **2005**, *21*, 12327.
[331] D.N. Mangos, T. Nakanishi, D.A. Lewis, *Sci. Technol. Adv. Mater.* **2014**, *15*, 015002.
[332] R. Jakobsen, F. Wasacz, J. Brasch, K. Smith, *Biopolymers* **1986**, *25*, 639.
[333] T.A. Giroux, S.L. Cooper, *J. Colloid Interface Sci.* **1990**, *139*, 351.
[334] N. Krithica, V. Natarajan, B. Madhan, P.K. Sehgal, A.B. Mandal, *Adv. Eng. Mater.* **2012**, *14*, B149.
[335] L. Cronje, B. Klumperman, *Eur. Polym. J.* **2013**, *49*, 3814.
[336] R.L. Rich, D.G. Myszka, *Curr. Opin. Biotechnol.* **2000**, *11*, 54.
[337] R. Méjard, H.J. Griesser, B. Thierry, *TrAC, Trends Anal. Chem.* **2014**, *53*, 178.
[338] R.J. Green, R.A. Frazier, K.M. Shakesheff, M.C. Davies, C.J. Roberts, S.J. Tendler, *Biomaterials* **2000**, *21*, 1823.
[339] P. Netsuwan, H. Mimiya, A. Baba, S. Sriwichai, K. Shinbo, K. Kato, F. Kaneko, S. Phanichphant, *Sens. Actuators, B* **2014**, *204*, 770.
[340] K. Knez, W. Noppe, N. Geukens, K.P. Janssen, D. Spasic, J. Heyligen, K. Vriens, K. Thevissen, B.P. Cammue, V. Petrenko, *Anal. Chem.* **2013**, *85*, 10075.
[341] T.M. Battaglia, J.-F. Masson, M.R. Sierks, S.P. Beaudoin, J. Rogers, K.N. Foster, G.A. Holloway, K.S. Booksh, *Anal. Chem.* **2005**, *77*, 7016.
[342] K. Tsuboi, H. Matsumoto, M. Minagawa, A. Tanioka, *Appl. Phys. Lett.* **2011**, *98*, 241109.
[343] B. Ding, J. Kim, Y. Miyazaki, S. Shiratori, *Sens. Actuators, B* **2004**, *101*, 373.
[344] M. Sun, B. Ding, J. Lin, J. Yu, G. Sun, *Sens. Actuators, B* **2011**, *160*, 428.
[345] M. Saitakis, E. Gizeli, *Cell. Mol. Life Sci.* **2012**, *69*, 357.
[346] F. Höök, B. Kasemo, in *Piezoelectric Sensors*, Edt: Springer, **2007**.
[347] G. Li, S. Ye, S. Morita, T. Nishida, M. Osawa, *J. Am. Chem. Soc.* **2004**, *126*, 12198.
[348] D. Rodoplu, M. Mutlu, *J. Eng. Fibers Fabr.* **2012**, *2*, 118.
[349] N. Wang, X. Wang, Y. Jia, X. Li, J. Yu, B. Ding, *Carbohydr. Polym.* **2014**, *108*, 192.
[350] S. Seker, Y.E. Arslan, Y.M. Elçin, *IEEE Sens. J.* **2010**, *10*, 1342.
[351] D. Rodoplu, Y. Sen, M. Mutlu, *Nanosci. Nanotechnol. Lett.* **2013**, *5*, 444.
[352] J. Cui, J. Iturri, U. Götz, M. Jimenez, A. del Campo, *Langmuir* **2013**, *29*, 6582.
[353] T.M.A. Gronewold, *Anal. Chim. Acta* **2007**, *603*, 119.
[354] B. Ding, M. Wang, X. Wang, J. Yu, G. Sun, *Mater. Today* **2010**, *13*, 16.

[355] Z. Hu, T. Cai, C. Chi, *Soft Matter* **2010**, *6*, 2115.
[356] D. Matatagui, M. Fernández, J. Fontecha, I. Sayago, I. Gràcia, C. Cané, M. Horrillo, J. Santos, *Talanta* **2014**, *120*, 408.
[357] D. Matatagui, M. Fernández, J. Santos, J. Fontecha, I. Sayago, M. Horrillo, I. Gràcia, C. Cané, *J. Nanomater.* **2014**, *2014*.
[358] A.C. Goodfriend, T.R. Welch, G. Barker, R. Ginther, M.S. Riegel, S.V. Reddy, J. Wang, A. Nugent, J. Forbess, *J. Biomed. Mater. Res., Part A* **2014**.
[359] S. El-Amin, H. Lu, Y. Khan, J. Burems, J. Mitchell, R. Tuan, C. Laurencin, *Biomaterials* **2003**, *24*, 1213.
[360] H. Tseng, T.E. Peterson, B.C. Berk, *Circul. Res.* **1995**, *77*, 869.
[361] D.-F. Liao, B. Monia, N. Dean, B.C. Berk, *J. Biol. Chem.* **1997**, *272*, 6146.
[362] S.D. Wolpe, G. Davatelis, B. Sherry, B. Beutler, D.G. Hesse, H.T. Nguyen, L.L. Moldawer, C.F. Nathan, S.F. Lowry, A. Cerami, *J. Exp. Med.* **1988**, *167*, 570.
[363] E. Cadman, J.R. Bostwick, J. Eichberg, *Anal. Biochem.* **1979**, *96*, 21.
[364] A.G. Gornall, C.J. Bardawill, M.M. David, *J. Biol. Chem.* **1949**, *177*, 751.
[365] G.R. Kingsley, *J. Biol. Chem.* **1939**, *131*, 197.
[366] A.A. Vertegel, R.W. Siegel, J.S. Dordick, *Langmuir* **2004**, *20*, 6800.
[367] P. Smith, R.I. Krohn, G. Hermanson, A. Mallia, F. Gartner, M. Provenzano, E. Fujimoto, N. Goeke, B. Olson, D. Klenk, *Anal. Biochem.* **1985**, *150*, 76.
[368] K.-N. Chua, W.-S. Lim, P. Zhang, H. Lu, J. Wen, S. Ramakrishna, K.W. Leong, H.-Q. Mao, *Biomaterials* **2005**, *26*, 2537.
[369] L. Cen, K. Neoh, E. Kang, *Langmuir* **2003**, *19*, 10295.
[370] J. Lin, S. Qiu, K. Lewis, A.M. Klibanov, *Biotechnol. Bioeng.* **2003**, *83*, 168.
[371] V. Ivanov, J. Behnisch, A. Holländer, F. Mehdorn, H. Zimmermann, *Surf. Interface Anal.* **1996**, *24*, 257.
[372] J.C. Tiller, C.-J. Liao, K. Lewis, A.M. Klibanov, *Proc. Natl. Acad. Sci. U. S. A.* **2001**, *98*, 5981.
[373] P. Wutticharoenmongkol, N. Sanchavanakit, P. Pavasant, P. Supaphol, *Macromol. Biosci.* **2006**, *6*, 70.
[374] A. Neamnark, N. Sanchavanakit, P. Pavasant, R. Rujiravanit, P. Supaphol, *Eur. Polym. J.* **2008**, *44*, 2060.
[375] K. Park, Y.M. Ju, J.S. Son, K.-D. Ahn, D.K. Han, *J. Biomater. Sci., Polym. Ed.* **2007**, *18*, 369.
[376] A. Martins, E.D. Pinho, S. Faria, I. Pashkuleva, A.P. Marques, R.L. Reis, N.M. Neves, *Small* **2009**, *5*, 1195.
[377] D.K. Mills, in *Orthopedic Biomaterials*, Edt: Springer, **2018**.
[378] K. Hurle, T. Christel, U. Gbureck, C. Moseke, J. Neubauer, F. Goetz-Neunhoeffer, *J. Mater. Sci. Mater. Med.* **2016**, *27*, 1.
[379] M. Rödel, J. Teßmar, J. Groll, U. Gbureck, *Acta Biomater.* **2018**, *79*, 182.
[380] I. Potapochkina, N. Korotkova, S. Loginova, V. Lebedev, *Polymer Science Series D* **2011**, *4*, 45.
[381] J. Groll, M. Möller, in *Encyclopedia of Polymeric Nanomaterials*, Edt: Springer, Berlin, Heidelberg, **2015**.
[382] J. Groll, M. Moeller, in *Encyclopedia of Biophysics*, Edt: Springer, Berlin, Heidelberg, **2013**.
[383] S. Chandra, Y. Ohama, *Polymers in concrete*, CRC press, **1994**.
[384] J. Dong, T. Uemura, Y. Shirasaki, T. Tateishi, *Biomaterials* **2002**, *23*, 4493.
[385] D. Chung, *J. Mater. Sci.* **2004**, *39*, 2973.
[386] D. Feldman, F. Denes, Z. Zeng, A. Denes, D. Banu, *J. Adhes. Sci. Technol.* **2000**, *14*, 1705.

[387] M. Al-Zahrani, M. Maslehuddin, S. Al-Dulaijan, M. Ibrahim, *Cem. Concr. Compos.* **2003**, *25*, 527.
[388] M. Ginebra, E. Fernandez, E. De Maeyer, R. Verbeeck, M. Boltong, J. Ginebra, F. Driessens, J. Planell, *J. Dent. Res.* **1997**, *76*, 905.
[389] U. Gbureck, O. Grolms, J. Barralet, L. Grover, R. Thull, *Biomaterials* **2003**, *24*, 4123.
[390] J. Wang, C. Liu, Y. Liu, S. Zhang, *Adv. Funct. Mater.* **2010**, *20*, 3997.
[391] L. Wistlich, A. Rücker, M. Schamel, A.C. Kübler, U. Gbureck, J. Groll, *Adv. Healthcare Mater.* **2017**, *6*, 1600902.
[392] X. Baur, W. Marek, J. Ammon, A. Czuppon, B. Marczynski, M. Raulf-Heimsoth, H. Roemmelt, G. Fruhmann, *Int. Arch. Occup. Environ. Health* **1994**, *66*, 141.
[393] J. An, J.G. Wolke, J.A. Jansen, S.C. Leeuwenburgh, *J. Mater. Sci. Mater. Med.* **2016**, *27*, 1.
[394] K.S. TenHuisen, P.W. Brown, *Biomaterials* **1998**, *19*, 2209.
[395] A. Jenni, L. Holzer, R. Zurbriggen, M. Herwegh, *Cem. Concr. Res.* **2005**, *35*, 35.
[396] R. Wang, J. Li, T. Zhang, L. Czarnecki, *Bull. Pol. Acad. Sci.: Tech. Sci.* **2016**, *64*, 785.
[397] N.L. Millar, T.A. Bradley, N.A. Walsh, R.C. Appleyard, M.J. Tyler, G.A. Murrell, *J. Shoulder Elbow Surg.* **2009**, *18*, 639.
[398] J. Ge, M. Trujillo, J. Stansbury, *Dent. Mater.* **2005**, *21*, 1163.
[399] D. Chattopadhyay, P. Prasad, B. Sreedhar, K. Raju, *Prog. Org. Coat.* **2005**, *54*, 296.
[400] M. Sterley, S. Trey, Å. Lundevall, S. Olsson, *J. Appl. Polym. Sci.* **2012**, *126*.
[401] C. Neuerburg, S. Recknagel, J. Fiedler, J. Groll, M. Moeller, K. Bruellhoff, H. Reichel, A. Ignatius, R.E. Brenner, *J. Mater. Sci. Mater. Med.* **2013**, *24*, 2417.
[402] J. Ferracane, E. Greener, *J. Dent. Res.* **1984**, *63*, 1093.
[403] H. Perez-Hernandez, T. Paumer, T. Pompe, C. Werner, A. Lasagni, *Biointerphases* **2012**, *7*, 1.
[404] W.D. Cook, *Polymer* **1992**, *33*, 600.
[405] V. Karageorgiou, D. Kaplan, *Biomaterials* **2005**, *26*, 5474.
[406] A. Rücker, *Entwicklung eines photochemisch vernetzbaren, methacrylat-und isocyanathaltigen Knochenklebers mit degradierbaren keramischen Füllstoffen*. **2017**, Würzburg.
[407] I. Sideridou, V. Tserki, G. Papanastasiou, *Biomaterials* **2002**, *23*, 1819.
[408] W.A. Rutala, D.J. Weber, **2008**.
[409] S. Duan, W. Zhu, L. Yu, J. Ding, *Chin. Sci. Bull.* **2005**, *50*, 1093.
[410] J.W. Hwang, S.M. Noh, B. Kim, H.W. Jung, *J. Appl. Polym. Sci.* **2015**, *132*.
[411] N.V. Shah, R. MeiSliN, *Orthopedics* **2013**, *36*, 945.
[412] M. Mehta, K. Shah, R. Bhatt, *J. Oral Maxillofac. Surg.* **1987**, *45*, 393.
[413] B. Vázquez Lasa, in *Orthopaedic bone cements*, Edt: S. Deb, CRC Press, Boca Raton, Boston, New York, Washington, DC, **2008**.
[414] A. Bou-Francis, A. Ghanem, *Int. J. Adhes. Adhes.* **2017**, *77*, 96.
[415] V. Bhagat, E. O'Brien, J. Zhou, M.L. Becker, *Biomacromolecules* **2016**, *17*, 3016.
[416] B. Cohen, M. Panker, E. Zuckerman, M. Foox, M. Zilberman, *J. Biomater. Appl.* **2014**, *28*, 1366.
[417] T. Kiguchi, H. Aota, A. Matsumoto, *Macromolecules* **2004**, *37*, 8249.
[418] D.A. Ossipov, *Expert Opin. Drug Delivery* **2015**, *12*, 1443.
[419] S.-M. Ho, A.M. Young, *Eur. Polym. J.* **2006**, *42*, 1775.

[420] P. Lucksanasombool, W. Higgs, R. Higgs, M. Swain, *Biomaterials* **2003**, *24*, 1159.
[421] W. MacDonald, E. Swarts, R. Beaver, *Clin. Orthop. Relat. R.* **1993**, 283.
[422] B. Van Meerbeek, J. De Munck, D. Mattar, K. Van Landuyt, P. Lambrechts, *Oper. Dent.* **2003**, *28*, 647.
[423] J. Vainio, J. Kilpikari, P. Törmälä, P. Rokkanen, *Arch. Orthop. Trauma Surg.* **1979**, *94*, 191.
[424] A. Bercier, S. Gonçalves, H. Autefage, F. Briand-Mesange, O. Lignon, J. Fitremann, *Materials* **2010**, *3*, 5111.
[425] K. Ishihara, N. Nakabayashi, *J. Biomed. Mater. Res., Part A* **1989**, *23*, 1475.
[426] L. Wistlich, J. Kums, A. Rossi, K.H. Heffels, H. Wajant, J. Groll, *Adv. Funct. Mater.* **2017**, *27*, 1702903.
[427] K.-H. Heffels, *Functional nanofibres for regenerative medicine*. **2012**, Würzburg.
[428] P.C. Weber, D. Ohlendorf, J. Wendoloski, F. Salemme, *Science* **1989**, *243*, 85.
[429] S.E. D'Souza, M.H. Ginsberg, E.F. Plow, *Trends Biochem. Sci.* **1991**, *16*, 246.
[430] S.L. Bellis, *Biomaterials* **2011**, *32*, 4205.
[431] E.M. Sussman, M.C. Halpin, J. Muster, R.T. Moon, B.D. Ratner, *Ann. Biomed. Eng.* **2014**, *42*, 1508.
[432] M.J. Smith, K.L. White Jr, D.C. Smith, G.L. Bowlin, *Biomaterials* **2009**, *30*, 149.
[433] V. Holan, M. Chudickova, P. Trosan, E. Svobodova, M. Krulova, S. Kubinova, E. Sykova, J. Sirc, J. Michalek, M. Juklickova, *J. Controlled Release* **2011**, *156*, 406.
[434] S. Jin, T.-M. Park, C.-H. Kim, J.-S. Kim, B.D. Le, Y.H. Jeong, J.-Y. Kwak, S. Yoon, *Biotechniques* **2015**, *58*, 285.
[435] D. Abebayehu, A. Spence, B.D. Boyan, Z. Schwartz, J.J. Ryan, M.J. McClure, *J. Biomed. Mater. Res., Part A* **2017**.
[436] S. Thangaraju, E. Subramani, B. Chakravarty, K. Chaudhury, *Gynecol. Oncol.* **2012**, *127*, 426.
[437] G. Chen, D.V. Goeddel, *Science* **2002**, *296*, 1634.
[438] L.A. Tartaglia, D.V. Goeddel, *Immunol. Today* **1992**, *13*, 151.
[439] S.R. Wiley, J.A. Winkles, *Cytokine Growth Factor Rev.* **2003**, *14*, 241.
[440] H. Wajant, *Br. J. Pharmacol.* **2013**, *170*, 748.
[441] R.E. Kontermann, P. Scheurich, K. Pfizenmaier, *Expert Opin. Drug Discov.* **2009**, *4*, 279.
[442] L.C. Burkly, *Semin. Immunol.* **2014**, *26*, 229.
[443] L.C. Burkly, J.S. Michaelson, T.S. Zheng, *Immunol. Rev.* **2011**, *244*, 99.
[444] J.R. Crowther, *ELISA: theory and practice*, Springer Science & Business Media, **1995**. Vol. 42.
[445] A. Fick, I. Lang, V. Schäfer, A. Seher, J. Trebing, D. Weisenberger, H. Wajant, *J. Biol. Chem.* **2012**, *287*, 484.
[446] B.A. Tannous, *Nat. Protoc.* **2009**, *4*, 582.
[447] S. Haddock, C. McDougall, J. Case, *The bioluminescence web page*. **2000**, University of California, Santa Barbara.
[448] K.L. Everton, D.R. Abbott, D.K. Crockett, K.S. Elenitoba-Johnson, M.S. Lim, *J. Chromatogr. B* **2009**, *877*, 1335.
[449] A. Einhauer, A. Jungbauer, *J. Biochem. Biophys. Methods* **2001**, *49*, 455.
[450] Q.P. Pham, U. Sharma, A.G. Mikos, *Tissue Eng.* **2006**, *12*, 1197.
[451] K. Klinkhammer, N. Seiler, D. Grafahrend, J. Gerardo-Nava, J. Mey, G.A. Brook, M. Möller, P.D. Dalton, D. Klee, *Tissue Eng., Part C* **2008**, *15*, 77.
[452] V.A. Schulte, K. Hahn, A. Dhanasingh, K.-H. Heffels, J. Groll, *Biofabrication* **2014**, *6*, 024106.

[453] Y.-L. Lu, F. Zhang, T. Chen, S.-N. Hu, W.-J. Kou, X.-L. Luo, L.-Q. Wang, C.-H. Cai, *Acta Polym. Sin.* **2016**, 650.
[454] S. Torres-Giner, M. Ocio, J. Lagaron, *Eng. Life Sci.* **2008**, *8*, 303.
[455] J. Trebing, I. Lang, M. Chopra, S. Salzmann, M. Moshir, K. Silence, S.S. Riedel, D. Siegmund, A. Beilhack, C. Otto, *mAbs* **2014**, *6*, 297.
[456] D.F. Legler, O. Micheau, M.-A. Doucey, J. Tschopp, C. Bron, *Immunity* **2003**, *18*, 655.
[457] Y. Wu, B. Zhou, *Br. J. Cancer* **2010**, *102*, 639.
[458] A. Krippner-Heidenreich, I. Grunwald, G. Zimmermann, M. Kühnle, J. Gerspach, T. Sterns, S.D. Shnyder, J.H. Gill, D.N. Männel, K. Pfizenmaier, *J. Immunol.* **2008**, *180*, 8176.
[459] H. Rauert, A. Wicovsky, N. Müller, D. Siegmund, V. Spindler, J. Waschke, C. Kneitz, H. Wajant, *J. Biol. Chem.* **2010**, *285*, 7394.
[460] M. Chopra, M. Biehl, T. Steinfatt, A. Brandl, J. Kums, J. Amich, M. Vaeth, J. Kuen, R. Holtappels, J. Podlech, *J. Exp. Med.* **2016**, 1881.
[461] B.N. Giepmans, S.R. Adams, M.H. Ellisman, R.Y. Tsien, *Science* **2006**, *312*, 217.
[462] L.D. Lavis, R.T. Raines, *ACS Chem. Biol.* **2008**, *3*, 142.
[463] S. Van De Linde, A. Löschberger, T. Klein, M. Heidbreder, S. Wolter, M. Heilemann, M. Sauer, *Nat. Protoc.* **2011**, *6*, 991.
[464] M. Sauer, *J. Cell Sci.* **2013**, *126*, 3505.
[465] D. Lando, U. Endesfelder, H. Berger, L. Subramanian, P.D. Dunne, J. McColl, D. Klenerman, A.M. Carr, M. Sauer, R.C. Allshire, *Open Biol.* **2012**, *2*, 120078.
[466] S. van de Linde, M. Heilemann, M. Sauer, *Ann. Rev. Phys. Chem.* **2012**, *63*, 519.
[467] S. van de Linde, S. Aufmkolk, C. Franke, T. Holm, T. Klein, A. Löschberger, S. Proppert, S. Wolter, M. Sauer, *Chem. Biol.* **2013**, *20*, 8.
[468] M. Heilemann, E. Margeat, R. Kasper, M. Sauer, P. Tinnefeld, *J. Am. Chem. Soc.* **2005**, *127*, 3801.
[469] J. Seibel, S. König, A. Göhler, S. Doose, E. Memmel, N. Bertleff, M. Sauer, *Expert Rev. Proteomics* **2013**, *10*, 25.
[470] G.T. Dempsey, J.C. Vaughan, K.H. Chen, M. Bates, X. Zhuang, *Nat. Methods* **2011**, *8*, 1027.
[471] M. Heilemann, S. van de Linde, A. Mukherjee, M. Sauer, *Angew. Chem., Int. Ed.* **2009**, *48*, 6903.
[472] M. Sauer, M. Heilemann, *Chem. Rev.* **2017**.
[473] S. Letschert, A. Göhler, C. Franke, N. Bertleff-Zieschang, E. Memmel, S. Doose, J. Seibel, M. Sauer, *Angew. Chem., Int. Ed.* **2014**, *53*, 10921.
[474] S. Stoyanov, I. Petkov, L. Antonov, T. Stoyanova, P. Karagiannidis, P. Aslanidis, *Can. J. Chem.* **1990**, *68*, 1482.
[475] R. Du, C. Liu, Y. Zhao, K.-M. Pei, H.-G. Wang, X. Zheng, M. Li, J.-D. Xue, D.L. Phillips, *J. Phys. Chem. B* **2011**, *115*, 8266.
[476] A. Rossi, *Development of functionalized electrospun fibers as biomimetic artificial basement membranes*. **2016**, Würzburg.
[477] T.G. Kim, T.G. Park, *Tissue Eng.* **2006**, *12*, 221.
[478] M. Paulsson, *Crit. Rev. Biochem. Mol. Biol.* **1992**, *27*, 93.
[479] M. Brinkley, *Bioconjugate Chem.* **1992**, *3*, 2.

Danksagung

Ich möchte mich am Ende bei den Menschen bedanken, die zum Gelingen dieser Arbeit beigetragen haben.

Ich danke Herrn Prof. Dr. Jürgen Groll, dass er mich am Lehrstuhl aufgenommen hat, nachdem ich nach einem Jahr pharmakologischer Doktorarbeit schon aufgeben wollte. Danke für die Möglichkeit, doch noch eine Promotion durchzuführen, mit der ich mich besser identifizieren konnte.

Besonders bedanke ich mich außerdem bei Prof. Dr. Uwe Gbureck. Danke, lieber Uwe, dass ich immer in dein Büro platzen durfte, um Fragen zu stellen oder auch mal nur, um kurz zu plaudern. Danke, dass du mich immer unterstützt hast, auch wenn ich eigentlich gar nicht zu deiner Gruppe gehört habe. Danke für das gute Essen und die vielen Grillfeste.

Danke auch an Dr. Jörg Teßmar und Dr. Andrea Ewald, an deren Tür man immer klopfen konnte, um sich Rat zu holen.

Außerdem danke ich dem ganzen FMZ für das angenehme und kollegiale Umfeld, den guten Zusammenhalt und allgemein für die tolle Zeit, die ich mit euch erleben durfte. Ich danke euch für die lustigen Mittagspausen und die vielen Freizeitgestaltungen. Ich freue mich, dass aus Kollegen Freunde geworden sind.

Ich danke insbesondere den technischen Mitarbeitern für ihre tatkräftige Unterstützung. Danke an Harald Hümpfer und Anton „Toni“ Hofmann, dass ihr es immer geschafft habt, Probleme zu lösen, ob es mit dem Computer oder mit dem Herstellen von Materialien, die man gerade ganz schnell brauchte, zu tun hatte. Außerdem möchte ich mich bei Simone Werner und Maria Aniolek für die biologische und mikrobiologische Unterstützung bedanken. Ferner möchte ich Judith Friedlein, Carina Blum und Philipp Stahlhut für die Hilfe mit dem REM danken. Großer Dank geht auch an Isabell Biermann, die immer eine große Unterstützung war und für alle organisatorischen Fragen ein offenes Ohr hatte.

Mein ganz besonderer Dank geht an die vielen tollen Menschen, die ich kennenlernen durfte: die „Oldies“ Michaela Rödel und Julia Blöhbaum, außerdem Theresa Brückner

und Martha Schamel, die es schon „geschafft“ haben. Danke an die „Hartzer“ Susanne Feineis, Simone Schäfer, Sarah Bertlein und Ilona Zilkowski.

Vielen Dank auch an Angela Rossi, danke für deine Unterstützung und Hilfe. Es war toll, dass du mit mir den Weg gegangen bist.

Ich danke außerdem meinen Kollaborationspartnern Prof. Dr. Harald Wajant und Dr. Juliane Medler, geb. Kums, von der Abteilung für Molekulare Innere Medizin für die gute Zusammenarbeit und die interessante Publikation, die daraus entstanden ist.

Als letztes möchte ich mich ganz herzlich bei meiner Familie, besonders meinen Eltern, bedanken und meinen Freunden, die mich unterstützt haben. Danke, Mama und Papa, dass ihr immer für mich da wart. Danke, Chris, dass du an meiner Seite bist. <3